Assembling dacite in a continental subduction zone: a case study of Tauhara volcano

Chelsea May Tutt

A thesis submitted in partial fulfilment of the requirements for the degree of Masters of Science with Honours in Geology

School of Geography, Environment and Earth Sciences,

Victoria University of Wellington

May 2011

ABSTRACT

Mount Tauhara is the largest dacitic volcanic complex of onshore New Zealand and comprises seven subaerial domes and associated lava and pyroclastic flows, with a total exposed volume of ca. 1 km^3. The dacites have a complex petrography including quartz, plagioclase, amphibole, orthopyroxene, clinopyroxene, olivine and Fe-Ti oxides and offer an excellent opportunity to investigate the processes and timescales involved in assembling dacitic magma bodies in a continental subduction zone with in situ and mineral specific analytical techniques.

Whole rock major and trace element data and Pb isotopes ratios define linear relationships indicating that the dacites are generated by mixing of silicic and mafic magmas. Two groups of samples define separate mixing trends between four endmembers on the basis of La/Yb ratios, $^{87}Sr/^{86}Sr$ ratios and Sr contents. The older Western and Central Domes have low $^{87}Sr/^{86}Sr$ (0.7042-0.7046) and high LREE/HREE (La_N/Yb_N = 8.0-11.5) and Sr (380-650 ppm) compared to the younger Hipaua, Trig M, Breached and Main Domes, which have higher $^{87}Sr/^{86}Sr$ (0.7047-0.7052) and lower LREE/HREE (La_N/Yb_N = 6.5-7.5) and Sr (180-400 ppm).

In situ mineral major and trace element chemistry of mineral phases, as well as Sr and Pb isotope ratios of mineral separates have been used to: (i) fingerprint the origin of each crystal phase; (ii) constrain the chemistry of the four endmembers involved in the mixing events and; (iii) estimate the timing of mixing relative to eruption and the ascent rate of the dacitic magmas. The presence of quartz and analyses of quartz-hosted melt inclusions are used to fingerprint the chemistry of the silicic endmembers, which is a rhyolitic melt with a major element chemistry similar to that of either the Whakamaru Group Ignimbrite melts (Western, Central and Trig M Domes) or intermediate between that of the Whakamaru and the Oruanui Ignimbrite melts (Hipaua, Breached and Main Domes). Similarly, Ba-Sr concentrations and Sr isotopic signatures of plagioclase show that this phenocryst phase also predominantly crystallized from the rhyolitic melt. Variations in the Mg# and trace element chemistry of clinopyroxenes suggest they were formed both in the mixed dacitic melts and in a mafic endmember. The chemistry of the mafic endmembers have been traced using a combination of back-calculated Sr melt concentrations from clinopyroxene with the highest Mg# in each sample group, and the linear trends between whole rock SiO_2 content and most elements. These results indicate that dacites erupted from the Western and Central Dome were generated by the mixing of a high alumina basalt and a rhyolitic melt and Trig M Dome dacites were generated by the mixing of an andesite with a rhyolitic melt. Magmas erupted from Hipaua, Breached and Main Domes were also produced by the mixing of an andesitic melt and a rhyolitic body with a composition intermediate between that of the Whakamaru and the Oruanui melt bodies.

Trace element data and $^{87}Sr/^{86}Sr$ ratios of amphibole demonstrate that it crystallized from the mixed dacitic melt. Thermobarometric conditions obtained from amphibole indicate that the magma mixing event that produced the dacites occurred within a magma chamber located at ca. 9 km depth and ca. 900 °C with the exception of Trig M Dome which occurred deeper at 13 km and 950 °C. Diffusion profiles of Ti in quartz and Fe-Mg in clinopyroxene indicate the magma mixing events occurred < 6 months prior to eruption. Amphibole reaction rims show the magma to have ascended over 2-3 weeks for each dome, with the exception of Main Dome where reaction rims were not present in the amphibole, suggesting the ascent rate was faster than 0.2 m/s (< 6 hours).

TABLE OF CONTENTS

CHAPTER 1: INTRODUCTION

CHAPTER 2: METHODS

CHAPTER 3: RESULTS

CHAPTER 4: DISCUSSION

CHAPTER 5: CONCLUSION

APPENDICES

LIST OF FIGURES

CHAPTER 1: INTRODUCTION

CHAPTER 2: METHODS

CHAPTER 3: RESULTS

CHAPTER 4: DISCUSSION

APPENDICES

LIST OF TABLES

CHAPTER 2: METHODS

CHAPTER 3: RESULTS

CHAPTER 4: DISCUSSION

APPENDICES

LIST OF PLATES

ACKNOWLEDGEMENTS

First and foremost, I would like to thank my three supervisors, Prof. Joel Baker, Dr Marc-Alban Millet and Dr Monica Handler, all of whom have dedicated their time, brains and hard work throughout this thesis. Your concise laboratory instructions and late night analytical assistance is dearly appreciated.

Tim Worthington is thanked for his previous work on Tauhara volcano and the samples collected during his thesis, which were used in this study.

I would like to thank Stewart Bush for the production of both thin and thick sections for all samples and the entertaining conversations which made polishing sections less mundane. Kate Saunders is thanked for the help in developing the perfect epoxy to hardener ratio and her assistance with the initial mounting of crystals for probe analyses. John Patterson is also thanked for his contribution to sample preparation by numerous inventions including the "magnet in a syringe". Julie Vry is thanked for her guidance in microscopy and sample crushing. Dan Morgan is thanked for kindly sharing his time, knowledge and spreadsheets on diffusion modelling.

John Patterson and Kate Saunders are thanked for help during electron microprobing on the 'old probe' and extending its lifetime expectancy through delicate maintenance. John Creech, Sarah Martin and Sophie Barton are thanked for assistance with the 'new' electron microprobe. Alex McCoy-West is thanked for his ICP-MS methods which were utilised in this study.

I would like to thank a number of staff and students of the Victoria University geology department who have contributed in numerous ways: Colin Wilson (for the discussions about thermometry, Mount Tauhara and related volcanology), Netty Bolton (for teaching me your technique of weighing really small things) and the laboratory team who provided much welcomed company in both the ultraclean lab and probe room. To my office buddies - Sarah, Sophie, Kirsty, Melissa, Chris, Kate, and Barbara – I dedicate alot of gratitude for "living" with me during the stressful and not-so-stressful times and providing answers to my numerous, typically out of the blue questions.

My mother Robyn Tutt is thanked for her love, patience, accommodation and food during the course of my studies. Lastly, Joel Pearson is thanked for his love, support, and the company to a multitude of bogan gigs which provided the momentary escapes from the science world.

CHAPTER 1

INTRODUCTION

Plate 1: Mount Tauhara looking southeast from across the township of Taupo (photograph courtesy of Sophie Barton).

1.1 INTRODUCTION

Average continental crust has a chemical composition similar to that of intermediate (andesite and dacite) igneous rocks (55-65% SiO_2) (Rudnick and Fountain, 1995; Taylor and McLennan, 1995). Therefore it is commonly conjectured that subduction zones, where andesitic volcanism is predominant, are the active sites of new continental crust generation (Tatsumi, 2008). However, partial melting of the upper mantle generates basaltic magmas (45-55% SiO_2) (Bacon et al., 1997; Ulmer, 2001), as is the case for both mid-ocean ridge basalts (MORB), and oceanic subduction zones where primary arc basalts are occasionally erupted, and as demonstrated by experimental studies on the melting of peridotite (Jaques and Green, 1980; Hirose and Kushiro, 1993; Takahashi et al., 2001). These mantle-derived products have significantly different major element, and compatible and incompatible trace element signatures as compared to continental crust, arc andesites and dacites. For example, Figure 1.1 shows typical N-MORB normalised ($N\text{-}MORB_N$) incompatible trace element patterns for average continental crust (Rudnick and Fountain, 1995) and a range of arc magmas. Andean andesites have $N\text{-}MORB_N$ trace element patterns similar to the average continental crust signature. Arc andesites, dacites and rhyolites and the average continental crust have a greater enrichment in the large ion lithophile elements, and the light rare earth elements relative to arc basalts. Therefore a range of secondary processes must contribute to the generation of intermediate and silicic magmas from basaltic melts in subduction zones and it is these processes that are key to understanding the formation of these evolved magmas and potentially the origins of continental crust. Thus detailed petrological and geochemical study of andesite and dacite rocks in subduction zones provides an opportunity to investigate the shallow crustal differentiation processes which modify mantle-derived arc basaltic melts *en route* to the surface and their contribution to generating new continental crust.

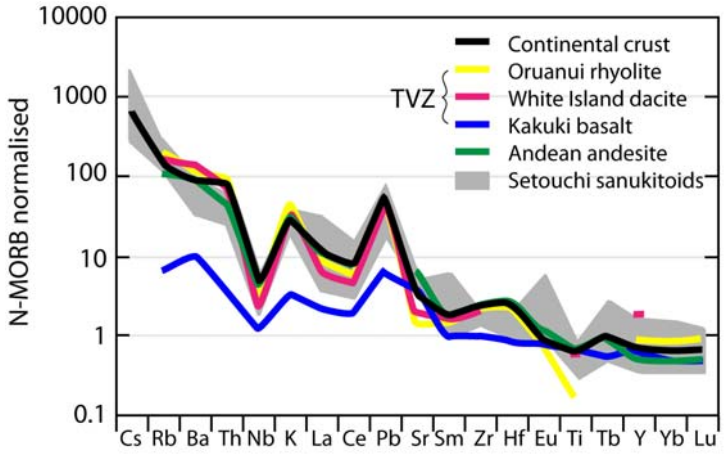

Figure 1.1: Multi-element plot showing N-MORB normalised incompatible trace element data for arc volcanic rocks (Oruanui rhyolite: Sutton et al., 1995; White Island dacite: Graham and Cole, 1991; Andean andesite : Weaver and Tarney, 1984; Kakuki basalt; Graham et al., 1995; Setouchi sanukitoids: Shimoda et al., 1998; Tatsumi et al., 2003) and average continental crust (Rudnick and Fountain, 1995). TVZ: Taupo Volcanic Zone.

1.2 OBJECTIVES OF THIS THESIS

This study aims to constrain the detailed mechanisms involved in the construction of an intermediate arc magmatic complex, using as a case study the largest dacitic volcano in the continental New Zealand arc, the Tauhara volcano. Previous work on the Tauhara volcano focused on major element chemistry investigations (Lewis, 1960; Reid and Cole, 1983; Worthington, 1985), and a limited amount of trace element and Sr isotopic study (Worthington and Graham, 1988), which were carried out more than 20 years ago. Recent advances in analytical techniques and, specifically, in situ analytical methods now makes it possible to undertake detailed whole rock and mineral specific chemical and isotopic studies providing greater insights into the sub-surface processes which generate dacitic magmas in a continental subduction zone setting.

This thesis presents a detailed study of six dacite domes which comprise the Tauhara volcano. Analytical methods employed included: (1) whole rock trace element chemistry by inductively coupled plasma mass spectrometry (ICP-MS), (2) in situ electron microprobe major element and laser ablation ICP-MS trace element analysis of individual phenocrysts and their hosted melt inclusions, and (3) Sr-Pb isotope measurements of whole rock, groundmass and phenocrysts by multi-collector ICP-MS.

1.3 SUBDUCTION ZONES

1.3.1 GENERAL CHARACTERISTICS

Subduction zones are formed during the convergence of two tectonic plates where the denser plate is thrust beneath the other. In a continental setting such as the Taupo Volcanic Zone (TVZ), the subducted oceanic lithosphere is cold, hydrated and dense and comprises oceanic crust that has been hydrated and altered through hydrothermal processes and mechanical fracturing prior to subduction (Tatsumi and Kogiso, 2003), unaltered anhydrous oceanic lithosphere and pelagic and terrigenous sediments deposited at both the subduction trench and onto the oceanic crust. During slab descent into the mantle and subsequent heating, subducted lithosphere dehydrates and releases fluids into the overlying mantle generating a serpentinised mantle (Figure 1.2). The serpentinised mantle is dragged down alongside the slab and subsequently heated further, thereby releasing fluids which lower the solidus of the overlying mantle wedge (Wysoczanski et al., 2006). This fluid flux, coupled with mantle decompression from subduction-induced corner flow triggers partial melting of the mantle wedge, resulting in the generation of a mantle-derived melt (Annen et al., 2006). During melt

ascent, the overlying low-density continental crust acts as a barrier, trapping the melt and resulting in crustal differentiation processes, such as fractional crystallisation, crustal assimilation and magma mixing, which all act to modify the chemistry of the primary mantle-derived melt (Tatsumi and Stern, 2006). The location of the volcanic arc relative to the trench is linked to the angle of subduction as volcanic arcs typically occur 108 ± 18 km (1σ) above the subducting slab surface (Tatsumi and Eggins, 1995). This depth is linked to a ca. 1300 °C isotherm where the amount of melting in the mantle wedge is sufficient to allow for the mechanical separation of parental arc magmas (Schmidt and Poli, 1998).

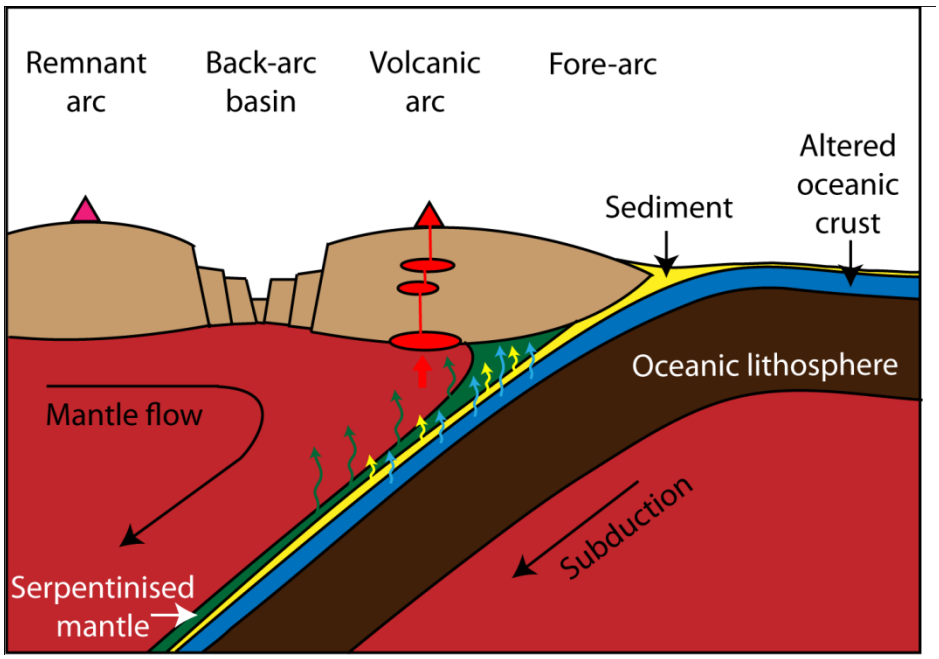

Figure 1.2: Schematic diagram of a subduction zone where oceanic lithosphere is subducted beneath continental crust. Figure taken and modified after Wysoczanski et al. (2006).

1.3.2 INTERMEDIATE ARC MAGMAS

HIGH MAGNESIUM ANDESITES (SANUKITOIDS)

The class of eruptives that most closely match the average geochemistry of the continental crust are high magnesium andesites (HMA), such as the Setouchi sanukitoids, Japan (Figure 1.1). HMA are characterised by high MgO contents (> 5% MgO), low FeO_{Tot} /MgO (< 1.0), and enrichment in Cr and Ni (Tatsumi, 2008). N-MORB normalised incompatible trace element data for the Setouchi sanukitoids are plotted in Figure 1.1 (Shimoda et al., 1998; Tatsumi et al., 2003). This HMA signature is also observed in Late Archaean terranes such as the Superior Province (Shirley and Hanson, 1984), south India (Moyen et al., 2003), Baltic Shield (Samsonov et al., 2005), and the central Pilbara Craton (Smithies and Champion, 1999).

The generation of Archaean HMA and modern-day sanukitoid magmas have been attributed to the direct production of andesitic melts in the mantle through the melting of the subducted oceanic lithospheric slab. Experimental studies by Nicholls and Ringwood (1973) and subsequent studies by Sekine et al. (1982), Rapp et al. (1991) and Wolf and Wyllie (1994) have shown that partial melting of subducted basaltic crust can produce *primary* HMA magmas as opposed to calc-alkaline and tholeiitic intermediate magmas that are typically erupted in modern arcs. However, because the solidus temperature of typical subducted anhydrous oceanic crust at modern arcs is higher than the estimated temperature along the subducted slab, oceanic crust cannot melt in typical modern subduction zones (Yasuda et al., 1994; Pertermann and Hirschmann, 1999). Slab melting was possible, however, during the Archean when both the mantle and lithosphere were hotter than the present day (Berry et al., 2008). Similarly, slab melting has also been postulated as a mechanism for the generation of intermediate magmas beneath the Setouchi volcanic belt (SVB) where young "hot" lithosphere of the Shikoku Basin is subducted into hot upper mantle (Tatsumi et al., 2003; England et al., 2004). Experiments by Liu et al. (1996) shows that slab melting of young oceanic crust is possible at depths shallower than 60 km along subduction zones where an average thermal gradient higher than 7 °C/km is present.

ADAKITES

In contrast to HMA, adakites form suites of intermediate to felsic rocks (SiO_2 > 56 wt.%) with basaltic members absent (Martin et al., 2005). Adakitic rocks also have high Na_2O (3.5-7.5 wt. %) correlating with low K_2O/Na_2O (~0.42), high Mg# (~0.51), high Ni and Cr (ca. 24 and ca. 36 ppm respectively) (Martin et al., 2005) and high Sr concentrations (>400 ppm with extreme concentrations up to 3000 ppm) (Defant and Drummond, 1990). The term adakite was first defined by Defant and Drummond (1990) in reference to the sodic and felsic 'slab-melts' of the magnesian andesites from Adak Island in the Aleutians (Kay, 1978) where these subduction zone magmas were produced by melting of subducted oceanic crust basalts. This slab melting genesis of adakites is supported by experimental work on water-saturated or dehydration melting of amphibolites (Beard and Lofgren, 1989; Rapp et al., 1991; Sen and Dunn, 1994). Martin and Moyen (2003) divided adakites into two main compositional groups, defined by silica content: high-SiO_2 adakites (HSA) (SiO_2 > 60 wt. %) as found in most of the Austral Volcanic zone of the Andes (Stern and Kilian, 1996) and localised volcanoes such as Mount St. Helens (USA; Smith and Leeman, 1987), and Sambe and Daisen (Japan; Morris, 1995), and low-SiO_2 adakites (LSA) (SiO_2 < 60 wt. %) such as Adak and Kormandosky (Aleutians; Kay, 1978; Yogodzinski et al., 1995), and Zamboanga (Phillipines; Sanjona et al., 1996). These two adakite

groups are formed by different processes. HSA are formed from the melting of subducted hydrated basalt with variable contamination of these slab melts by peridotite assimilation in the mantle wedge whereas LSA are generated in a two-phase process consisting of complete metasomatism between slab melt and peridotite, followed by the melting of this metasomatised peridotite (Martin et al., 2005).

THOLEIITIC VERSUS CALC-ALKALINE ARC MAGMAS

The majority of magmas erupted in modern arcs have tholeiitic and calc-alkaline intermediate compositions. These two types of distinctive non-alkaline trends present in modern subduction zones characterize the presence (tholeiitic) or absence (calc-alkaline) of iron-enrichment (Nockolds and Allen, 1953). The trends are distinguished quantitatively using the Miyashiro (1974) method of plotting FeO*/MgO versus SiO_2 (FeO* = total iron as FeO) where the calc-alkalic series plot on a shallower trend and tholeiitic series plot on a steeper trend than the line defined by this equation:

$$SiO_2 \text{ (wt\%)} = 6.4 \times FeO^*/MgO + 42.8$$

Tholeiitic and calc-alkalic rocks of northeast Japan are compared to average continental crust (Tatsumi and Kogiso, 2003) in Figure 1.3 where FeO*/MgO and MgO are plotted versus SiO_2. This demonstrates that continental crust possesses chemical signatures closer to those of calc-alkaline rather than tholeiitic andesites. Tholeiitic trends can be explained by the fractional crystallisation from a basaltic parent (as modelled by MELTS: Ghiorso and Sack, 1995). In contrast, the linear calc-alkaline signature cannot be explained by fractional crystallisation processes alone, and therefore, other processes must contribute to the generation of the calc-alkaline magmas in a subduction zone setting.

Numerous mechanisms have been proposed for the generation of these andesitic magmas in modern subduction zones, however, most can be divided into these groups:

1. Producing H_2O-rich melts in deep crustal hot zones through either the partial melting of pre-existing crustal rocks or the partial crystallisation of basaltic sills in the lower crust with subsequent crystallisation of the melt only at shallow depths (Annen et al., 2006).

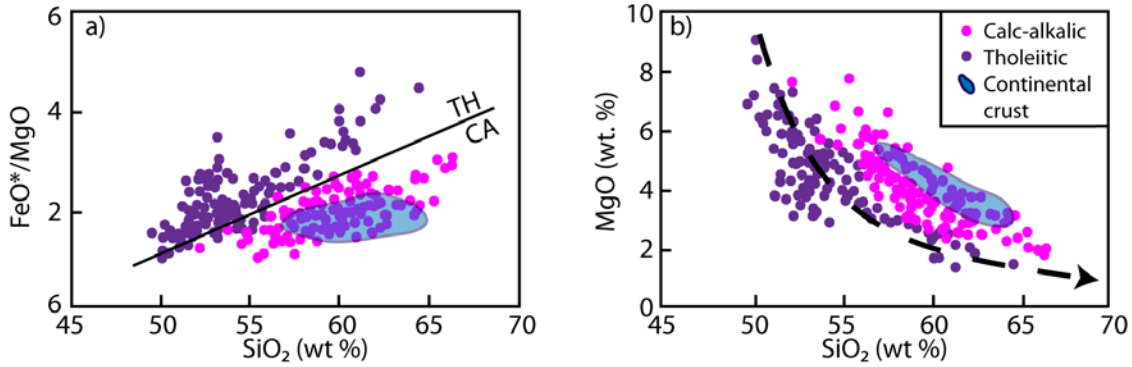

Figure 1.3: FeO*/MgO (a) and MgO (b) versus SiO_2 for calc-alkaline and tholeiitic rocks from the northeastern Japan volcanic arc. (a) shows the discrimination between calc-alkaline (CA) and tholeiitic (TH) rocks where they plot below and above, respectively, the line described by Miyashiro (1974). (b) shows the tholeiitic and calc-alkaline rocks in respect to MgO where only the tholeiitic trend can be explained by crystallisation from a basaltic melt (black dashed line) as modelled by MELTS (Ghiorso and Sack, 1995).

2. Slab derived melts reacting with mantle wedge peridotites generating a mantle partial melt with subsequent shallow crustal differentiation en route to the surface (Kelemen, 1995; Rapp et al., 1999).

3. Basaltic underplating, followed by anatexis of such initial crust and subsequent delamination of residual, mafic lower crust (Turcotte, 1989; Kay and Kay, 1993).

4. Mixing between silicic magmas and mantle-derived mafic magmas (Heiken and Eichelberger, 1980; Annen et al., 2006).

The reactions between slab-derived fluids and mantle peridotite and basaltic underplating with subsequent residue delamination are the preferred mechanisms for the generation of post-Archean andesites and thus the modern continental crust (Tatsumi and Kogiso, 2003). A more plausible mechanism for generation of calc-alkaline andesites, and thus the continental crust is the mixing of mantle derived basalts and crustally-derived silicic magmas either in the shallow crust (scenario 2) or deep crustal hot zones (scenario 1).

1.3.3 MAGMATIC DIFFERENTIATION PROCESSES THAT OCCUR IN ARCS

In a continental setting, multiple differentiation processes modify the mantle derived melts en route to the surface generating more silicic melts in the crust. These main processes are fractional crystallisation, crustal assimilation, and magma mixing.

ASSIMILATION FRACTIONAL CRYSTALLISATION

Fractional crystallisation is an important process in the evolution of many igneous rocks where magmas go through a liquid line of descent en route to the surface. This is where the residual liquid evolves though the differentiated withdrawal of minerals (Bowen, 1928). Gravity separates the dense crystals from the less dense melt, preventing re-equilibration with the liquid (Carmichael et al., 1974). The latent heat in the magma, as a result of fractional crystallisation generates sufficient thermal energy to melt and assimilate crustal wallrock (Bowen, 1928). The amount of wall rock assimilation is dependent on the amount of fractional crystallisation and the physical parameters including temperature contrast between wallrock and magma, magma ascent rate and solidus temperature of the wallrock (DePaolo, 1981). Crustal contamination can be identified by correlations between country rock age and the $^{143}Nd/^{144}Nd$ ratios observed in igneous rocks (DePaolo, 1981).

MAGMA MIXING

Magma mixing is the blending of two or more magma batches to form a hybrid magma which inherits properties intermediate to those of the parental magmas. Magma mixing clearly requires an open system. Since thermal diffusion rates are faster than chemical diffusion rates, temperature homogenization occurs initially. Chemical equilibration is thus dependent on physical properties after thermal equilibration such as viscosity and crystal content of the magmas (Sparks and Marshall, 1986). Complete mixing is only plausible in two scenarios where: (a) the physical properties (temperature, viscosity) of both end-members are similar e.g. an andesite and a dacite or (b) > 50% of a mafic end-member is present. When the mafic input is <50%, the viscosity increases rapidly in the mafic end-member due to crystallisation induced from thermal equilibration and reaches a point where it is effectively solid. Therefore, complete magma mixing cannot occur between the mafic and silicic end-members and the mafic magma is instead dispersed as cognate xenoliths, enclaves or veins within the silicic magma (Sparks and Marshall, 1986).

Magma mixing in a suite of magmatic rocks can be recognised by either petrographic or geochemical evidence. Evidence for magma mixing is provided by phenocryst disequilibrium features such as sieve textures, atoll and swallow-tail structures, and resorption and reaction rims. The petrological diversity of the Mount St. Helens andesites and dacites, for example, is governed by the mixing of a felsic dacite (or rhyodacite) and a basalt (Gardner et al., 1995). Geochemically, magma mixing in a suite of related igneous rocks produces linear arrays on

bivariate plots of element concentrations, as opposed to hyperbolic trends observed in the tholeiites (Figure 1.3) which are generated by fractional crystallisation.

1.4 GEOLOGICAL BACKGROUND TO THE TAUHARA VOLCANO

The North Island of New Zealand lies on an active convergent plate boundary where the Pacific Plate is obliquely subducted beneath the Australian Plate at ca. 50 mm/yr beneath the North Island (Cole and Lewis, 1981) to form the Taupo-Hikurangi arc-trench system (Figure 1.4). The Taupo-Hikurangi system marks the southernmost 300 km of the 2000-km-long Tonga-Kermadec-Taupo volcanic arc and associated Lau-Havre-Taupo back-arc system, which is undergoing a southward propagation from rifting to spreading (Parson and Wright, 1996). The Taupo Volcanic Zone (TVZ) is an active region of back-arc rifting and Cenozoic arc volcanism. The extensional regime of the TVZ began ca. 4 Ma with present day extension rates between 12 to 20 mm/yr and up to 3 mm/yr subsidence (Parson and Wright, 1996). The tectonic fabric of the TVZ is characterised by steeply dipping (60°) en echelon faults, striking between 040˚ and 080˚ (Cole, 1990). The extensional regime has thinned the crust from a normal thickness of 25 km to a present day thickness of 15 km (Wilson et al., 1995; Stratford and Stern, 2006). The crust beneath the TVZ is abnormally thin for a continental setting, generating an extreme heat flow of 800 mW/m^2 (Stern 1985, 1987), which is ca. 12 times greater than typical continental heat flow. This heat flow is highest in the eastern side of the TVZ where andesitic and dacitic volcanism are principally focused.

Subduction related volcanism in the TVZ began ca. 2 Ma with andesitic volcanism. This was followed by rhyolitic (with minor basaltic, andesitic and dacitic) activity from ca. 1.6 Ma (Wilson et al., 1995). The TVZ can be divided into three segments: northern and southern regions dominated by basaltic andesite to dacite volcanics and a central 125 km segment dominated by 8 caldera forming rhyolitic centres (Figure 1.5) (Healy, 1962). Older basaltic and dacitic eruptives, especially in the central segment are buried by the Whakamaru eruptions (0.34 Ma), hence the Whakamaru eruptions are used as a marker between “old TVZ” (pre-Whakamaru) and “young TVZ’” (post-Whakamaru) volcanic products. Eruptive volumes for basalt, andesite, dacite and rhyolite from the “young TVZ” are 5, 300, 20 and 3000 km^3, respectively, with a 15,000 km^3 total volume of rhyolitic eruptives for both the “old” and “young TVZ” compared to a total of ca. 20,000 km^3 for all erupted TVZ volcanic material (Wilson et al., 1995).

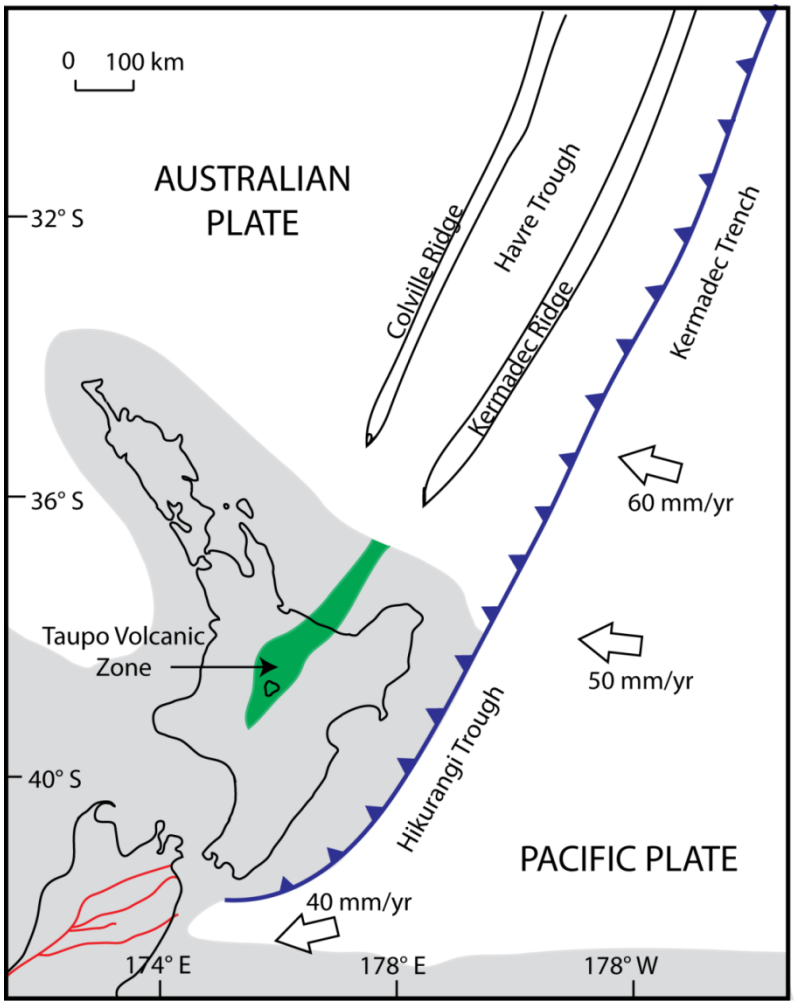

Figure 1.4: Map showing the location of the Kermadec Ridge and Taupo Volcanic Zone arcs in relation to the subduction zone plate boundary. Arrows show the motion of the Pacific Plate in relation to the Australian Plate. Shaded region represents continental crust and the unshaded region is oceanic crust.

1.4.1 TVZ ANDESITES

Andesites in the TVZ are the second most voluminous eruptives after rhyolitic magmatism. Eruptions typically form cone-forming composite volcanoes with minor occurrences of pyroclastic falls and flows with the cones ranging in volume from ca. 10 to > 200 km^3 (Wilson et al., 1995). Individual volcanoes are generally long-lived with volcanoes such as Ruapehu and Tongariro having been active for > 240 kyr. TVZ andesites are petrographically diverse and have been characterised into nine types (six in the Tongariro Volcanic Centre alone) based on variable mineral assemblages. All contain plagioclase, pyroxene and Fe-Ti oxides with the main variations being reflected in the presence or absence of olivine and hornblende (Graham et al., 1995). A wide range of processes have been proposed to be responsible for generating TVZ andesites including fractional crystallisation and assimilation from a low-alumina or tholeiitic basalt, assimilation of the meta-greywacke basement and magma mixing. Andesitic volcano locations within the TVZ are shown in Figure 1.5.

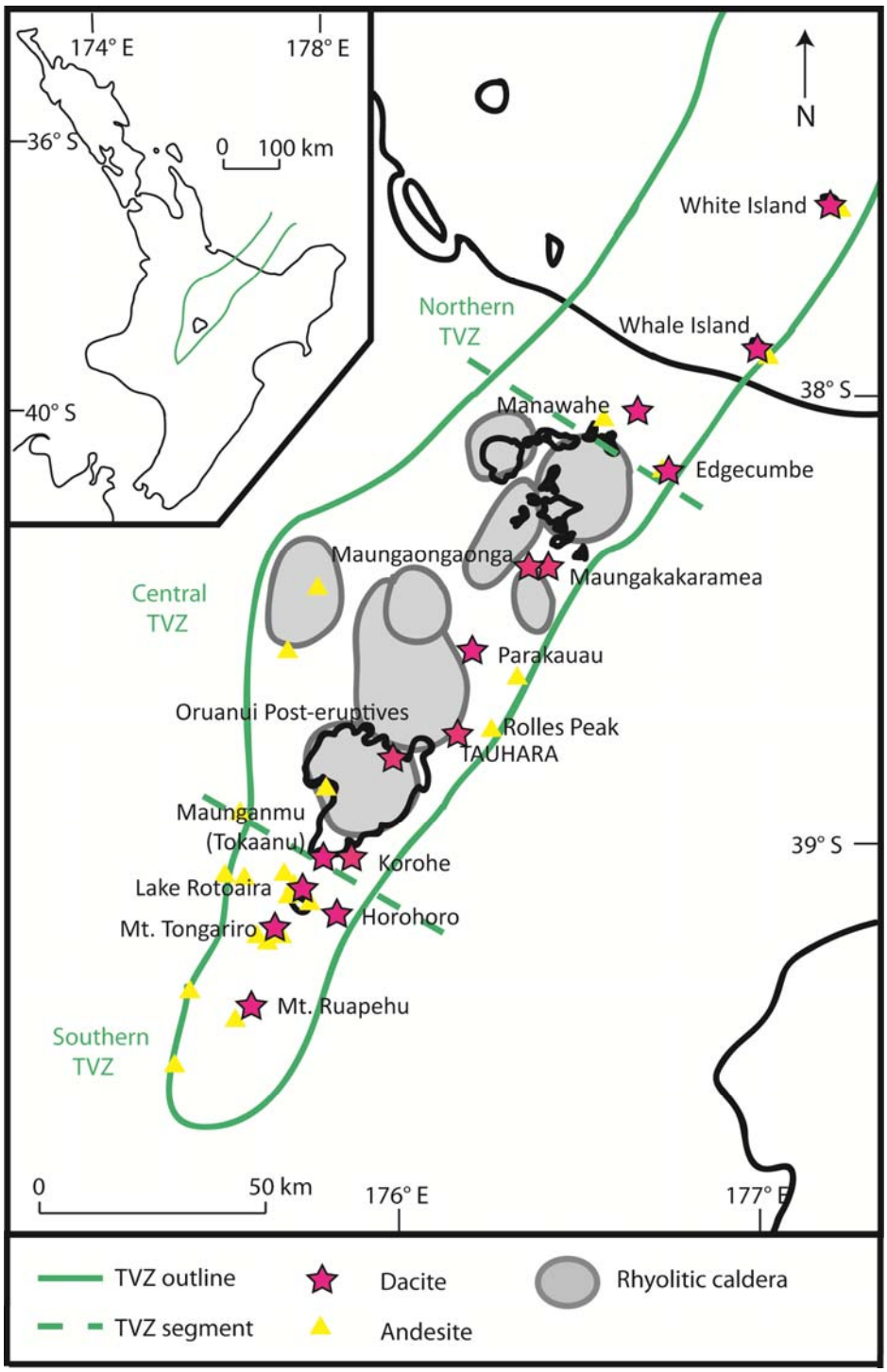

Figure 1.5: Map showing the areal extent of the Taupo Volcanic Zone (TVZ) and its segments as described by Healy (1962) and Wilson et al. (1995), and the locations of andesite and dacite volcanoes (labelled) and the 8 calderas formed by rhyolitic pyroclastic eruptions. Rolles Peak andesite is also labelled.

1.4.2 TVZ DACITES

Dacites make up less than 0.1% of the total volume of TVZ eruptives (< 5 km^3 total) with no individual volcanic complex or flow having a volume of more than 3 km^3 (Graham and Worthington, 1988). All exposed dacites post-date the 340-320 ka Whakamaru group Ignimbrites perhaps due to burial or destruction during the Whakamaru caldera collapse.

Figure 1.5 shows the location of subaerial dacites in the TVZ. These have been divided into two geochemical groups (Type A and B) by Graham et al., (1995).

Type A dacites are postulated to have formed by the fractionation of a high-alumina basalt (HAB) and are commonly associated with the HAB andesite sequence with ≤ 67 wt% SiO_2. These andesite-dacites are thought to mark the TVZ arc front. Examples of Type A dacites in the TVZ are White Island volcano and Mt Edgecumbe. Type B dacites are typically found in the central TVZ and have 64-70 wt% SiO_2 and lower concentrations of large ion lithophile elements and lower Sr isotopic ratios than Type A dacites. Type B dacites appear to be genetically related to rhyolites either through fractionation-accumulation or magma mixing processes. Both groups of dacites have been erupted as either individual cones and domes or dome/cone complexes and associated pyroclastic/lava flows with short lifespans and associated with discrete sub-plinian to plinian fall deposits (Wilson et al., 1995). Mt Tauhara is the site of the largest known TVZ dacitic complex, and is classified as a Type B dacite.

1.5 THE TAUHARA VOLCANO

1.5.1 GEOLOGY

The Tauhara volcano is situated 5 km northeast of the city of Taupo, and is located on the eastern rim of the TVZ (Figure 1.5). The Tauhara volcano comprises six dacitic domes (Western, Central, Hipaua, Trig M, Breached and Main), one rhyolite flow (Trig 9471), and two inferred dacite domes: a cryptodome (Buried Dome) beneath a pyroclastic flow erupted from Breached Dome and an inferred dacite dome adjacent to the main edifice (Waipahihi) (Figure 1.6). The total exposed volume of dacite is estimated to be ca. 1 km^3. The rhyolite of Trig 9471 and adjacent Rubbish Tip dome are chemically unrelated to the Tauhara dacites and are more closely related to the ca. 50 ka Ngangiho Dome (Sutton et al., 1995). The current height of the volcano is marked by a collapsed crater at the top of Main Dome, 555 m above the surrounding pumice plain. The base of the volcano is buried by younger ignimbrites and airfall deposits (e.g. eruptives from the Taupo caldera: Wilson, 1993), suggesting the entire volume of the Tauhara volcano is considerably larger than the 1 km^3 estimate.

The first significant geological investigation of the Tauhara volcano was made by Lewis (1960, 1968a) who defined five domes based on structure: Main, Western, Hipaua, Trig M and Breached Domes, where the later named Central Dome (Worthington, 1985) was thought to

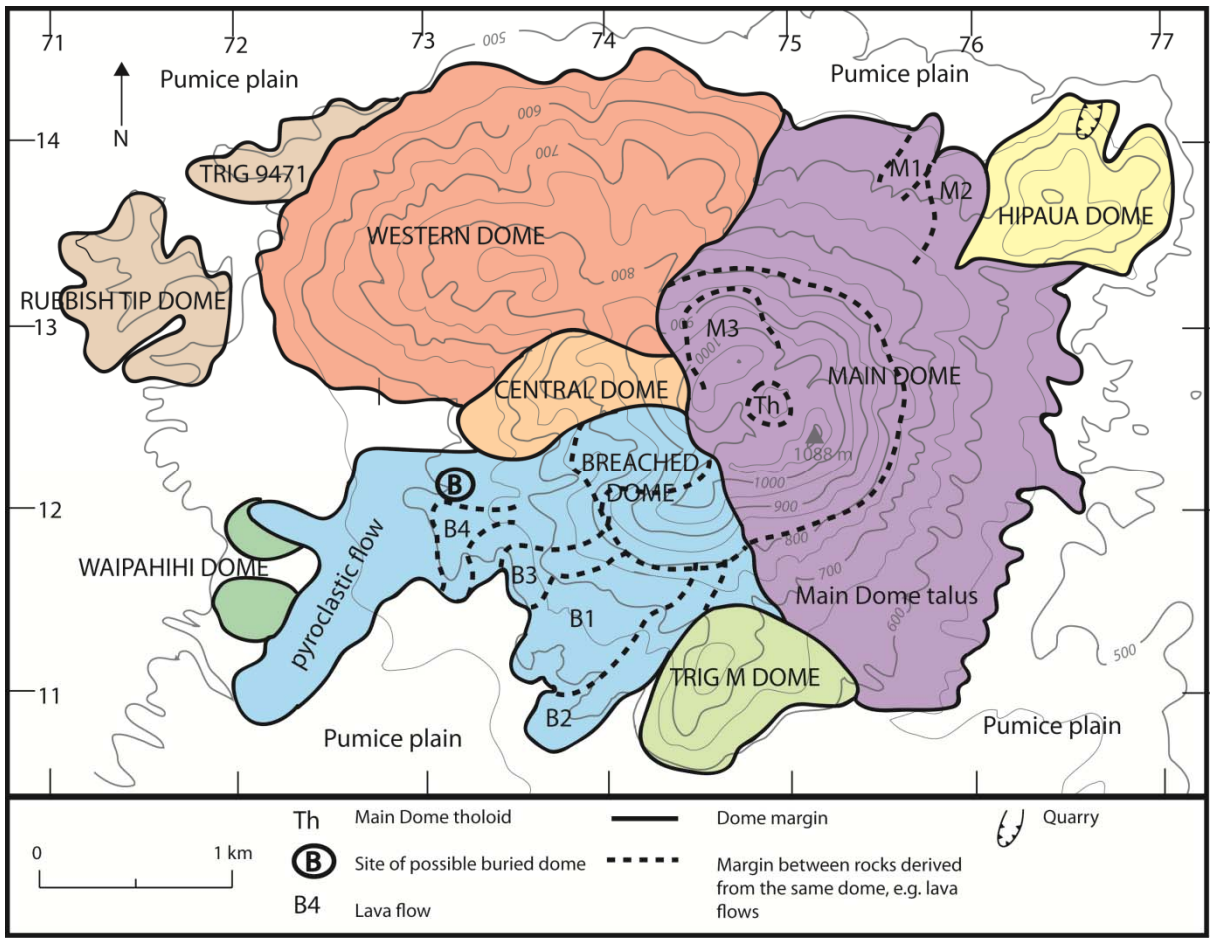

Figure 1.6: Map of the Tauhara volcano showing the location and extent of domes, lava flows and other features as identified by Worthington (1985).

form the northern rim of Breached Dome. The eruption style of the Tauhara dacites is described as semi-plastic lava extruded from separate vents and small fissures (Lewis, 1968a). However, the presence of *in situ* dacitic pumice on Main Dome as well as pyroclastic and lava flows associated with Breached and Main Dome suggest the eruption style was more explosive. Recent exposures at the quarry on Hipaua Dome reveal Huka Falls sediments displaced by around 150 m suggesting that Hipaua Dome growth began as a cryptodome that upthrust the overlying sediments (Rosenberg and Kilgour, 2003). Initial eruptive deposits of Hipaua Dome dacite are lapilli and ash intermixed with sandstone clasts from the Huka Falls Formation, mud-coated clasts and liquefied fine ash indicating that the Hipaua Dome dacite magma subsequently erupted through saturated lake sediments generating a phreatomagmatic eruption.

Relative ages of the domes are based on the fieldwork of Worthington (1985), with Western Dome the oldest, followed by Central Dome. Hipaua, Trig M, Buried and Waipahihi Domes follow as isolated domes and are only known to be older than Breached and Main Domes. Superimposed on all domes is the youngest and largest dome of Main Dome. A schematic diagram is presented in Figure 1.7 showing the relative chronology of the Tauhara domes.

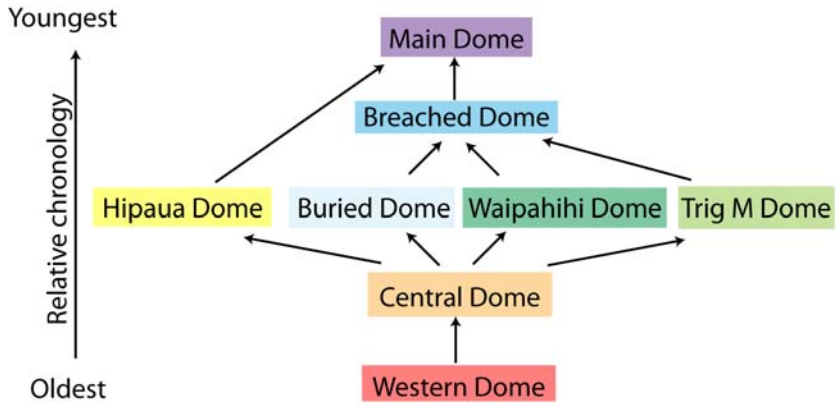

Figure 1.7: Relative chronology of the dacite domes. Arrows show chronological relationships based on geology.

WESTERN DOME

Western Dome was first named by Lewis (1968a) and rises 340 m above the pumice plain. It is a typical dome shape with its axis striking 050˚ and has a total volume of 0.3 km^3. The western half of the dome is assymetrical with a bulge on its northern flank possibly caused by a eastward continuation of the later emplacement of Trig 9471 flow beneath it (Figure 1.6) (Worthington, 1985). The eastern half of Western Dome is uplifted and deeply incised by streams. These sections have been uplifted by the emplacement of younger Central and Main Domes. The southern section of the eastern half has fractures concentric to the emplacement of Central Dome, which have uplifted this section by approximately 15 m. The easternmost section of the eastern half has wedges with fractures roughly concentric to the emplacement of Main Dome, where the wedge has been uplifted approximately 10 m on its western side and 15 m on its eastern side, closest to Main Dome. These uplifted wedges imply that Western Dome is older than Central and Main Dome and therefore is the oldest dome of the TDC (Worthington, 1985).

CENTRAL DOME

Central Dome forms a semi-circular ridge south of Western Dome, west of Main Dome and north of Breached Dome. Central Dome was initially thought to be a northern flank of the larger Breached Dome to the south (Lewis, 1968a), however chemical and geological evidence presented by Worthington (1985) does not support this. Central Dome is chemically distinct from Breached Dome and is more closely related to that of Western Dome and a concentric fractured wedge of Central Dome's southern flank bounded by Breached Dome has been uplifted approximately 10 m. The concentric fractures change direction to circular around a point west of Breached Dome where uplift increases by approximately 20 m. This abrupt

change is thought to be caused by the emplacement of the Buried Dome cryptodome. Therefore, it has been concluded that Central Dome is a separate dome, distinct from that of Breached Dome. Central Dome rises 275 m above the pumice plain with an estimated volume of 0.039 km^3 (Worthington, 1985). The southern half of Central Dome is missing, possibly destroyed by the emplacement of Breached Dome.

HIPAUA DOME

Hipaua Dome is a small horseshoe-shaped dome northeast of Main Dome and rises 170 m above the pumice plain with a total estimated volume of 0.031 km^3 (Worthington, 1985). Flow M2 from Main Dome has been deflected by Hipaua Dome and therefore Hipaua Dome is interpreted to be older than Main Dome. The axis of the "horseshoe" limbs strike 000˚. The only quarry in the Tauhara volcano, Burrows Quarry, is situated on eastern limb of this dome and therefore, most information is known of this dome. The dome axis of the eastern limb is marked by three spines 5, 10 and 20 m in diameter. The ease of sampling Hipaua Dome has led to its use as being representative for the whole Tauhara volcano. However, the chemical and petrological variations seen in Hipaua Dome samples do not encompass the full range of the Tauhara volcano (Graham and Worthington, 1988). Enclaves (Cole et al., 2001) of quartz microdiorite containing quartz, amphibole, plagioclase (An_{88-47}), orthopyroxene (En_{76-77}), clinopyroxene ($En_{37-47}Fs_{8-21}Wo_{45-47}$), magnetite and ilmenite are abundant in Hipaua Dome.

TRIG M DOME

Trig M Dome is a small steep-sided dome (0.02 km^3) located south of Breached and Main Domes. The dome axis, striking 000˚ is marked by three peaks interpreted to be collapsed and eroded spines with diameters of 100 m each (Worthington, 1985). The tallest spine peak reaches 190 m above the pumice plain. Lava flow B2 from Breached Dome is deflected around Trig M Dome and therefore Trig M Dome is interpreted to be older than Breached Dome.

WAIPAHIHI DOME

Waipahihi Dome consists of two small domes rising 40 m above the pumice plain. It is located west of Breached Dome and has markedly different topography from the undulating landscape formed by the pyroclastic flows of Breached Dome. The Breached Dome pyroclastic flow is deflected and diverges around a point east of the Waipahihi Dome implying that Waipahihi Dome is older than Breached Dome. No rock exposures are present on either mound and its composition is only inferred from an electrical resistivity survey by Dawson and Thompson (1981) that supports the hypothesis by Worthington (1985) of a buried dacite dome or lava flow that is at least 100 m thick. The chronological relationship between Hipaua, Trig M and Waipahihi Domes is unknown due to their isolated nature, but they are all older than Breached and Main Domes.

BURIED DOME

The presence of Buried Dome is implied by the field observations of Worthington (1985); deflections in stream patterns concentric around a point immediately west of Breached Dome and a 90° deflection of lava flow B4 from Breached Dome about the same point. This behaviour is consistent with a buried feature, although not necessarily a dome. This object is older than Breached Dome.

BREACHED DOME

Breached Dome is the second youngest dome of the Tauhara volcano rising 435 m above the pumice plain with a total estimated volume of 0.19 km^3 (Worthington, 1985). As its name suggests, its crater is breached due to the collapse of the dome to the west. Associated with the formation of Breached Dome are four small lava flows that form steep ridges with abrupt terminations, suggesting viscous compositions. A large pyroclastic flow (initially assumed to be a lahar by Lewis (1968a) extends 2.8 km from its crater. The texture of the Breached Dome pyroclastic flow varies with distance from its source with the rounding of breccia clasts and decreasing ash matrix evident with distance from source. This variation is interpreted to represent a pyroclastic flow comparable to those from the modern Merapi volcano (Indonesia) (Worthington, 1985), where the modern volcano is characterised by the continuous growth of a summit dome and its periodic collapses generating block and ash flows with associated surges (Camus et al., 2000). Like Breached Dome, the previous stages of the Merapi eruptions

were characterised by long effusive lava flows (Camus et al., 2000). The pyroclastic flow has a total volume of 0.067 km^3.

MAIN DOME

Main Dome is the largest and youngest dome of the Tauhara volcano and rises 555 m above the pumice plain with a total approximate volume of 0.41 km^3 (Worthington, 1985). Main dome has a 610 m diameter crater with a 70 m high tholoid present at the top of the dome. The crater has been breached to the north by pyroclastic flows M1 and M2. These pyroclastic flows resemble Pelean-type pyroclastic flows based on the juvenile ash matrix and unaltered clasts. Talus surrounding Main Dome is interpreted to be sourced from the dome as it grew, possibly covering other lava and pyroclastic flows and yields a total erupted volume (dome and talus) of 0.52 km^3 (Worthington, 1985).

1.5.2 AGE

A minimum age of 9 ka was initially established by Lewis (1960) based on the mantling of the complex by the Waitahanui breccias. The first direct age was attained using K-Ar dating of Hipaua Dome lavas producing an age of 31 ± 3 ka (Stipp, 1968). This is in agreement with the detailed tephrostratigraphy of the Taupo area by Vucetich and Howarth (1976) showing that eruptive activity ceased at Hipaua Dome between 19-20 ka and at Main Dome between 15-20 ka. These ages, however, are inconsistent with an $^{40}Ar/^{39}Ar$ age of ca. 190 ka for Hipaua Dome (Wilson et al., 1995) which is in agreement with the recent exposure of the upthrust Huka Falls lake sediments (Huka Falls Formation dates between the ca. 330 ka Whakamaru group ignimbrites and 22.6 ka Oruanui ignimbrite).

1.5.3 PETROLOGY

In depth petrographic descriptions were conducted by Worthington (1985) on 122 thin sections from the Tauhara volcano. Average modal analyses are comparable between domes with ca. 18% mineral phenocryst content. Plagioclase is the most abundant phenocryst (ca. 8%) and are separated into two groups. Plagioclase A form oscillatory zoned euhedral to anhedral crystals with diameters ~1.5 mm and plagioclase B form ~0.8 mm euhedral to subhedral crystals with no zoning with the exception of rims. Both groups of plagioclase are chemically similar with An_{23-91}. Orthopyroxene is also present in two populations with orthopyroxene A forming ca. 0.6 mm euhedral to anhedral minerals occurring either as

individual crystals or in clusters with plagioclase A. Orthopyroxene A have En_{47-67}. Orthopyroxene B occur in various modes; large euhedral crystals of ~1.3 mm within orthopyroxene-clinopyroxene-olivine clusters, ~0.8 mm euhedral to subhedral individual crystals and small (~0.3 mm) acicular crystals forming either as reaction coronas around olivine or monomineralic clusters. Orthopyroxene B have En_{69-79}. Clinopyroxene phenocrysts can be divided into two groups, A and B, although both are chemically indistinguishable with ca. $En_{45}Fs_{12}Wo_{43}$. Clinopyroxene A forms monomineralic clusters of crystals ~ 0.2 mm in diameter whereas clinopyroxene B forms individual crystals either ca. 1.5 mm or 0.8 mm in diameter. Hornblende comprises ca. 3% of the rocks with crystals range from anhedral to euhedral with average diameters of 1.2 mm. Quartz is also present, occurring typically as anhedral crystals with abundant fractures. Olivine (Fo_{80-82}) is present in trace amounts in the dacites, forming subhedral to anhedral crystals 0.5 – 2.0 mm in size. Biotite is present in 25% of samples, occurring as subhedral to anhedral crystals ca. 0.4 mm in size.

Table 1.1: Dome averaged modal analyses for dacites from the Tauhara volcano taken from Worthington (1985).

Modal analyses	Western Dome	Central Dome	Hipaua Dome	Trig M Dome	Breached Dome	Main Dome
Groundmass	81.3	81.6	83.4	83.9	80.6	84.2
Plagioclase	8.9	8.5	7.5	7.1	10.8	9.3
Orthopyroxene A	0.1	0.5	0.3	0.3	0.3	0.4
Orthopyroxene B	0.6	0.2	1.1	1.1	1.1	0.9
Clinopyroxene A	1.0	0.7	1.3	0.7	1.5	0.6
Clinopyroxene B	0.9	1.7	1.1	2.0	0.8	2.0
Hornblende	4.9	4.1	3.1	2.5	2.5	0.9
Quartz	1.6	2.2	1.4	1.5	1.3	1.2
Opaques	0.7	0.6	0.7	0.9	1.1	0.5
Biotite	trace	0.1	0.1	0.1	trace	trace
Olivine	trace	n.p.	trace	0.1	trace	n.p.

n.p.: not present.

1.5.4 PETROGENESIS

Marshall (1908) during his general geology investigation of the North Island identified Mt. Tauhara as a hypersthene-dacite, the only “cone” rising above the pumice plain not to be formed of hypersthene-augite-bearing andesite. The first chemical and petrological investigation of the Tauhara volcano was undertaken by Grange (1937). Microscopy of three thin sections from Breached Dome showed the dacite to contain feldspar, quartz, clinopyroxene, orthopyroxene, and hornblende with resorbed cores. The major element chemistry of one sample was used to conclude that Mt Tauhara is “yellowstonose” using the CIPW classification, a group which encompasses most of the world’s dacites.

Detailed petrological work by Lewis (1968b) revealed that the observed phenocryst phases are not in equilibrium, and also not in equilibrium with the groundmass. This is shown by a range in mineral textures and compositions of the main phenocryst phases, such as resorbed quartz rims, resorbed atoll-structured hornblende with varying degrees of oxidation, and bimodal compositions of feldspar (An_{27} and An_{48}). Lewis (1968b) also noted the minor presence of anhedral olivine "xenocrysts" (antecrysts). Major element whole rock data from Lewis (1968b) defined a narrow range in chemical variation for the Tauhara volcano with SiO_2 = 65.8 to 68.0 wt %. This narrow range of compositions with no discrete major element variations suggested to Lewis that the Tauhara volcano was formed from only one magma body and ruled out fractional crystallisation as a governing differentiation process. A lack of xenoliths other than cognate xenoliths found by Lewis (1968b) also apparently ruled out crustal assimilation as the primary process in the generation of the Tauhara dacites. Lewis (1968b) proposed two processes that could have formed the Tauhara volcano; magma mixing between a rhyolitic magma and an olivine-bearing basalt in a ratio of 3:1, and his preferred hypothesis of fusion of dacitic crustal rocks (greywacke) or rocks of more basic composition. The small range in mineralogy and chemistry was attributed to variations in physical parameters such as pressure and temperature and minor amounts of assimilation-fractional crystallisation.

A later study by Reid and Cole (1983) disagreed with these earlier studies. Reid and Cole (1983) used average major and trace element analyses of six samples to place constraints on the genesis of the entire Tauhara volcano. Partial melting, fractional crystallisation and magma mixing models were used to conclude that the Tauhara dacitic magma was generated through partial melting of western basement greywacke of the Waipapa Formation with a minor mafic mixing component. A more detailed study of the Tauhara volcano was carried out by Worthington (1985). Worthington collected 292 samples from the Tauhara volcano and conducted modal and chemical analyses on 115 representative samples. Twenty-one samples were then analysed for whole rock Sr isotopes (Graham and Worthington, 1988). An origin of magma mixing was proposed to account for mineral disequilibrium amongst phenocryst phases and groundmass, bimodal compositions of orthopyroxene (En_{44-51} and En_{69-79}) and plagioclase (An_{23-43} and An_{66-91}) phases, resorption textures and the coupled variations in major element concentrations and Sr isotope ratios. Mixing between rhyolite and various mafic end-members was concluded to be the major process in generating the dacites of the Tauhara volcano.

The mixing mechanisms, nature of the endmembers involved, and timescales and location of the mixing process in assembling this dacite dome complex are the key questions addressed here, using in situ, mineral-specific analytical techniques.

1.6 THESIS OUTLINE

This thesis is structured as follows:

Chapter 1: *Introduction:* A review of the generation of intermediate rocks in subduction zones in relation to the formation of continental crust, with a review of the Taupo Volcanic Zone, and the geology of the Tauhara volcano.

Chapter 2: *Methods:* An outline of the analytical techniques used in this study and an evaluation of data precision and accuracy.

Chapter 3: *Results:* Description of the geochemical results obtained for the Tauhara Dacite Complex including new whole rock trace element data, Sr-Pb isotope ratios, *in situ* mineral major and trace element and Sr-Pb isotopic data.

Chapter 4: *Discussion:* Insights into the magmatic processes responsible for the geochemical variations in the Tauhara volcano and generating the Tauhara dacites and how this compares to other worldwide examples of dacitic volcanoes.

Chapter 5: *Conclusions:* The conclusions reached in this study of how the Tauhara volcano was formed.

Supplementary Information

Appendix 1: Sample list and descriptions.

Appendix 2: EPMA major element data for minerals and melt inclusions.

Appendix 3*:* LA-ICP-MS trace element data for minerals and melt inclusions.

Appendix 4*:* Whole rock major and trace element data.

Appendix 5*:* Sr-Pb isotopic data.

Appendix 6: Thermobarometry, oxybarometry and hygrometry.

Appendix 7: Diffusion modelling.

CHAPTER 2

METHODS

2.1 INTRODUCTION

A range of analytical techniques were employed to determine the chemical and isotopic composition of samples from Tauhara Volcano. Solution inductively coupled plasma mass spectrometry (ICP-MS) was used to determine whole rock trace element concentrations. Mineral *in situ* major element analyses were conducted by electron probe microanalysis (EPMA). Phenocrysts were imaged using backscattered electron imaging for clinopyroxene, orthopyroxene, plagioclase, and Fe-Ti oxides to resolve major element zoning. Cathodoluminescence imaging was used to determine Ti zoning in quartz as well as look for the presence of quartz-hosted melt inclusions. Mineral *in situ* trace element analyses were performed by laser ablation ICP-MS. Sr-Pb isotopic ratios of whole rock, groundmass and mineral separates were determined using multi-collector ICP-MS.

2.2 SAMPLE SELECTION AND PREPARATION

2.2.1 SAMPLE SELECTION

All rock samples used in this study come from the Victoria University of Wellington (VUW), New Zealand collection 19421-19527. This sample suite was collected by Tim Worthington (Worthington, 1985) and was based on outcrop locations and accessibility. Overall, 292 samples in total were collected from 6 domes; Western, Central, Hipaua, Trig M, Breached and Main Domes, as well as associated pyroclastic flows. From these, 115 samples were selected by Worthington for whole rock major and trace element analyses. 33 samples were selected for further study in this thesis based on major element variations, and to be representative of each dome (Figure 2.1). These samples exclude xenoliths. Amongst those, 21 samples were analysed for Sr-Pb isotopes. Six representative samples (one from each dome) have been subjected to detailed *in situ* mineral major and trace element analysis.

2.2.2 ROCK CRUSHING AND MINERAL SEPARATION

Weathered surfaces were removed using a diamond rock saw and the remaining unaltered rock was cut into domino-sized slabs. One slab was used to make thin sections (30 µm thick) for petrography, another to make thick sections (100 µm thick) for detailed mineral major and trace element analysis and 40-50 g of rock chips were pulverised using a Fritsch

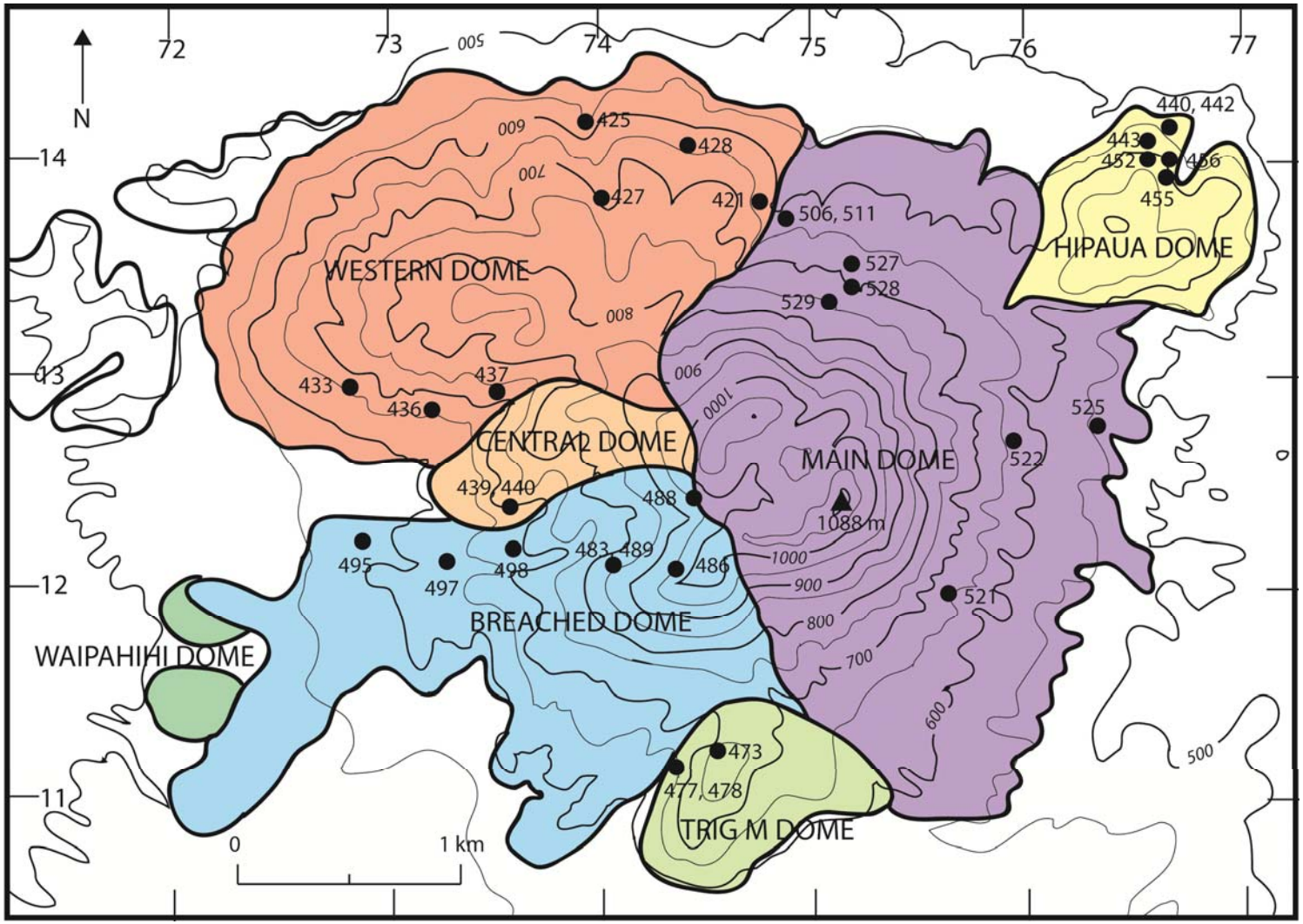

Figure 2.1: Simplified topographic map of Tauhara volcano showing domes and sample locations (Worthington, 1985).

Pulverisette 13 to extract rock chips and crystals ranging from 5 mm to <250 µm in size. Crushed rock was passed through a 250 µm sieve to remove any powder and fine crystal fragments. A strong magnet was passed over the samples to separate magnetite-bearing groundmass from its crystal cargo. Groundmass chips 1-2 mm in size that excluded phenocrysts were then extracted from this separate for isotope analysis. Specific crystal groups were picked under a binocular microscope from the crystal separate, which included: clinopyroxene, amphibole, and small plagioclase (<1 mm) crystals for bulk Pb and Sr isotope analyses; large (>2 mm) plagioclase phenocrysts were picked for single grain Pb and Sr isotope analyses and; whole quartz crystals were picked for cathodoluminescence (CL) imaging. All crystal and rock chip fractions were rinsed with >18.2 MΩ H_2O (MQ) and placed in an ultrasonic tank for 5 min. Each sample was then rinsed three times using MQ and the solution decanted before drying in an oven at 50 °C. Whole quartz crystals were mounted in Epo-tek 301 1LB kit epoxy using 3:1 epoxy resin to hardener and set at 60 °C prior to carbon coating. The quartz grains were orientated so that the C-axis was flat.

2.3 WHOLE ROCK ANALYSES

2.3.1 WHOLE ROCK MAJOR ELEMENT ANALYSES

Whole rock major element concentrations were previously determined using X-ray fluorescence spectrometry on an automated Siemens SRS-1 X-ray Spectrometer at Victoria University of Wellington, New Zealand (VUW) (Worthington, 1985). Sample powders were fused with ammonium nitrate to oxidise all Fe to the ferric state. Multiple fusions were conducted for each sample and the values averaged if totals were acceptable between 99.3-100.3 wt %.

2.3.2 WHOLE ROCK TRACE ELEMENT ANALYSES

Whole rock trace element concentrations were determined by solution ICP-MS at VUW. Samples were introduced using a peristaltic pump into the nebuliser.

REAGENTS

Whole rock powders were digested using Seastar® ultrapure acid (SS) to reduce contamination. Analytical grade (AR) concentrated acids used for beaker cleaning were sub-boiled (SB) distilled at VUW (quartz stills for HNO_3 and Teflon stills for HCl). Millipore® H_2O (MQ) was only used when its resistivity measured > 18.2 MΩ. Concentrated SS and SB acids were diluted by mixing with MQ, checking molarity with a density meter.

BEAKER PREPARATION

Savillex® teflon beakers (23 mL) were used for sample digestions. The beakers were pre-cleaned using a general cleaning procedure as follows. Beakers were soaked for 24 hr in AR-grade 6M HCl followed by 24 hr flux in 7 M HNO_3 on a hotplate at 120 °C. Beakers were then individually fluxed in AR-grade 7M HNO_3 SB for 24 hr. The beakers were rinsed three times using MQ between each step. Following this general cleaning procedure, the beakers were fluxed for 24 hr in 2 mL 7 M HNO_3 SS + 0.2 mL of 29 M HF SS to ensure all trace elements were removed including remnant high field strength elements (Zr, Hf, Nb etc.) and Pb.

DIGESTION

60 to 75 mg of whole rock powders were weighed into beakers, using a Sartorious balance (± 0.01 mg). Digestions were conducted in ultraclean class 10 PicoTrace laminar flow hoods. The samples were first digested in 1 mL of 29 M HF SS with 0.3 mL of 16 M HNO_3 SS and left on a hotplate at 120 °C for 5 days. After allowing the beakers to cool, the acid was evaporated and the sample then nitrified by evaporating in 1 mL of 16 M HNO_3 at 120 °C. The samples were then digested in 4 mL of 6M HCl SS for 24 hr and inspected for solids. If the samples were solid free, the acid was evaporated and the sample nitrified by evaporating in 1 mL of 16 M HNO_3 SS at 120 °C twice before adding 10 mL of 1M HNO_3 SS and leaving on the hotplate for 2 days, allowing the samples to fully dissolve before analysis. If, however, solids were present, the digestion procedure was repeated again from the initial HF-HNO_3 step.

DILUTIONS

Once fully in solution in 10 mL of 1 M HNO_3, samples were diluted using a further 20 mL of 1 M HNO_3 SS to a total of 30 mL solution in pre-cleaned (2% HNO_3 SS for 14 days) 60 mL Nalgene

LDPE bottles to ensure elements remained in solution. A 300 µL aliquot was extracted and diluted with 10 mL of 1% HNO_3 SS in pre-cleaned centrifuge tubes (2% HNO_3) ready for analysis. The samples were weighed at each step of the dilution process to enable the precise calculation of dilution factors of the sample and standards.

TUNING

An Agilent 10 ppb tuning solution containing Li, Co, Y, Ce, and Tl was diluted to 1 ppb for tuning (9 mL 0.5% HNO_3 SS and 1 ml of tuning solution) where analytical conditions such as torch position and carrier gas flow were optimised for sensitivity whilst maintaining low oxide generation. ^{7}Li, ^{55}Co, ^{89}Y, ^{140}Ce, and ^{205}Tl were monitored to achieve the lowest relative standard deviations possible, typically < 4% and to optimise sensitivity. CeO^{+}/Ce was used to monitor oxide generation. Analytical conditions were set such that maximum oxide production was always < 2%. Analytical conditions are listed in Table 2.1.

Signal intensity was measured using an electron multiplier in either pulse (P) or analog (A) counting mode. The pulse counting method of ion concentration is defined by a linear equation in relation to counts per second (CPS) to determine analyte concentrations of 1 ppt - 100 ppb. Element concentrations which yield count rates greater than one million CPS cannot be determined by pulse counting so the analog counting method is applied which is defined by a different linear equation. By switching between pulse and analog counting, both low and high concentrations can be measured during the same scan. P/A factors were calibrated using BHVO-1 and BCR-2 standards for Ca, V, Cr, Ni, Sr, Zr, Mo, Ba, and Ce.

CONCENTRATION ANALYSIS

A typical run consisted of the following sequence: primary standard (BHVO-1), 2 samples, secondary standard (either BCR-2 or BHVO-2), 2 samples and then finishing with another BHVO-1 standard.

Each sample was calibrated to the USGS rock standard BHVO-1, which was digested and analysed under the same conditions as the samples. ^{43}Ca was used as an internal calibration using CaO wt% previously determined by XRF (Worthington, 1985) or reference values for standards. For every element, CPS values were corrected for background levels by averaging 30 s of background counts and deducting this from a 60 s average of sample counts. The trace element concentration of element X (C^{X}) was then determined using the following equations:

1) $$X_1^{sam} = G_X^{std} \times \left(CPS_X^{sam}/CPS_X^{std}\right) \times \left(Dil^{std}/Dil^{sam}\right)$$

2) $$C^X = X_1^{sam} \times \left(CaO_{XRF}^{sam}/Ca_1^{sam}\right)$$

X_1^{sam}, Ca_1^{sam} = primary standard BHVO-1 and dilution corrected element X and Ca respectively.

G_X^{std} = Georem reference value for BHVO-1 standard of element X

CPS_X^{sam}, CPS_X^{std} = background corrected counts per second of element X in the sample/standard BHVO-1

Dil^{sam}, Dil^{std} = dilution factors for the samples and standard BHVO-1 respectively

$CaO_{XRF}^{sam}, CaO_{Ref}^{std},$ = pre-existing CaO values determined by XRF (Worthington, 1985) and standard reference values respectively.

Due to the lack of certified Georem values for certain trace elements, preferred standard values were compiled from Georem preferred values (http://georem.mpch-mainz.gwdg.de) and Baker et al. (2002). The list of chosen values and sources is given in Table 2.2.

PRECISION AND ACCURACY OF TRACE ELEMENT DATA

Repeated digestions and dilutions of the USGS standards BHVO-2 and BCR-2 were used to assess data accuracy and reproducibility (precision). A summary of secondary standard data is provided in Table 2.3 and Table 2.4. Elements are typically accurate to within ±5% for both secondary standards, with the exception of Pb and Mo. Mo is accurate to -17% in BHVO-2 only, however this value for BHVO-2 is not well constrained. Accuracy for Pb is +14% and +10% for BHVO-2 and BCR-2, respectively. Eu and Zr concentrations were determined by monitoring two isotopes (^{90}Zr, ^{91}Zr, ^{151}Eu, ^{153}Eu). Zr data are identical when calculated using either ^{90}Zr or ^{91}Zr, however Eu data are significantly different with ^{153}Eu concentrations systematically higher than ^{151}Eu. This is due to interference of ^{137}Ba + ^{16}O which attributes to mass 153 and hence provides lower ^{151}Eu/^{153}Eu ratios between 0.88-0.96 (Table 2.5).

Table 2.1 ICP-MS instrumental and analytical conditions.

ICP-MS system	Agilent 7500CS octopole
Acquisition mode	Peak hopping
Detection mode	Pulse and analogue counting (mostly pulse)
Standards and Calibration	
Calibration standard	BHVO-1
Secondary standard	BHVO-2, BCR-2
Internal Standard	^{43}Ca
Method	
Background acquisition	90 s
Sample/standard acquisition	180 s
Washout time	210 s
Measured isotopes and integration times	10 ms: ^{43}Ca, ^{45}Sc, ^{53}Cr, ^{51}V, ^{60}Ni, ^{63}Cu, ^{66}Zn, ^{71}Ga, ^{86}Sr, ^{89}Y, ^{90}Zr, ^{91}Zr, ^{93}Nb, ^{137}Ba, ^{139}La, ^{140}Ce, ^{146}Nd 20 ms: ^{85}Rb, ^{141}Pr, ^{147}Sm, ^{157}Gd, ^{163}Dy 50 ms: ^{95}Mo, ^{133}Cs, ^{151}Eu, ^{153}Eu, ^{159}Tb, ^{165}Ho, ^{166}Er, ^{169}Tm, ^{172}Yb, ^{175}Lu, ^{178}Hf, ^{181}Ta, ^{208}Pb, ^{232}Th, ^{238}U
Tuning	
Tuning standard	Agilent 1 ppb solution (Li, Co, Y, Ce, Tl)
Monitored isotopes during tuning	^{7}Li, ^{89}Y, ^{140}Ce, ^{205}Tl (% RSD for each isotope typically <4%)
Calibration standard	BHVO-1
Monitored isotopes during calibration	^{43}Ca, ^{60}Ni, ^{86}Sr, ^{89}Y, ^{137}Ba, ^{140}Ce, ^{208}Pb, ^{232}Th (% RSD for each isotope typically <4%)
Background	^{43}Ca typically < 2000 cps, always <3000 cps (% of BHVO-1 cps = < 0.1%)
Oxides	CeO^{+}/Ce^{+}: 1 ppb solution ≤ 2%
Carrier gas (Ar)	1.07-1.13 L/min
Makeup gas (Ar)	0 L/min
RF power	1500 W
RF matching	1.68-1.75 V
Sample depth (z)	7-8 mm

Table 2.2: Preferred trace element concentrations of the USGS rock standards.

Element	BHVO-1		BHVO-2		BCR-2	
Sc (ppm)	31.0	G	32.0	G	33.0	G
V	318	G	317	G	416	G
Cr	287	G	280	G	16.0	1
Ni	118	G	119	G	13.0	1
Cu	137	G	127	G	21.0	G
Zn	106	G	103	G	130	G
Ga	21.0	G	22.0	G	22.0	1
Rb	9.19	G	9.11	G	46.9	G
Sr	396	G	396	G	340	G
Y	26.0	G	26.0	G	36.0	1
Zr	174	G	172	G	189	1
Nb	18.6	G	18.1	G	13.0	G
Mo	1.00	G	4.00	G	250	G
Cs	0.090	G	0.100	G	1.10	G
Ba	133	G	131	G	677	G
La	15.5	D	15.2	G	25.1	D
Ce	38.2	D	37.5	G	53.3	D
Pr	5.41	D	5.35	G	6.76	D
Nd	24.7	D	24.5	G	28.7	D
Sm	6.14	D	6.07	G	6.58	D
Eu	2.07	D	2.07	G	1.94	D
Gd	6.29	D	6.24	G	6.73	D
Tb	0.960	G	0.920	G	1.07	G
Dy	5.36	D	5.31	G	6.44	D
Ho	0.980	G	0.980	G	1.28	G
Er	2.57	D	2.54	G	3.71	D
Tm	0.330	G	0.330	G	0.540	G
Yb	1.98	D	2.00	G	3.34	D
Lu	0.279	D	0.274	G	0.499	D
Hf	4.51	D	4.36	G	4.97	D
Ta	1.21	G	1.14	G	0.8	1
Pb	2.40	G	1.60	G	11.0	G
Th	1.23	G	1.22	G	5.90	1
U	0.409	G	0.403	G	1.69	G

G: Georem preferred values.

D: Danish Lithospheric Centre ID-MC-ICP-MS data (Baker et al., 2002).

1: Lack of data for BCR-2, so better constrained BCR-1 values were used for these elements.

Table 2.3: ICP-MS trace element data of repeat digestions and dilutions of USGS rock standard BHVO-2.

Digestion	A	B	C	C	C	D	D	E	F	Mean	Georem	% Offset	2 s.d.	% 2 s.d.
Dilution	1	1	1	2	3	1	2	1	1					
Sc (ppm)	32.3	30.8	30.6	31.6	31.1	31.2	31.0	31.0	30.4	31.1	32.0	-2.8	1.1	3.6
V	323	314	319	321	319	318	319	322	315	319	317	+0.6	6	1.9
Cr	289	288	294	291	290	299	289	296	293	292	280	+4.3	7	2.6
Ni	116	118	118	115	114	119	119	119	118	117	119	-1.3	4	3.4
Cu	129	132	132	127	129	132	128	130	128	130	127	+2.0	4	2.8
Zn	103	107	109	103	104	107	106	106	105	105	103	+2.3	4	4.0
Ga	20.9	21.0	21.1	20.6	20.7	21.4	20.8	21.0	20.8	20.9	22.0	-4.9	0.5	2.2
Rb	8.88	9.18	9.32	8.86	8.89	9.37	9.00	9.17	9.01	9.07	9.11	-0.4	0.39	4.3
Sr	388	391	409	391	394	402	399	404	386	396	396	+0.0	16	4.1
Y	25.7	25.6	26.3	25.5	25.7	26.6	26.1	26.3	25.6	25.9	26.0	-0.3	0.8	3.0
Zr	171	171	177	173	176	181	178	182	170	176	172	+2.1	9	5.2
Nb	18.0	18.3	18.5	18.1	18.2	19.1	18.5	18.8	18.1	18.4	18.1	+1.7	0.7	3.8
Mo	4.18	2.62	4.41	3.03	3.03	3.19	3.15	3.11	3.18	3.32	4.00	-16.9	1.16	35.0
Cs	0.088	0.090	0.098	0.088	0.089	0.093	0.090	0.085	0.094	0.091	0.100	-9.3	0.008	8.5
Ba	129	130	137	130	132	137	135	134	132	133	131	+1.4	6	4.4
La	15.0	15.1	15.9	15.1	15.3	15.9	15.5	15.5	15.0	15.4	15.2	+1.1	0.7	4.7
Ce	36.9	37.3	39.1	36.9	37.8	39.3	37.8	38.3	37.2	37.8	37.5	+0.9	1.8	4.7
Pr	5.18	5.27	5.58	5.25	5.35	5.54	5.42	5.38	5.31	5.37	5.35	+0.3	0.26	4.9
Nd	23.6	24.2	25.4	24.1	24.5	25.1	24.9	24.9	24.0	24.5	24.5	+0.1	1.2	4.7
Sm	5.90	5.97	6.35	5.96	6.13	6.25	6.09	6.13	6.06	6.09	6.07	+0.4	0.29	4.7
Eu	1.99	2.01	2.12	2.01	2.04	2.12	2.08	2.08	2.00	2.05	2.07	-1.0	0.10	5.0
Gd	6.11	6.11	6.35	6.07	6.29	6.53	6.37	6.24	6.15	6.25	6.24	+0.1	0.31	4.9
Tb	0.927	0.932	0.994	0.936	0.956	1.00	0.964	0.979	0.944	0.959	0.920	+4.2	0.053	5.6
Dy	5.17	5.22	5.56	5.22	5.28	5.54	5.40	5.44	5.26	5.34	5.31	+0.6	0.29	5.4
Ho	0.940	0.955	1.02	0.949	0.979	1.02	0.984	0.983	0.953	0.975	0.980	-0.5	0.058	5.9
Er	2.47	2.49	2.68	2.51	2.56	2.63	2.60	2.59	2.54	2.56	2.54	+0.9	0.14	5.4
Tm	0.320	0.320	0.343	0.319	0.326	0.343	0.334	0.328	0.333	0.330	0.330	-0.1	0.018	5.6
Yb	1.89	1.93	2.05	1.92	1.97	2.05	2.03	1.98	1.94	1.97	2.00	-1.3	0.12	6.1
Lu	0.271	0.268	0.285	0.268	0.283	0.284	0.286	0.280	0.274	0.277	0.274	+1.3	0.015	5.5
Hf	4.31	4.36	4.67	4.46	4.58	4.80	4.68	4.72	4.42	4.56	4.36	+4.6	0.35	7.6
Ta	1.15	1.17	1.25	1.16	1.20	1.24	1.22	1.23	1.18	1.20	1.14	+5.2	0.07	6.1
Pb	1.57	2.02	1.80	1.84	1.91	1.96	1.85	1.75	1.73	1.83	1.60	+14.1	0.27	14.9
Th	1.20	1.20	1.31	1.20	1.23	1.28	1.23	1.26	1.19	1.23	1.22	+1.2	0.09	6.9
U	0.386	0.394	0.429	0.382	0.406	0.421	0.406	0.416	0.403	0.405	0.403	+0.4	0.032	7.8

NB: Each letter represents a separate digestions and numbers represent different dilutions of the same digestion.

Table 2.4: ICP-MS trace element of repeat digestions and dilutions of USGS rock standard BCR-2.

Digestion	A	B	B	C	C	D	Mean	Preferred	% Offset	2 s.d.	% 2 s.d.
Dilution	1	1	2	1	2	1					
Sc (ppm)	32.7	32.4	32.7	32.9	32.2	33.3	32.7	33.0	-0.9	0.7	2.2
V	408	416	414	413	423	423	416	416	+0.1	12	2.8
Cr	15.1	15.5	15.6	14.8	14.9	15.0	15.1	16.0	-5.4	0.6	4.2
Ni	12.0	11.9	11.8	12.3	11.6	12.6	12.0	13.0	-7.4	0.7	5.7
Cu	21.5	21.0	20.3	20.1	20.5	19.0	20.4	21.0	-2.9	1.6	8.0
Zn	132	132	132	133	135	134	133	130	+2.3	2	1.7
Ga	-	21.3	21.4	21.1	21.6	21.6	21.4	22.0	-2.7	0.5	2.1
Rb	46.3	47.9	46.5	45.8	46.0	48.0	46.7	46.9	-0.4	1.9	4.2
Sr	347	343	340	333	339	344	341	340	+0.3	10	2.8
Y	35.5	35.2	35.1	34.9	35.1	36.0	35.3	36.0	-1.9	0.8	2.2
Zr	190	190	190	190	193	192	191	189	+0.9	3	1.5
Nb	12.4	12.4	12.3	12.1	12.4	12.6	12.4	13.0	-5.0	0.3	2.5
Mo	241	236	238	239	243	230	238	250	-4.8	9	3.9
Cs	1.06	1.11	1.09	1.06	1.06	1.12	1.08	1.10	-1.5	0.05	4.7
Ba	670	677	665	665	691	694	677	677	+0.0	26	3.8
La	24.8	25.0	24.8	24.5	24.9	25.8	25.0	25.1	-0.6	0.89	3.6
Ce	53.0	53.3	52.6	51.3	53.2	54.1	52.9	53.3	-0.8	1.9	3.6
Pr	6.77	6.82	6.78	6.63	6.74	6.92	6.78	6.76	+0.3	0.19	2.8
Nd	28.6	28.6	28.5	27.6	28.3	29.4	28.5	28.7	-0.7	1.2	4.2
Sm	6.49	6.55	6.60	6.28	6.66	6.71	6.55	6.58	-0.5	0.30	4.6
Eu	1.97	1.99	1.97	1.94	2.05	2.03	1.99	1.94	+2.3	0.08	4.1
Gd	6.77	6.86	6.80	6.76	6.96	6.94	6.85	6.73	+1.8	0.17	2.5
Tb	1.08	1.08	1.06	1.04	1.08	1.10	1.07	1.07	+0.2	0.04	3.8
Dy	6.33	6.39	6.41	6.20	6.44	6.49	6.38	6.44	-1.0	0.20	3.1
Ho	1.27	1.28	1.27	1.24	1.28	1.30	1.27	1.28	-0.5	0.04	3.3
Er	3.65	3.66	3.61	3.56	3.70	3.74	3.65	3.71	-1.5	0.13	3.4
Tm	0.511	0.510	0.512	0.497	0.510	0.527	0.511	0.540	-5.3	0.019	3.8
Yb	3.30	3.33	3.29	3.21	3.32	3.38	3.31	3.34	-1.0	0.11	3.3
Lu	0.501	0.505	0.489	0.493	0.510	0.504	0.500	0.499	+0.2	0.016	3.1
Hf	4.99	5.07	5.03	4.95	5.12	5.14	5.05	4.97	+1.6	0.15	2.9
Ta	0.796	0.808	0.798	0.771	0.799	0.831	0.801	0.810	-1.2	0.038	4.8
Pb	12.1	12.5	12.3	12.7	13.2	9.43	12.0	11.0	+9.4	2.7	22.2
Th	5.80	5.99	5.93	5.75	5.98	5.94	5.90	5.90	+0.0	0.20	3.3
U	1.59	1.62	1.61	1.57	1.63	1.71	1.62	1.69	-3.9	0.09	5.6

NB: Each letter represents a separate digestions and numbers represent different dilutions of the same digestion.

Table 2.5: Zr and Eu concentration data calculated using two different isotopes of each of these elements.

	421	**425**	**427**	**428**	**433**	**436**	**437**	**439**	**440**	**442**	**443**
^{90}**Zr**	112	75.7	83.3	107	83.8	97.7	80.2	92.9	62.6	100.3	95.2
^{91}**Zr**	111	84.2	83.9	106	82.0	96.8	78.3	90.7	60.8	95.8	95.7
^{90}***Zr/^{91}Zr***	*1.01*	*0.90*	*0.99*	*1.00*	*1.02*	*1.01*	*1.02*	*1.02*	*1.03*	*1.05*	*0.99*
^{151}**Eu**	1.00	0.762	0.867	0.935	0.701	0.885	0.837	0.697	0.711	0.784	0.765
^{153}**Eu**	1.10	0.821	0.920	1.01	0.755	0.980	0.946	0.741	0.758	0.848	0.832
^{151}***Eu/^{153}Eu***	*0.91*	*0.93*	*0.94*	*0.93*	*0.93*	*0.90*	*0.88*	*0.94*	*0.94*	*0.92*	*0.92*
	444	**452**	**455**	**456**	**473**	**477**	**478**	**483**	**486**	**488**	**489**
^{90}**Zr**	58.1	97.5	84.8	56.4	85.4	81.7	79.3	75.5	83.2	85.3	86.0
^{91}**Zr**	58.2	96.5	83.3	54.7	84.9	81.3	78.3	74.5	83.3	85.1	85.9
^{90}***Zr/^{91}Zr***	*1.00*	*1.01*	*1.02*	*1.03*	*1.01*	*1.01*	*1.01*	*1.01*	*1.00*	*1.00*	*1.00*
^{151}**Eu**	0.558	0.797	0.670	0.745	0.809	0.788	0.768	0.788	0.728	0.828	0.723
^{153}**Eu**	0.598	0.893	0.707	0.798	0.851	0.845	0.811	0.854	0.785	0.901	0.776
^{151}***Eu/^{153}Eu***	*0.93*	*0.89*	*0.95*	*0.93*	*0.95*	*0.93*	*0.95*	*0.92*	*0.93*	*0.92*	*0.93*
	495	**497**	**498**	**506**	**511**	**521**	**522**	**525**	**527**	**528**	**529**
^{90}**Zr**	92.4	114	106	100	101	104	107	98.3	68.4	97.0	90.9
^{91}**Zr**	92.2	111	105	100	98.6	101	105	97.2	67.9	95.3	89.5
^{90}***Zr/^{91}Zr***	*1.00*	*1.02*	*1.01*	*1.01*	*1.02*	*1.03*	*1.01*	*1.01*	*1.01*	*1.02*	*1.02*
^{151}**Eu**	0.818	0.918	0.814	0.785	0.793	0.810	0.826	0.795	0.659	0.899	0.83
^{153}**Eu**	0.893	1.00	0.868	0.861	0.840	0.845	0.879	0.883	0.709	0.985	0.88
^{151}***Eu/^{153}Eu***	*0.92*	*0.92*	*0.94*	*0.91*	*0.94*	*0.96*	*0.94*	*0.90*	*0.93*	*0.91*	*0.94*

2.4 MINERAL *IN SITU* ANALYSES

Two different electron probe microanalysers (EPMA) were used during the course of this study, both at VUW. The JEOL superprobe JXA-8230 was used for back scattered electron imaging and all major element analyses, whereas a JEOL 733 superprobe was used for cathodoluminescence imaging. All analyses were performed on carbon coated 100 µm thick thin sections.

2.4.1 IMAGING

BACKSCATTERED ELECTRON IMAGING

Backscattered electron imaging (BSE) was conducted using an accelerating voltage of 15 kV. A backscatter electron detector measures the average atomic number at the electron beam focus point. A brighter point is equal to a higher average atomic mass of the mineral and can therefore reveal major element zoning in phenocrysts. BSE imaging was used to examine zoning of different elements in various crystals. These include Fe-Mg zoning in clinopyroxene, orthopyroxene, and hornblende and Ca-Na zoning in plagioclase.

CATHODOLUMINESCENCE IMAGING

Cathodoluminescence imaging (CL) of quartz crystals was conducted using a photomultiplier with an accelerating voltage of 15 kV and a 12 nA beam current. A cathode gun is used to bombard the sample with a high energy electron beam which produces short lived phosphorescence. The degree of luminescence generated is dependent on variations such as trace element impurities in crystal structures. Ti concentration in quartz is one such impurity where an increase in luminescence correlates to an increase in Ti (Wark and Spear, 2005). Images were scanned and saved at highest resolution for diffusion modelling of Ti in quartz.

2.4.2 EPMA *IN SITU* ANALYSES

Mineral major element concentrations were measured using five wavelength dispersive spectrometers and determined using the ZAF correction method. The ZAF method corrects for the matrix effects of mass number (Z), absorbance (A) and fluorescence (F). In order to reduce matrix effects the EPMA is calibrated using homogeneous natural mineral phases of similar composition to the minerals being analysed. The utilised mineral standards are listed in Table 2.6. For elements with <1 wt% concentrations in the standard minerals, the element was calibrated on a synthetic oxide standard. Calibration analysis consisted of 60 s on-peak and a 30 s background measurement per element on both sides of the peak. Minerals, including plagioclase, clinopyroxene, orthopyroxene, hornblende and oxides, were measured using a focused electron beam with a current of 12 nA and an accelerating voltage of 15 kV. For synthetic and natural glass analyses, the beam was defocused to a diameter of 10 µm and with an 8 nA current to reduce the release of volatiles and damage to the glass matrix. During analysis, peaks were measured for 30 s and background for 15 s. Alkali elements such as Na and K were measured first to minimise volatile loss.

Standards used for calibration were analysed three to five times at the beginning of each analytical run and measurements averaged. Correction factors were calculated using the published values of the standards and were applied to the samples analysed in the following run. The calibrated standards were run as unknown secondary standards throughout the runs to monitor precision, accuracy and drift of the spectrometers. EPMA precision and accuracy for the mineral and glass standards are shown in Table 2.7.

PRECISION AND ACCURACY OF EPMA DATA

Repeat analyses of the calibrated standards are typically accurate to within ±5 % with precision typically < 5 wt % for oxides > 1 wt % in the standards. When Cr and Mn concentrations are low (< 1 wt %) they are susceptible to fluorescence and absorbance interferences which results in offset peak counts and greater standard errors. Cr and Mn have therefore also been measured using LA-ICP-MS where higher precision and accuracy can be attained.

Table 2.6: EPMA calibration and secondary standards.

Mineral	Standard
Clinopyroxene	Kakanui Augite (USNM 122142) [2,3]
Orthopyroxene	Hypersthene, Johnstown meteorite (USNM 746) [2]
Hornblende	Engels Amphibole[1]
Plagioclase	Plagioclase (Labradorite) Lake County, OR (NMNH 96189) [2]
Oxides	Ilmenite, Ilmenite Mountains, USSR (NMNH 96189) [2]
Glass	VG-A99 Basaltic Glass (USNM 113498/1) [2]

1: Ingamells (1980) 2: Jarosewich et al. (1980) 3: Klügel et al. (2005).

Table 2.7: Precision and accuracy of EPMA data for secondary standards.

ENGELS AMPHIBOLE (n = 17)

	Reference	Mean	% Offset	2 s.d.	% 2 s.d.
SiO_2 (wt %)	42.14	42.30	+0.4	0.47	1.1
TiO_2	0.94	0.93	- 1.0	0.07	7.5
Al_2O_3	12.09	12.16	+ 0.6	0.29	2.4
FeO	19.05	18.96	- 0.5	0.40	2.1
MnO	0.63	0.64	+ 1.5	0.05	7.7
MgO	8.67	8.74	+ 0.8	0.18	2.1
CaO	11.56	11.56	0.0	0.23	2.0
Na_2O	1.63	1.66	+ 1.6	0.12	7.1
K_2O	0.91	0.89	- 2.1	0.05	5.4
Total	97.62	97.83			

KAKANUI AUGITE (n = 11)

	Reference	Mean	% Offset	2 s.d.	% 2 s.d.
SiO_2	50.73	50.57	- 0.3	0.45	0.9
TiO_2	0.74	0.73	- 1.6	0.03	4.6
Al_2O_3	8.73	8.63	- 1.1	0.23	2.7
Cr_2O_3	0.15	0.17	+ 14.5	0.04	25.3
FeO	6.34	6.29	- 0.3	0.36	5.7
MnO	0.13	0.12	-10.0	0.03	25.6
MgO	16.65	16.62	- 0.2	0.29	1.7
CaO	15.82	15.88	+ 0.9	0.17	1.1
Na_2O	1.27	1.25	- 1.2	0.24	19.2
Total	100.39	101.21			

n.d.: Not determined.

Table 2.7 *(continued)*: Precision and accuracy of EPMA data for secondary standards.

ILMENITE (n = 12)

	Reference	Mean	% Offset	2 s.d.	% 2 s.d.
SiO_2	n.d.	0.01		0.02	155
TiO_2	45.7	45.74	+ 0.1	0.36	0.8
Al_2O_3	n.d.	0.02		0.02	124
FeO	46.5	46.34	- 0.3	1.21	2.6
MnO	4.77	4.75	- 0.3	0.21	4.4
MgO	0.31	0.32	+ 4.5	0.03	9.6
Total	97.28	97.20			

HYPERSTHENE (n = 9)

	Reference	Mean	% Offset	2 s.d.	% 2 s.d.
SiO_2	54.09	54.14	+ 0.1	0.73	1.3
TiO_2	0.16	0.14	- 11.1	0.04	25.9
Al_2O_3	1.23	1.21	- 1.5	0.35	28.9
Cr_2O_3	0.75	0.96	+ 28.0	0.41	42.6
FeO	15.22	15.25	+ 0.2	1.01	6.6
MnO	0.49	0.40	-18.0	0.12	30.9
MgO	26.79	26.85	+ 0.2	1.09	4.1
CaO	1.52	1.46	- 4.2	0.17	12.0
Na_2O	n.d.	0.02		0.02	133
Total	100.25	99.89			

PLAGIOCLASE (n = 22)

	Reference	Mean	% Offset	2 s.d.	% 2 s.d.
SiO_2	51.25	51.28	+ 0.1	1.14	2.2
TiO_2	0.05	0.06	+ 13.1	0.04	78.5
Al_2O_3	30.91	30.90	- 0.02	0.52	1.7
FeO	0.46	0.46	- 0.3	0.11	23.3
MgO	0.14	0.15	+ 4.6	0.03	21.0
Na_2O	26.79	26.85	+ 0.2	1.09	4.1
CaO	13.64	13.62	- 0.2	0.18	1.3
K_2O	0.18	0.19	+ 2.8	0.03	15.6
Total	100.08	100.09			

VG-A99 (n = 6)

	Reference	Mean	% Offset	2 s.d.	% 2 s.d.
SiO_2	51.15	51.12	- 0.1	0.85	1.7
TiO_2	4.11	4.14	+ 0.8	0.04	0.9
Al_2O_3	12.38	12.42	+ 0.3	0.25	2.0
FeO	13.35	13.28	- 0.5	0.51	3.8
MnO	0.20	0.21	+ 3.8	0.04	19.9
MgO	5.07	5.03	- 0.8	0.06	1.3
CaO	9.26	9.28	+ 0.2	0.05	0.5
Na_2O	2.68	2.64	- 1.5	0.12	4.5
K_2O	0.83	0.84	+ 1.1	0.06	5.3
Total	99.02	99.00			

2.5 LASER ABLATION ICP-MS TRACE ELEMENT ANALYSIS

2.5.1 SAMPLE PREPARATION

To prepare thick sections for laser ablation, the carbon coating from previous EPMA analyses was removed using a 1 µm diamond polish and methanol. The slides were then cut into half mount sections to fit in the ablation holder using a small slow-speed diamond saw. The cuts were oriented to preserve the phenocrysts previously measured by EPMA analyses.

2.5.2 LASER ABLATION

Mineral trace element concentrations were analysed by laser ablation (LA)-ICP-MS at VUW. The VUW LA-ICP-MS system comprises of a solid state New Wave deep ultra-violet (193 nm) laser ablation system coupled to an Agilent 7500 cs ICP-MS. Helium is used to carry the ablation material to the plasma source of the ICP-MS. Typical analysis conditions are given in Table 2.8. P/A factors were measured for the isotopes ^{24}Mg, ^{29}Si and ^{55}Mn for clinopyroxene and hornblende, and ^{29}Si for plagioclase and melt inclusions.

2.5.3 CONCENTRATION CALCULATIONS

Trace element abundances are calculated using the same principles as for solution ICP-MS analyses (section 2.3.2) where each analysis is bracketed by USGS glass standards, in this case BCR-2G and NIST612. BCR-2G was used as a primary standard for clinopyroxene and amphibole measurements, whereas NIST612 was used for plagioclase and melt inclusion analyses. A typical run consisted of the sequence: standard, 5 samples, standard. This sequence allows for the middle primary standard to be analysed as a secondary standard when calculated as an unknown. Secondary standard analyses for BCR-2G and NIST612 are presented in Tables 2.9 and 2.10, respectively. Element concentrations were typically accurate to within ±5% for BCR-2G and 2-3% for NIST612. ^{43}Ca was used as an internal standard using CaO wt % previously determined by EPMA for clinopyroxene, amphibole and plagioclase phenocrysts whereas ^{29}Si was used as the internal element standard for melt inclusions.

Trace element concentrations were obtained using similar equations to that for solution ICP-MS data reduction, without the dilution correction. Background corrections were applied to each sample signal. CPS for every element were graphed against the acquisition time and outliers from each plot were deleted from the data. The background-corrected and screened CPS were averaged before applying the following equations:

3) $$X_1^{sam} = G_X^{std} \times \left(CPS_X^{sam}/CPS_X^{std}\right)$$

4) $$C^X = X_1^{sam} \times \left(CaO_{EPMA}^{sam}/Ca_1^{sam}\right)$$

X_1^{sam}, Ca_1^{sam} = Concentration of element X and Ca in the sample respectively.

G_X^{std} = Standard Georem reference concentration value for element X.

CPS_X^{sam}, CPS_X^{std} = background and outlier corrected CPS of element X in the sample and standard.

CaO_{EPMA}^{sam} = sample CaO values determined by EPMA.

2.6 ISOTOPE MEASUREMENTS

All sample digestions and chemical separations were conducted in ultraclean class 10 PicoTrace laminar flow hoods in the Class 10 clean lab at VUW. Pb and Sr were separated from the same sample digestion with Pb separated first, and Sr then separated from the remaining sample.

2.6.1 REAGENTS

Seastar® ultrapure acid (SS) was used for Pb isotope digestion, chemical separation and dilutions for analyses to minimise blanks. For Sr chemistry, however, SB acids were used with the exception of HF where Seastar® acid was used in the initial digestion step. A density meter was used to check molarity of the acids.

2.6.2 BEAKER PREPARATION

Teflon beakers (7 mL) were cleaned using the following general cleaning procedure. Beakers were soaked for 24 hr in AR-grade 6M HCl followed by 24 hr in AR-grade 7 M HNO_3 on a hotplate at 120 °C. Beakers were then individually fluxed in 7M HNO_3 SB for 24 hr. The beakers were rinsed 3 times in MQ between each acid step. This general cleaning procedure is sufficient for Sr isotope chemistry. However, beakers used for Pb isotope chemistry underwent

additional cleaning steps consisting of 24 hr with 7M HNO_3 SS at 120 °C, followed by 6M HCl SS, and were stored with 6 M HCl SS until used.

Table 2.8: LA-ICP-MS instrumental and analytical conditions.

Laser Ablation	
Laser Ablation System	New Wave 193 nm (deep UV) solid state laser
Ablation Mode	Static spot analyses
Spot size	20 or 35 µm
Repetition rate	5 Hz
Laser Power	65%
ICP-MS	
ICP-MS system	Agilent 7500CS octopole
Acquisition mode	Peak hopping
Detection mode	Pulse and analogue counting (mostly pulse)
Standards and Calibration	
Calibration standard	BCR-2G, NIST612
Internal standard	^{43}Ca or ^{29}Si
Method	
Background acquisition	60 s
Sample/standard acquisition	60 s
Washout time	90 s
Measured isotopes and integration times	
Clinopyroxene and hornblende:	10 ms: ^{7}Li, ^{11}B, ^{24}Mg, ^{29}Si, ^{43}Ca, ^{45}Sc, ^{47}Ti, ^{51}V, ^{53}Cr, ^{55}Mn, ^{60}Ni, ^{63}Cu, ^{66}Zn, ^{85}Rb, ^{88}Sr, ^{89}Y, ^{90}Zr, ^{93}Nb, ^{133}Cs, ^{137}Ba, ^{139}La, ^{140}Ce, ^{141}Pr, ^{146}Nd, ^{147}Sm, ^{153}Eu, ^{157}Gd, ^{159}Tb, ^{163}Dy, ^{165}Ho, ^{166}Er, ^{169}Tm, ^{172}Yb, ^{175}Lu, ^{178}Hf, ^{181}Ta, ^{182}W, ^{208}Pb, ^{232}Th, ^{238}U
Plagioclase:	10 ms: ^{29}Si, ^{43}Ca, ^{88}Sr, ^{137}Ba, ^{138}Ba 20 ms: ^{7}Li, ^{24}Mg, ^{25}Mg, ^{139}La, ^{140}Ce 50 ms: ^{85}Rb, ^{89}Y, ^{133}Cs, ^{141}Pr, ^{146}Nd, ^{147}Sm, ^{153}Eu, ^{157}Gd, ^{208}Pb
Melt inclusions:	10 ms: : ^{7}Li, ^{11}B, ^{24}Mg, ^{29}Si, ^{43}Ca, ^{45}Sc, ^{51}V, ^{53}Cr, ^{55}Mn, ^{60}Ni, ^{63}Cu, ^{66}Zn, ^{85}Rb, ^{88}Sr, ^{89}Y, ^{90}Zr, ^{93}Nb, ^{137}Ba, ^{139}La, ^{140}Ce, ^{141}Pr, 20 ms: ^{47}Ti, ^{133}Cs, ^{146}Nd, ^{147}Sm, ^{153}Eu, ^{157}Gd, ^{159}Tb, ^{163}Dy, ^{165}Ho, ^{166}Er, ^{169}Tm, ^{172}Yb, ^{175}Lu, ^{178}Hf, ^{181}Ta, ^{182}W, ^{208}Pb, ^{232}Th, ^{238}U
Tuning	
Tuning standard	BCR-2G, NIST 612
Ablation Mode	Rastering (2 µm/s) beneath a 50 µm spot
Monitored isotopes during tuning	^{7}Li, ^{24}Mg, ^{29}Si, ^{43}Ca, ^{88}Sr, ^{138}Ba, ^{208}Pb (% RSD for each isotope typically <5%, always <9%)
Background	^{43}Ca typically < 200 cps, always <300
Oxides	ThO^{+}/Th^{+}: typically < 0.5%, always <0.8%
Carrier gas (Ar)	0.83 L/min
Ablation gas (He)	85%
RF power	1500 W
RF matching	1.68 V
Sample depth (z)	3.5 mm

Table 2.9: LA-ICP-MS trace element data for the glass standard BCR-2G.

Run	1	2	3	4	5	6	7	8	9	10	11	Average	Georem	% Offset	2 s.d.	% 2 s.d.
Li (ppm)	8.68	9.01	9.07	9.08	9.16	9.73	8.58	8.90	8.80	8.37	9.39	8.98	9.00	-0.2	0.76	8.4
B	5.71	8.86	8.30	5.12	7.05	5.03	7.76	5.49	6.55	5.98	5.69	6.97	6.00	+8.4	2.63	40.5
Mg	3.55	3.51	3.50	3.50	3.49	3.63	3.59	3.68	3.53	3.54	3.63	3.56	3.56	0.0	0.13	3.5
Si	53.0	53.4	53.8	53.7	53.1	55.2	54.9	55.9	53.8	55.1	55.1	54.3	54.4	-0.2	2.0	3.6
Sc	31.5	31.2	33.7	31.4	31.4	34.5	31.7	34.8	33.7	33.3	33.8	32.8	33.0	-0.6	2.8	8.4
Ti	2.30	2.27	2.22	2.26	2.23	2.33	2.26	2.35	2.28	2.19	2.32	2.27	2.27	+0.2	0.09	4.1
V	423	420	420	420	417	436	425	439	418	429	435	425	425	+0.1	16	3.7
Cr	18.7	18.0	13.0	15.8	15.9	17.1	13.9	17.2	19.0	12.0	16.8	16.1	17.0	-5.1	4.6	28.7
Mn	0.189	0.189	0.189	0.188	0.188	0.193	0.191	0.192	0.189	0.190	0.192	0.190	0.190	0.0	0.003	1.8
Ni	12.2	12.6	14.1	14.6	12.5	12.2	12.9	13.0	14.4	13.2	14.9	13.3	13.0	+2.5	2.0	14.8
Cu	21.3	20.8	20.9	21.5	18.8	19.3	21.5	21.1	21.2	22.6	20.8	20.9	21.0	-0.5	2.1	9.8
Zn	120	122	126	122	128	133	129	136	122	123	125	126	125	+0.8	10	8.1
Rb	48.0	46.8	47.1	47.6	46.4	48.3	47.9	48.0	45.7	45.7	46.6	47.1	47.0	+0.2	1.9	4.0
Sr	344	339	341	344	335	349	355	350	347	335	346	344	342	+0.7	12	3.7
Y	36.2	35.0	34.1	34.1	33.5	34.7	34.5	36.3	33.9	35.3	34.9	34.8	35.0	-0.6	1.8	5.1
Zr	188	182	184	183	180	193	187	190	186	179	184	185	184	+0.6	8	4.5
Nb	12.5	12.4	12.2	12.5	11.8	12.9	13.6	12.6	12.2	12.2	12.5	12.5	12.5	0.0	0.9	7.4
Cs	1.26	1.24	1.09	1.01	1.07	1.21	1.27	1.31	1.09	1.09	1.15	1.16	1.16	+0.4	0.20	17.0
Ba	693	682	679	677	654	710	685	706	689	675	692	686	683	+0.4	31	4.5
La	25.1	24.6	24.6	24.9	24.2	24.7	24.5	25.7	24.3	24.4	24.9	24.7	24.7	+0.1	0.9	3.4
Ce	53.4	52.5	52.9	53.2	52.6	55.1	55.1	55.7	54.1	54.5	54.2	53.9	53.3	+1.2	2.2	4.0
Pr	6.72	6.75	6.42	6.63	7.02	6.74	6.58	7.21	6.52	6.51	6.68	6.71	6.70	+0.1	0.46	6.9
Nd	29.6	29.9	29.2	28.7	27.9	30.2	29.0	28.8	28.9	27.9	27.9	28.9	28.9	+0.0	1.6	5.4
Sm	5.99	6.23	6.19	6.72	6.20	7.51	7.26	7.25	6.32	6.58	6.45	6.61	6.59	+0.3	1.03	15.6
Eu	1.88	1.94	1.94	1.85	2.02	1.91	2.02	2.13	2.09	2.18	1.75	1.97	1.97	+0.2	0.26	13.1
Gd	6.75	6.95	8.18	6.42	6.69	7.98	7.34	6.92	7.88	7.28	5.83	7.11	6.71	+6.0	1.43	20.0
Tb	1.01	0.908	0.910	0.920	0.991	1.01	0.993	1.07	1.02	0.985	0.966	0.981	1.02	-3.9	0.101	10.3
Dy	6.96	6.76	6.48	6.62	6.51	7.16	6.90	7.50	6.51	5.51	6.06	6.63	6.44	+3.0	1.07	16.2
Ho	1.35	1.35	1.19	1.19	1.39	1.21	1.33	1.38	1.14	1.25	1.37	1.29	1.27	+1.4	0.18	14.2
Er	4.20	4.17	3.48	3.97	3.50	3.56	3.57	3.76	4.13	3.48	4.10	3.81	3.70	+3.0	0.61	16.0
Tm	0.466	0.492	0.560	0.525	0.508	0.586	0.554	0.533	0.471	0.386	0.437	0.502	0.510	-1.6	0.118	23.4
Yb	3.48	3.40	3.20	3.27	3.80	3.72	3.49	3.53	3.61	3.22	3.85	3.51	3.39	+3.4	0.45	12.8
Lu	0.534	0.524	0.473	0.477	0.427	0.531	0.554	0.502	0.465	0.559	0.463	0.501	0.503	-0.4	0.085	17.0
Hf	4.80	4.79	4.81	5.18	4.79	5.44	5.02	5.66	4.72	4.93	4.74	4.99	4.84	+3.1	0.63	12.5
Ta	0.757	0.753	0.830	0.712	0.655	0.939	0.758	0.802	0.833	0.824	1.019	0.808	0.780	+3.5	0.203	25.2
W	0.510	0.550	0.481	0.357	0.486	0.361	0.335	0.986	0.249	0.757	0.659	0.521	0.500	+4.2	0.427	81.9
Pb	10.7	11.1	10.7	11.4	10.1	11.2	11.0	11.9	11.0	10.9	10.6	11.0	11.0	-0.3	0.9	8.1
Th	5.77	5.65	5.99	5.71	6.21	6.15	6.14	6.56	5.67	6.02	6.06	5.99	5.90	+1.6	0.56	9.3
U	1.66	1.66	1.64	1.59	1.60	1.57	1.74	1.81	1.63	1.74	1.80	1.68	1.69	-0.8	0.17	9.9

Table 2.10: LA-ICP-MS trace element data for the glass standard NIST612.

Run	1	2	3	4	5	6	7	8	Average	Georem	% Offset	2 s.d.	% 2 s.d.
Li	42.7	44.8	41.4	41.0	42.8	41.2	43.7	41.7	42.4	42.0	+1.0	2.7	6.4
Mg	78.8	77.9	76.4	75.6	78.6	78.2	76.1	77.2	77.4	77.0	+0.5	2.4	3.2
Si (wt %)	72.8	73.0	72.4	70.9	73.0	72.5	72.7	70.6	72.2	71.9	+0.5	1.9	2.6
Rb	31.7	31.6	32.3	30.4	32.6	33.5	31.3	30.1	31.7	31.4	+0.9	2.2	7.0
Sr	31.7	32.0	32.6	30.6	33.6	32.6	31.9	30.2	31.9	31.4	+1.6	2.2	7.0
Y	38.0	38.4	38.4	38.2	40.2	39.9	38.7	35.2	38.4	38.0	+1.0	3.0	7.8
Cs	41.8	42.9	42.4	41.3	44.1	43.4	44.1	39.5	42.5	42.0	+1.1	3.2	7.4
Ba	39.2	38.1	41.2	36.1	41.4	39.2	39.4	39.0	39.2	39.7	-1.3	3.3	8.5
Ba	38.7	38.8	40.6	37.9	40.9	39.4	42.4	38.9	39.7	39.7	0.0	3.0	7.5
La	35.4	36.4	36.6	35.7	37.1	36.5	37.8	35.9	36.4	35.8	+1.7	1.6	4.3
Ce	38.9	39.2	39.1	37.6	41.1	38.3	40.3	37.5	39.0	38.7	+0.8	2.4	6.3
Pr	37.8	38.0	37.6	37.0	39.1	37.3	38.2	35.3	37.5	37.2	+0.9	2.2	5.8
Nd	35.6	36.6	36.4	35.6	37.9	35.8	37.1	34.5	36.2	35.9	+0.7	2.1	5.8
Sm	38.2	38.4	39.3	37.9	40.2	37.1	39.6	36.9	38.5	38.1	+0.9	2.3	6.1
Eu	35.3	35.6	35.6	33.7	36.2	34.2	35.2	34.8	35.1	35.0	+0.2	1.6	4.6
Gd	35.7	36.9	36.8	37.2	37.7	36.6	38.0	36.8	37.0	36.7	+0.7	1.4	3.7
Pb	38.4	40.4	38.7	37.6	38.7	39.4	38.9	38.7	38.9	38.6	+0.7	1.6	4.1

NB: concentrations are in ppm unless specified.

2.6.3 SAMPLE LEACHING

All samples were acid leached to remove any anthropogenic contamination using procedures detailed in Table 2.11. This process involves acid leaching the rock particles in acid to remove only their exterior. Samples were centrifuged at 2000 rpm for 5 min and the leachate was pipetted out and discarded. The samples were then rinsed three times in MQ to remove all the remaining leachate. If more than one acid leaching step was necessary, the samples were rinsed once with MQ between leaches. The leaching process was modified depending on sample type. The rock standards JB-2 and BHVO-2 were not leached.

Table 2.11: Leaching processes adopted in this study.

Sample Type	Sample weight	Acid	Temperature	Duration	Repetition
Whole rock powders	500 mg	6 M HCl SS	120 °C	2 hr	1x
Groundmass rock chips (1-2 mm)	50 mg	2 M HCl SS	120 °C	2 hr	2x
Individual plagioclase phenocrysts	1 mg	2 M HCl SS	20 °C	20 min	3x
Bulk clinopyroxene, hornblende and plagioclase phenocrysts	5-20 mg	2 M HCl SS	20 °C	20 min	3x

2.6.4 Pb-Sr ISOTOPE ANALYSIS

DIGESTION

All samples were digested in 1 mL of 29 M HF SS with 0.2 mL 16 M HNO3 SS for 24 hr at 120 °C and then evaporated. The samples were then nitrified twice by evaporating 1 mL of 16 M HNO_3 SS. The samples were then brought into solution in 3 mL 0.8 M HBr SS at 120°C for 24 hr to equilibrate the sample into bromide form. Samples were then dried down and re-dissolved in 1.5 mL of 0.8 M HBr SS ready for Pb separation.

Pb SEPARATION

1 mL pipette tips were converted into columns by placing polypropylene frits at the tip. The columns were soaked in 2 M HCl SS until use (at least 7 days). Each column was rinsed three times in MQ water prior to adding 5 mm of anion exchange resin AG-1X8. The Pb separation

process is illustrated in Figure 2.2. Samples were centrifuged for 5 min at 2000 rpm to separate out un-dissolved solids from the solution. This solution was extracted using a pipette and loaded directly on to the resin. The empty beakers were then fluxed in 6M HCl SS at 120 °C for the duration of Pb separation. Sr in the sample passes through the resin in 0.8 M HBr SS and was collected in pre-cleaned 7 mL Teflon beakers. This solution is then nitrified to be used for Sr chemistry. This cut was then fluxed in 1.5 mL 3 M HNO_3 SB for 2 hr prior to Sr separation. The cleaned Pb beakers were rinsed three times in MQ. Pb was eluted from the columns in 6M HCl SS and collected in the recleaned beakers. The Pb cut was evaporated and nitrified twice before being redissolved in 1 mL of 0.8 M HBr SS for a second pass through the Pb columns to completely remove matrix elements from the Pb cut. After that the samples are ready for dilution and isotopic analysis.

Sr SEPARATION

Sr separation columns were constructed in the same manner as the Pb columns and rinsed with MQ three times before filling with 5 mm of Sr specific resin (EiChrom Sr.spec™). The Sr separation process is summarised in Figure 2.3. The Sr cut was evaporated, nitrified and then brought back into solution in 1 mL of 3M HNO_3 SB. The Sr cut underwent a second pass through the columns to remove any Rb, Ba or Ca which would result in matrix effects when analysed.

Pb ISOTOPE RATIO ANALYSES

The separated Pb was taken into solution in 2 mL 0.5% HNO_3 SS. Using total Pb concentrations from previous ICP-MS whole rock solution analyses, a calculated aliquot of 90 ppb sample Pb was extracted into acid-washed and MQ-cleaned micro-centrifuge tubes. These were then topped up to 1.5 mL with 0.5% HNO_3 SS to generate a 30 ppb Pb solution for analysis. The sample dilutions were analysed using a Nu Plasma multi-collector (MC)-ICP-MS at VUW coupled to a desolvating nebuliser system (DSN). Using the DSN reduces the volume of solvent (mostly water) reaching the plasma, improving ionization efficiency, and reduces interferences in isotopic ratio measurements. The MC-ICP-MS was tuned using a 30 ppb solution of the Pb standard SRM981. Tuning consisted of adjusting the nebuliser gas flow, the torch position and voltage across each lens to optimise sensitivity to ca. 8 V for ^{208}Pb. Accuracy was monitored using JB2 as a secondary standard. The background was measured for 60 s prior to analysis and this was automatically deducted from measurements. Isotope masses ^{208}Pb, ^{207}Pb, ^{206}Pb and

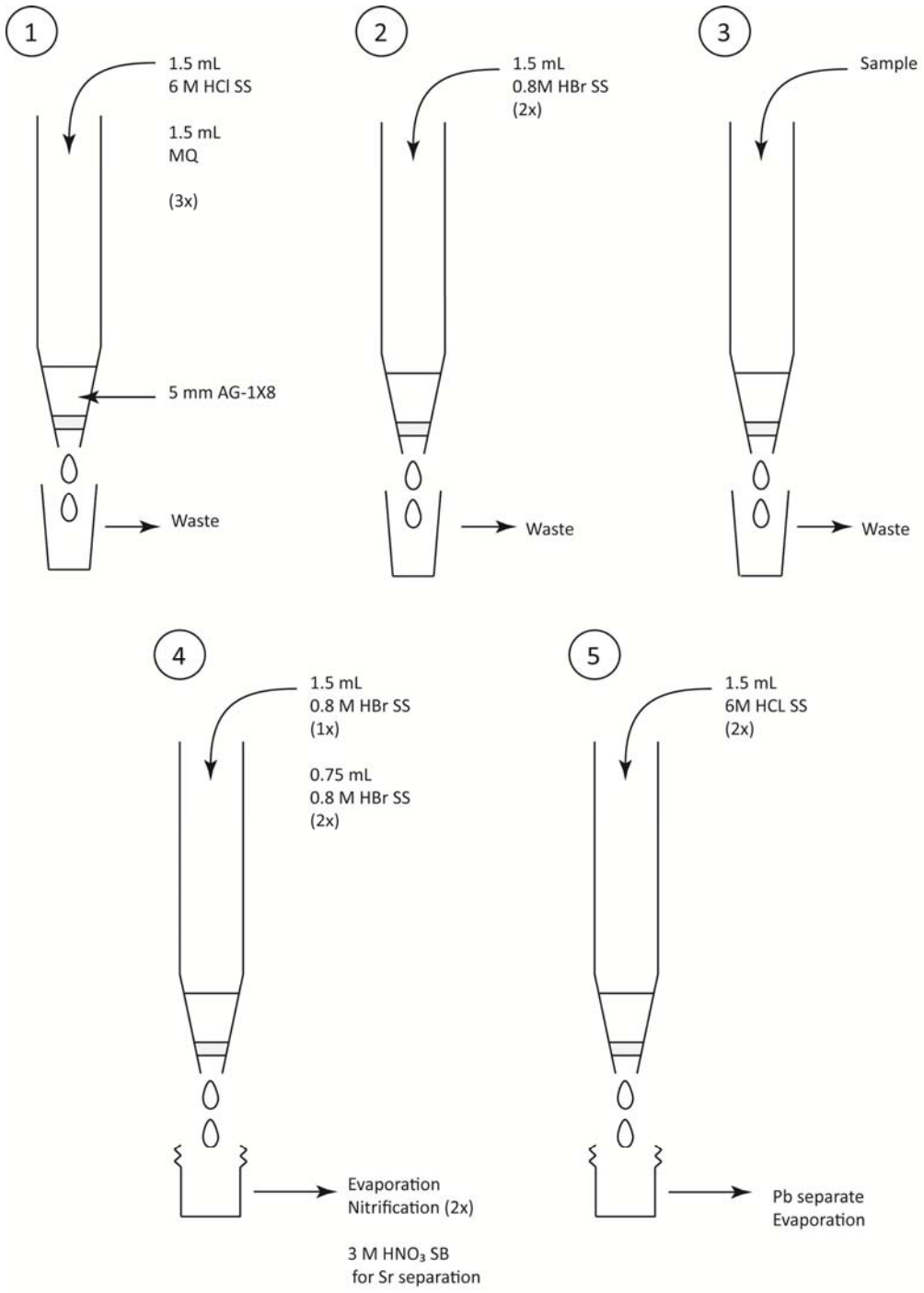

Figure 2.2 Diagram illustrating the Pb chemical separation process.

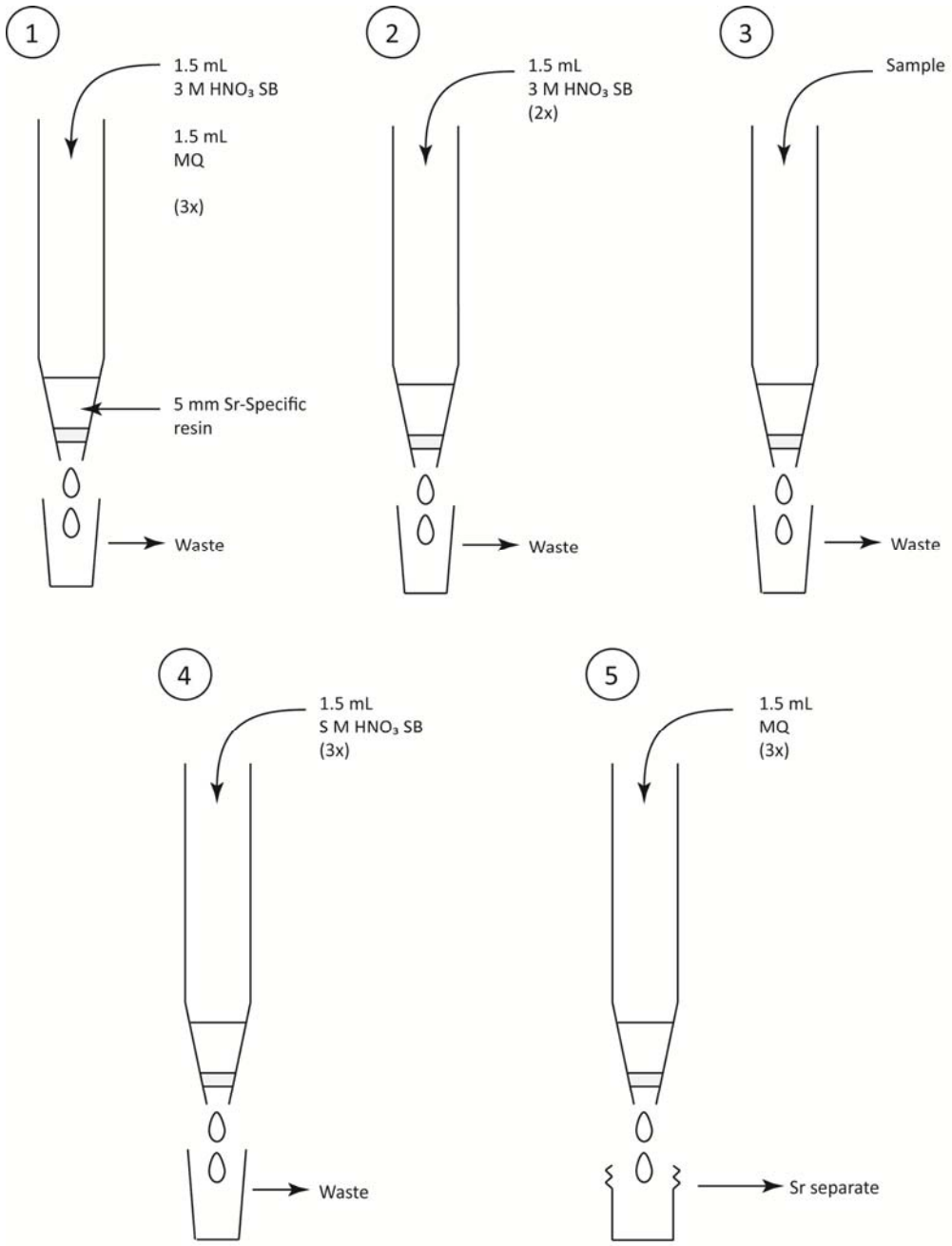

Figure 2.3: Diagram illustrating the Sr chemical separation process.

^{204}Pb were measured in the H4, H3, H2 and Ax Faraday cups, respectively. The isotopic mass of ^{202}Hg was also measured in cup L2, to monitor mercury interferences which were deducted from the 204 signal. Pb isotopic ratios were measured for two blocks of 25 five second integrations with background measurements taken before each block. Due to Pb possessing only 1 non-radiogenic isotope, fractionation of Pb during analysis was corrected for by running each Pb measurement individually and bracketing these with the SRM981 Pb standard. Analyses of repeat digestion and dilutions of the secondary standard JB-2 are listed in Table 2.12. Analyses are within the error of the preferred values of Baker et al. (2004). Measured blanks were insignificant at < 14 pg compared to sample Pb of 90 ng.

Table 2.12: Reproducibility of JB-2 during Pb isotope analysis.

JB-2*	^{208}Pb/^{204}Pb	^{207}Pb/^{204}Pb	^{206}Pb/^{204}Pb
A1	38.282 ± 2	15.563 ± 1	18.344 ± 1
A2	38.281 ± 4	15.563 ± 1	18.343 ± 1
B1	38.266 ±3	15.558 ± 1	18.342 ± 1
B2	38.274 ± 3	15.561 ± 1	18.342 ± 1
B3	38.281 ± 3	15.562 ± 1	18.343 ± 1
C1	38.278 ± 4	15.563 ± 1	18.341 ± 2
C2	38.274 ± 4	15.562 ± 2	18.339 ± 2
C3	38.272 ± 3	15.563 ± 1	18.337 ± 1
D1	38.276 ± 2	15.561 ± 1	18.342 ± 1
Mean	38.276 ± 5	15.562 ± 2	18.341 ± 2
Preferred	38.276 ± 5	15.562 ± 2	18.344 ± 2
2 SD ppm	138	109	120

Preferred values those of Baker et al. (2004) n = 14;*Letters are separate digestions whereas numbers indicate separate dilutions of the same digestion.

Sr ISOTOPE ANALYSIS

The Sr separate was brought up into solution in 2 mL of 0.5% HNO_3 SS for analysis. Using previously measured ICP-MS whole rock Sr concentrations, a 100 ppb sample aliquot was extracted into pre-cleaned (1.2 M HCl) micro-centrifuge tubes and topped up to 1.5 mL with 0.5% HNO_3 SS to create a 70 ppb Sr solution for analysis.

Sr isotopes were measured using the MC-ICP-MS. The MC-ICP-MS was tuned using a 70 ppb solution of Sr standard SRM987. Prior to every measurement, a blank was measured which was automatically deducted from the sample analysis. Analyses consisted of 90 five second integrations. Isotopic masses ^{87}Sr and ^{86}Sr were measured in the H2 and Ax Faraday cups, respectively. Isotopic interferences were monitored by measuring ^{88}Sr, ^{85}Rb and ^{84}Sr in the H4, L2 and L3 cups, respectively. A linear interpolation was applied to the samples to correct for any drift and bias of the MC-ICP-MS using SRM987 as a bracketing standard. Accuracy and reproducibility were monitored using BHVO-2 as a secondary standard. Repeat analyses of the secondary standard BHVO-2 are given in Table 2.13. Precision for BHVO-2 is better than 1.5 x

10^{-5} when run at 8 V for ^{88}Sr. However for individual plagioclase crystal analyses, maximum attainable sensitivity was 2 V. In order to test the reproducibility for this data, the BHVO-2 standards were diluted to match the 2 V maximum. This produced two sigma errors ranging from 2-5 x 10^{-5}. Note that although these errors are quite large, the variations measured in the isotopic ratios of the samples are significantly larger than the errors. Procedural Sr blanks were < 90 pg, which is insignificant, compared to sample Sr contents.

Table 2.13: Reproducibility of BHVO-2 Sr isotope measurements.

8V	**$^{87}Sr/^{86}Sr$**	**2V**	**$^{87}Sr/^{86}Sr$**
A1	0.703471 ± 11	E2	0.703452 ± 35
A2	0.703486 ± 12	E3	0.703542 ± 49
A3	0.703467 ± 10	E4	0.703518 ± 20
B1	0.703452 ± 6		
B2	0.703464 ± 7		
B3	0.703455 ± 8		
C1	0.703452 ± 9		
C2	0.703465 ± 15		
C3	0.703464 ± 10		
C4	0.703457 ± 15		
C5	0.703455 ± 11		
E1	0.703465 ±11		
Mean	0.703463 ± 19	Mean	0.703504 ± 94
Georem	0.703469 ± 17	Georem	0.703469 ± 17
2SD ppm	27	2 SD ppm	291

*Letters are separate digestions; numbers are separate dilutions of the same digestion. Georem reference is a mean data value from http://georem.mpch-mainz.gwdg.de/.

CHAPTER 3

RESULTS

3.1 MINERAL PETROGRAPHY AND CHEMISTRY

One representative sample from each dome (Western, Central, Hipaua, Trig M, Breached and Main Dome) containing clinopyroxene, orthopyroxene, amphibole, plagioclase, quartz, ilmenite and titanomagnetite mineral phases was analysed for major and trace element chemistry. Major element chemistry was measured by EPMA for clinopyroxene, orthopyroxene, amphibole, plagioclase, ilmenite and titanomagnetite, whereas trace elements were measured by LA-ICP-MS for only plagioclase, clinopyroxene and amphibole. All phenocrysts were imaged using BSE with the exception of quartz where CL was used. All mineral phases have previously been petrographically described in detail by Worthington (1985) and therefore this information has only been summarised in this thesis. Dome average modal analysis is presented in Table 3.1. All domes have comparable total phenocryst assemblages with 13 to 19% crystal content. Western and Central Domes are distinct with the presence of less orthopyroxene (~0.5%) and more hornblende (~4.5%) in comparison to Hipaua, Trig M, Breached and Main Domes with ~1.4 and ~2.2% (with the exception of Main Dome with ~1% hornblende), respectively. Traces of biotite are only present in Western, Central, Hipaua and Main Domes and traces of olivine are only present in Western Dome.

Table 3.1: Average dome modal analyses (volume %) for the selected samples from Tauhara volcano.

Dome	Total Xl.	Plag	Opx	Cpx	Hbl	Qz	Opq	Bt	Ol
Western	17.58	7.90	0.50	1.82	4.97	1.72	0.65	0.02	0.02
Central	18.35	8.50	0.60	2.35	4.10	2.20	0.55	0.05	
Hipaua	17.05	8.50	1.13	2.50	2.80	1.25	0.78	0.08	
Trig M	13.07	6.77	1.27	1.17	2.23	0.87	0.77		
Breached	18.36	8.84	1.79	2.67	2.21	1.83	1.01		
Main	15.60	9.09	1.44	2.34	0.99	1.25	0.49	0.01	

3.1.1 AMPHIBOLE

Amphibole phenocrysts are abundant in the Tauhara dacites ranging between 6 – 41 modal % of total phenocrysts (Worthington, 1985). Representative amphibole phenocrysts from each dome are shown in Figure 3.1. Phenocryst a-axes are typically 3-6 mm long in Western, Hipaua and Trig M dome samples. Core dissolution to varying degrees is evident in all samples, resulting in atoll and swallow-tail phenocryst textures (Figure 3.1). Strong zoning is visible in Western, Breached and Main Dome amphiboles with less zoning in Hipaua and Trig M Dome crystals. Zoning features in Central Dome amphibole phenocrysts are obscured by prolific disequilibrium features such as resorbed cores and reaction rims.

3.1.1.1 AMPHIBOLE MAJOR ELEMENT CHEMISTRY

Aluminium number (Al# = Al_{VI} /(Al_{VI}+Al_{IV}) on the basis of 13 cations) for amphibole phenocrysts is presented in Figure 3.2. Amphibole Al# is unimodal for all domes except Main Dome, which has two distinct populations. Western, Central, Hipaua, Trig M and Breached Dome amphiboles are normally distributed with Al# peaks at 0.16. The higher Al# peak, consisting primarily of phenocryst cores, have the same compositional range as amphiboles from the other domes (Al# = 0.10 – 0.20). The second Main Dome peak at Al# = 0.00 – 0.08, comprises both middle and rim zones of crystals.

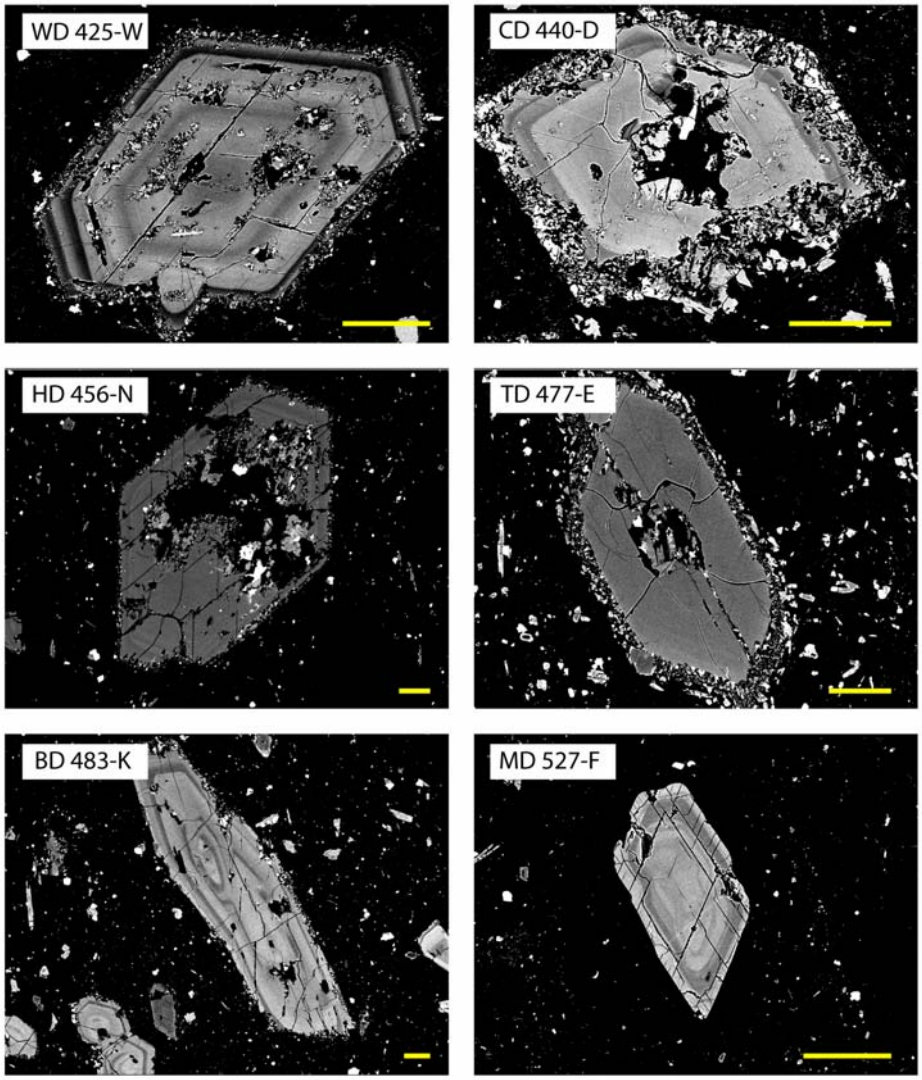

Figure 3.1: BSE images of representative amphibole phenocrysts from the Tauhara volcano. Yellow scale bars are 100 µm long. WD: Western Dome, CD: Central Dome, TD: Trig M Dome, BD: Breached Dome, MD: Main Dome.

`

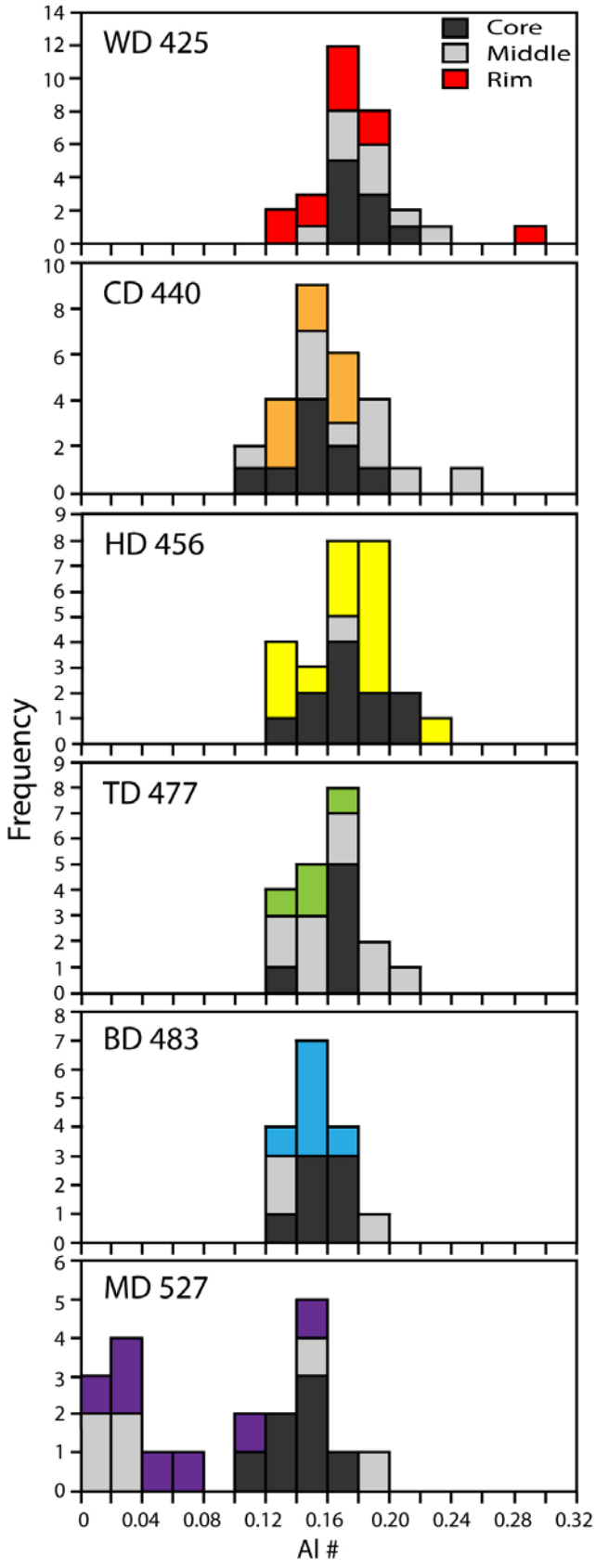

Figure 3.2: Al# histograms for amphibole phenocrysts of the Tauhara volcano.

3.1.1.2 AMPHIBOLE TRACE ELEMENT CHEMISTRY

Representative chondrite-normalised rare earth element (REE) data for amphiboles from each dome are presented in Figure 3.3. Western, Central, Hipaua, Trig M and Breached Dome amphiboles have amphibole with restricted REE concentrations and an average pattern for amphibole from each dome is shown. In contrast, Main Dome amphibole has two REE populations: high and low REE and therefore averages of both populations are represented. These two REE signatures correspond to the two Al# populations with the low Al# amphiboles having the high REE concentrations. Overall there is no systematic variation between Western, Central, Hipaua, Trig M, Breached and the low REE Main Dome amphiboles. The high REE Main Dome amphiboles have the same shaped REE pattern as the other amphiboles, but are an order of magnitude higher in concentration than the other low REE amphibole from the same dome. A strong negative Eu_N anomaly is also observed in the high REE (low Al#) Main Dome amphiboles.

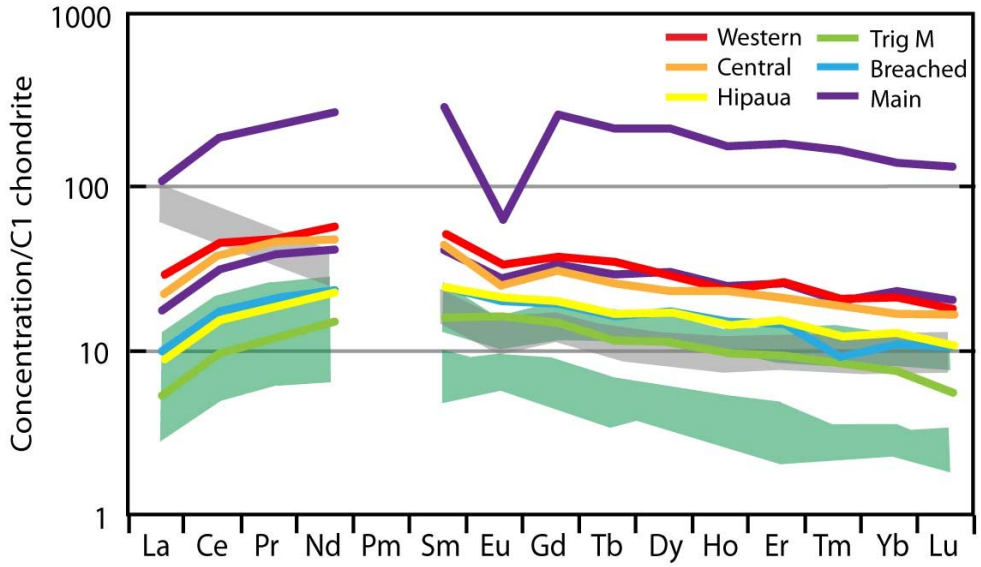

Figure 3.3: Representative chondrite-normalised (Sun and McDonough, 1989) REE patterns for amphiboles from the Tauhara Dacite Complex. Chondrite-normalised clinopyroxene (green shaded fields) and whole rock (grey shaded field) REE concentrations are also shown.

Trace element data for amphiboles plotted against Al_2O_3 are presented in Figure 3.4. Trace elements compatible in amphibole correlate with Al_2O_3 such as Mn and Zn. Other elements such as Cu, Sr and V and Eu anomalies show scattered negative correlations with Al_2O_3 whereas Pb shows a scattered positive correlation. There are no systematic differences between domes for these trace elements at a given Al_2O_3 with the exception of Western Dome amphibole which have higher Sr and Cu concentrations than the other domes. The Main Dome

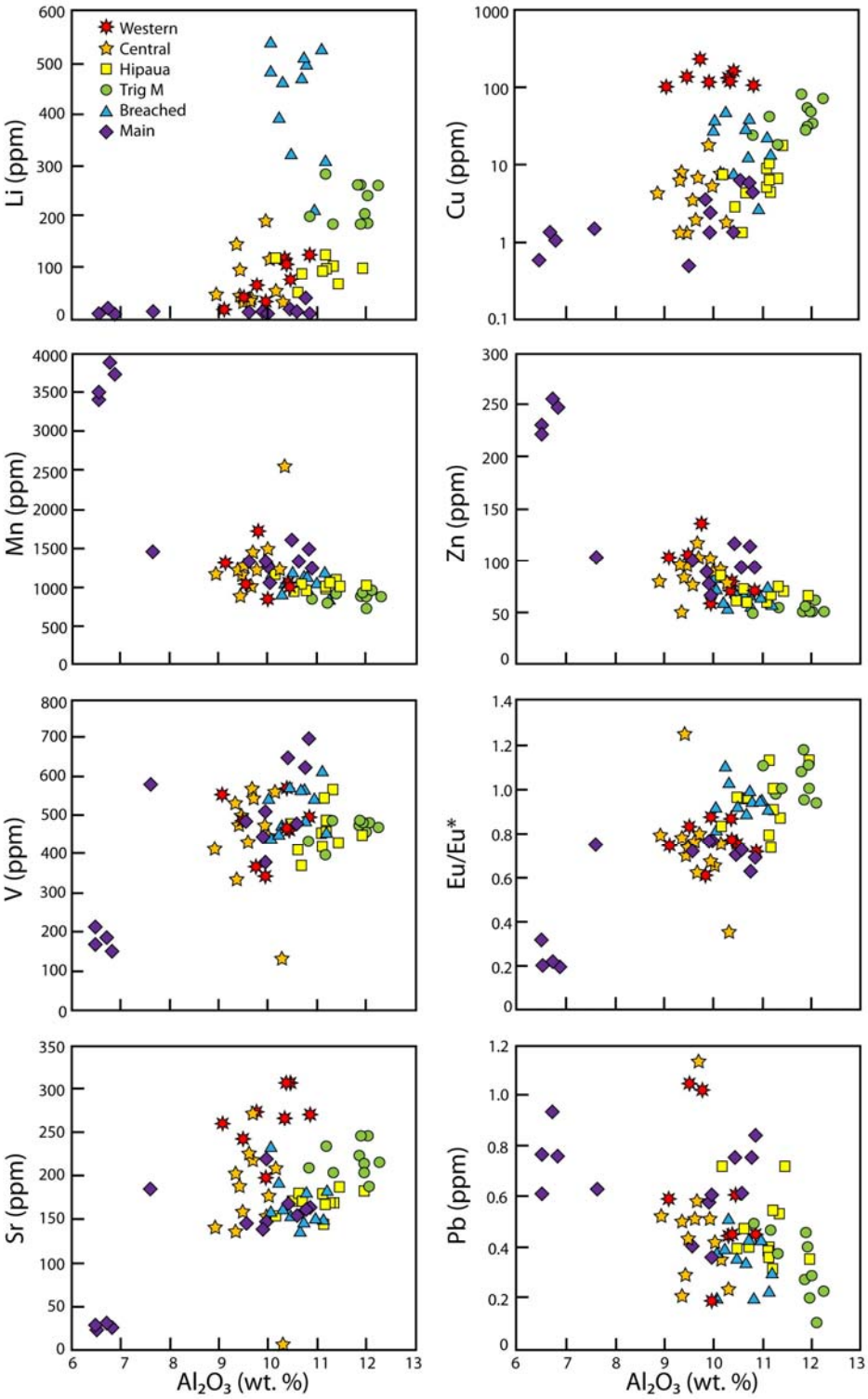

Figure 3.4: Amphibole trace element concentrations plotted versus Al_2O_3 for the Tauhara volcano.

low Al# amphibole population shows markedly different trace element concentrations to the other amphiboles but extends the overall trends observed e.g. high Mn and Zn and low Sr and V. Li in amphibole has a large range in concentration (ca. 0-550 ppm) which does not correlate with Al_2O_3. Amphibole from each dome has distinct Li concentrations with Main Dome amphibole having very low Li (> 40 ppm) whereas Breached Dome crystals have high Li concentrations up to 550 ppm. Western, Central and Hipaua Dome amphibole have the same Li concentrations (ca. 100 ppm) whereas Trig M Dome phenocrysts are higher in Li (ca. 200-300 ppm).

3.1.1.3 AMPHIBOLE THERMOBAROMETRY, OXYBAROMETRY AND HYGROMETRY

Amphibole has been widely used as a geobarometer for calc-alkaline sub-volcanic rocks where the Al content is solely controlled by pressure (Hammerstrom and Zen, 1986). Recent research by Ridolfi et al. (2010) provides an improved geobarometer and the development of other methods to determine physical parameters such as temperature and oxygen fugacity where pressure is calculated from Al^T, temperature is based on Si index, Mg index is used to calculate oxygen fugacity and Al index is used for H_2O_{melt}. Each parameter is calculated independently from the other. Dome-averaged amphibole rim temperature, pressure, oxygen fugacity and melt water content (H_2O_{melt}) are presented in Table 3.2. Core values for Main Dome amphibole are also presented. Figure 3.5a shows temperature versus depth for core and rim analyses of calc-alkaline amphiboles of the Tauhara volcano. There is no systematic variation between Western, Central, Hipaua, Breached Dome amphiboles and high Al# Main Dome cores which cluster between 850–940 °C and 6–12 km. Trig M Dome amphiboles formed at higher temperatures and greater depths. Some Main Dome cores and all Main Dome rims (low Al#) crystallised at lower temperatures (750-850 °C) and depths (3-4 km) than the high Al# amphibole cores.

Table 3.2: Average rim temperature, pressure, oxygen fugacity and water content of amphiboles from the Tauhara Dacite Complex.

Sample	Dome	T (°C)	P (MPa)	Depth* (km)	log fO_2	H_2O_{melt} (wt. %)
425	Western	889	214	8.1	-10.8	5.8
440	Central	886	213	8.1	-10.9	6.0
456	Hipaua	915	287	10.8	-10.5	6.6
477	Trig M	946	351	13.2	-9.7	6.6
483	Breached	904	251	9.5	-10.4	6.2
527	Main	796	101	3.8	-12.4	4.7
527c	Main	895	235	8.9	-10.6	6.1

*Depth is based on an average continental crust density of 2700 kg/m^3. 527c: Core averages representing the second Main Dome amphibole population.

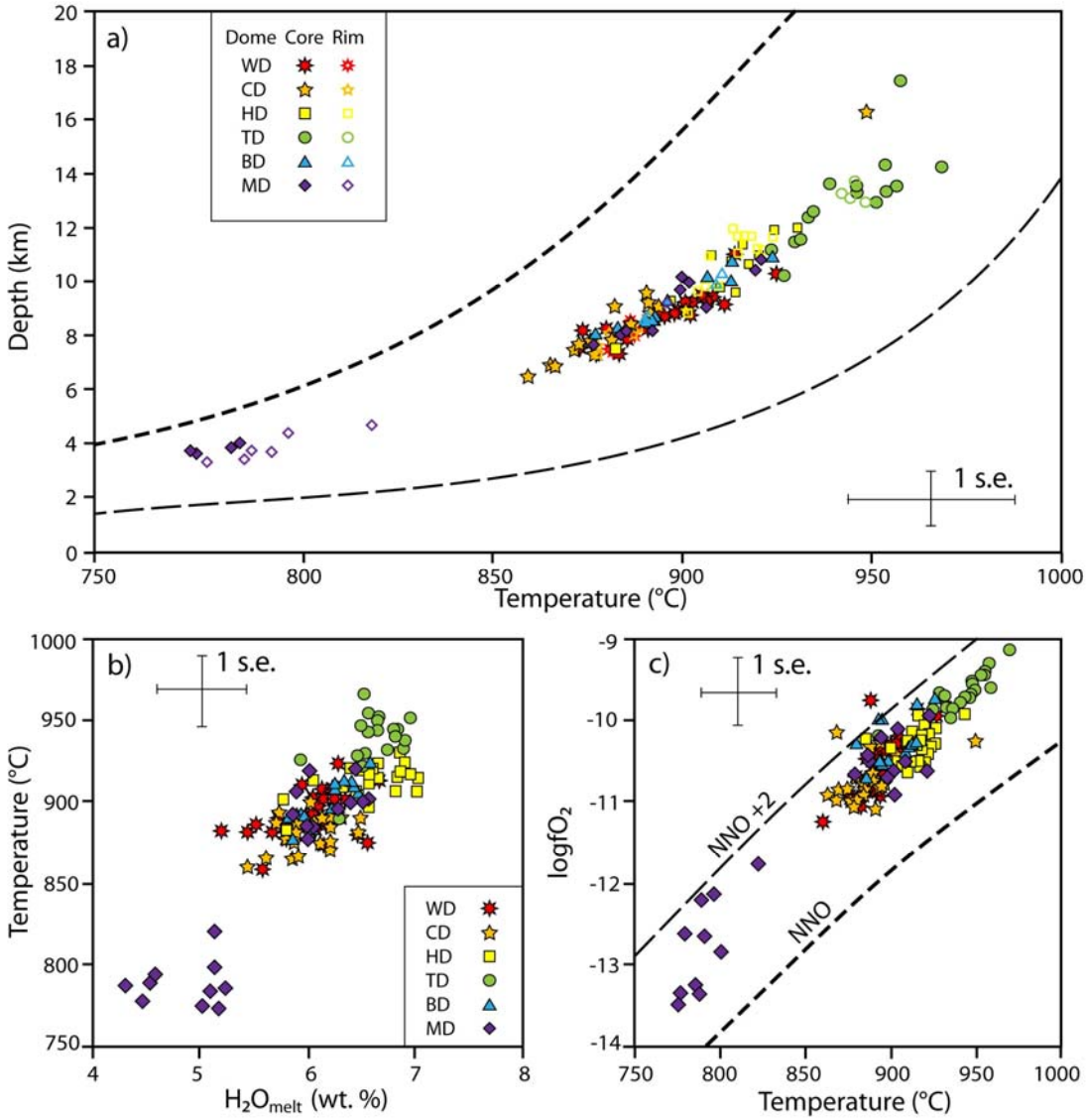

Figure 3.5: Depth-T (a), T-H_2O_{melt} (b) and logfO_2-T (c) diagrams for amphiboles of the Tauhara volcano calculated using the equations of Ridolfi et al. (2010). Error bars presented are 1 standard error. Heavy dashed line in (a) represents the upper limit of consistent amphiboles and light dashed line is the maximum amphibole thermal stability curve. Symbols for (c) are the same as (b). NNO buffers in (c) are from O'Neill and Pownceby (1993).

Figure 3.5b shows temperature versus H_2O_{melt} for all amphibole phenocryst zones. Although most amphiboles have calculated H_2O_{melt} just within 1 se of each other, a broad trend is seen in Trig M and Hipaua Dome with higher H_2O_{melt} contents than Breached, Western, Central and Main Dome. The low Al#, low temperature amphibole from Main Dome yield distinctly lower H_2O_{melt} of 4.5 wt. % (versus 6 wt. % in high Al# Main Dome zones).

Oxygen fugacity is positively correlated with temperature as shown in Figure 3.5c. Central, Breached, Western, Hipaua and high temperature Main Dome amphiboles cluster above the NNO buffer, at around -10.8 logfO_2. Trig M Dome amphibole oxygen fugacity is higher than the other dome clusters with values around -9.7 logfO_2. The low temperature Main Dome

amphibole yield lower oxygen fugacity than the high temperature Main Dome amphibole by up to 2 log units, between -11.7 to -13.5.

3.1.2 PYROXENE

Clinopyroxenes make up 2-33 modal % of total phenocrysts in the Tauhara dacites (Worthington, 1985) and are present in two forms: stubby crystals forming monomineralic clusters and euhedral clinopyroxene phenocrysts. Orthopyroxene is less abundant, comprising 0-20 modal % of total phenocrysts, and is either euhedral or intermixed within some clinopyroxene clusters. Representative pyroxene crystals are presented in Figure 3.6. Clinopyroxene phenocryst 425-E has an Fe-rich core, Mg-rich middle and resorbed Fe-rich rim, typical of clinopyroxene from Western Dome. A spongy sieved core texture is present in some clinopyroxenes, as displayed by phenocryst 440-B. 456-E illustrates a clinopyroxene monomineralic cluster common in all domes except Western Dome. Clinopyroxene 456-L and orthopyroxene 456-F are intergrown, both displaying similar zoning patterns. Spongy sieved cores are also prevalent in orthopyroxenes with Fe-rich cores such as 483-J. Strong oscillatory zoning as shown by orthopyroxene 483-D is also a common feature in orthopyroxene. Oscillatory zoning was not observed in any clinopyroxene crystals.

3.1.2.1 PYROXENE MAJOR ELEMENT CHEMISTRY

Pyroxene wollastonite (Wo), enstatite (En) and ferrosilite (Fs) contents are displayed in Figure 3.7. Core and rim analyses for both orthopyroxene and clinopyroxene are presented. Western and Central Dome orthopyroxene were not present in thin section for the selected samples. Low En orthopyroxene compositions (En_{47}) are not presented in the figure to preserve the resolution of the main orthopyroxene population but are included in Figure 3.8. Clinopyroxenes plot within a field of $Wo_{40\text{-}50}En_{30\text{-}50}Fs_{20\text{-}0}$ with no systematic variation between domes. Both core and rim compositions are the same for clinopyroxene from Hipaua, Breached and Main Domes. Western Dome clinopyroxene show bimodal cores and homogenised rims, whereas both Central and Trig M Dome clinopyroxene rims are higher in Fs than the cores. Orthopyroxene phenocrysts plot in a field defined by $Wo_{0\text{-}5}En_{65\text{-}80}Fs_{35\text{-}20}$ with no systematic variation between Hipaua, Trig M and Main Domes. The rims of Hipaua, Trig M and Main Domes are higher in Fs than the cores. Orthopyroxene from Breached Dome has higher

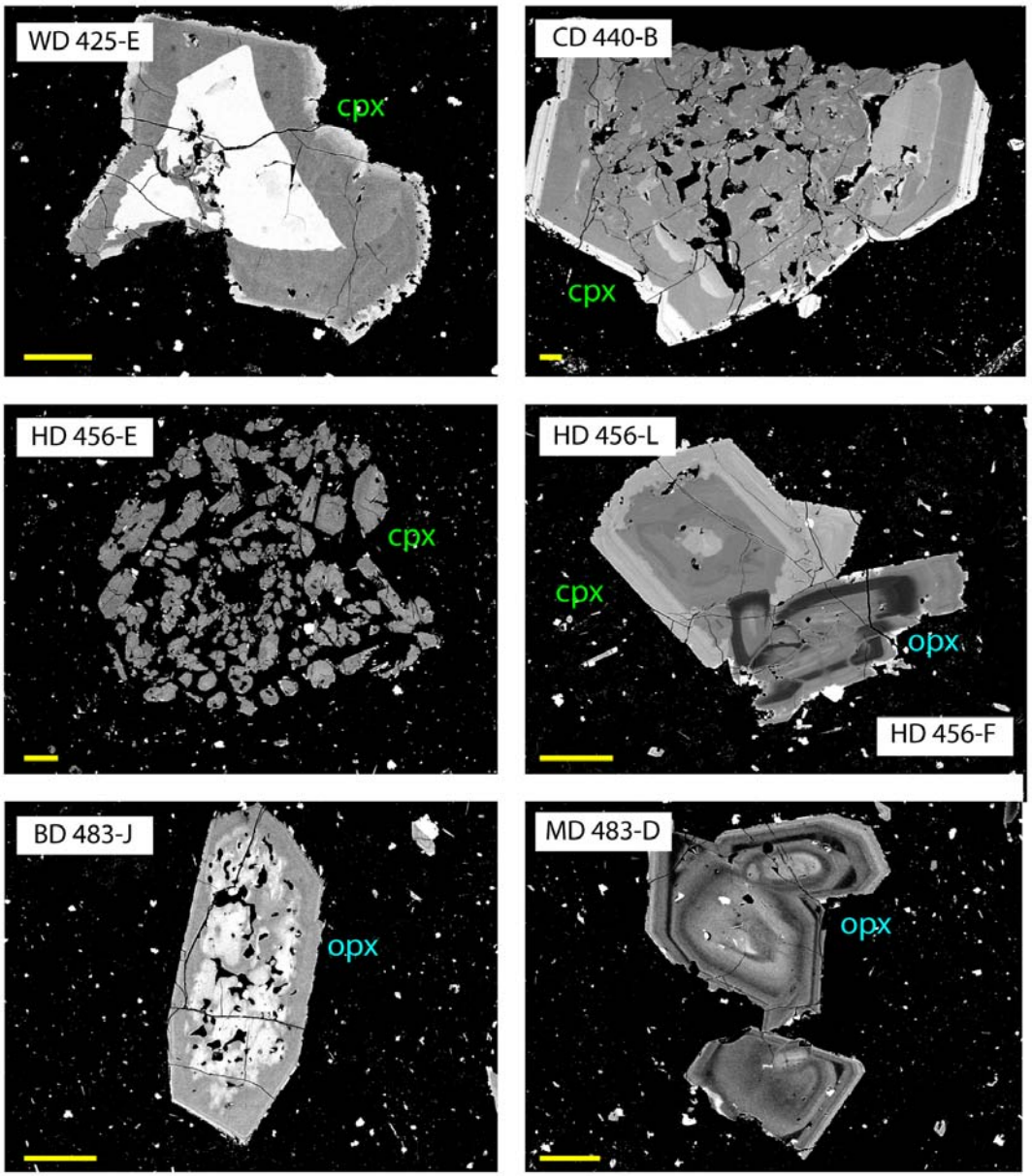

Figure 3.6: BSE images of representative clinopyroxene and orthopyroxene phenocrysts of the Tauhara volcano. Yellow scale bars are 100 µm. WD: Western Dome, CD: Central Dome, HD: Hipaua Dome, BD: Breached Dome, MD: Main Dome.

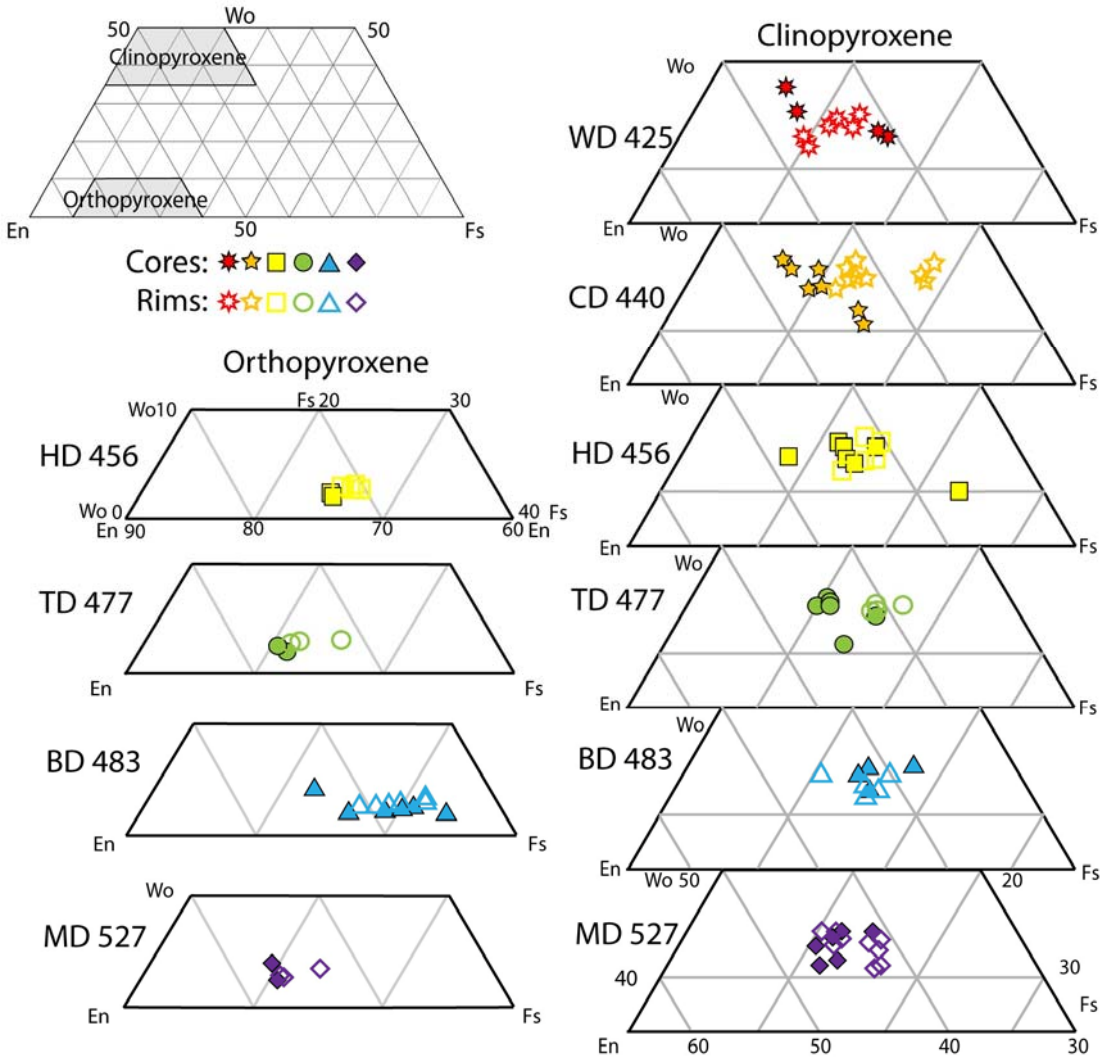

Figure 3.7: Pyroxene ternary diagrams showing pyroxene core and rim data for each dome. WD: Western Dome, CD: Central Dome, HD: Hipaua Dome, TD: Trig M Dome, BD: Breached Dome, MD: Main Dome.

Fs than the other domes. Pyroxene Mg# histograms are presented in Figure 3.8 with the inclusion of middle zones. Where more than one middle zone was present, one representative zone was selected per phenocryst. Clinopyroxene phenocrysts show no systematic variation between domes with all domes peaking around Mg# = 74-80. High Mg# (Mg# > 86) core and middle zones are only observed in clinopyroxene phenocrysts from Hipaua, Central and Western Domes. One low Mg# core is present in Hipaua Dome. Except for Western Dome clinopyroxene which has bimodal core and middle zones with rims of homogenized composition, all crystal zones share the same range in composition. Orthopyroxene phenocrysts have the same Mg# as the clinopyroxene with the exception of Breached Dome with orthopyroxene having lower Mg# = 68-70. Low Mg# (46-52) orthopyroxene is only present in Breached and Hipaua Domes.

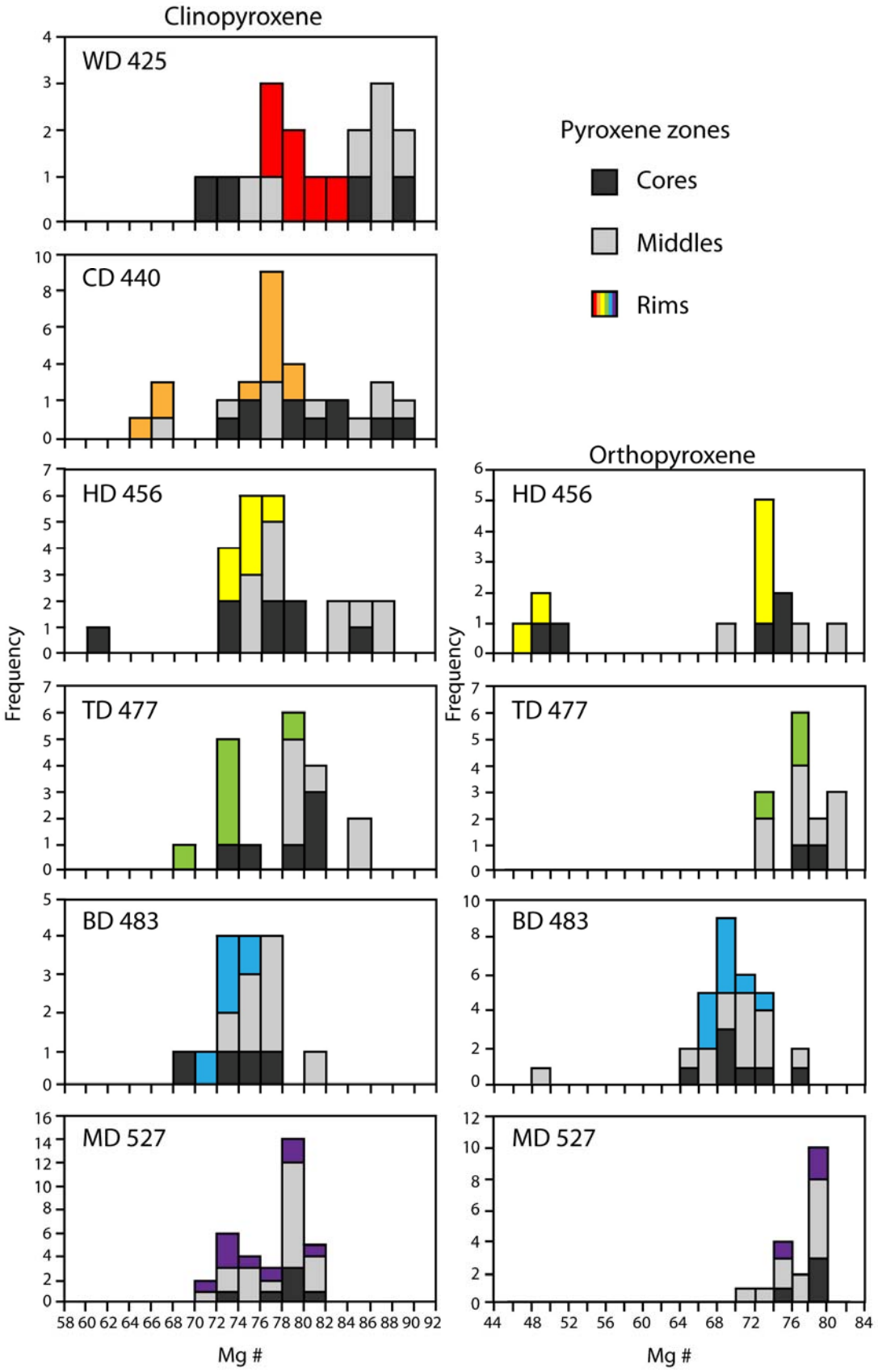

Figure 3.8: Clinopyroxene and orthopyroxene histograms showing Mg# for core, middle and rim zones of crystals for the Tauhara volcano.

3.1.2.2 CLINOPYROXENE TRACE ELEMENT DATA

LA-ICP-MS trace element analyses were only carried out on clinopyroxene phenocrysts. Representative chondrite-normalised rare earth element (REE) data for clinopyroxenes from each dome are presented in Figure 3.9. Only one population of clinopyroxene phenocrysts were present in the REE signatures from Western and Hipaua Domes. Two populations of clinopyroxene REE signatures were observed in Central, Trig M, Breached and Main Dome clinopyroxene of high-REE and low-REE contents. All clinopyroxene show the same convex upward patterns. The high REE population is ca. 3 times greater than the low REE for light- and middle-REE (LREE and MREE). This distinction is greater for the heavy-REE (HREE). The high REE population have similar MREE and HREE to the Tauhara dacite whole rocks and the low Al# amphibole with a small negative Eu anomaly also observed in the clinopyroxenes. The low REE clinopyroxene population is similar to the high Al# amphibole REE patterns.

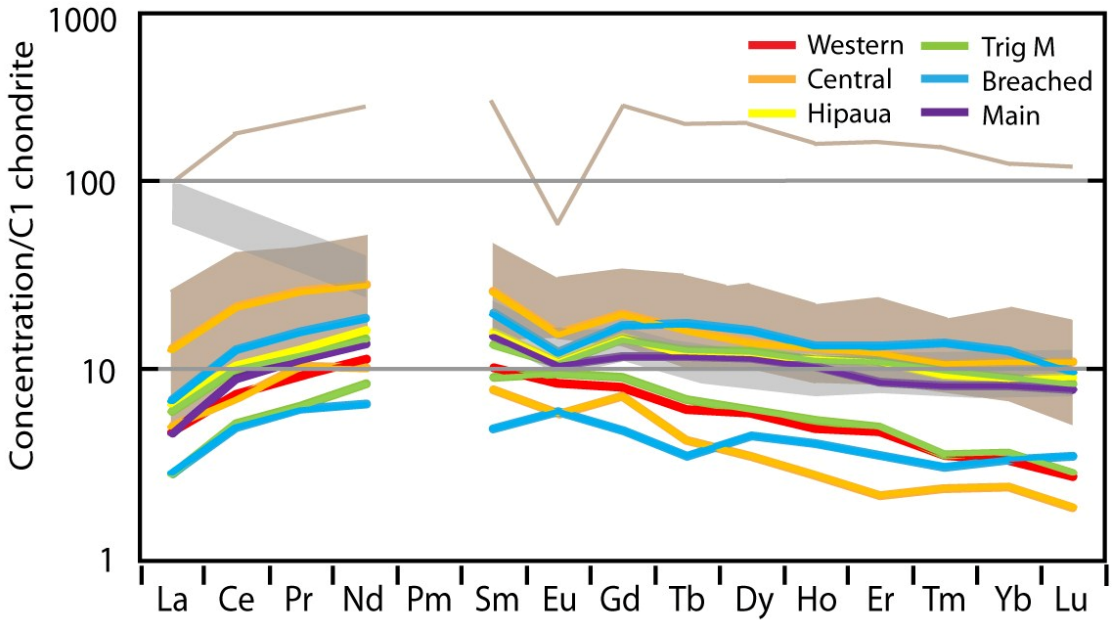

Figure 3.9: Representative chondrite-normalised (Sun and McDonough, 1989) REE data for clinopyroxenes from the Tauhara volcano. Chondrite-normalised amphibole (brown shaded field) and whole rock (grey shaded field) REE data are also shown.

Clinopyroxene trace element data plotted versus Mg# are presented in Figure 3.10. Trace element variations with Mg# are observed for compatible and moderately incompatible elements such as Ni, Zn, V and Sr and Eu/Eu*. There is no covariation of Mg# with trace elements such as Pb, Cu and Li. The range in concentrations for both Li and Cu are large with concentrations of Li and Cu in Western, Central and Hipaua Dome clinopyroxenes greater than Breached, Trig M and Main Dome clinopyroxenes.

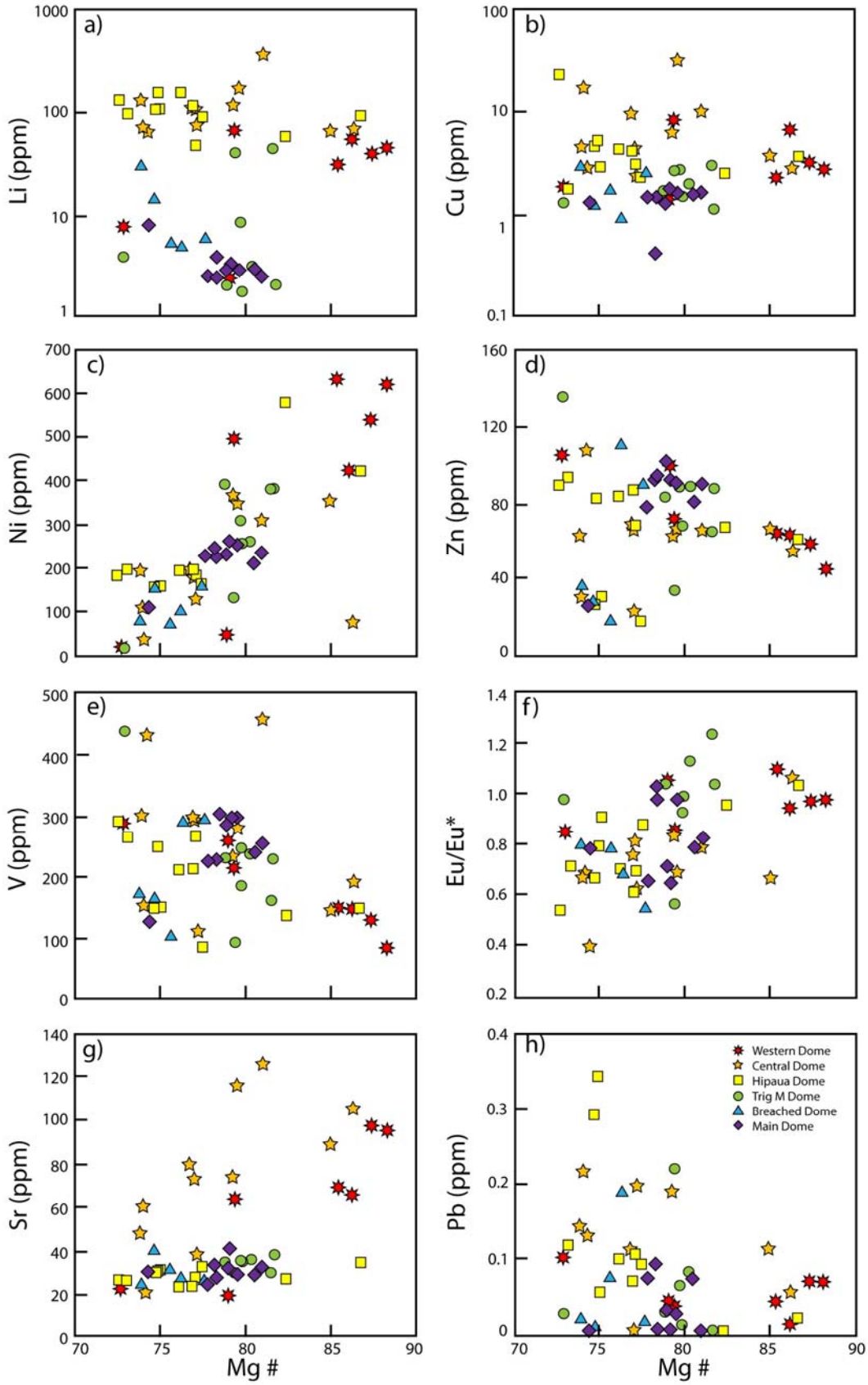

Figure 3.10: Clinopyroxene trace element data plotted versus Mg# for dacites of the Tauhara volcano.

3.1.2.3 TWO-PYROXENE THERMOMETRY

Two-pyroxene thermometry was applied to orthopyroxene-clinopyroxene pairs in equilibrium. Equilibrium was tested using the Fe-Mg exchange method of Putirka (2008). Temperature was calculated based on the widely used Brey and Köhler (1990) model T_{BKN} thermometer adapted by Putirka (2008). The pressure input was calculated by Putirka's equation 38 (2008) which is temperature independent. Details of the thermometry calculations with equations are given in Appendix A6.2. Two-pyroxene thermometry is presented in Figure 3.11. The two-pyroxene thermometer has a standard error of ±66 °C. Orthopyroxene was absent in the selected Western and Central Dome samples and therefore temperatures were not calculated for these domes. Two-pyroxene temperatures for the Hipaua, Trig M, Breached and Main Dome phenocrysts cluster between 920-960 °C with no systematic variation between domes. Average rim thermometry analyses are presented in Table 3.3.

3.1.2.4 CLINOPYROXENE DIFFUSION MODELLING

Diffusion modelling was applied to clinopyroxene phenocryst rims using the 1-D method of Morgan (2004). The process of diffusion modelling is detailed in Appendix A7. Diffusion coefficients were calculated using Dimanov and Wiedenbeck (2006). Two-pyroxene temperatures were used for Hipaua, Trig M, Breached and Main Dome. Where orthopyroxene was absent, temperatures were taken from amphibole thermometry (section 3.1.4). Amphibole oxygen fugacities were also used. Amphibole conditions were used rather than two-pyroxene and Fe-Ti oxide thermometers because they have the lowest uncertainties and diffusion modelling is highly dependent on temperature. Only rim temperatures and fugacities were used. Modelled clinopyroxenes are presented in Figure 3.12. The random orientation of clinopyroxene within the thin sections results in the calculation of maximum ages. Straight rim boundaries were not present in Breached Dome clinopyroxene and therefore could not be modelled. Diffusion ages with utilised temperatures, oxygen fugacities and calculated coefficients are given in Table 3.4. Diffusion modelling dates the Fe-rich clinopyroxene rims to have formed less than 3 yr prior to eruption. Western, Central and Hipaua Dome clinopyroxenes yield ages between 1-3 yr with Trig M and Main Dome clinopyroxene rims yielding ages of less than 1 yr.

Table 3.3: Two-pyroxene average rim temperatures for the Tauhara volcano.

Sample	Dome	Temperature (°C)
456	Hipaua	910
477	Trig M	909
483	Breached	933
527	Main	951

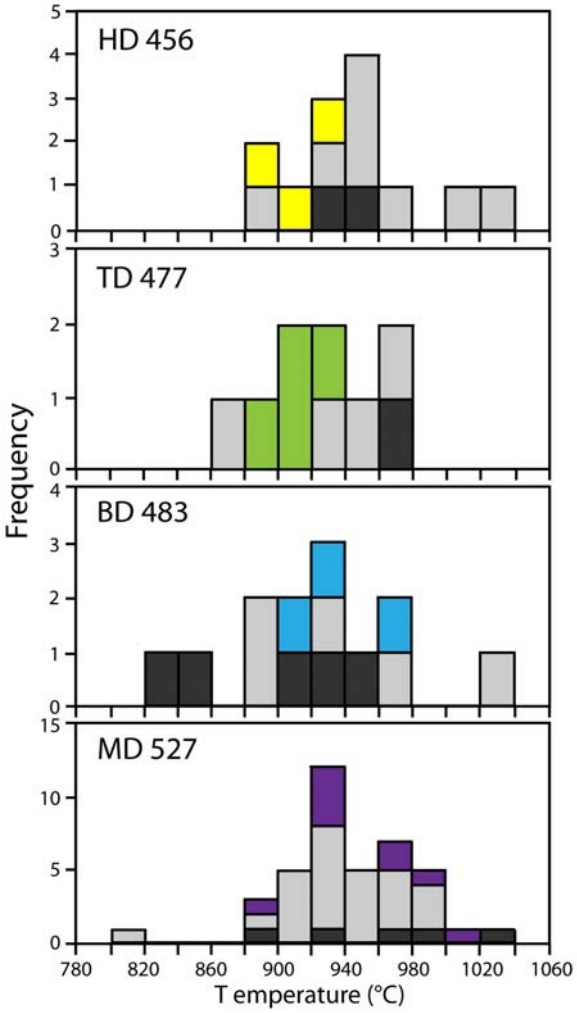

Figure 3.11: Two-pyroxene thermometry temperature histograms for the Tauhara volcano. The average absolute deviation is ±66 °C.

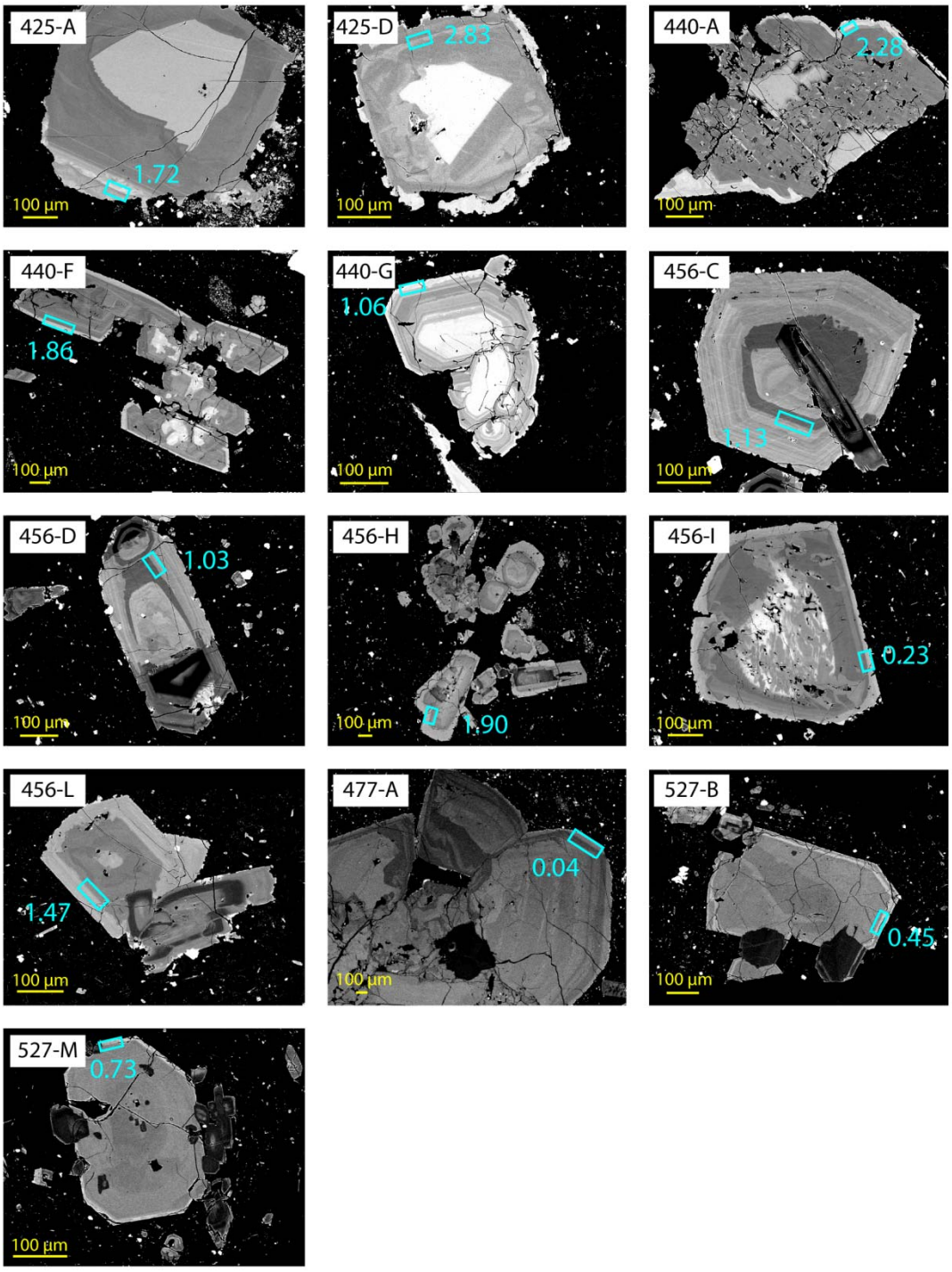

Figure 3.12: BSE images of clinopyroxene utilised for Fe-Mg exchange diffusion modelling. Zone boundaries used are marked by blue boxes. Ages are in years.

Table 3.4: Diffusion ages for clinopyroxene phenocryst rims of the Tauhara volcano.

Sample	Dome	Crystal	T °C	pO_2	D	**Age (years)**	Hot	Cold
425	Western	A	889	2.00E-05	2.00E-21	**1.72**	0.61	4.97
425	Western	D	889	2.00E-05	2.00E-21	**2.83**	1.00	8.16
440	Central	A	886	1.84E-05	1.80E-21	**2.28**	0.80	6.60
440	Central	F	886	1.84E-05	1.80E-21	**1.86**	0.65	5.37
440	Central	G	886	1.84E-05	1.80E-21	**1.06**	0.37	3.06
456	Hipaua	C	910	2.85E-05	4.16E-21	**1.13**	0.41	3.13
456	Hipaua	D	910	2.85E-05	4.16E-21	**1.03**	0.38	2.85
456	Hipaua	H	910	2.85E-05	4.16E-21	**1.90**	0.70	5.29
456	Hipaua	I	910	2.85E-05	4.16E-21	**0.23**	0.09	0.65
456	Hipaua	L	910	2.85E-05	4.16E-21	**1.47**	0.54	4.09
477	Trig M	A	909	6.00E-05	5.92E-21	**0.04**	0.01	0.10
527	Main	B	951	4.14E-06	4.30E-21	**0.45**	0.16	1.31
527	Main	M	951	4.14E-06	4.30E-21	**0.73**	0.26	2.16

Hot and cold represent 1 standard error of time based on the temperature standard errors of: amphibole ±22 °C and two-pyroxene ±30 °C and amphibole oxygen fugacity error of ±0.22 log units. Hot temperature and high pO_2 yields the lowest age whereas low temperature and low fO_2 results in maximum ages.

3.1.3 PLAGIOCLASE

Plagioclase is abundant in the Tauhara Dacite Complex representing up to 70 modal % of total phenocrysts. Crystal lengths range in size up to 7 mm (Trig M Dome). Plagioclase crystals are typically oscillatory zoned with anorthite (An) rich cores. Multiple disequilibrium features are observed in the same sample with varying degrees of resorption. Representative images of plagioclase phenocrysts are presented in Figure 3.13. Crystal 425-ZO has an An-rich core with resorbed and oscillatory zoning. Sponge sieved texture is evident in the core of 440-I. Phenocryst 456-H shows a completely sieved textured plagioclase with an An-rich rim. This entirely sieved texture is referred to as “dusty” by Worthington (1985). Plagioclase 477-W has plagioclase phenocrysts with resorbed rims. 483-ZD is similar to 477-W but has an extra An-rich rim. Perfect oscillatory zoning with no disequilibrium textures is seen in plagioclase 527-K.

3.1.3.1 PLAGIOCLASE MAJOR ELEMENT DATA

A feldspar ternary diagram is displayed in Figure 3.14 showing rim and core analyses for plagioclase from each dome. There is no systematic variation between domes with all plagioclase falling within a field of $Ab_{0\text{-}75}Or_{0\text{-}15}An_{20\text{-}100}$ with high anorthite ($>An_{70}$) plagioclase absent in Western, Central and Main Dome. Rim analyses for Western, Central and Hipaua Dome plagioclase have a higher orthoclase content than the cores in contrast to Trig M,

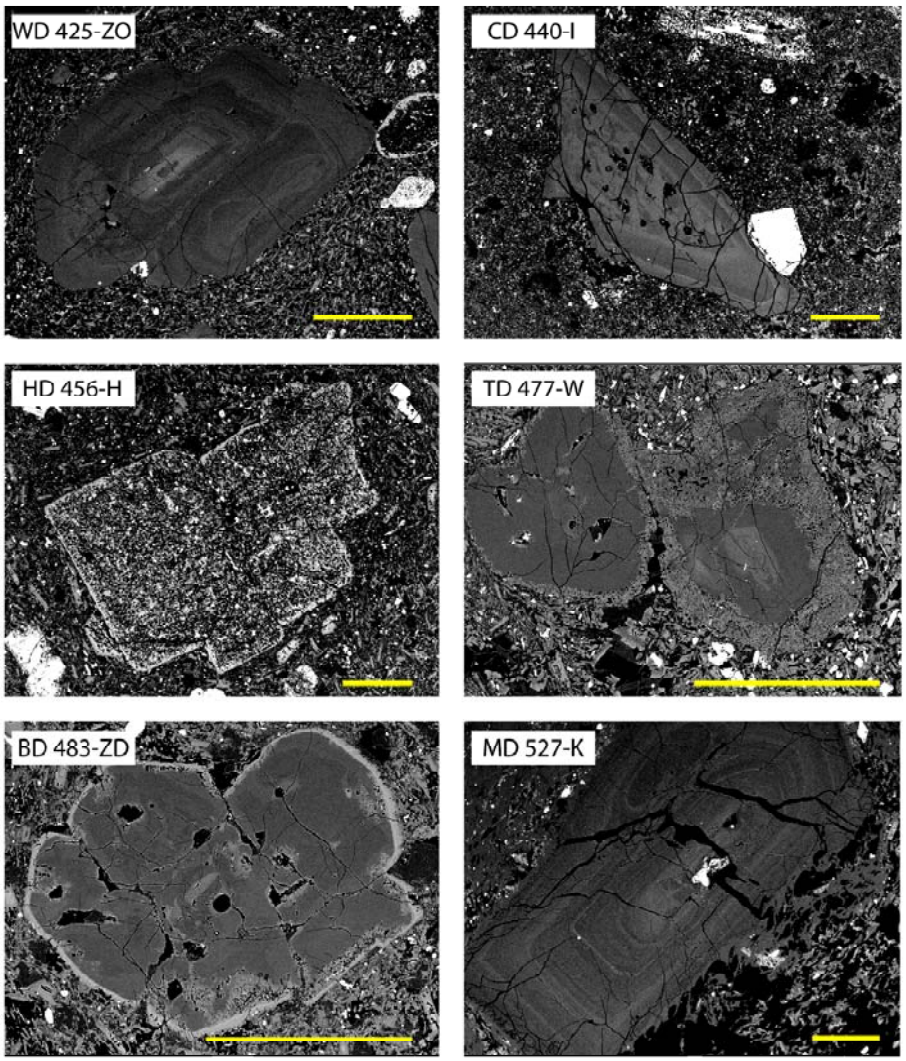

Figure 3.13: BSE images of representative plagioclase phenocrysts from the Tauhara volcano showing variable degrees of disequilibrium textures. Yellow scale bars are 500 µm in length. WD: Western Dome, CD: Central Dome, HD: Hipaua Dome, TD: Trig M Dome, BD: Breached Dome, MD: Main Dome.

Breached and Main Dome plagioclase where there is no difference between cores and rims. An# histograms are presented in Figure 3.15 showing analyses of rim, middle and core zones for plagioclase from the Tauhara volcano. The An# distribution is unimodal with the peaks of all domes falling between An# = 24-36 with no systematic variations between domes or zones.

3.1.3.2 PLAGIOCLASE TRACE ELEMENT DATA

Average chondrite-normalised trace element data for plagioclase phenocrysts from each dome are presented in Figure 3.16. Ba is greatly enriched with Ba_N ~ 100 and the LREE decrease from La_N ca. 12 to Sm_N ca. 1 with the exception of Eu_N ca. 12. There is no systematic variation in plagioclase trace element chemistry between domes.

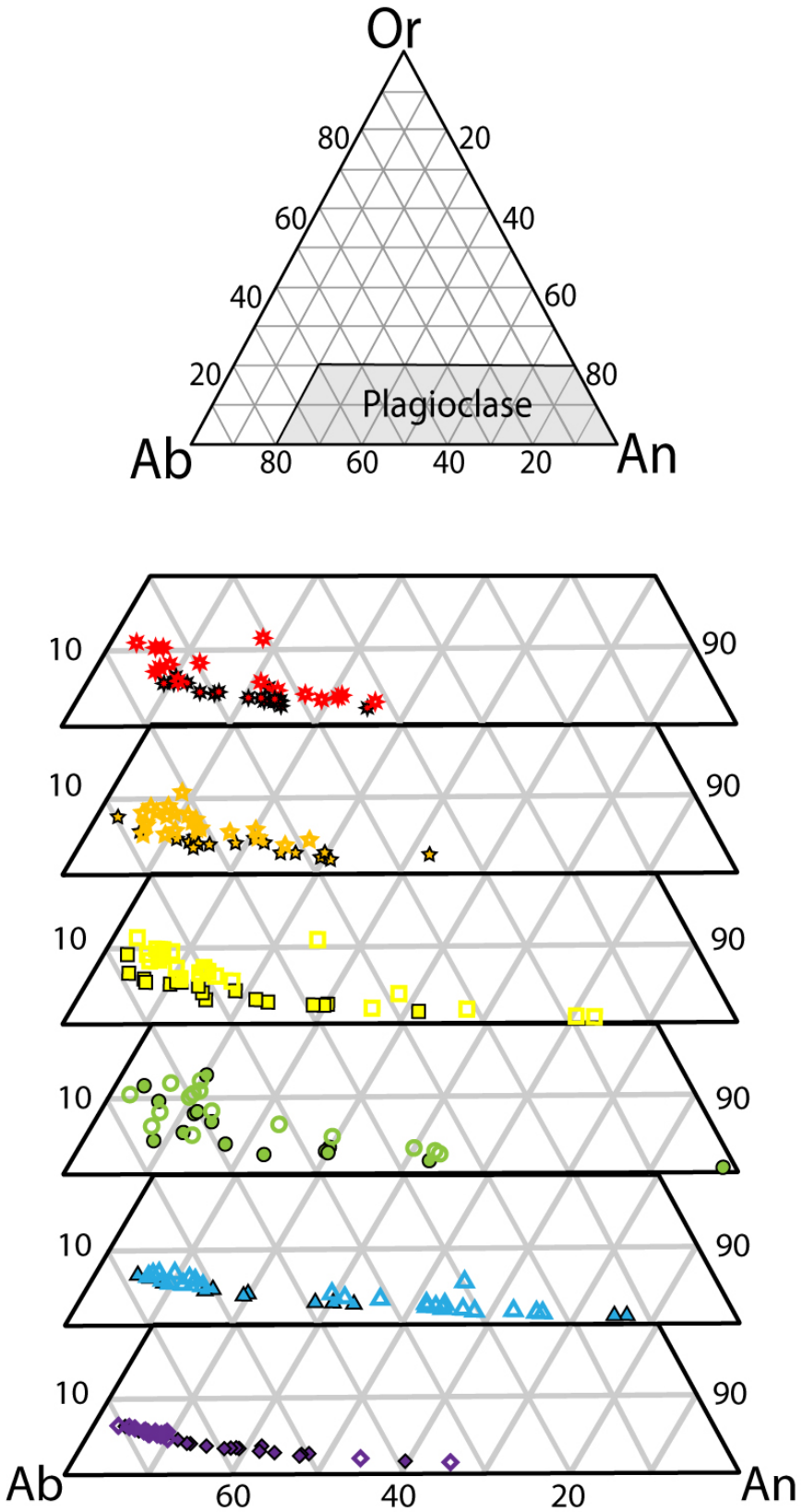

Figure 3.14: Feldspar ternary diagram showing plagioclase phenocryst data for core and rim zones. Symbols are the same as Figure 3.7.

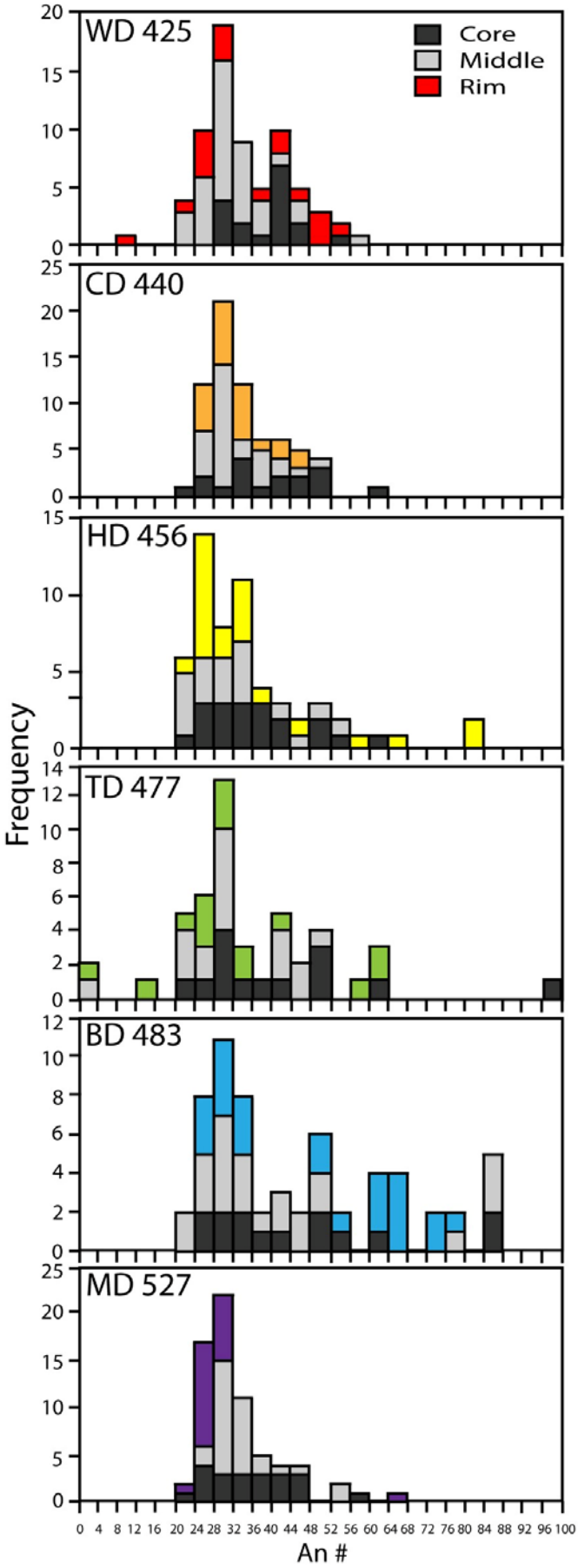

Figure 3.15: An# histograms showing analyses of core, middle and rim zones of plagioclase phenocrysts from the Tauhara volcano.

Plagioclase trace element concentrations are plotted versus An# in Figure 3.17. Trace elements such as Sr, Ba, Rb and Eu correlate with An# as expected with Pb also showing covariance. There is no systematic variation between domes for these elements. In contrast, Li shows no co-variation with An# (with the exception of Breached Dome plagioclase with An# > 60) and clear differences between domes are observed. Hipaua Dome plagioclase crystals have high Li concentrations with ca. 55 ppm Li in contrast to plagioclase crystals from Hipaua Dome which have ca. 40 ppm Li. Main and Breached Dome plagioclase have the lowest Li concentrations (ca. 25 ppm). Western Dome plagioclase Li concentrations extend the range of both Hipaua and Central Dome plagioclase (30-60 ppm). Similarly Trig M Dome plagioclases overlap the Li concentrations of Central, Breached and Main Dome plagioclase (20-50 ppm).

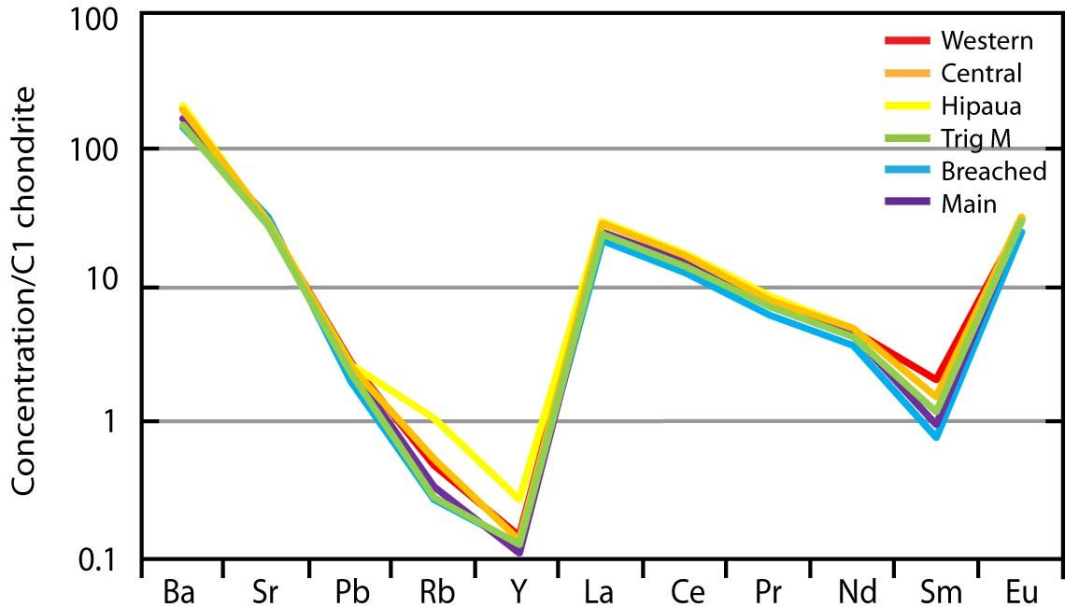

Figure 3.16: Chondrite-normalised (Sun and McDonough, 1989) multi-element plot showing dome-averaged chondrite-normalised trace element data for plagioclase from the Tauhara volcano.

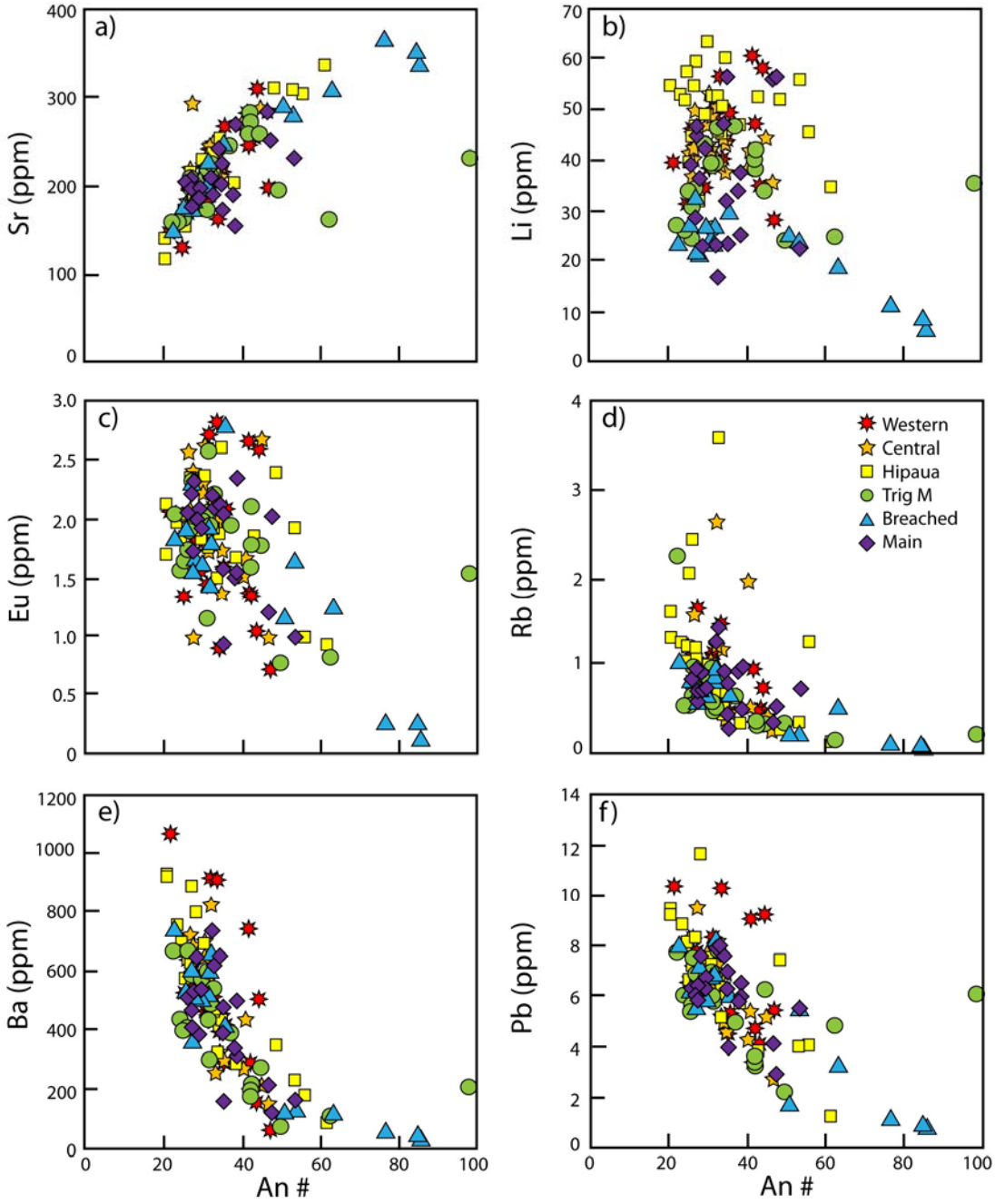

Figure 3.17: Trace element data plotted versus An# for plagioclase phenocrysts of the Tauhara volcano.

3.1.4 QUARTZ

Quartz comprises 0-22 modal % of total phenocrysts of the Tauhara volcano with the highest abundance of quartz present in the most acidic dacites. Quartz is present in two main sizes: 1 mm (small) or > 2 mm (large). TiO_2 zoning is prevalent with resorption evident between zones. Quartz crystals are typically anhedral and reversely zoned with Ti-rich rims. Melt inclusions and oscillatory zoning are also common in the large crystals.

3.1.4.1 QUARTZ DIFFUSION MODELLING

Rim zones have been modelled using the 1-D strategy of Morgan et al. (2004). Amphibole rim temperatures (section 3.1.4) were utilised. Diffusion coefficients were calculated using the method of Cherniak et al. (2007). Modelled quartz phenocrysts are presented in Figure 3.18. Diffusion ages with temperature and diffusion coefficients are given in Table 3.5. Western Dome quartz rims yield ages of 0.3 to 0.5 yr compared to Central Dome which yield ages of ca. 0.75 yr. Trig M Dome quartz rims yield ages less than 0.3 yr and Breached Dome quartz rims yield ages less than 0.25 yr. Only one quartz rim from Main Dome was satisfactory for diffusion modelling and provides an age of 0.25 yr.

Table 3.5: Quartz rim diffusion ages of the Tauhara volcano.

Sample	Dome	Crystal	T (°C)	D	**Age (years)**	Hot*	Cold*
425	Western	bH	889	3.76E-20	**0.30**	0.18	0.58
425	Western	bO	889	3.76E-20	**0.51**	0.30	0.93
425	Western	bW	889	3.76E-20	**0.33**	0.20	0.61
440	Central	bM	886	3.49E-20	**0.76**	0.44	1.41
440	Central	sT	886	3.49E-20	**0.74**	0.43	1.37
477	Trig M	bG	945	1.38E-19	**0.34**	0.22	0.56
477	Trig M	sH	945	1.38E-19	**0.24**	0.15	0.39
477	Trig M	sI	945	1.38E-19	**0.06**	0.04	0.10
477	Trig M	sL	945	1.38E-19	**0.08**	0.05	0.14
477	Trig M	sQ	945	1.38E-19	**0.07**	0.05	0.11
477	Trig M	sY	945	1.38E-19	**0.22**	0.14	0.36
483	Breached	bM	904	5.39E-20	**0.25**	0.15	0.44
483	Breached	sP	904	5.39E-20	**0.22**	0.15	0.39
483	Breached	bR	904	5.39E-20	**0.19**	0.11	0.34
527	Main	sY	894	4.24E-20	**0.25**	0.15	0.46

* Hot and cold represent 1 standard error of time based on the temperature standard errors of amphibole thermometry ±22 degrees. Hot temperature yields the lowest age whereas low temperature results in maximum ages.

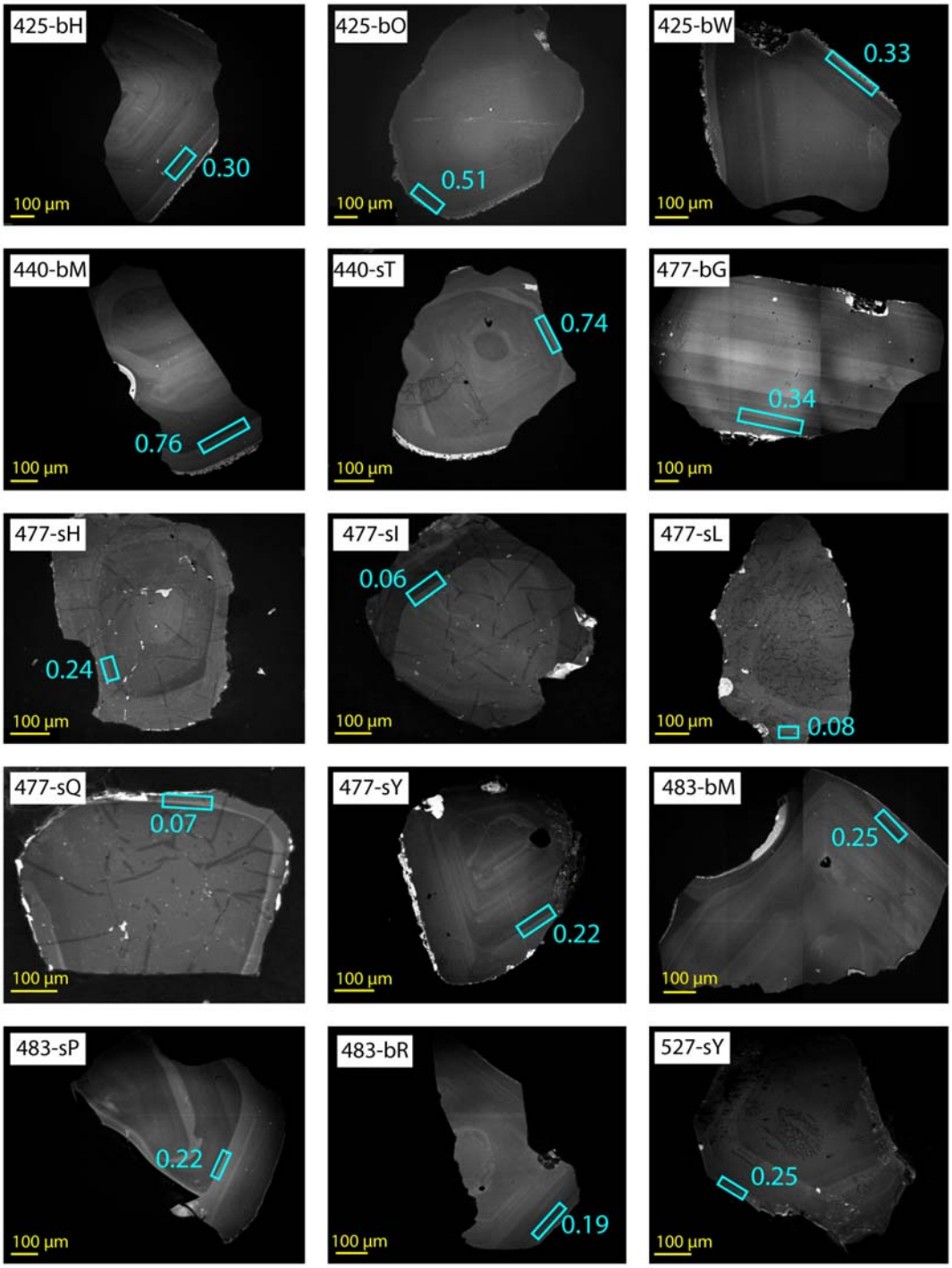

Figure 3.18: Cathodoluminescence images of diffusion modelled quartz phenocrysts from the Tauhara volcano. Blue boxes show modelled zone boundaries. Ages are in years.

3.1.5 Fe-Ti OXIDES

Fe-Ti oxides are common in the Tauhara dacites as individual phenocrysts, hosted by other phenocrysts (clinopyroxene, amphibole and plagioclase) and groundmass microlites. Titanomagnetite is more abundant than ilmenite in all forms. Individual oxide phenocrysts and phenocryst hosted oxides are both typically 100 – 500 µm in diameter. Groundmass oxide microlites have diameters of 2-20 µm. Oxide images are displayed in Figure 3.19.

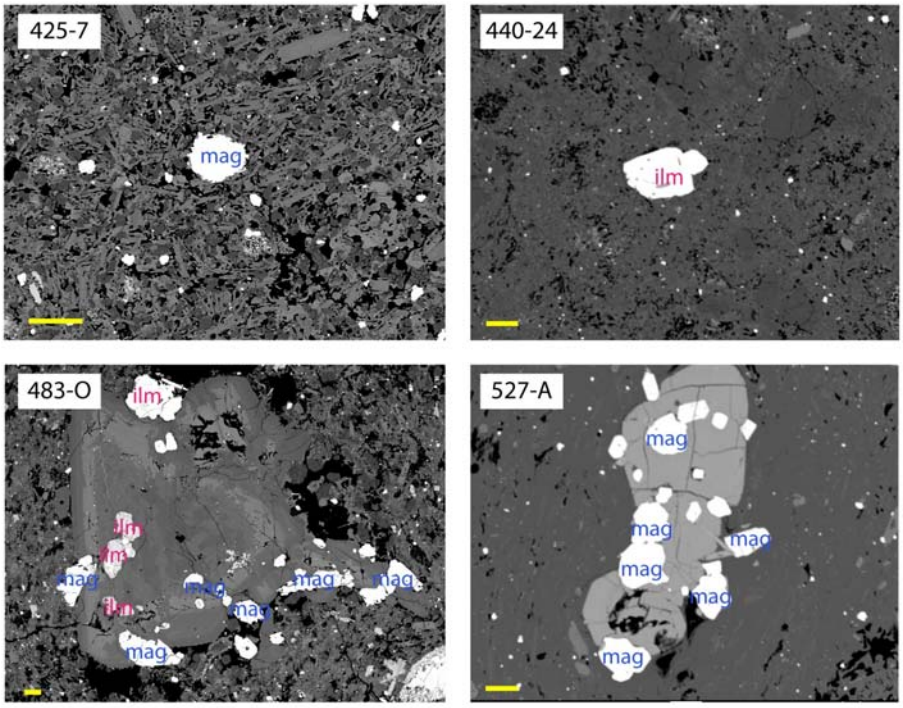

Figure 3.19: BSE images of ilmenite and titanomagnetite phenocrysts in groundmass (425-7 and 440-24) and hosted in plagioclase (483-O) and clinopyroxene (527-A). Yellow scale bars are 100 µm in length. Abundant oxide microlites are visible in all images.

3.1.5.1 Fe-Ti OXIDE MAJOR ELEMENT DATA

Ilmenite and titanomagnetite major element data are plotted in an oxide ternary diagram in Figure 3.20. Ilmenite crystals plot on the ilmenite-rhombic boundary and extend towards the cubic line (red shade field). Conversely, titanomagnetite crystals plot on the magnetite-cubic boundary and extend towards the rhombic line. Magnetites are present in two populations: low-Ti with 0 -15% TiO_2 marked by the blue shaded field and high-Ti with 20-30% TiO_2. High-Ti magnetites are only present in Western, Central, Hipaua and Breached Domes and are phenocrysts. Microlitic magnetite (black solid symbols) have similar chemistries to the large low-Ti phenocrysts for Central, Hipaua, Trig M and Breached Domes where as the microlites are richer in TiO_2 for Western Dome and TiO_2-poor for Main Dome. Ilmenite microlites were only found in Western, Hipaua and Main Domes where they have lower TiO_2 than the large phenocrysts.

3.1.5.2 Fe-Ti OXIDE THERMOMETRY AND OXYBAROMETRY

Fe-Ti oxide thermometry was applied to ilmenite-magnetite pairs in equilibrium using the Ghiorso and Evans (2008) thermometer. Equilibrium was verified using the Mg-Mn test of Bacon and Hirschmann (1988). Fe-Ti oxide thermometry utilises the temperature dependent exchange of of Fe^{2+} + Ti^{4+} for $2Fe^{3+}$ between ilmenite and magnetite phases whereas oxygen fugacity is determined by the magnetite-haematite iron redox reaction. Details of the Fe-Ti oxide thermometry and equations are given in Appendix A6.4. Fe-Ti oxide temperatures and oxygen fugacities are given in Table 3.6. Oxide pairs are divided into groundmass and phenocryst hosted types. Temperature versus oxygen fugacity is presented in Figure 3.21. Central and Hipaua Dome phenocryst hosted oxides yield temperatures and fO_2 between 680-755 °C and -14 to -16 logfO_2. Western and Hipaua Dome groundmass oxides have higher temperatures with 790–810 °C and -12 to -13 logfO_2. Trig M Dome phenocryst hosted oxides have the highest temperatures with 880-895 °C and -10.7 to -11.5 logfO_2. All Western, Central, Hipaua and Trig M Domes have oxygen fugacities ~NNO+1. Both Main Dome groundmass and phenocryst hosted oxides align with the NNO with temperatures between 770–900 °C.

Table 3.6: Fe-Ti oxide temperatures and oxygen fugacities.

Groundmass

Sample	Dome	Ilmenite*	Magnetite*	T (°C)	ΔNNO	log fO_2
425	Western	s5	s1	804	1.58	-12.24
425	Western	s7	s9	812	1.55	-12.10
456	Hipaua	s2	s10	790	1.21	-12.91
527	Main	s1	s8	860	0.03	-12.67
527	Main	s10	s8	899	0.31	-11.67
527	Main	L18	L17	767	0.26	-14.37

*s: microlite; L: phenocryst

Crystal hosted pairs

Sample	Dome	Host	Ilmenite	Magnetite	T (°C)	ΔNNO	log fO_2
440	Central	amphibole	4	3	724	1.49	-14.15
440	Central	amphibole	8	7	697	1.24	-15.09
440	Central	amphibole	18	17	741	1.25	-13.98
440	Central	clinopyroxene	23	22	741	1.22	-14.01
456	Hipaua	clinopyroxene	2	3	682	0.99	-15.73
456	Hipaua	clinopyroxene	20	19	755	0.94	-13.96
477	Trig M	clinopyroxene	6	7	895	1.01	-11.04
477	Trig M	clinopyroxene	15	16	884	0.77	-11.48
477	Trig M	amphibole	17	18	911	1.02	-10.75
527	Main	clinopyroxene	13	14	776	0.20	-14.22

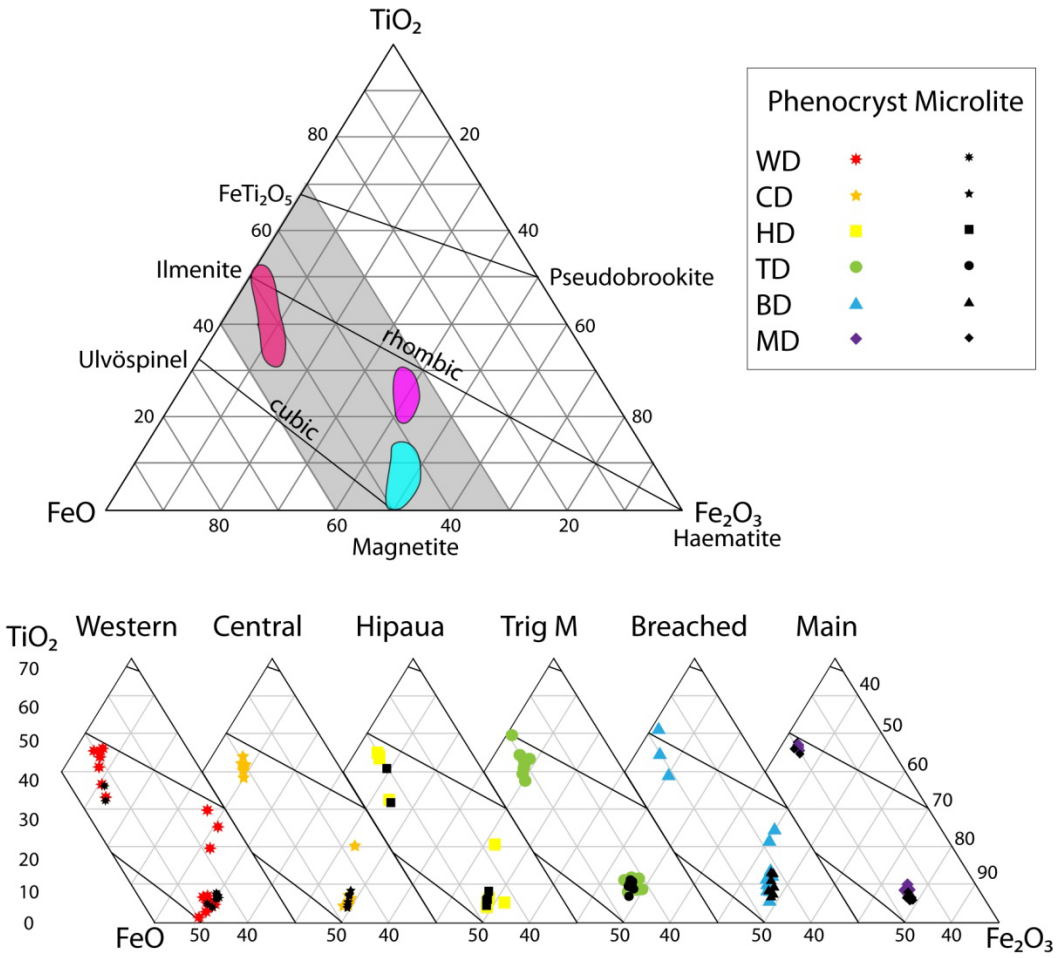

Figure 3.20: Fe-Ti oxide ternary diagram showing ilmenite and titanomagnetite data for both phenocryst and microlite oxides of the Tauhara volcano.

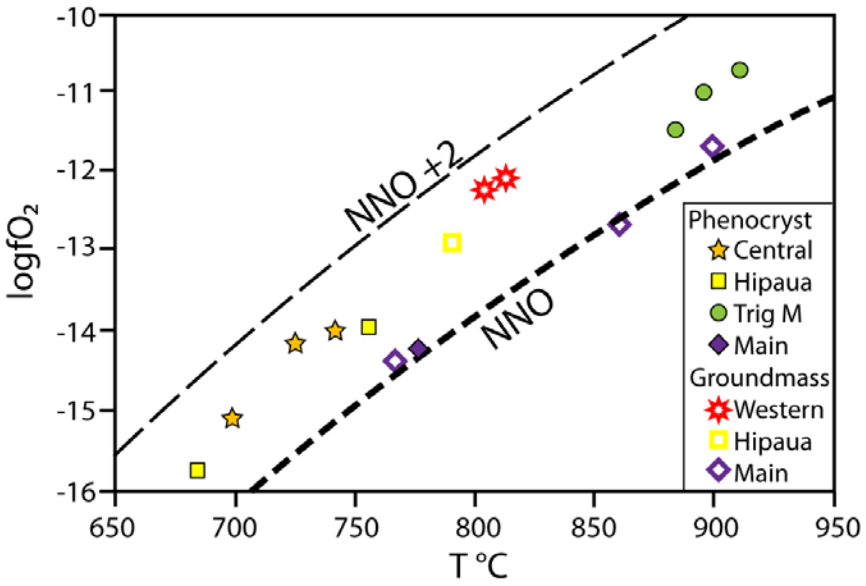

Figure 3.21: Fe-Ti oxide temperatures and oxygen fugacities calculated from the Ghiorso and Evans (2008) thermometer. NNO buffers from O'Neill and Pownceby (1993).

Dome average temperatures for the oxides and the thermometers used in this thesis is presented in Table 3.7. Main Dome is divided into two populations: the high and low temperatures groups identified in amphibole and oxide thermometry. Amphibole and two-pyroxene temperatures are within error of each other and the oxide temperatures from Trig M and Main Domes. Oxide thermometry for Western, Central and Hipaua Dome reveal temperatures outside of uncertainties of amphibole and two-pyroxene temperatures and are 80°, 160° and 170 °C lower, respectively.

Table 3.7: Dome average temperatures from thermometers used in this thesis.

Dome	**Amphibole rims** (°C, ±22 s.d.)	**Two-pyroxene rims** (°C, ± 66 aad)	**Fe-Ti oxide** (°C, ±44 aad)
Western	889		808
Central	886		726
Hipaua	915	910	742
Trig M	946	909	897
Breached	904	933	
Main H	895	951	899
Main L	796 (c)		772

Main L: Amphibole rims and low temperature oxide population, Main H: amphibole cores and high temperature oxide population.

3.2 WHOLE ROCK CHEMISTRY

3.2.1 WHOLE ROCK AND MELT INCLUSION MAJOR ELEMENT DATA

Whole rock XRF data from the Tauhara volcano (Worthington, 1985) plot in the dacite field, just extending into the rhyolite field on a TAS classification diagram (Le Bas et al., 1986) (Figure 3.22). There is a strong positive correlation between total alkalis and SiO_2 with $Na_2O + K_2O$ ranging between 64.6–71.5 wt % and 5.4 – 6.4 wt %, respectively. The different domes have overlapping compositions in Figure 3.22. Quartz-hosted melt inclusions from the TDC have been analysed by EPMA (this study) and plot within the rhyolite field with SiO_2 = 75.5 – 80.7 wt % and total alkalis = 6.7 - 9.5 wt %. Overall there is a negative trend for the melt inclusions with $Na_2O + K_2O$ in Western, Central and Trig M Dome melt inclusions being greater than in Main, Hipaua and Breached Dome melt inclusions. Hipaua and Breached Dome melt inclusions have the lowest total alkalis, however only one melt inclusion per dome was analysed. Dome averages for the Tauhara dacites and quartz-hosted melt inclusions are presented in Tables 3.8 and 3.9, respectively.

Mafic igneous rocks previously studied in association with the Tauhara volcano are also shown in Figure 3.22. These mafic samples include basaltic andesite to dacite xenoliths collected and

analysed by Worthington (1985); microdiorite enclaves collected from Hipaua Dome and analysed by Cole et al. (2001) and the Rolles Peak andesite located 5 km northeast of the Tauhara volcano, collected and analysed by Worthington (1985). The Kakuki basalt, which is one of the most primitive basalts found in the TVZ (Gamble et al., 1993) is also plotted as a reference. Of these mafic rocks, the Tauhara dacites appear to fall on a linear array between the most silica rich quartz-hosted melt inclusions, the Rolles Peak andesite, the Kakuki basalt and two quartz-microdiorite enclaves. All other mafic materials lie significantly above this trend.

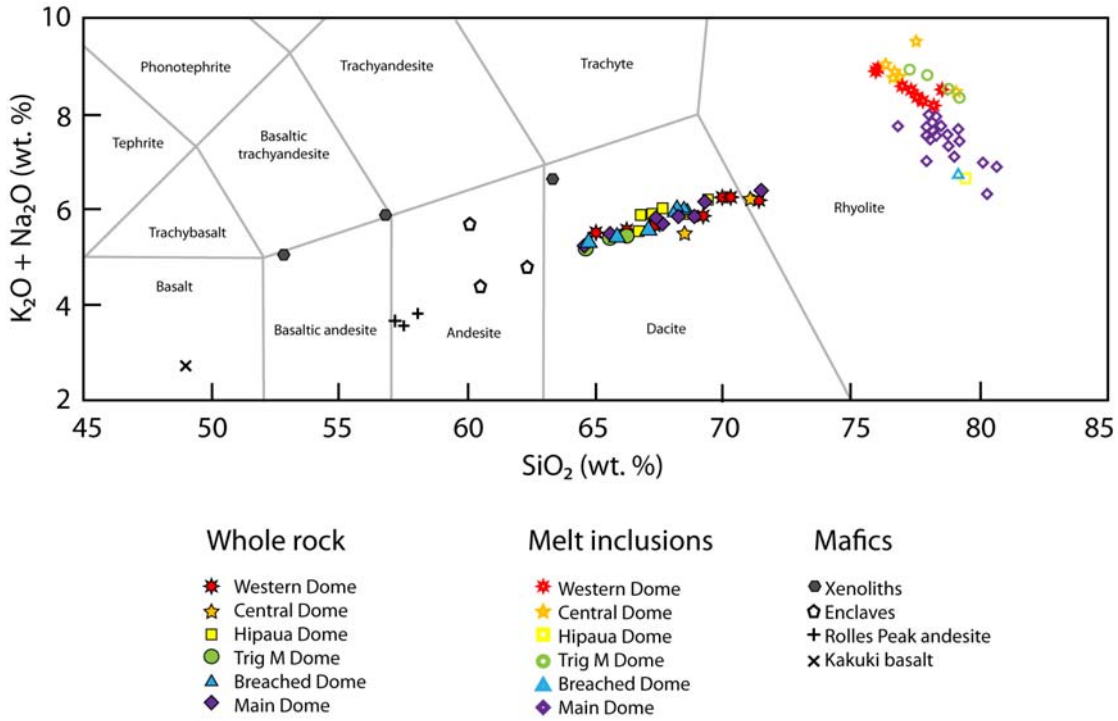

Figure 3.22: Total alkalis ($K_2O + Na_2O$) versus SiO_2 classification diagram showing the composition of Tauhara dacites (Worthington, 1985) and quartz-hosted melt inclusions (this study). Mafic igneous rocks referred to in this study are also plotted and include xenoliths and Rolles Peak andesites (Worthington, 1985), enclaves from Hipaua Dome (Cole et al., 2001) and Kakuki basalt (Graham et al., 1993).

Table 3.8: Average whole rock XRF data for the Tauhara volcano domes (from Worthington, 1985).

Dome	Western	Central	Hipaua	Trig M	Breached	Main
n	*7*	*2*	*6*	*3*	*7*	*8*
SiO_2 (wt. %)	68.45	69.77	67.70	65.46	67.25	67.86
TiO_2	0.36	0.35	0.37	0.44	0.40	0.41
Al_2O_3	14.94	14.66	14.76	15.73	15.05	14.68
Fe_2O_3	3.74	3.48	4.20	5.04	4.45	4.23
MnO	0.07	0.08	0.08	0.10	0.09	0.08
MgO	2.16	1.68	2.44	2.78	2.36	2.34
CaO	4.34	4.06	4.46	5.02	4.53	4.48
Na_2O	3.60	3.58	3.69	3.43	3.62	3.56
K_2O	2.31	2.28	2.23	1.92	2.17	2.28
P_2O_5	0.08	0.08	0.08	0.08	0.08	0.09
LOI	0.77	0.85	0.33	0.90	1.09	1.39
Original total	99.79	99.90	99.89	99.84	99.77	99.90
Total alkali	5.91	5.86	5.93	5.34	5.78	5.84

Table 3.9: Average quartz-hosted melt inclusion EPMA data from the Tauhara volcano domes.

Dome	Western	Central	Hipaua	Trig M	Breached	Main
n	*11*	*6*	*1*	*4*	*1*	*20*
SiO_2 (wt. %)	77.30	77.21	79.48	78.35	79.19	78.67
TiO_2	0.10	0.11	0.06	0.06	0.06	0.10
Al_2O_3	12.27	12.40	12.11	11.45	11.80	11.83
FeO	1.11	0.82	0.35	0.90	1.27	1.04
MnO	0.02	0.03	0.00	0.03	0.03	0.04
MgO	0.07	0.05	0.00	0.06	0.06	0.10
CaO	0.61	0.48	1.35	0.50	0.82	0.76
Na_2O	3.13	2.96	3.88	3.23	2.88	3.45
K_2O	5.38	5.94	2.77	5.42	3.88	4.02
Total	99.26	99.70	100.30	98.43	100.29	95.88
Total alkali	8.52	8.91	6.65	8.65	6.76	7.47

Note: Oxides are normalised to 100 wt. %. Total refers to average original analytical total.

Major element data for the Tauhara dacites are presented Harker diagrams (Figure 3.23) for the 33 representative samples studied in this thesis. Total SiO_2 ranges between 64.6 - 71.5 wt % with both Western and Main Domes spanning this entire range. Only two samples were collected from Central Dome which have 68.5 and 71.0 SiO_2 wt %. Hipaua Dome samples show a smaller SiO_2 range between 66.7 - 69.4 wt %. Trig M Dome samples show a smaller variation in SiO_2 (64.6 - 66.2 SiO_2 wt %) but with values more mafic than Hipaua Dome. Samples from the Breached Dome edifice have SiO_2 contents comparable to the Trig M dome falling between 64.7-67.0 wt % whereas samples from the Breached Dome pyroclastic flow are tightly clustered between 75.5-80.7 SiO_2 wt %.

Major element oxides correlate strongly and generally linearly, with SiO_2. A negative trend between SiO_2 and TiO_2, Al_2O_3, FeO_{Tot}, MgO and CaO is observed whereas the alkalis Na_2O and K_2O show positive trends. The different domes have overlapping arrays for Na_2O, K_2O, CaO and MgO in contrast to TiO_2, Al_2O_3 and FeO_{Tot} where two subparallel arrays are observed. Main Dome and Breached Dome edifice samples form the high array for TiO_2 where the low TiO_2 array is comprised of Western, Central and Hipaua Dome samples. Samples from the Breached Dome pyroclastic flow plot separately, below the lowest TiO_2 trend. Trig M Dome samples fall on both TiO_2 arrays. Al_2O_3 versus SiO_2 compositions show the high Al_2O_3 array comprising of Trig M, Western, Central and Breached Dome pyroclastic flow samples, whereas Breached Dome edifice samples and the samples from Main and Hipaua Domes form the lower Al_2O_3 array. Samples from Western and Central Dome comprise the low FeO_{Tot} array, in contrast to Hipaua, Trig M, Breached (both edifice and pyroclastic flow) and Main Dome samples which form the high FeO_{Tot} array.

Quartz-hosted melt inclusion major element data are shown in Figure 3.24. SiO_2 ranges between 75.5–80.7 wt % for all melt inclusions. Two populations of melt inclusions can be

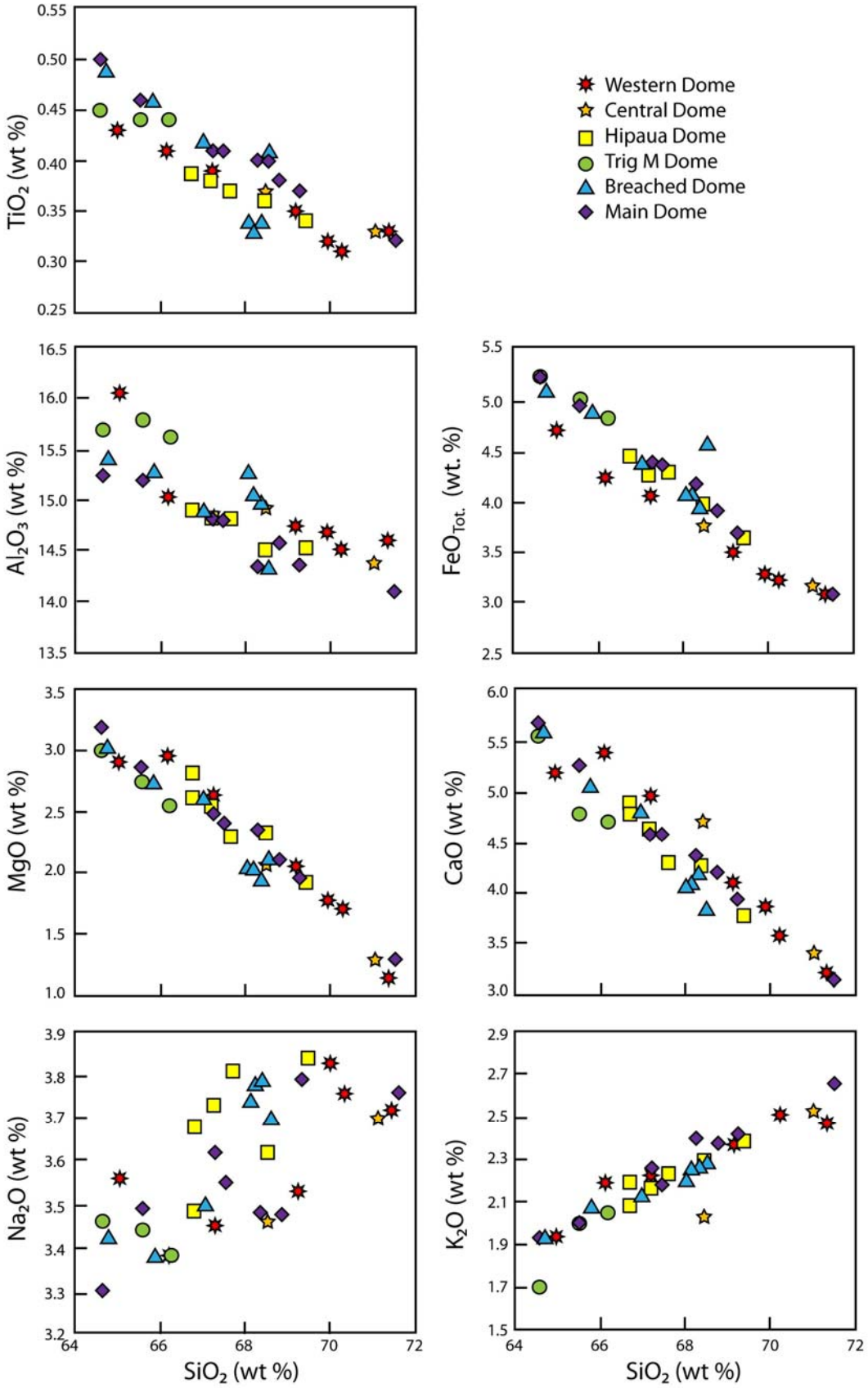

Figure 3.23: Harker diagrams for the Tauhara dacites (Worthington, 1985).

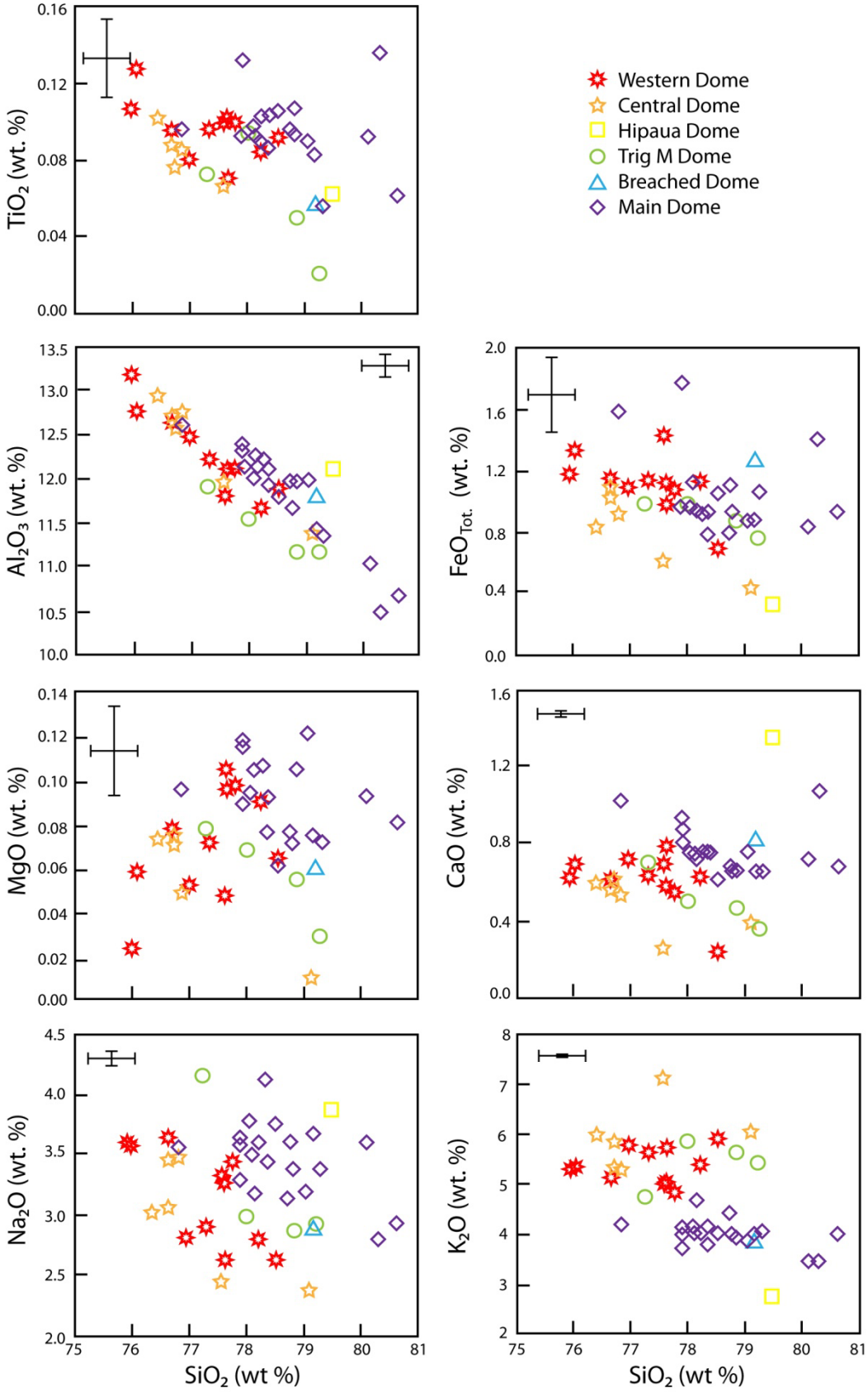

Figure 3.24: Major element data plotted versus SiO_2 for quartz-hosted melt inclusions in the Tauhara dacites. Error bars are 2 s.d.

identified: Western, Central and Trig M dome inclusions have 75.5–79.4 SiO_2 and Main, Hipaua and Breached Dome inclusions have 77.5–79.5 SiO_2 with outliers extending to 76.8–80.7 wt. %. For essentially the same SiO_2 range, Western, Central and Trig M Dome inclusions have K_2O > 4.7 wt % whereas Main, Hipaua and Breached Dome inclusions have K_2O < 4.6 wt %. In addition, two subparallel arrays are observed for Al_2O_3 where Main, Hipaua and Breached Domes have higher Al_2O_3 than Western, Central and Trig M domes for a given SiO_2. A broad scatter is observed in Na_2O where for a given SiO_2, Main, Breached and Hipaua Dome inclusions have higher Na_2O than the inclusions from Western and Central Domes with Trig M Dome inclusions straddling the groups. Both populations of melt inclusions show no clear variations in TiO_2, FeO_{Tot} and CaO relative to SiO_2.

Major element variations of the Tauhara dacite whole rocks are shown in Figure 3.25 for FeO_{Tot}, Al_2O_3 and CaO in relation to the rhyolitic melt inclusions and the mafic samples highlighted in Figure 3.1. The Tauhara dacites define a linear array between the inclusions and the enclaves and xenoliths. The Kakuki basalt falls below this trend for both Al_2O_3 and FeO_{Tot} and the Rolles Peak andesite lies above this trend for Al_2O_3.

3.2.2 WHOLE ROCK AND MELT INCLUSION TRACE ELEMENT DATA

Dome averages of whole rock trace element data for the Tauhara dacites and quartz-hosted melt inclusions are presented in Tables 3.10 and 3.11, respectively, with all data listed in Appendices 3 and 4. Trace element concentrations normalised to N-MORB and chondrite (Sun and McDonough, 1989) are shown in Figure 3.26. The Tauhara dacites have a typical subduction signature with enrichments in fluid-mobile large ion lithophile elements (Cs-K and Pb) relative to N-MORB (Figure 3.26a). The high field strength elements (HFSE) (Nb, Ta, and Ti) also show negative anomalies typical of subduction zone volcanism. There is no discernable difference in trace elements relative to N-MORB between the domes of the TDC except for Sr where Western and Central domes have significantly higher Sr concentrations than Main, Breached, Trig M and Hipaua Domes. The averaged quartz-hosted melt inclusion composition overlaps the whole rock data with the exception of the elements Cs-U which are enriched and Eu, Ti and Sr which are depleted.

Rare earth element (REE) data (Figure 3.26b) of Tauhara dacite whole rocks normalised to chondrite are enriched in the light REE (LREE) (La –Nd) (100 x chondrite) and decrease to 10 x chondrite for the heavy REE (HREE) (Dy-Lu). A slight U shaped pattern is evident in the middle

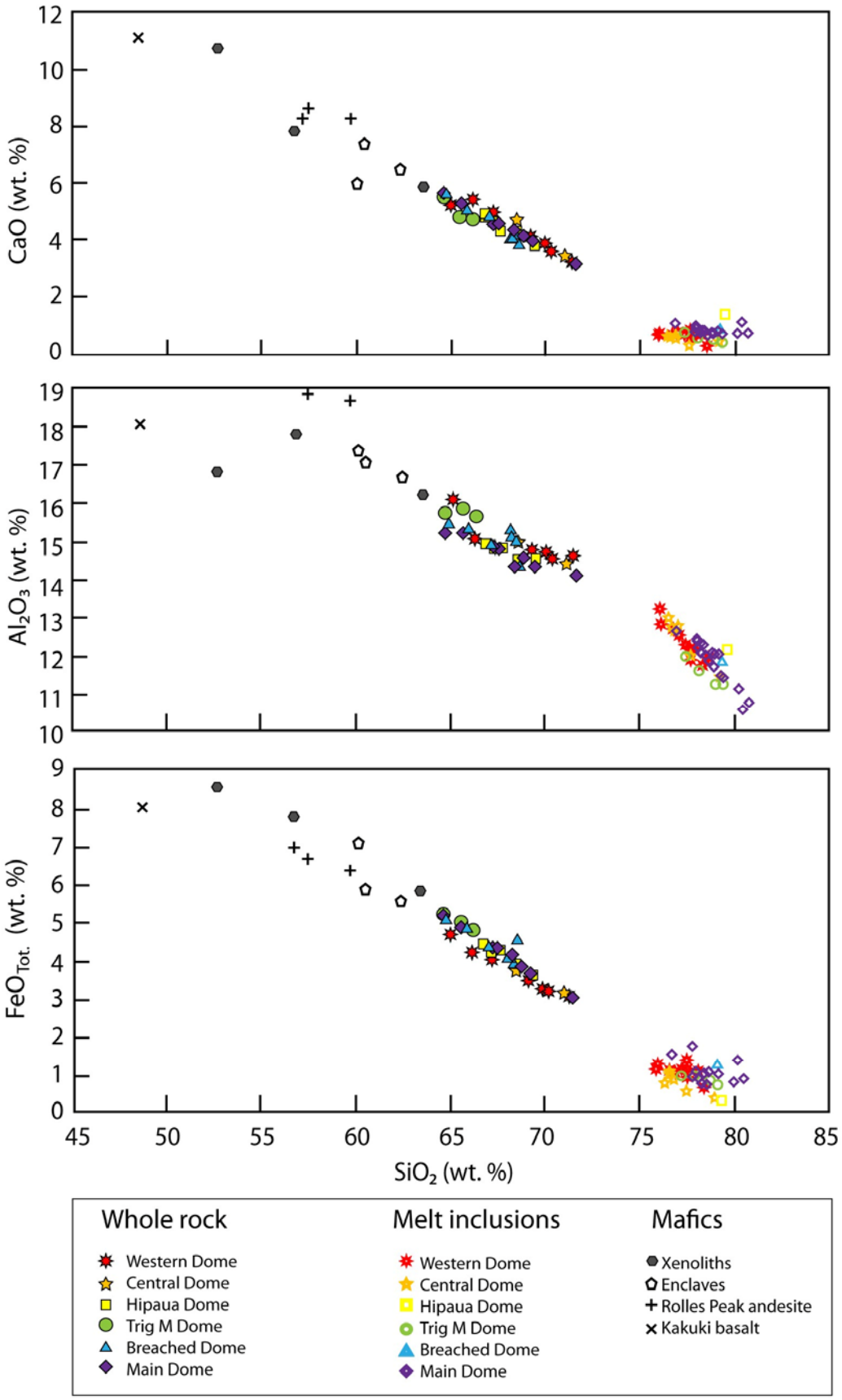

Figure 3.25: CaO, Al_2O_3 and FeO_{Tot} plotted versus SiO_2 showing data for the Tauhara dacite whole rocks (Worthington, 1985) and the quartz-hosted melt inclusions (this study). The Tauhara dacites define a linear trend between the rhyolitic melt inclusions and a more mafic end-member represented by the enclaves (Cole et al., 2001), xenoliths and Rolles Peak andesite (Worthington, 1985) and Kakuki basalt (Graham et al., 1995).

Table 3.10: Average dome whole rock trace element data from the Tauhara volcano.

Dome	Western	Central	Hipaua	Trig M	Breached	Main
n	*7*	*2*	*6*	*3*	*7*	*8*
Sc (ppm)	10.1	8.15	10.8	12.3	12.1	12.4
V	58.9	55.7	76.6	102	78.3	79.0
Cr	42.9	28.4	42.9	32.5	31.7	37.6
Ni	31.3	17.8	31.5	31.2	16.4	18.5
Cu	37.7	30.6	17.2	20.4	16.4	16.5
Zn	44.4	47.0	49.1	57.6	52.6	52.0
Ga	16.3	n.m.	15.8	16.7	18.2	15.3
Rb	64.7	65.3	65.1	50.9	64.1	66.6
Sr	502	472	301	360	302	283
Y	15.3	14.1	16.4	14.9	17.0	18.3
Zr	91.4	77.8	83.1	82.1	91.7	95.8
Nb	5.31	5.05	4.84	4.54	5.29	5.39
Mo	0.609	0.663	0.704	0.929	0.891	0.983
Cs	2.19	2.34	2.17	1.78	2.78	3.02
Ba	563	489	474	467	490	492
La	21.2	17.6	16.9	15.1	17.6	17.8
Ce	41.1	36.8	34.0	29.8	35.8	36.2
Pr	4.67	3.84	3.88	3.42	4.04	4.16
Nd	16.9	14.0	14.4	13.0	14.9	15.6
Sm	3.19	2.64	2.93	2.75	3.00	3.17
Eu	0.856	0.704	0.733	0.789	0.802	0.800
Gd	3.17	2.69	2.95	2.76	3.08	3.26
Tb	0.454	0.390	0.450	0.429	0.468	0.496
Dy	2.64	2.30	2.70	2.57	2.85	3.01
Ho	0.531	0.464	0.552	0.526	0.586	0.620
Er	1.60	1.41	1.66	1.58	1.78	1.87
Tm	0.237	0.209	0.248	0.234	0.267	0.280
Yb	1.60	1.40	1.68	1.61	1.81	1.88
Lu	0.244	0.215	0.258	0.248	0.282	0.295
Hf	2.77	2.30	2.45	2.50	2.71	2.71
Ta	0.567	0.484	0.451	0.506	0.704	0.553
Pb	10.5	11.2	9.65	10.4	12.0	10.8
Th	8.32	6.82	7.08	6.88	7.43	7.52
U	1.77	1.53	1.61	1.58	1.65	1.76

n.m: not measured due to analytical error.

REE (MREE) to HREE (Gd-Lu) part of the patterns. Western and Central Domes show steeper REE patterns with both higher LREE and lower HREE relative to the other domes (Hipaua, Trig M, Breached and Maim domes). This is more clearly displayed in Figure 3.26c; $(La/Yb)_N$ versus $(Gd/Yb)_N$ which is a plot of a typical LREE/HREE versus MREE/HREE ratio. Main, Breached, Trig M and Hipaua Domes cluster together between $(La/Yb)_N$: 6.5-7.5 and $(Gd/Yb)_N$: 1.32-1.52 whereas the Western and Central Domes range between 8-11.5 and 1.45-1.78 for $(La/Yb)_N$ and $(Gd/Yb)_N$ respectively. One Breached Dome outlier is present with higher $(La/Yb)_N$ (8.5) in relation to other Breached Dome samples (~6.5) with comparable $(Gd/Yb)_N$. An anomalously high La concentration of 21 ppm in this sample compared to other Breached Dome samples with 15 to 18 ppm La, is responsible for this difference.

Table 3.11: Average dome quartz-hosted melt inclusion trace element data from the Tauhara volcano.

Dome	Western	Central	Main
n	*5*	*1*	*9*
Li (ppm)	397	418	46.2
B	38.0	24.9	27.6
Mg	535	528	777
Ca	0.539	0.520	0.586
Sc	3.51	5.41	4.75
Ti	584	655	762
V	1.39	0.573	2.10
Cr	10.2	b.d.l.	4.76
Mn	268	265	273
Ni	3.77	0.560	1.59
Cu	3.58	1.52	16.0
Zn	43.4	40.2	36.6
Rb	213	161	143
Sr	47.8	29.2	44.4
Y	17.8	17.7	17.9
Zr	83.6	70.5	71.5
Nb	7.71	7.34	6.26
Cs	7.67	7.64	6.93
Ba	599	610	593
La	18.7	18.4	18.7
Ce	48.0	47.2	43.7
Pr	4.36	3.96	4.10
Nd	15.7	12.5	14.7
Sm	2.83	2.40	3.09
Eu	0.327	0.282	0.276
Gd	2.95	1.96	2.21
Tb	0.490	0.371	0.359
Dy	3.63	2.27	2.49
Ho	0.779	0.464	0.515
Er	1.69	1.67	1.56
Tm	0.306	0.328	0.246
Yb	2.30	1.94	2.14
Lu	0.211	0.383	0.314
Hf	2.60	1.99	2.22
Ta	0.747	0.644	0.680
W	2.06	1.61	1.42
Pb	17.5	17.6	15.9
Th	12.2	11.0	11.6
U	3.50	3.82	3.31

b.d.l.: below detection limits.

Trace element data are presented in Figure 3.27 for the Tauhara dacites, in addition to those for the rhyolitic melt inclusions and the mafic igneous rocks highlighted in Figures 3.22 and 3.25. Compatible elements V and Ni show strong linear negative trends with SiO_2. This trend is evident for other compatible elements such as Cr and Sc. The Tauhara dacites fall on a linear array between the rhyolitic melt inclusions and the Kakuki basalt and quartz-microdiorite enclaves. Various different trends in Ni are observed between domes. Western and Hipaua Domes form a steeper array between the melt inclusions and the Kakuki basalt whereas Breached and Main Dome trend between the quartz-microdiorite enclaves and the melt inclusions.

The incompatible elements Ba, Th and Pb have scattered positive correlations with SiO_2 where the Tauhara dacites plot between the melt inclusions with high very incompatible element (VICE) concentrations and mafic igneous rocks with lower VICE concentrations.

Sr defines two different linear arrays with SiO_2 where Western and Central Domes show a strong negative trend with Sr concentrations declining from 650 to 380 ppm with increasing SiO_2. This array falls between the melt inclusions and a high Sr mafic rock represented by the Rolles Peak

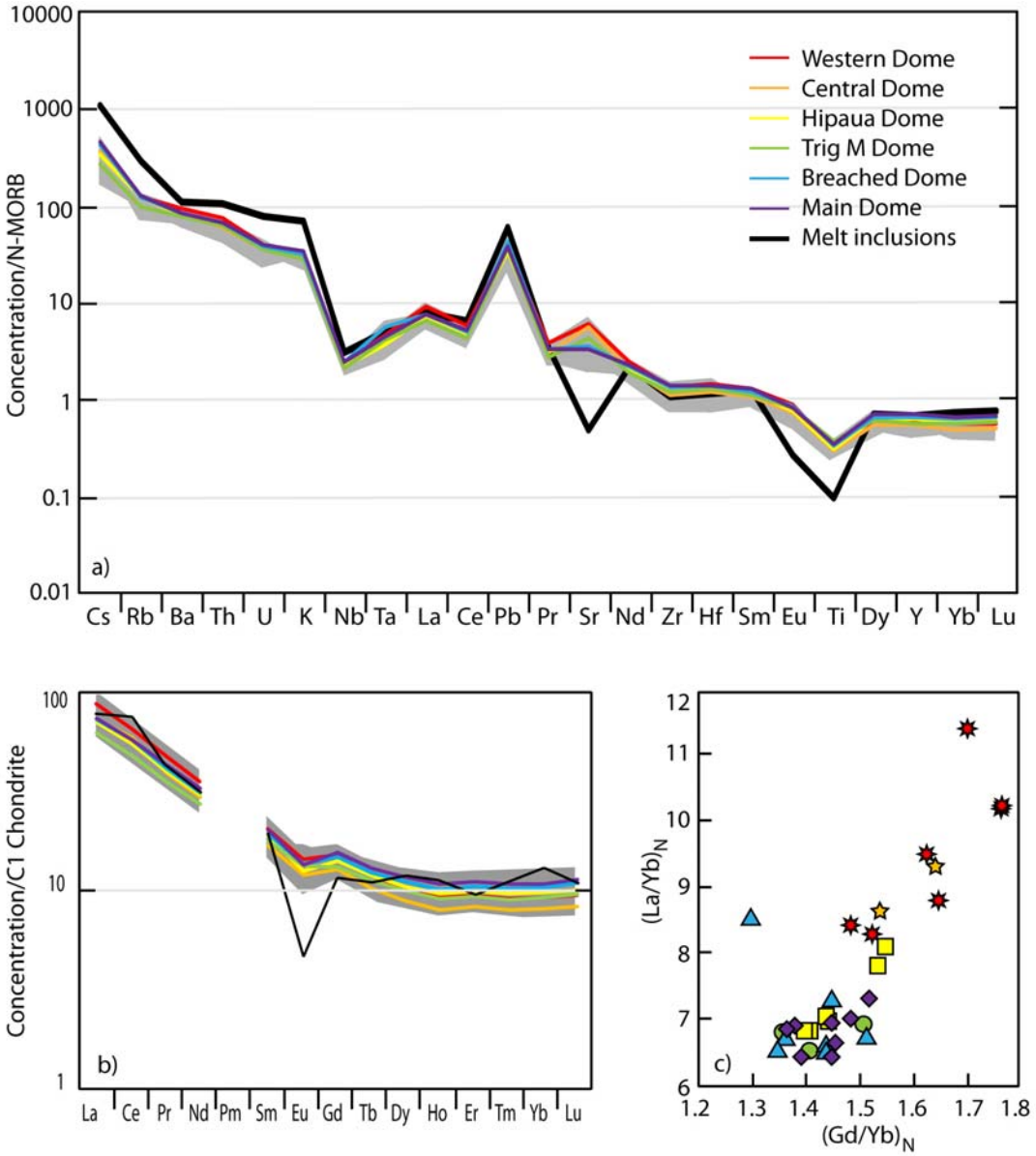

Figure 3.26: a) Multi-element plots of trace element data for Tauhara dacite whole rock samples and averaged melt inclusion data normalised to N-MORB (Sun and McDonough, 1989). Dome averages are marked by coloured lines whereas the whole variation is marked by the grey shaded field. b) Tauhara dacite whole rock REE data normalised to chondrite (Sun and McDonough, 1989). Colours are the same as a). c) Plot showing chondrite normalised whole rock variations between LREE (La) and MREE (Gd) relative to HREE (Yb).

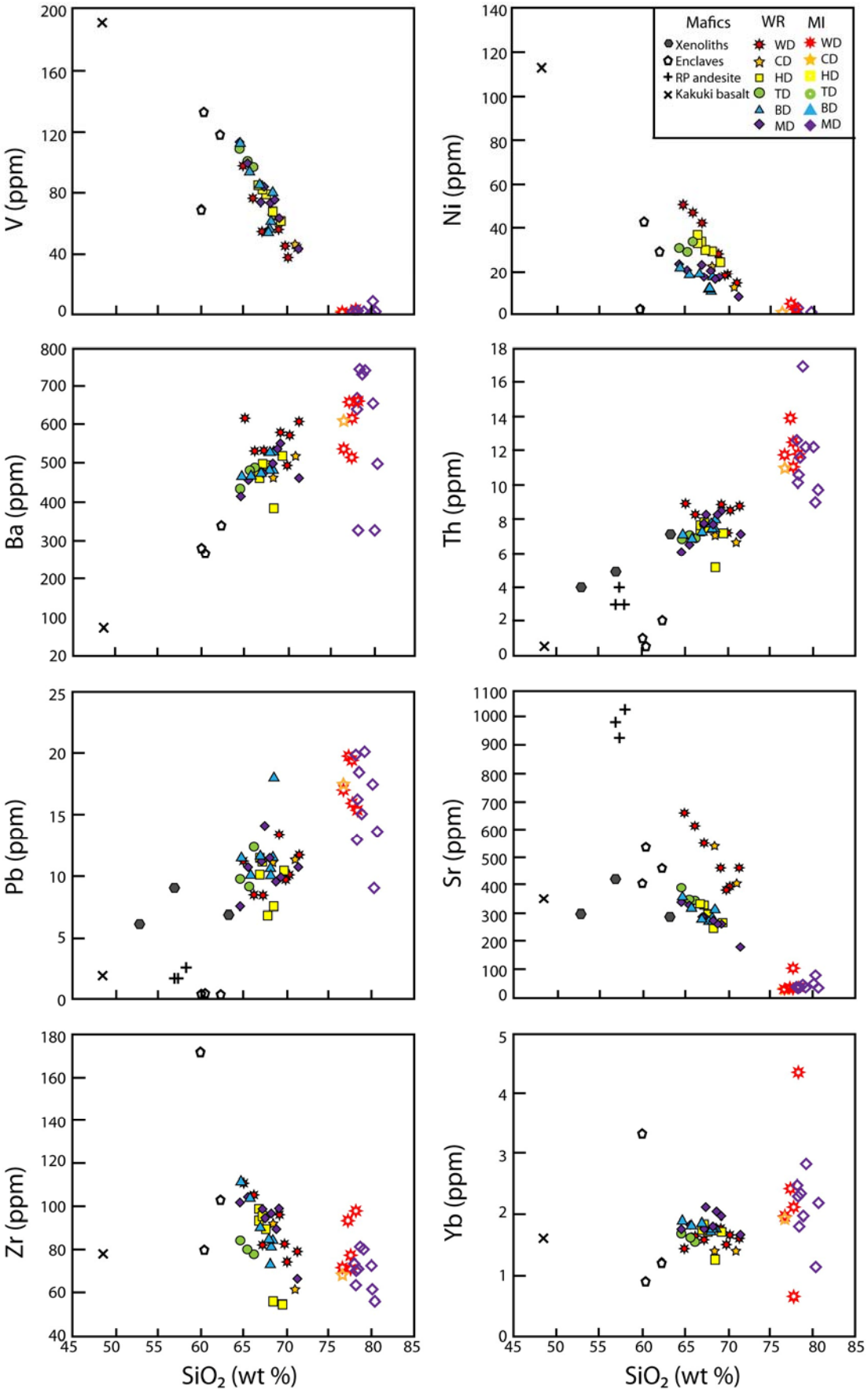

Figure 3.27: Trace element data plotted versus SiO_2 showing the Tauhara dacite whole rock and quartz-hosted melt inclusions. Data for enclaves (Cole et al., 2001) and the Kakuki basalt (Graham et al., 1995) are also plotted. WD: Western Dome, CD: Central Dome, HD: Hipaua Dome, TD: Trig M Dome, BD: Breached Dome, MD: Main Dome.

andesite. The Rolles Peak andesite is the only exposed volcanic rock in the TVZ with such high Sr concentrations. Main, Breached, Trig M and Hipaua Domes have Sr concentrations from 400 to 180 ppm, and all define a strong array between the melt inclusions and the enclaves. The xenoliths and the Kakuki basalts have Sr concentrations which fall below both trends.

Moderately incompatible elements (MICE) such as Zr and Yb show no clear relationship to SiO_2. Concentrations are typically around 80-90 ppm for Zr and 2 ppm for Yb. The variation of Yb in the melt inclusions is greater than the range displayed by the dacites.

3.2.3 Sr-Pb ISOTOPIC DATA

Groundmass Sr-Pb isotope ratios analysed for 22 representative dacite samples are presented in Table 3.12. Pb isotopic data define a linear array between both $^{208}Pb/^{204}Pb$ and $^{207}Pb/^{204}Pb$ versus $^{206}Pb/^{204}Pb$ (Figure 3.28a, b). All domes broadly follow the same trend. Groundmass Sr isotope ratios, however, show two separate populations independent of $^{206}Pb/^{204}Pb$ (Figure 3.28c). Western and Central Dome groundmasses cluster between $^{87}Sr/^{86}Sr$ = 0.7042-0.7046 whereas Main, Breached, Trig M and Hipaua Domes have higher $^{87}Sr/^{86}Sr$ falling between $^{87}Sr/^{86}Sr$ = 0.7047– 0.7052 with a Main Dome outlier within the Western-Central Dome data at $^{87}Sr/^{86}Sr$ = 0.7043.

One representative sample per dome was selected for mineral specific Sr-Pb isotope analyses. Sr-Pb isotope analyses were carried out on individual large plagioclase with c-axes > 2 mm and bulk small whole plagioclase with c-axes < 1 mm to avoid bias yet to obtain sufficient Sr to measure by MC-ICP-MS. Bulk clinopyroxene and amphibole crystals and whole rock Sr isotopic ratios and whole rock Pb isotopic ratios were also measured for these selected whole rock samples.

Pb isotope ratios reveal that plagioclase phenocrysts have more radiogenic Pb than both the groundmass and whole rocks (Figure 3.28d, e). This isotopic difference is also seen in the Sr isotopic signature (Figure 3.28f) where the plagioclase crystals have higher $^{87}Sr/^{86}Sr$ than the groundmass. Although the errors for the individual plagioclase crystals are relatively large, the difference between the plagioclase and dacite is larger than analytical uncertainties. Whole rock isotopic signatures are also different from the groundmass where Pb isotope ratios for Western, Trig M, Breached and Main Domes are higher than the groundmass and Central and Hipaua Dome whole rock have lower Pb isotope ratios. The isotopic difference is also seen in $^{87}Sr/^{86}Sr$ for Central, Hipaua and Main Domes where the whole rock is again higher than

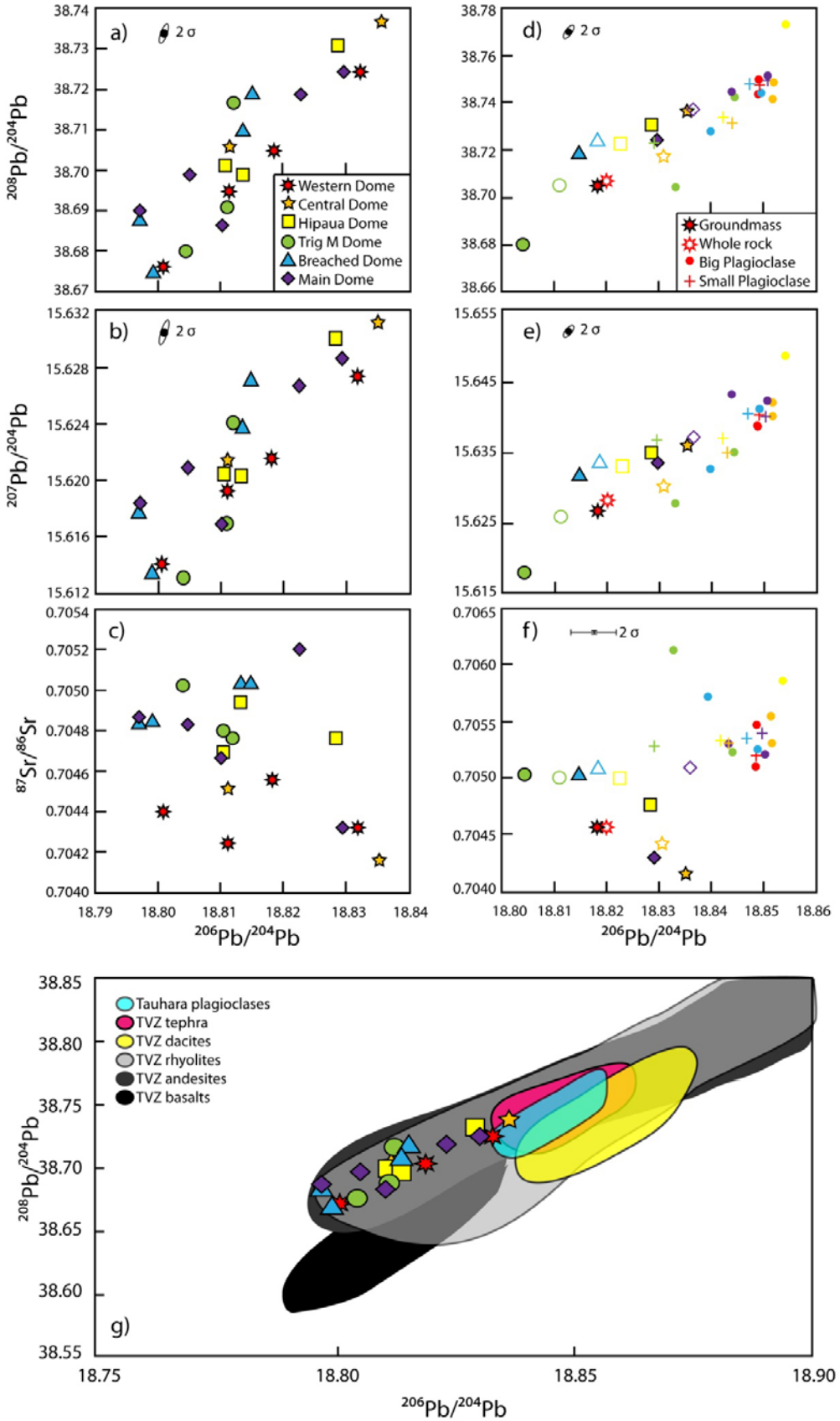

Figure 3.28: Sr-Pb isotopic plots of the Tauhara dacite groundmass (a, b, c,). 2 sigma errors for c) are smaller than the symbols. Plots c), d) and e) show the Sr-Pb isotopic ratio variation between groundmass, whole rock, individual large plagioclase (> 2 mm) and bulk small plagioclase (< 1 mm). Maximum plagioclase errors are defined in f) where as whole rock and groundmass errors are smaller than the symbols. Plot g) shows $^{208}Pb/^{204}Pb$ versus $^{206}Pb/^{204}Pb$ for the Tauhara dacite groundmass and plagioclase with respect to other TVZ igneous rock including other dacites, rhyolites, andesites and basalts (Graham et al., 1992), and TVZ rhyolitic tephra (Allan, 2008).

Table 3.12: Sr-Pb isotope ratios for the groundmass of 22 Tauhara dacites.

Dome	Sample #	$^{87}Sr/^{86}Sr$	*2σ*	$^{206}Pb/^{204}Pb$	*2σ*	$^{207}Pb/^{204}Pb$	*2σ*	$^{208}Pb/^{204}Pb$	*2σ*
Western	421	0.704402	*0.00012*	18.801	*0.001*	15.614	*0.001*	38.676	*0.003*
	425	0.704558	*0.00008*	18.818	*0.001*	15.622	*0.001*	38.705	*0.004*
	427	0.704245	*0.00006*	18.811	*0.001*	15.192	*0.001*	38.695	*0.003*
	437	0.704322	*0.00011*	18.832	*0.001*	15.627	*0.001*	38.724	*0.004*
Central	439	0.704513	*0.00008*	18.811	*0.001*	16.621	*0.001*	38.706	*0.003*
	440	0.704158	*0.00009*	18.835	*0.001*	15.631	*0.001*	38.737	*0.002*
Hipaua	443	0.704696	*0.00009*	18.811	*0.001*	15.620	*0.001*	38.701	*0.003*
	455	0.704946	*0.00011*	18.813	*0.001*	15.620	*0.001*	38.699	*0.003*
	456	0.704764	*0.00007*	18.828	*0.001*	16.630	*0.001*	38.731	*0.002*
Trig M	473	0.704758	*0.00007*	18.812	*0.001*	15.624	*0.001*	38.717	*0.003*
	477	0.705029	*0.00013*	18.804	*0.001*	15.613	*0.001*	38.680	*0.003*
	478	0.704802	*0.00007*	18.811	*0.001*	15.617	*0.001*	38.691	*0.003*
Breached	483	0.705041	*0.00009*	18.815	*0.001*	15.627	*0.001*	38.719	*0.003*
	486	0.705037	*0.00012*	18.813	*0.001*	15.624	*0.001*	38.710	*0.003*
	497	0.704842	*0.00013*	18.797	*0.001*	15.618	*0.001*	38.688	*0.003*
	498	0.704853	*0.00013*	18.799	*0.001*	15.613	*0.001*	38.675	*0.004*
Main	511	0.705205	*0.00010*	18.823	*0.001*	15.627	*0.001*	38.719	*0.003*
	521	0.704866	*0.00009*	18.797	*0.001*	15.618	*0.001*	38.691	*0.002*
	522	0.704825	*0.00014*	18.805	*0.001*	15.621	*0.001*	38.699	*0.003*
	527	0.704293	*0.00011*	18.829	*0.002*	15.629	*0.002*	38.725	*0.005*
	528	0.704677	*0.00010*	18.810	*0.001*	15.617	*0.001*	38.686	*0.003*

groundmass. However, there is no difference in the Sr isotope ratio between whole rock and groundmass for Western, Trig M and Breached Domes. The whole rock isotopic signature, although variable, still remains in the isotopic range for the total Tauhara dacite groundmass and distinct from the plagioclase. Sr-Pb isotopic data for whole rock and mineral separates are presented in Table 3.13.

A plot of $^{206}Pb/^{204}Pb$ versus $^{208}Pb/^{204}Pb$ for the Tauhara dacite groundmass and plagioclase is presented in Figure 3.28g compared to other volcanic rocks. All TVZ volcanic eruptives plot above the Northern Hemisphere Reference Line (Hart, 1984). The Tauhara plagioclase crystals plot within the field of data for rhyolitic tephra erupted from the TVZ (Allan, 2008) and overlap with the TVZ rhyolites. The Tauhara dacites plot within the andesite and rhyolite fields, but has lower $^{206}Pb/^{204}Pb$ than all other TVZ dacites and higher $^{208}Pb/^{204}Pb$ than the TVZ basalts. The Tauhara dacites plot as a mixing trend between the Tauhara plagioclase and andesites such as the Rolles Peak and Ohakune.

$^{87}Sr/^{86}Sr$ ratios were also analysed for bulk amphibole and clinopyroxene phenocrysts for each representative dome sample and are presented in Figure 3.29. Small bulk plagioclase phenocrysts (< 1 mm) and large individual plagioclase phenocrysts (> 2 mm) plot within the rhyolite fields represented by the TVZ tephra collected from ODP site 1123 (Allan, 2008) and plagioclase sourced from the rhyolites erupted from the Maroa Caldera (McCulloch et al., 1994). Clinopyroxene and amphibole separates yield $^{87}Sr/^{86}Sr$ ratios which fall between the groundmass and plagioclase for Western, Central and Main Domes. In contrast, the Hipaua,

Breached and Trig M Dome amphibole and clinopyroxene have the same Sr isotopic ratios as both the whole rock and groundmass (though only the whole rock for Hipaua Dome). Amphiboles have higher $^{87}Sr/^{86}Sr$ for all domes except Main Dome where clinopyroxene is higher. Amphibole abundance in the Central Dome samples was not sufficient to obtain enough material to analyse.

Table 3.13: Sr-Pb isotope data for whole rock and crystal separates of the Tauhara dacite.

Dome	Sample #	Type*	$^{87}Sr/^{86}Sr$	*2σ*	$^{206}Pb/^{204}Pb$	*2σ*	$^{207}Pb/^{204}Pb$	*2σ*	$^{208}Pb/^{204}Pb$	*2σ*
Western	425	WR	0.704561	*0.00009*	18.820	*0.002*	15.623	*0.002*	38.707	*0.005*
		LP 1	0.705468	*0.00035*	18.849	*0.009*	15.635	*0.008*	38.750	*0.019*
		LP 3	0.705098	*0.00041*	18.849	*0.009*	15.635	*0.008*	38.744	*0.019*
		SP	0.705194	*0.00024*	18.849	*0.002*	15.635	*0.002*	38.748	*0.004*
		Cpx	0.704643	*0.00087*						
		Amph	0.704833	*0.00022*						
Central	440	WR	0.704420	*0.00011*	18.831	*0.002*	15.625	*0.001*	38.718	*0.004*
		LP 1	0.705544	*0.00022*	18.851	*0.004*	15.635	*0.003*	38.742	*0.009*
		LP 8	0.705307	*0.00037*	18.852	*0.004*	15.637	*0.004*	38.749	*0.009*
		SP	0.705305	*0.00010*	18.843	*0.001*	15.630	*0.001*	38.732	*0.003*
		Cpx	0.704624	*0.00034*						
Hipaua	456	WR	0.704995	*0.00011*	18.823	*0.003*	15.628	*0.001*	38.723	*0.004*
		LP 6	0.705858	*0.00023*	18.854	*0.005*	15.644	*0.004*	38.774	*0.011*
		SP	0.705338	*0.00013*	18.842	*0.003*	15.632	*0.003*	38.734	*0.006*
		Cpx	0.705035	*0.00012*						
		Amph	0.705054	*0.00024*						
Trig M	477	WR	0.705000	*0.00009*	18.811	*0.002*	15.621	*0.002*	38.705	*0.005*
		LP 3	0.706134	*0.00087*	18.833	*0.007*	15.623	*0.006*	38.704	*0.015*
		LP 9	0.705229	*0.00083*	18.844	*0.007*	15.635	*0.041*	38.743	*0.014*
		SP	0.705285	*0.00015*	18.829	*0.001*	15.632	*0.001*	38.723	*0.004*
		Cpx	0.705009	*0.00009*						
		Amph	0.705115	*0.00012*						
Breached	483	WR	0.705082	*0.00009*	18.818	*0.002*	15.629	*0.002*	38.724	*0.003*
		LP 7	0.705716	*0.00047*	18.840	*0.004*	15.628	*0.004*	38.728	*0.009*
		LP 8	0.705255	*0.00017*	18.849	*0.005*	15.636	*0.004*	38.745	*0.011*
		SP	0.705352	*0.00010*	18.847	*0.002*	15.636	*0.002*	38.748	*0.005*
		Cpx	0.705058	*0.00009*						
		Amph	0.705125	*0.00026*						
Main	527	WR	0.705098	*0.00009*	18.836	*0.001*	15.632	*0.001*	38.737	*0.003*
		LP 3	0.705302	*0.00015*	18.844	*0.005*	15.638	*0.004*	38.745	*0.010*
		LP 6	0.705212	*0.00033*	18.850	*0.005*	15.637	*0.004*	38.752	*0.010*
		SP	0.705395	*0.00010*	18.850	*0.004*	15.635	*0.003*	38.750	*0.007*
		Cpx	0.704907	*0.00013*						
		Amph	0.704743	*0.00068*						

* Sample types: WR = Whole rock, LP = individual large plagioclase, SP = bulk small plagioclase, Cpx = bulk clinopyroxene, Amph = bulk amphibole.

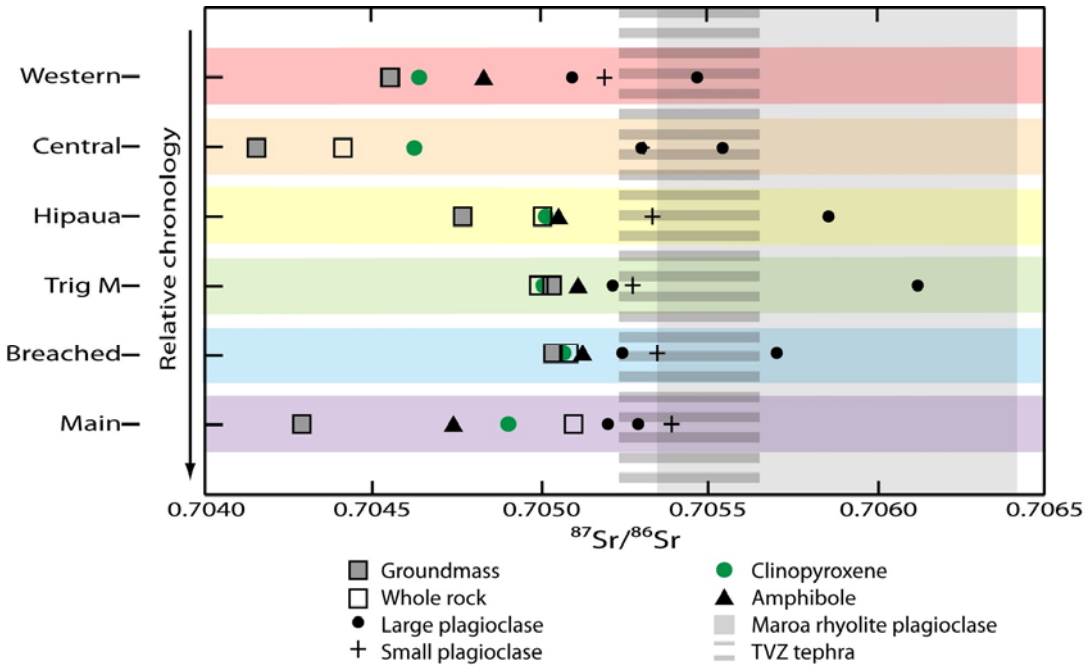

Figure 3.29: $^{87}Sr/^{86}Sr$ isotopic ratios for groundmass, whole rock and mineral separates from each dome of the Tauhara volcano. Errors are smaller than symbols. Plagioclase phenocrysts plot within the rhyolitic fields defined by the data for TVZ tephra (Allan, 2008) and the Maroa Caldera plagioclase (McCulloch et al., 1994). Relative chronology is based on geological observations by Worthington (1985).

Whole rock major and trace elements are plotted versus groundmass $^{206}Pb/^{204}Pb$ and $^{87}Sr/^{86}Sr$ isotope ratios for samples from the TDC in Figure 3.30. Strong elemental-isotopic linear co-variations are observed for elements such as SiO_2, MgO, Sr and V with $^{206}Pb/^{204}Pb$. In contrast $^{87}Sr/^{86}Sr$ ratios of the groundmass shows no clear correlation with major or trace elements. The two populations of $^{87}Sr/^{86}Sr$ ratios (Western and Central Dome samples with groundmass < 0.7051 and Main, Breached, Trig M and Hipaua Dome samples with groundmass > 0.7052) share the same range in V, SiO_2 and CaO contents. Distinct variations are observed for Sr where the low $^{87}Sr/^{86}Sr$ Western and Central Dome population has higher Sr concentration (> 400 ppm) than the Main, Breached, Trig M and Hipaua Dome population (< 400 ppm). Similarly, Ba versus $^{87}Sr/^{86}Sr$ shows only Western Dome samples with higher Ba concentrations (> 520 ppm) and Central Dome falling within the concentrations of Main, Breached, Hipaua and Trig M Domes of 410–550 ppm.

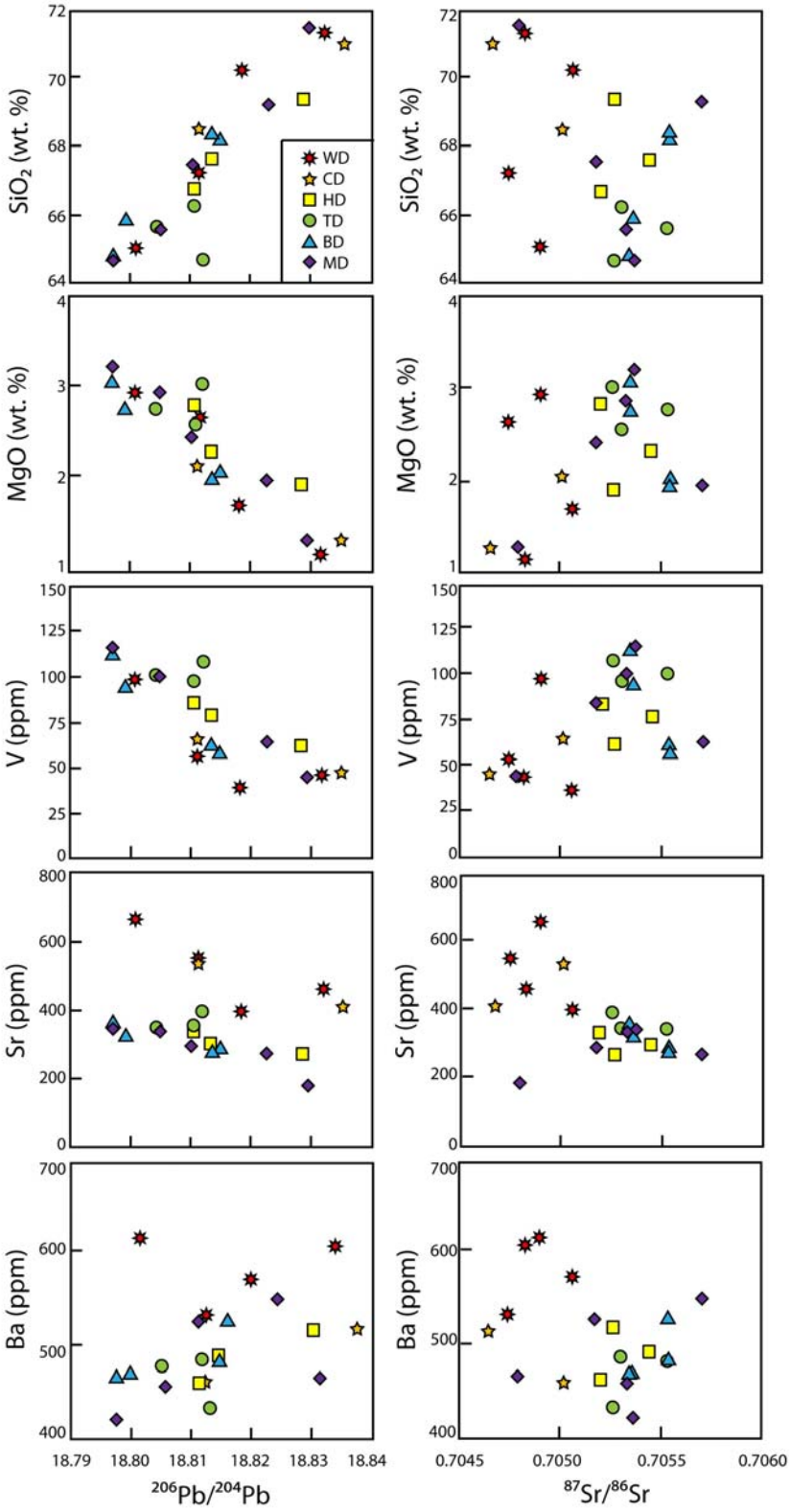

Figure 3.30: Major (SiO_2 and MgO) and trace element (V, Sr and Ba) whole rock data plotted versus groundmass $^{206}Pb/^{204}Pb$ and $^{87}Sr/^{86}Sr$ for Tauhara volcano samples. WD: Western Dome, CD: Central Dome. HD: Hipaua Dome, TD: Trig M Dome, BD: Breached Dome, MD: Main Dome.

CHAPTER 4

DISCUSSION

4.1: MAGMATIC PROCESSES RESPONSIBLE FOR GEOCHEMICAL VARIATION IN THE TAUHARA VOLCANO

The chemistry and petrology of Tauhara volcano provides insights into the physical and chemical processes that generated the dacites, which are discussed sequentially below.

4.1.1: GEOCHEMICAL VARIATION

Pb isotopic ratios are a useful tool in determining the parental magmas and processes that generate volcanic rocks as they are not affected by fractional crystallisation and changes in isotopic composition can only be due to magma mixing and/or crustal assimilation (Davidson et al., 2007). Plots of $^{206}Pb/^{204}Pb$ versus $^{208}Pb/^{204}Pb$, $^{87}Sr/^{86}Sr$, SiO_2 and Sr are presented in Figure 4.1 for the Tauhara dacites and other TVZ igneous rocks. Isotopic variation is observed in the Pb isotopic ratios for the Tauhara dacite groundmass indicating an open magmatic system, and that fractional crystallisation can be ruled out as a major process for the generation and evolution of the dacites. Major and trace element concentrations plotted versus the Pb isotopic composition of the dacites show linear trends suggesting further that magma mixing is the primary process in generating almost all aspects of the chemistry of the Tauhara dacites. Both SiO_2 and Sr plotted versus $^{206}Pb/^{204}Pb$ show linear trends that extend between the TVZ rhyolites and TVZ andesites. A similar conclusion was reached by Worthington (1985) and Graham and Worthington (1988).

The whole rock chemistry and Sr-Pb isotope ratios of the Tauhara groundmass do not however, provide quantitative information of the nature of the mixing endmembers and these are best explored by examination of the crystal cargo.

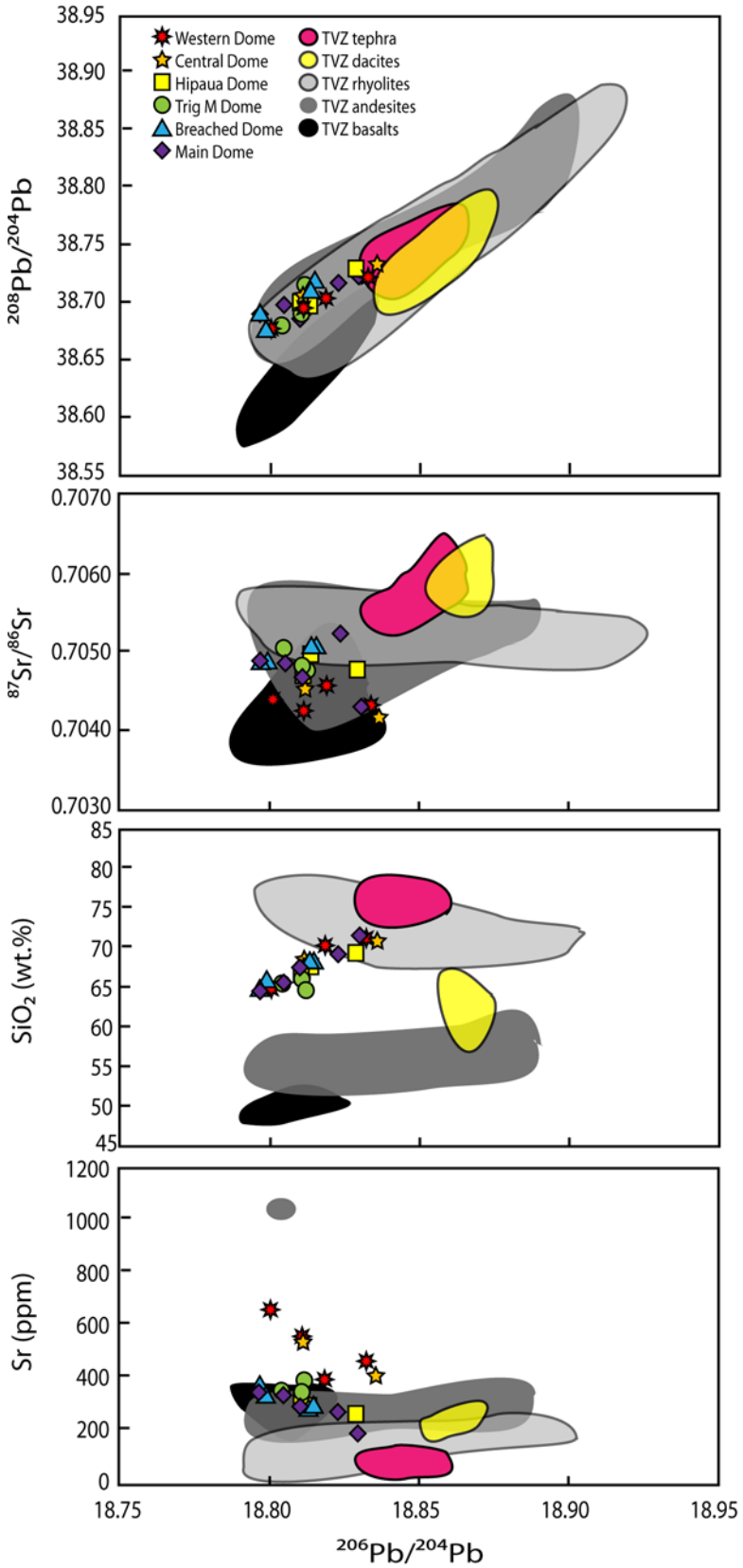

Figure 4.1: $^{206}Pb/^{204}Pb$ versus $^{208}Pb/^{204}Pb$, $^{87}Sr/^{86}Sr$, SiO_2 and Sr for the Tauhara dacites with other TVZ volcanic rocks shown for comparison (Graham et al., 1992; Graham and Hackett, 1987; Gamble et al., 1990, 1993; Graham and Cole, 1991; Graham and Worthington, 1988; Browne et al., 1992; McCulloch et al., 1994; Allan, 2008; Burt et al., 1996; Brown et al., 1998; Schmitz and Smith, 2004). Pb isotopes from Graham et al. have been corrected to SRM981 $^{206}Pb/^{204}Pb$ = 16.9416 and $^{208}Pb/^{204}Pb$ = 36.7262. All Sr isotopes are corrected to $^{87}Sr/^{86}Sr$ = 0.710248 for SRM987.

4.1.2 ORIGINS OF THE CRYSTAL CARGO

4.1.2.1 QUARTZ

Quartz phenocrysts from the Tauhara Dacite Complex are characterised by reverse zoning in TiO_2, resorption rims and abundant melt inclusions. The quartz-hosted melt inclusion major element chemistry is bimodal with two populations of rhyolitic melt: the Western, Central and Trig M Dome melt inclusions have higher K_2O and lower SiO_2 and Al_2O_3 compared to Hipaua, Breached and Main Dome inclusions. However, trace element chemistries are comparable for both populations however.

The majority of the population of quartz crystals show reverse zoning in TiO_2 characterised by bright rims. The concentration of TiO_2 in quartz is governed by the Ti activity, temperature and abundance of Ti in the melt (Wark and Watson, 2006). Assuming no major changes occurred in the Ti activity of the melt, the observed changes in Ti content reflect an increase of either temperature (Shane et al., 2008) or Ti in the melt, both consistent with the addition of a mafic melt to a rhyolitic reservoir. With thermal equilibration occurring before chemical re-equilibration during magma mixing (Sparks and Marshall, 1986) the Ti-rich rims are interpreted to have formed in the rhyolitic melt during thermal equilibration. The resorption of these Ti-rich rims from disequilibrium between the quartz rims and the final melt then occurred during chemical equilibration between the two parental melts.

In quartz, the source magma is constrained from melt inclusions, however for the other mineral phases, reliable melt inclusion data is absent, and a different approach is required. Therefore isotopic and trace element concentrations of the crystals are used instead.

4.1.2.2 PLAGIOCLASE

Pb-Sr isotopic variation is observed in plagioclase phenocrysts where both individual large and bulk small plagioclase crystals have different isotopic signatures than the dacite groundmass, indicating that plagioclase crystallised from magma(s) with different isotopic compositions to the dacite. Plagioclase crystals are more radiogenic than the dacite and fall within fields marked by both plagioclase phenocrysts from the rhyolitic Maroa Caldera (McCulloch et al., 1994) and TVZ tephra glass (Allan, 2008) (Figure 3.29). This observation suggests the plagioclase antecrysts also crystallised in the rhyolitic endmember melt along with the quartz crystals.

The concentrations of Ba and Sr in plagioclase can be used to evaluate the composition of the rhyolitic endmember magma. Partitioning of Sr and Ba between plagioclase and melt is strongly dependent on anorthite content, therefore partition coefficients calculated using the method of Blundy and Wood (1991) have been used to back-calculate melt concentrations. Temperatures from amphibole rims were used for the back-calculations as the Ridolfi et al. (2010) thermometer is the most reliable of those utilised in this study. The rhyolites, however, may have had temperatures lower than that recorded by the amphibole which results in a small overestimate of the Ba (<20 ppm/100 °C) and a small underestimate of Sr (>10 ppm/100 °C) concentrations in the melt. However, these uncertainties are insignificant in comparison to the concentrations of Sr and Ba in the quartz-hosted melt inclusions.

The back-calculated Ba and Sr melt concentrations are plotted in Figure 4.2 in relation to the dacite whole rock and quartz-hosted melt inclusions. Calculated Sr melt concentrations overlap the melt inclusion field with a few outliers falling between the melt and whole rock samples between 150-250 ppm. Back-calculated melt Ba concentrations show a wider range (100-1200 ppm) compared to the quartz-hosted melt inclusion field (300-800 ppm) and the whole rock field (400-600 ppm). Figure 4.2 clearly shows the reconstructed melt, from which the plagioclase crystallized, shares the same Sr and Ba concentrations as the quartz-hosted melt inclusions and plagioclase can therefore be interpreted to have largely originated in the rhyolitic endmember.

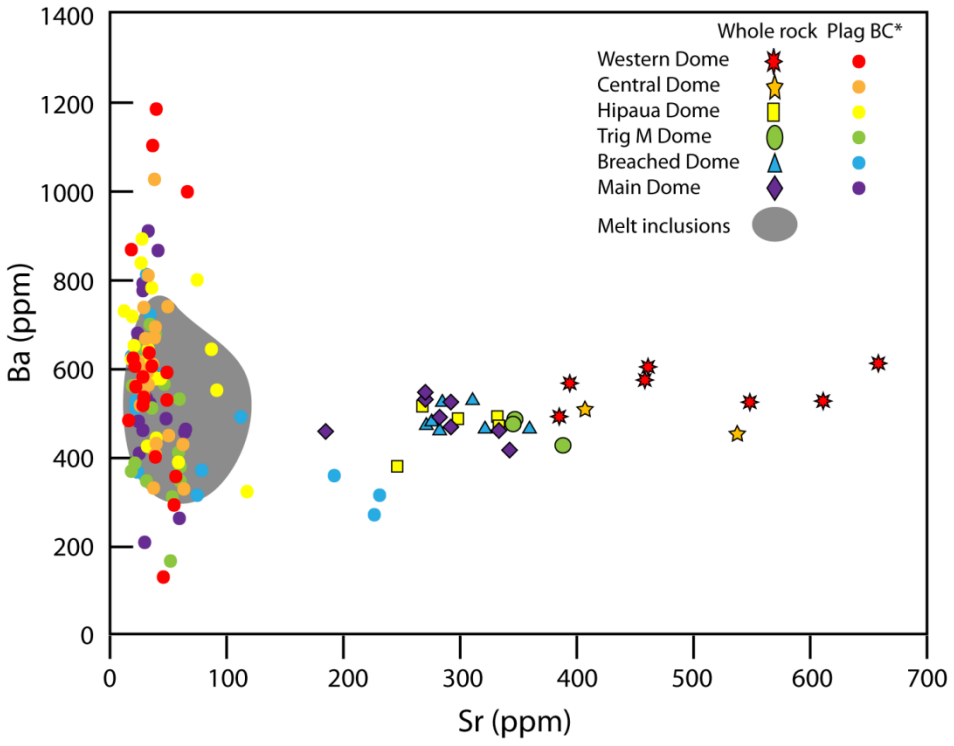

Figure 4.2: Plagioclase Sr and Ba concentrations back-calculated to melt concentrations (Plag BC*) using the methods of Blundy and Wood (1991) and utilising temperatures from amphibole thermometry. Quartz-hosted melt inclusion and Tauhara dacite whole rock Sr and Ba concentrations are also plotted.

Further evidence supporting this interpretation comes from the presence of amphibole, interpreted as crystallising in the mixed magma (see below). Amphibole hygrometry indicates the water content in the melts to be between 5 to 7 wt% for Western, Central, Hipaua, Trig M and Breached core and rims and Main Dome cores with the lower temperature, shallow depth Main Dome rims recording between 4 to 5.5 wt % H_2O. These water contents are consistent with the crystallisation of amphibole without the crystallisation of plagioclase during the magma mixing, as water concentrations in the melt above 5.5 wt% allow for crystallisation of amphibole with the suppression of plagioclase crystallisation (Carmichael et al., 1996; Jackson et al., 1998).

4.1.2.3 AMPHIBOLE

The origin of the amphiboles can be evaluated from their trace element signatures, specifically their REE concentrations. Amphibole rare earth element concentrations back-calculated to melt compositions using dacitic partition coefficients from Sisson (1994) are presented in Figure 4.3. The main population of amphibole crystals with Al# from 0.10 to 0.24, including all Western, Central, Trig M, Hipaua and Breach Dome crystals and the core and middle zones of Main Dome amphibole, has back-calculated melt REE concentrations comparable to the Tauhara whole rocks. This suggests these high Al# amphibole crystallised in the melt during or shortly after the magma mixing event. The low Al# (0-0.08) Main Dome amphibole rims have an order of magnitude greater REE concentrations than the other amphiboles and their origins remain unclear.

Sr isotopic ratios for bulk amphibole fall within the same field as the whole rock and clinopyroxene separates further supporting the interpretation that amphibole crystallised in the dacite. Although there are two populations of Main Dome amphibole, the low Al#, high REE rims have <40 ppm Sr, compared to the cores with ca. 150 ppm, so that the Main Dome rims have a negligible effect on the $^{87}Sr/^{86}Sr$ ratio of the bulk signature of the Main Dome amphiboles.

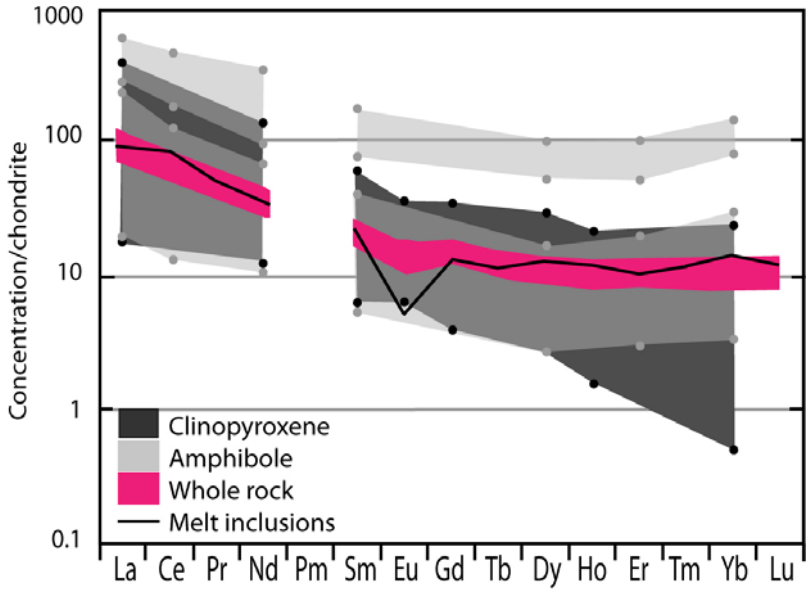

Figure 4.3: Chondrite normalised melt clinopyroxene and amphibole REE back-calculated to melt concentrations relative to the whole rock and melt inclusions. Dots represent the high and low back-calculated values.

4.1.2.4 CLINOPYROXENE

Clinopyroxene REE concentrations back-calculated to melt compositions using dacitic partition coefficients from Severs (2009) are presented in Figure 4.3. The REE signature of the back-calculated melts have similar values to both the whole rock and back-calculated amphibole melts. A greater range in back-calculated clinopyroxene melt concentrations are observed with the HREE concentrations extending to an order of magnitude lower than those calculated from the amphiboles, suggesting some clinopyroxene crystallised from the mafic mixing endmember.

Bulk clinopyroxene Sr isotopic ratios suggest they crystallised from a magma with a Sr isotopic signature comparable to the dacite. However, because this interpretation is based on the isotopic composition of bulk clinopyroxenes, it shows only an average of the isotopic concentrations weighted by the abundance of Sr in the mineral and may mask variations. Those clinopyroxenes that may have crystallised from the mafic endmember would also be expected to have lower Sr concentrations than those crystallising from the dacite.

4.1.3 CHARACTERISATION OF MIXING ENDMEMBERS

Two distinct dacite chemistries are observed in the genesis of the Tauhara volcano: Type 1: Western and Central Domes and Type 2: Hipaua, Trig M, Breached and Main Domes, which can only be explained by mixing events between two chemically distinct mafic endmembers. Figure

4.4 illustrates major element, trace element and isotopic variations between these two types of dacite. Type 1 dacites show steeper chondrite-normalised REE patterns where the Type 1 dacites are enriched in LREE and less enriched in HREE relative to the Type 2 dacites. This REE trend is further expressed in the plot of La_N/Yb_N versus Gd_N/Yb_N representing the relative enrichments between LREE and MREE to HREE, respectively. It is evident that the Type 1 dacites have greater enrichment in the LREE (8-12 times) and MREE (1.5-1.8 times) relative to HREE than the Type 2 dacites, with 6-8 times and 1.3-1.6 times, respectively. Sr shows the greatest difference between the two dacitic trends with the Type 1 dacites having higher Sr concentrations at a given silica content, e.g. 700 ppm (Type 1) versus 400 ppm (Type 2) for 65 wt% SiO_2. Type 1 dacites also have less radiogenic Sr with $^{87}Sr/^{86}Sr$ = 0.7041-0.7046 compared to Type 2 dacites with $^{87}Sr/^{86}Sr$ = 0.7046 - 0.7052.

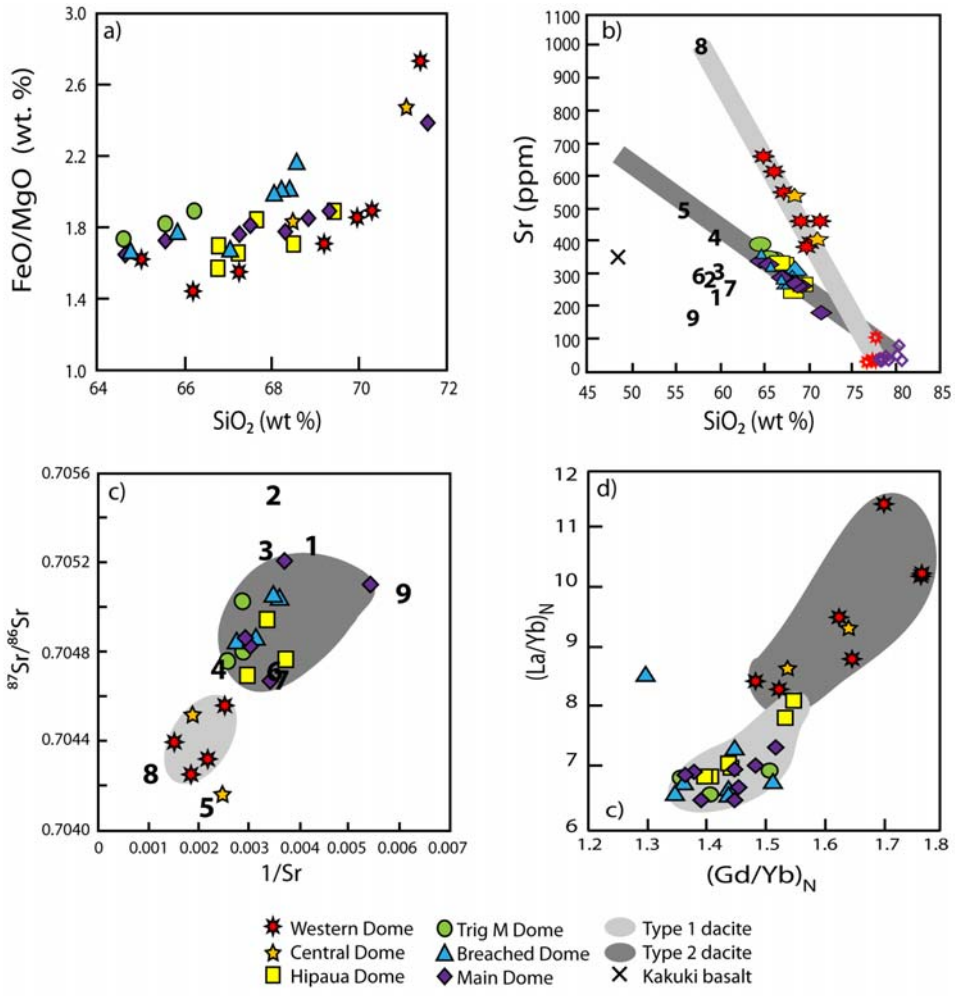

Figure 4.4: Plots showing the geochemical distinctions between type 1 and type 2 dacites identified in this study. Numbers in b) and c) refer to averages for types of andesites identified by Graham et al. (1995). Note andesite type 8 is the Rolles Peak andesite which is the only andesite with high Sr contents.

The Type 1 dacites appear to be the product of mixing between rhyolite and a mafic endmember with relatively lower HREE, higher LREE-MREE and Sr concentrations, and less radiogenic Sr. This is in contrast to the Type 2 dacites which are a product of the mixing between rhyolite and mafic endmembers with higher FeO_{Tot} and HREE, lower LREE-MREE and Sr concentrations and more radiogenic Sr.

THE RHYOLITE ENDMEMBER

Quartz-hosted melt inclusions provide a proxy for the chemistry of the rhyolitic endmembers. Major element data for Tauhara quartz-hosted melt inclusions are plotted in Figure 4.5 with the TVZ rhyolitic eruptives of Whakamaru (340 ka), Oruanui (26.5 ka), Rotorua ash (15.8 ka) and Taupo (1.8 ka) shown for comparison. Two distinct rhyolite melts can be principally distinguished by K_2O where Western, Central and Trig M Domes have high K_2O (>4.7 wt %) and Hipaua, Breached and Main Dome melts have low K_2O (<4.6 wt %). Western, Central and Trig M Dome inclusions fall within the field of the Whakamaru rhyolites where as the Hipaua, Breached and Main Dome inclusions overlap with the both the Whakamaru rhyolites and the high K_2O and low CaO and FeO quartz-hosted melt inclusions of the Oruanui rhyolite. However, all Tauhara melt inclusions have Al_2O_3 concentrations lower than the Whakamaru, Oruanui and Taupo rhyolites, and follow a similar trend to the Rotorua ash albeit extending to lower concentrations. Although the melt inclusions are akin to both the Whakamaru and Oruanui rhyolites, temporal relationships exclude both rhyolites to be an actual mixing endmember.

The Tauhara melt inclusions have a distinct trace element signature that is characterised by very low Sr (typically between 30-50 ppm), high Cu (up to 55 ppm) and low Ti and Mn (450-1000 and 230-300 ppm, respectively). The Tauhara melt inclusions have trace element concentrations that more closely match the tephra (Allan, 2008), glass (Brown et al., 1998) and quartz-hosted melt inclusion (Saunders et al., 2010) analyses from the Whakamaru eruptives than the Oruanui, Taupo, Maunganamu and Trig 9471 rhyolites.

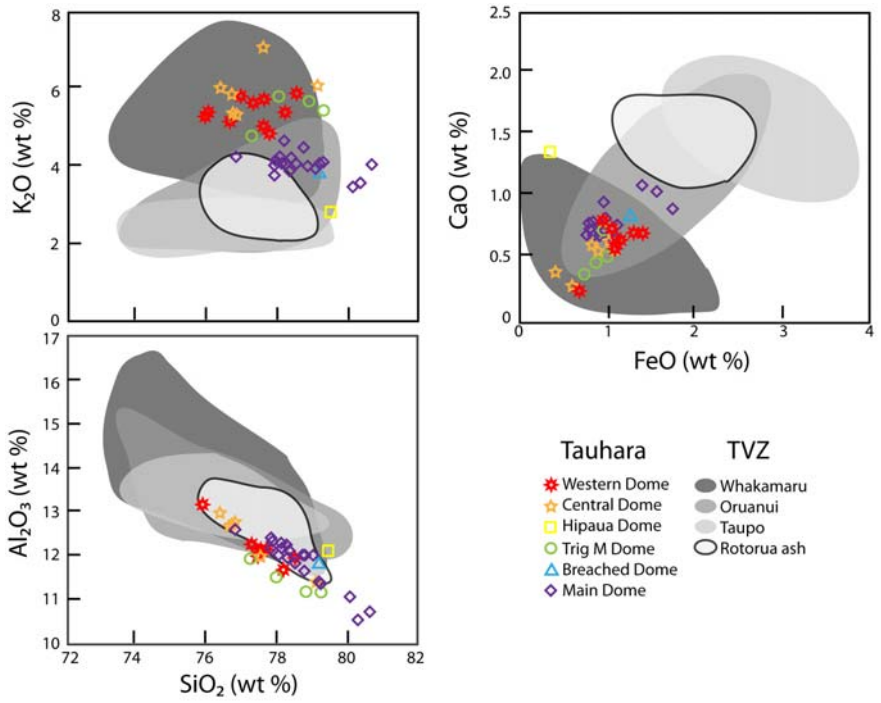

Figure 4.5: Selected major element plots for the quartz-hosted melt inclusions from the Tauhara volcano showing quartz-hosted melt inclusions from various TVZ rhyolites (Saunders et al., 2010) for comparison.

THE MAFIC ENDMEMBERS

No enclaves or xenoliths found within the Tauhara dacite have appropriate compositions to represent either mafic mixing endmember for all trace elements (Figures 3.22, 3.25 and 3.27). The Kakuki basalt, one of the most primitive arc basalts found in the TVZ also falls below the mixing trends and does not represent an appropriate mafic endmember. Nine types of andesites have been identified by Graham et al. (1995) in the TVZ, and have been plotted on Figure 4.4. Rolles Peak, the only type 8 andesite located 5 km NE of Tauhara volcano is the only subaerial andesite that has sufficiently high Sr and low $^{87}Sr/^{86}Sr$ to qualify as a potential endmember for the Type 1 dacites. Type 4 andesites are the only type of mafic endmember to satisfy both the Sr isotopes and concentration for the Type 2 dacites. Type 4 andesites are also the only andesites in the TVZ with amphibole phenocrysts.

There are no direct samples of either of the mafic endmembers in the form of melt inclusions, to evaluate the major element composition of these mixing endmembers, i.e. how mafic the endmembers were. Consequently, the clinopyroxene population that appears to derived from the mafic endmembers, as defined by having low REE concentrations, may be used to constrain the chemistry of the mafic mixing endmembers. A negative relationship is observed between clinopyroxene Yb concentration and Mg#, suggesting that the high Mg# (> 84), low HREE bearing clinopyroxene are derived from the mafic endmember(s) (Figure 4.6). These

clinopyroxenes were used to back-calculate the Sr concentration of the melt in which they crystallised using a partition coefficient of 0.08 (Rollinson, 1993). Partition coeffients calculated from Sobolev et al. (1995), which account for the effect of temperature, were not used as they resulted in anomalously high Sr concentrations of >4000 ppm. The back-calculated Sr values were then extrapolated onto the linear trends observed in the Tauhara dacite whole rock data and used to estimate the SiO_2 content of the endmember melt (Figure 4.6). These SiO_2 values were then applied to other major and trace elements that define linear whole rock trends to determine the chemistry of the mafic endmembers involved in the mixing events (Figures 3.23 and 3.27). Table 4.1 summarises the chemistry calculated for the most primitive mafic endmember from each mixing event.

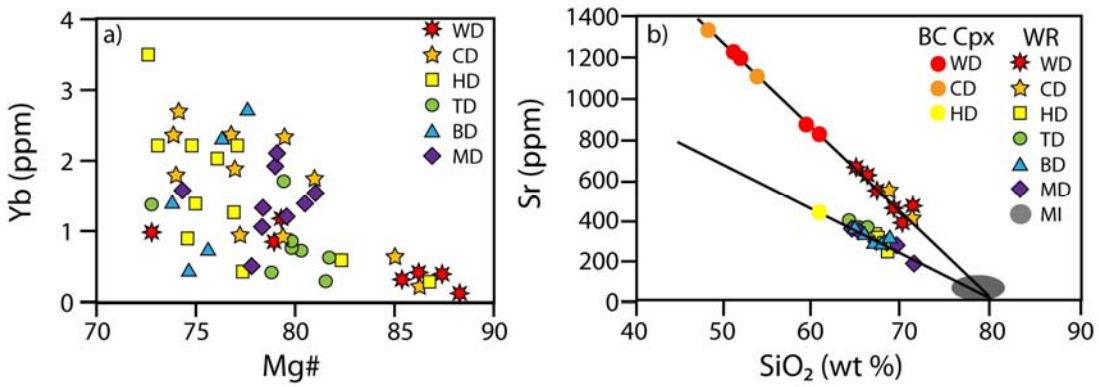

Figure 4.6: a) Yb versus Mg# for clinopyroxene crystals from the Tauhara Volcano. b) Back-calculated melt Sr from the mafic clinopyroxene from the Tauhara Volcano extrapolated onto the linear trends defined by SiO_2 versus Sr for the Tauhara dacite whole rock. WD: Western Dome; CD: Central Dome; HD: Hipaua Dome; TD: Trig M Dome; BD: Breached Dome; MD: Main Dome; MI: quartz-hosted melt inclusions; BC Cpx: Back-calculated clinopyroxene. Clinopyroxene from the mafic endmembers were not present in Trig M, Breached and Main Dome thin sections.

Table 4.1: Major and trace element chemistry of the Tauhara volcano mixing endmembers.

Element	Rhyolite 1	Rhyolite 2	Mafic 1	Mafic 2
SiO_2 (wt %)	77.47	78.73	48.56	61.06
TiO_2	0.09	0.09	0.74	0.58
Al_2O_3	12.15	11.84	20.17	15.94
Fe_2O_3	0.99	1.02	8.91	6.38
MgO	0.02	0.09	7.86	4.13
CaO	0.55	0.79	11.41	6.94
Na_2O	3.10	3.44	2.55	3.16
K_2O	5.55	3.95	0.67	1.54
Sc (ppm)	3.83	4.75	26.1	19.7
V	1.18	2.10	223	145
Cr	10.2	4.76	217	63.8
Ni	2.70	1.59	157	30.8
Zn	42.9	36.7	71.0	72.0
Sr	44.7	43.7	1322	429
Zr	81.4	71.5	71.0	72.3
Eu	0.319	0.276	3.02	0.926
$^{206}Pb/^{204}Pb$			38.598	38.669
$^{207}Pb/^{204}Pb$			15.589	15.610
$^{208}Pb/^{204}Pb$			18.730	18.785

The two mafic endmembers are chemically distinct in both major and trace element characteristics. Mafic endmember 1, the mafic endmember for Western and Central Domes, has a SiO_2 concentration within the basaltic field and overall major element chemistry comparable to the TVZ Kakuki basalt or Tatua basalt (Gamble et al., 1993). The trace element signature is also similar to a HAB, but with significantly higher Cr and Sr than any TVZ HAB. Mafic endmember 2, the mafic mixing member for Hipaua, Trig M, Breached and Main Domes, is a silicic andesite with ca. 61. wt% SiO_2 and a major and trace element signature comparable to andesites from the Wahianoa, Mangawhero and Whakapapa Formations from Mt. Ruapehu (Graham and Hackett, 1987), with the exception of Sr which is ~100 ppm lower in the Ruapehu eruptives than in the calculated endmember (ca. 300 ppm).

Approximate relative proportions of the mafic and rhyolitic endmembers that hybridized to produce the dacites can be quantified by using, for example, the SiO_2 contents of the endmembers from the back-calculated clinopyroxene modelling. For the high-Sr dacite array (Western and Central Domes), the mixing proportions were ca. 40% HAB and ca. 60% rhyolite, whereas for the low-Sr dacite array (other domes) the mixing proportions were ca. 60% andesite and ca. 40% rhyolite.

4.2: MECHANICS OF MAGMA MIXING IN THE GENERATION OF THE TAUHARA DACITES

4.2.1: PHYSICAL CONDITIONS: TEMPERATURE, PRESSURE, DEPTH AND WATER CONTENT

Temperature constraints were obtained from three mineral phases in the Tauhara volcano suite: amphibole, clinopyroxene and Fe-Ti oxides hosted in both phenocrysts and in the groundmass. Amphibole, pyroxene and Fe-Ti oxide temperatures are presented in Figure 4.7. The amphibole and pyroxene of phenocrysts, amphibole and pyroxene, will preserve crystallisation temperatures of from the melts, whereas the Fe-Ti oxides may have re-equilibrated during cooling. The rims of both pyroxene and amphibole phenocrysts record fairly homogeneous temperatures of 900 °C, whereas values for the mineral cores are heterogeneous and range from 850 to 1050 °C, with the exception of the Main Dome amphibole rims which record a lower temperature of 800 °C. Trig M Dome phenocryst-hosted Fe-Ti oxides record the same temperatures as the pyroxene rims. Main Dome groundmass Fe-Ti oxides record the same temperatures as the pyroxene rims and amphibole cores, whereas the phenocryst-hosted Fe-Ti oxides record a lower temperature, similar to the amphibole rims.

Both Central and Hipaua Dome oxides show temperatures lower than the amphibole and pyroxene temperatures. The amphibole and pyroxene temperatures record the temperature of the melt during magma mixing from which they crystallised. As all amphibole phenocrysts crystallised during or shortly after the mixing event (section 4.1.2.3) and the thermometer carries the smallest uncertainties, the crystal inner zones record temperatures during the magma mixing event (850-950 °C). The consistency of the rim temperatures indicate thermal equilibration prior to eruption and it was these temperatures the magmas were erupted (ca. 900 °C).

These temperatures parallel the magma mixing temperature of Mount Unzen, Japan where a rhyodacitic magma of 790 ± 20 °C was intruded and subsequently mixed with an andesite of >1030 °C and generated a thermally equilibrated dacitic eruption temperature of 890 ± 20 °C (Venezky and Rutherford, 1999) Similarly, Fe-Ti oxide thermometry of Volcán Ceboruco, Mexico shows the mixed dacite magma to have thermally equilibrated at ~890 °C prior to intrusion of a ~1030 °C mafic magma (Chertoff and Gardner, 2004) and the dacites of the 1980 Mount St. Helens eruption yield Fe-Ti oxide temperatures of 880 - 920 °C (Geschwind and Rutherford, 1995).

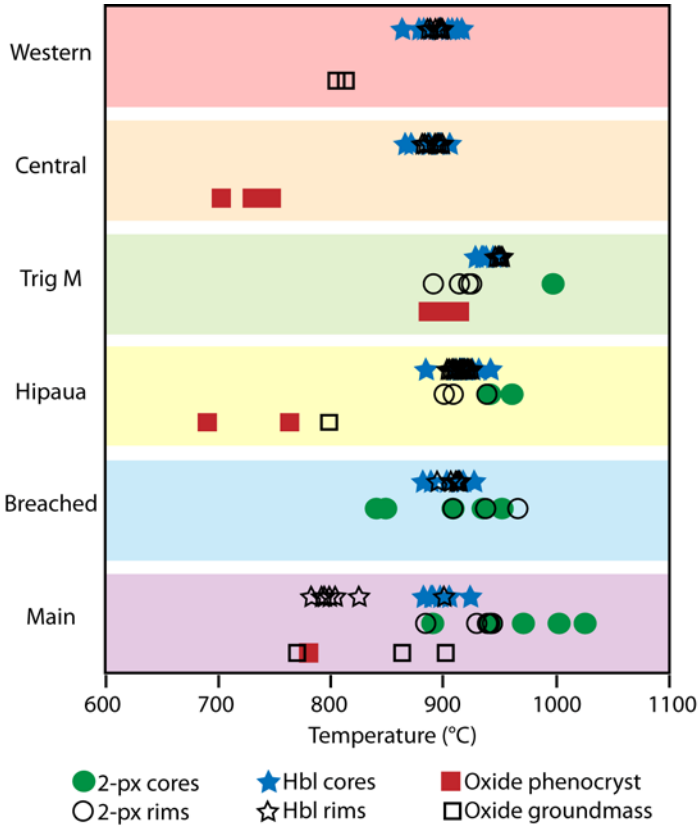

Figure 4.7: Temperatures calculated from phenocrysts and groundmass Fe-Ti oxides from the Tauhara volcano: hornblende thermometry from Ridolfi et al. (2010); two-pyroxene thermometry adapted from the Brey and Köhler (1990) thermometer, and Fe-Ti oxide thermometry from Ghiorso and Evans (2008). 1 standard errors are ±22 °C, ±30 °C and ±44 °C, respectively. 2-px = two pyroxene, Hbl = hornblende, oxide = Fe-Ti oxides.

Pressures were only calculated using amphibole barometry as the uncertainties associated with two-pyroxene barometry are large. Western, Central, Hipaua, and Breached Dome amphibole core and rims and Main Dome amphibole rims record pressures between 210-290 MPa, which equates to depths of 7 - 12 km based on an average continental crust density of 2700 kg/m^3. Trig M Dome amphibole rims record a greater pressure of 351 MPa, equating to depths of 13 km (Figure 3.5). As amphibole largely crystallised during or after the magma mixing event where the mafic melts were intruded into the silicic melts (and hosted crystals), the average rim depths recorded for each dome are used as an estimate of the location of the rhyolite reservoir. This implies these reservoirs were likely located at ca. 8 km depth for Western and Central Domes, 11 km for Hipaua Dome, 13 km for Trig M and 9 km for Breached and Main Domes (cores only). Main Dome amphibole rims record shallower depths (101 MPa) suggesting the mixed magma stalled on ascent at depth of 4 km.

4.2.2: MAGMATIC TIMESCALES

Chemical zoning in crystals are disequilibrium features due to changes in the main physical properties of the magma such as pressure, temperature, and chemistry (Costa and Morgan, 2010). Over time, these sharp boundaries decay by the kinetic process of diffusion and form smoother, broader profiles, (Morgan et al., 2004). If the rate of diffusion is known, the time since the formation of that boundary can be calculated from the width of the boundary, (Morgan et al., 2004). Chemical gradients in phenocrysts have been used here to determine the timing of mixing events during generation of the Tauhara dacites, as marked by high-Ti quartz rims and low-Mg rims present on clinopyroxene. Relative probability curves were calculated using the method of Martin et al. (2008) and provide a visual representation of the diffusion ages and associated uncertainties (Figure 4.8). The envelopes of best fit are presented for the quartz (thick pink lines) and clinopyroxene (thick black lines) rim diffusion ages and relative probability curves for individual crystals are also shown, marked by thin pink lines for quartz, and thin grey lines for clinopyroxene. Diffusion in quartz shows peak probabilities for ages consistently < 6 months. This is also comparable with the clinopyroxene diffusion modelling for Hipaua, Trig and Main Domes. However, Western and Central Domes have clinopyroxene diffusion ages of 1-3 yr, similar to the secondary peak for Hipaua Dome at ca. 1-2 yr. This may suggest that these clinopyroxene rims did not form during the mixing event, but prior to mixing. However, the clinopyroxene in the thick sections used for analysis were randomly oriented and the ages calculated from clinopyroxene diffusion modelling are therefore maximum ages, owing to the potentially oblique nature of the modelled boundary zones. The Fe-Mg diffusion coefficient was also only calculated for zones parallel to the c-axis

and therefore whether diffusivity is isotropic is uncertain. The longer timescales may therefore be an artefact of these effects.

Diffusion profiles in plagioclase and magnetite phenocrysts from Volcán Ceboruco, Mexico indicate that the mixing between mafic and dacite magma occurred 1-2 months prior to eruption (Chertkoff and Gardner, 2004). Diffusion in olivine was used to determine the timescale of magma mixing between andesite and dacite endmembers for multiple eruptions from the 1953-1974 eruptions of Southwest Trident volcano, Alaska (Coombs et al., 2000). Olivine profiles from the initial 1953 eruption yield mixing ages between two weeks to one month prior to eruption with subsequent flows ranging from six months up to two years.

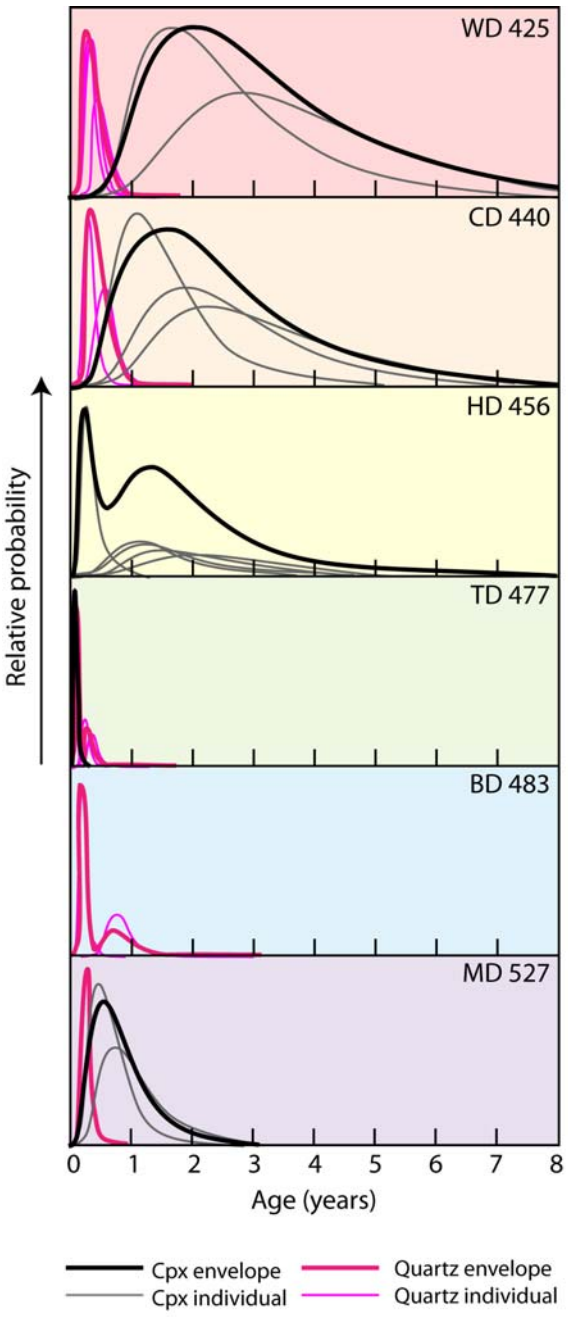

Figure 4.8: Relative probability envelopes for the modelled diffusion ages for clinopyroxene and quartz for each dome.

4.2.3: MAGMA ASCENT RATES

Amphibole reaction rims can be used for determining the rate of magma ascent as the thickness of the reaction rims are dependent on how long the magma resides outside the hornblende stability field during ascent (Rutherford and Hill, 1993; Browne and Gardner, 2006). Reaction rims develop due to the decrease in pressure and water content in the melt during magma ascent (Rutherford and Devine, 2002). Amphibole reaction rim thicknesses in the Tauhara dacite are presented in Figure 4.9 and calculated ascent rates are presented in Table 4.2. Ascent rates were calculated from experiments by Rutherford and Hill (1993) using isothermal constant-rate decompression at 900 °C where:

Reaction rim thickness = 2.98* [duration of ascent between 160 to 2 MPa (d)] -10.4

where R^2 = 0.99. Due to the random orientation of the amphibole analysed in the thin section, oblique sections are presented. Therefore measured reaction rims are maximum thicknesses, resulting in maximum estimates of the ascent rates.

Assuming magma ascent occurred at a constant rate from the magmatic chamber to the surface of the crust, this ascent rate was applied to the depths modelled from the amphibole rim barometry to generate the total duration of magma ascent. Western, Central, Hipaua, Trig M and Breached Domes all exhibit reaction rims. Based on their thicknesses, it took 2-3 weeks on average, for the magma to rise from the crustal magma chambers to the surface. These ascent rates are comparable to the dacites of Mt. St. Helens (Rutherford and Hill, 1993).

By contrast, reaction rims are absent from Main Dome amphibole phenocrysts. The absence of reaction rims in the Main Dome amphibole suggest the exhumation of the magma occurred at rates >0.2 m/s, as witnessed in the 1995-2002 eruptions of Soufrière Hills (Rutherford and Devine, 2002).

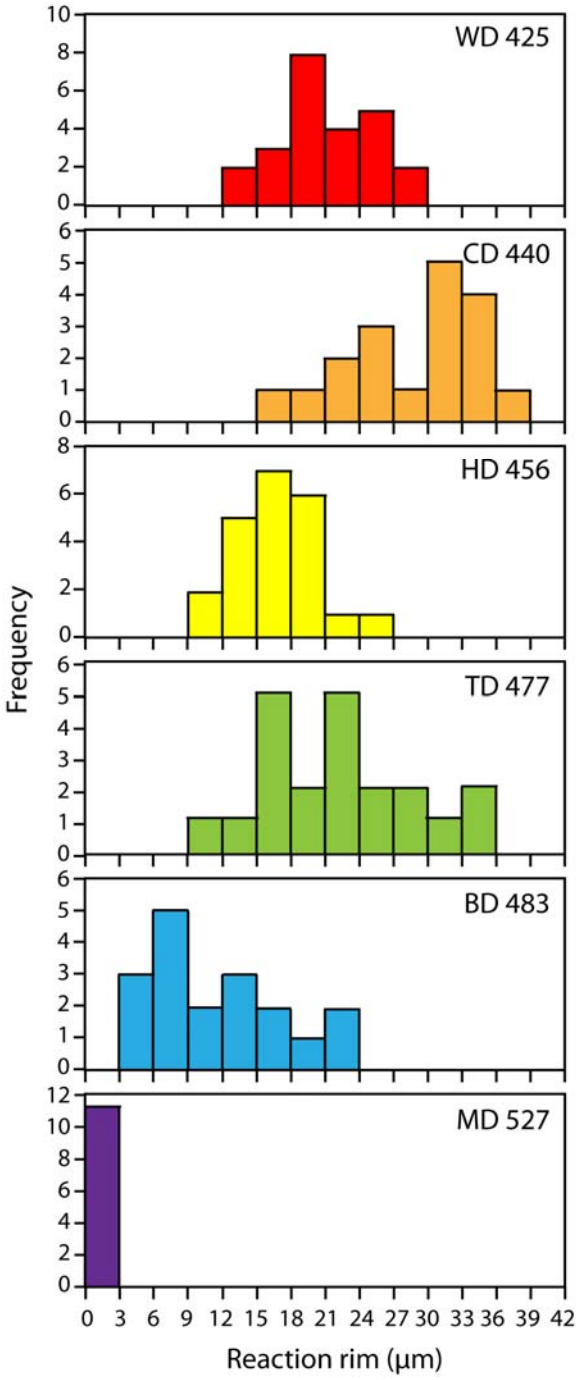

Figure 4.9: Measured thicknesses of amphibole reaction rims of the Tauhara volcano.

Table 4.2: Magma ascent rates calculated from amphibole reaction rim thickness.

Dome	Average reaction rim thickness (µm)	Ascent from 160 MPa (km/d)*	Source depth (km)	Total ascent duration (d)
Western	18	0.613	8.1	13.2
Central	27.3	0.462	8.1	17.5
Hipaua	13.9	0.717	10.8	15.1
Trig M	19.3	0.586	13.2	22.5
Breached	8.8	0.907	9.5	10.5
Main	0	N.A.		

*Depth based on average continental crust density of 2700 kg/m^3.

N.A: Not applicable as Main Dome amphiboles do not possess reaction rims.

4.1.3 ASSEMBLY AND ERUPTION OF TAUHARA DACITE DOMES

The chemistry of the crystal cargo allows for the following magmatic evolution of the Tauhara volcano to be determined (Figure 4.10).

1) The initial rhyolitic reservoir at 8 km depth, consisted primarily of a rhyolitic melt defined by the Type 1 quartz-hosted melt inclusions (rhyolite 1) with a chemistry comparable to the Whakamaru rhyolites and an assemblage of plagioclase and quartz with traces of biotite. A HAB melt (with high Sr and Cr) containing low-REE clinopyroxene and traces of olivine crystals, was intruded into the rhyolitic magma body and incomplete magma mixing occurred between the rhyolitic and basaltic melts. Mixing occurred over 6 months within the chamber generating a high-Sr, low $^{87}Sr/^{86}Sr$ dacitic melt during which amphibole, high-REE clinopyroxene and orthopyroxene crystallised in the magma. The resultant magma at temperatures of 890 °C, ascended to the surface in ca. 13 days.

2) The chemistries of Western and Central Dome are indistinguishable, with the only difference observed in the mixing timescale where the mixing between the HAB and rhyolite endmembers occurred over 6 months for Western Dome and 9 months for Central Dome. It is therefore proposed that the dacites which form both domes are generated from the same mixing event with the eruption of Central Dome 3 months later. The Central Dome magma ascended to the surface in ca. 18 days.

3) An andesitic melt chemically similar to TVZ Type 4 (Endmember 2) with clinopyroxene and traces of olivine crystals was then intruded into Rhyolite 1 in a chamber at 13 km depth, where magma mixing occurred over 4 months. Clinopyroxene (high REE, $En_{38-45}Fs_{10-20}Wo_{40-45}$), orthopyroxene ($En_{70-80}Fs_{20-25}Wo_{2-5}$, in equilibrium with the clinopyroxene) and amphibole (Al# = 0.12-0.22) crystallised during and shortly after the magma mixing. The mixed magma of low-Sr and high $^{87}Sr/^{86}Sr$ and 945 °C ascended to the surface over ca. 23 days resulting in the eruption of Trig M Dome.

4) Recharging of the magma chambers occurred with the Rhyolite 2 endmember, which comprised a rhyolitic melt with a chemistry comparable to the Whakamaru and Oruanui rhyolites, containing quartz, plagioclase and traces of biotite crystals. Subsequent intrusion of an andesite (similar in chemistry to TVZ Type 4, and the andesite involved in the generation of Trig M Dome) into the rhyolitic melt resulted in incomplete magma mixing between the two endmember melts. The chronological relationship between

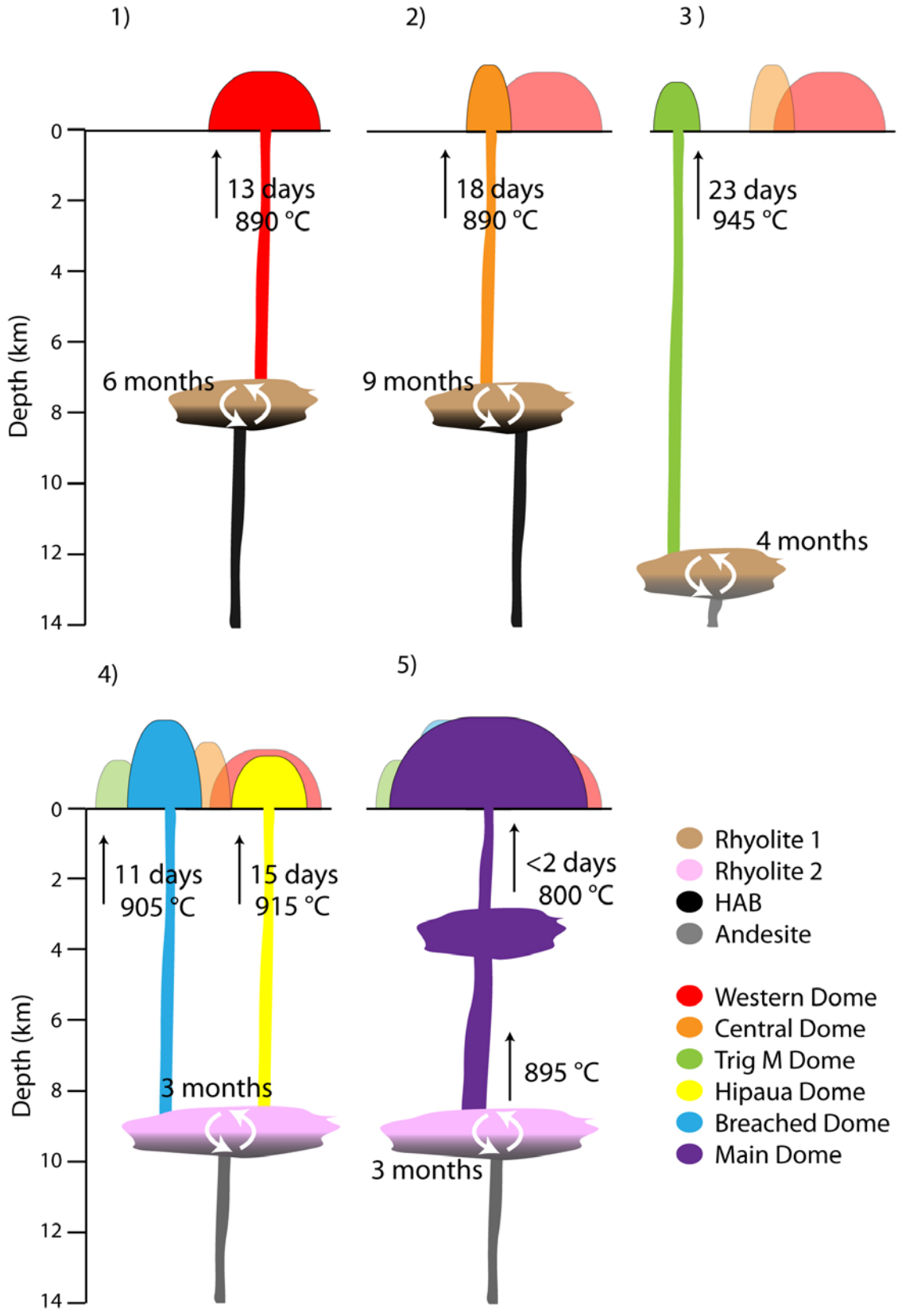

Figure 4.10: Schematic diagram showing the assembly of Tauhara volcano.

Breached and Hipaua Domes cannot be constrained due to the isolated location of the domes and they share chemically comparable endmembers. Magma mixing occurred over 3 months for both domes generating dacites of 905 °C for Breached Dome and 915 °C for Hipaua Dome. Breached Dome magma ascended to the crust over ca. 11 days and Hipaua Dome magma over ca. 15 days.

5) As was the case in the generation of Hipaua and Breached Domes, the generation of the Main Dome dacite was a result of magma mixing over 3 months between Rhyolite 2 and the intrusion of a Type 4 andesite. Clinopyroxene (low REE, Mg#: 68-88, $En_{35-50}Fs_{10-20}Wo_{40-45}$), orthopyroxene (Mg#: 62-82, $En_{65-80}Fs_{20-35}Wo_{2-5}$) and amphibole (Al#: 0.10-0.24) crystallised in the heterogeneous melt during the mixing of the two melts at 9 km depth. The ascent of the Main Dome dacite magma appears to have stalled en route to the surface at 4 km depth allowing crystallisation of amphibole rims of Al#: 0-0.08 and cooling of the magma to 800 °C. Plagioclase crystal rims appear to be in equilibrium with this final melt of Main Dome. Amphibole reaction rims were not present in the Main Dome amphibole indicating the final phase of magmatic ascent to the surface occurred in < 2 days.

CHAPTER 5

CONCLUSIONS

5.1 CONCLUSIONS

A detailed chemical and isotopic study of dacitic melt and its mineral assemblage from the Tauhara dacite volcano located in New Zealand's continental subduction zone of the Taupo Volcanic Zone has shown that:

1) The Tauhara Dacite Complex comprises at least six domes of bulk dacitic composition that formed as the result of magma mixing processes between rhyolitic and mafic endmember magmas.

2) Two separate phases of eruptions occurred: (1) HAB (Western and Central Domes) and an andesite magma (Trig M Dome) mixing with a rhyolitic magma with a chemical signature comparable to Whakamaru rhyolites, and (2) andesite magmas mixing with a rhyolitic body with chemistry overlapping both the Oruanui and Whakamaru rhyolites (Hipaua, Breached and Main Domes). The relative proportions of the mafic and rhyolitic magmas mixing to produce each dacite dome vary slightly, but are generally subequal.

3) Abundant disequilibrium textures (sieve, resorption, and atoll structures) are evident in all phenocryst mineral phases and with reverse zoning present in quartz, consistent with rhyolitic magma mixing with injected basaltic and andesitic endmembers increasing temperatures. All quartz, plagioclase and biotite phenocrysts originated from the rhyolitic endmember melts whereas low-REE clinopyroxene and olivine phenocrysts originated from the mafic endmembers. Clinopyroxene, amphibole and orthopyroxene crystallised during and shortly after the magma mixing events.

4) The intrusion of the mafic endmembers and subsequent mixing occurred at varying depths; 8 km (Western and Central Domes), 9 km (Main and Breached Domes), 11 km (Hipaua Dome) and 13 km (Trig M Dome). The Main Dome magma stalled en route to the surface at ca. 4 km depth.

5) Temperatures during magma mixing initially varied between 850 - 940 °C (Western, Central, Hipaua, Breached and Main Domes) and between 920 - 970 °C (Trig M Dome) and were homogenized by the mixing process towards intermediate temperatures of 900 and 950 °C, respectively, prior to eruption.

6) The duration of magma mixing prior to eruption varied between the domes, but were all on timescales of months; Western Dome: 6 months, Central Dome: 9 months, Trig M Dome, 4 months and Breached, Hipaua and Main Domes: 3 months.

7) The ascent of magma from reservoir to the surface occurred over 2-3 weeks for all dome eruptions except Main Dome, where eruption from the 4 km depth chamber occurred in < 2 days.

REFERENCES

Allan, A. S. R. (2008). *An elemental and isotopic investigation of Quaternary silicic Taupo Volcanic Zone tephras from ODP Site 1123: chronostratigraphic and petrogenetic applications.* M.Sc. thesis, Victoria University, Wellington, New Zealand.

Andersen, D. J. & Lindsley, D. H. (1998). Internally consistent solution models for Fe-Ti-Mg-Mn oxides – Fe-Ti oxides. *American Mineralogist* **73**, 714-726.

Andersen, D. J., Lindsley, D. H. & Davidson, P. M. (1993). QUILF: a Pascal program to assess equilibria among Fe-Mg-Mn-Ti oxides, pyroxenes, olivine and quartz. *Computers and Geosciences* **19***,* 1333-1350.

Annen, C., Blundy, J. D. & Sparks, R. S. J. (2006). The genesis of intermediate and silicic magmas in deep crustal hot zones. *Journal of Petrology* **47**, 505-539.

Bacon, C. R. & Druitt, T. H. (1988). Compositional evolution of the zoned calc-alkaline magma chamber of Mount Mazama, Crater Lake, Oregon. *Contributions to Mineralogy and Petrology* **98***,* 224-256.

Bacon, C. R. & Hirschmann, M. M. (1988). Mg/Mn partitioning as a test for equilibrium between coexisting Fe-Ti oxides. *American Mineralogist* **73***,* 57-61.

Bacon, C. R., Gunn, S. H., Lanphere, M. A. & Wooden, J. L. (1994). Multiple isotopic components in Quaternary volcanic rocks of the Cascade Arc near Crater Lake, Oregon. *Journal of Petrology* **35**, 1521-1556.

Bacon, C. R., Bruggman, P. E., Christiansen, R. L., Clynne, M. A., Donnelly-Nolan, J. M. & Hildreth, W. (1997). Primitive magmas at five Cascade volcanic fields: melts from hot, heterogenous sub-arc mantle. *Canadian Mineralogist* **35***,* 397-423.

Baker, J. A., Waight, T. E. & Ulfbeck, D. G. (2002). Rapid and highly reproducible analysis for rare earth elements by multiple collector inductively coupled plasma mass spectrometry. *Geochimica et Cosmochimica Acta* **66***,* 3635-3646.

Baker, J. A., Peate, D., Waight, T. E. & Meyzen, C. (2004). Pb isotopic analysis of standards and samples using a ^{207}Pb-^{204}Pb double spike and thallium to correct for mass bias with a double focusing MC-ICP-MS. *Chemical Geology* **211**, 275-303.

Beard, J. S. & Lofgren, G. E. (1989). Effect of water on the composition of partial melts of greenstones and amphibolites. *Science* **144***,* 195-197.

Berry, A. J., Danyushevsky, L. V., O'Neill, H. St. C., Newville, M. & Sutton, S. R. (2008). Oxidisation state of iron in komatiitic melt inclusions indicates hot Archaean mantle. *Nature* **455***,* 960-963.

Blundy, J. D. & Cashman, K. V. (2008). *Petrologic reconstruction of magmatic system variables and processes.* In: Putirka, K. D. &Tepley, F. J. (eds) *Minerals, Inclusions and Volcanic Processes. Reviews in Mineralogy and Geochemistry* **69***,* 179-239.

Blundy, J. D. & Wood, B. J. (1991). Crystal-chemical controls on the partitioning of Sr and Ba between plagioclase feldspar, silicate melts, and hydrothermal solutions. *Geochimica et Cosmochimica Acta* **55**, 193-209.

Bowen, N. L. (1928). *The evolution of igneous rocks.* Princton, N.J.: Princton University Press.

Brey, G. P. & Köhler, T. (1990). Geothermobarometry in four-phase lherzolites II. New thermobarometers, and practical assessment of existing thermobarometers. *Journal of Petrology* **31***,* 1353-1378.

Brown, S. J. A., Wilson, C. J. N., Cole, J. W. & Wooden, J. (1998). The Whakamaru group ignimbrites, Taupo Volcanic Zone, New Zealand: evidence for reverse tapping of a zoned silicic magmatic system. *Journal of Volcanology and Geothermal Research* **84**, 1-37.

Browne, B. L. & Gardner, J. E. (2006). The influence of magma ascent path on the texture, mineralogy, and formation of hornblende reaction rims. *Earth and Planetary Science Letters* **246***,* 161-176.

Browne, P. R. L., Graham, I. J., Parker, R. J. & Wood, C. P. (1992). Subsurface andesite lavas and plutonic rocks in the Rotokawa and Ngatamariki geothermal systems, Taupo Volcanic Zone, New Zealand. *Journal of Volcanology and Geothermal Research* **51**, 199-215.

Burt, R. M., Cole, J. W. & Vroon, P. Z. (1996). Volcanic geology and geochemistry of Motuhora (Whale Island), Bay of Plenty, New Zealand. *New Zealand Journal of Geology and Geophysics* **39***,* 565-580.

Camus, G., Gourgard, A., Mossand-Berthommier, P. –C. & Vincent, P. –M. (2000). Merapi (Central Java, Indonesia): An outline of the structural and magmatological evolution, with a special emphasis to the major pyroclastic events. *Journal of Volcanology and Geothermal Research* **100**, 139-163.

Carmichael, I. S. E., Turner, F. J. & Verhoogen, J. (1974). *Igneous petrology*. New York: McGraw-Hill.

Carmichael, I. S. E., Lange, R. A. & Luhr, J. F. (1996). Quaternary minettes and associated volcanic rocks of Mascota, western Mexico: a consequence of plate extension above a subduction modified mantle wedge. *Contributions to Mineralogy and Petrology* **124**, 302-333.

Cherniak, D. J. (2010). *Diffusion in quartz, melilite, silicate perovskite, and mullite*. In: Zhang, Y. & Cherniak, D. J. (eds) *Diffusion in Minerals and Melts. Reviews in Mineralogy and Geochemistry* **72**, 735-756.

Cherniak, D. J. & Dimanov, A. (2010). *Diffusion in pyroxene, mica and amphibole*. In: Zhang, Y. & Cherniak, D. J. (eds) *Diffusion in Minerals and Melts. Reviews in Mineralogy and Geochemistry* **72**, 641-690.

Cherniak, D. J., Watson, E. B. & Wark, D. A. (2007). Ti diffusion in quartz. *Chemical Geology* **236***,* 65-74.

Chertkoff, D. G. & Gardner, J. E. (2004). Nature and timing of magma interactions before, during, and after the caldera-forming eruption of Volcán Ceboruco, Mexico. *Contributions to Mineralogy and Petrology* **146**, 705-735.

Cole, J. W. (1990). Structural control and origin of volcanism in the Taupo Volcanic Zone, New Zealand. *Bulletin of Volcanology* **52***,* 445-459.

Cole, J. W. & Lewis, K. B. (1981). Evolution of the Taupo-Hikurangi subduction system. *Tectonophysics* **72**, 1-21.

Cole, J. W., Gamble, J. A., Burt, R. M., Carroll, L. D. & Shelley, D. (2001). Mixing and mingling in the evolution of andesite-dacite magmas; evidence from co-magmatic plutonic enclaves, Taupo Volcanic Zone, New Zealand. *Lithos* **59***,* 25-46.

Coombs, M. L., Eichelberger, J. C. & Rutherford, M. J. (2000). Magma storage and mixing conditions for the 1953-1974 eruptions of Southwest Trident volcano, Katmai National Park, Alaska. *Contributions to Mineralogy and Petrology* **140**, 99-118.

Costa, F. & Chakraborty, S. (2004). Decadal time gaps between mafic intrusion and silicic eruption obtained from chemical zoning patterns in olivine. *Earth and Planetary Science Letters* **227**, 517-530.

Costa, F. & Morgan, D. J. (2010*). Time constraints from chemical equilibration in magmatic crystals.* In: Dosseto, A., Turner, S. P. & Orman, J. A. V. (eds) *Timescales of magmatic processes: from core to atmosphere.* Oxford: Wiley-Blackwell, pp. 125-159*.*

Davidson, J. P., Morgan, D. J. & Charlier, B. L. A. (2007). Isotopic microsampling of magmatic rocks. *Elements* **3**, 253-259.

Dawson, G. B. & Thompson, G. E. (1981). Groundwater survey at Taupo, Part 2: Relationships geophysical, geochemical and geological. *Geophysics Division Report*, D. S. I. R., Wellington.

Defant, M. J. & Drummond, M. S. (1990). Derivation of some modern arc magmas by melting of young subducted lithosphere. *Nature* **347**, 662-665.

DePaolo, D. J. (1981). Trace element and isotopic effects of combined wallrock assimilation and fractional crystallisation. *Earth and Planetary Science Letters* **53***,* 189-202.

Dimanov, A. & Sautter, V. (2000). "Average" interdiffusion of (Fe,Mn)-Mg in natural diopside. *European Journal of Mineralogy* **12**, 749-760.

Dimanov, A. & Wiedenbeck, M. (2006). (Fe,Mn)-Mg interdiffusion in natural diopside: effect of pO_2. *European Journal of Mineralogy* **18***,* 705-708.

Eichelberger, J. C. (1975). Origin of andesite and dacite: evidence of mixing at Glass Mountain in California and at other circum-Pacific volcanoes. *Geological Society of America Bulletin* **86***,* 1381-1391.

England, P., Engdahl, R. & Thatcher, W. (2004). Systematic variation in the depths of slabs beneath arc volcanoes. *Geophysical Journal International* **156***,* 377-408.

Gamble, J. A., Smith, I. E. M., Graham, I. J., Kokelaar, B. P., Cole, J. W., Houghton, B. F. & Wilson, C. J. N. (1990). The petrology, phase relations and tectonic setting of basalts from the Taupo Volcanic Zone, New Zealand and the Kermadec Island Arc - Havre Trough, SW Pacific. *Journal of Volcanology and Geothermal Research* **43***,* 253-270.

Gamble, J. A., Smith, I. E. M., McCulloch, M. T., Graham, I. J. & Kokelaar, B. P. (1993). The geochemistry and petrogenesis of basalts from the Taupo Volcanic Zone and Kermadec Island Arc, S. W. Pacific, *Journal of Volcanology and Geothermal Research* **54**, 265-290.

Gardner, J. E., Carey, S., Rutherford, M. J. & Sigurdsson, H. (1995). Petrologic diversity in Mount St. Helens dacites during the last 4,000 years: implications for magma mixing. *Contributions to Mineralogy and Petrology* **119**, 224-238.

Gardner, J. E., Rutherford, M. J., Cary, S. & Sigurdsson, H. (1995). Experimental constraints on pre-eruptive water contents and changing magma storage prior to explosive eruptions of Mount. St Helens volcano. *Bulletin of Volcanology* **57***,* 1-17.

Geschwind, C. –H. & Rutherford, M. J. (1995). Crystallisation of microlites during magma ascent: the fluid mechanics of 1980-1986 eruptions at Mount St. Helens. *Bulletin of Volcanology* **57***,* 356-370.

Ghiorso, M. S. & Sack, R. O. (1991). Fe-Ti oxide geothermometry - thermodynamic formulation and the estimation of intensive variables in silicic magmas. *Contributions to Mineralogy and Petrology* **108***,* 485-510.

Ghiorso, M. S. & Sack, R. O. (1995). Chemical mass transfer in magmatic processes; IV, a revised and internally consistent thermodynamic model for the interpolation and extrapolation of liquid-solid equilibria in magmatic systems at elevated temperatures and pressures. *Contributions to Mineralogy and Petrology* **119**, 197-212.

Ghiorso, M. S. & Evans, B. W. (2008). Themodynamics of rhombohedral oxide solid solutions and a revision of the Fe-Ti two-oxide geothermobarometer and oxygen-barometer. *American Journal of Science* **308***,* 957-1039.

Graham, I. J. & Hackett, W. R. (1987). Petrology of calc-alkaline lavas from Ruapehu volcano and related vents, Taupo Volcanic Zone, New Zealand. *Journal of Petrology* **28***,* 531-567.

Graham, I. J. & Worthington, T. J. (1988). Petrogenesis of Tauhara Dacite (Taupo Volcanic Zone, New Zealand) - evidence for magma mixing between high-alumina andesite and rhyolite. *Journal of Volcanology and Geothermal Research* **35**, 279-294.

Graham, I. J. & Cole, J. W. (1991). Petrogenesis of andesites and dacites of White Island volcano, Bay of Plenty, New Zealand, in light of new geochemical and isotopic data. *New Zealand Journal of Geology and Geophysics* **34***,* 303-315.

Graham, I. J., Gulson, B. L., Hedenquist, J. W. & Mizon, K. (1992). Petrogenesis of Late Cenozoic volcanic rocks from the Taupo Volcanic Zone, New Zealand, in the light of new lead isotope data. *Geochimica et Cosmochimica Acta* **56***,* 2797-2819.

Graham, I. J., Cole, J. W., Briggs, R. M., Gamble, J. A. & Smith, I. E. M. (1995). Petrology and petrogenesis of volcanic rocks from the Taupo Volcanic Zone: a review. *Journal of Volcanology and Geothermal Research* **68***,* 59-87.

Grange, L. I. (1937). The geology of the Rotorua-Taupo subdivision*. New Zealand Geological Survey Bulletin* **37**.

Hammarstrom, J. & Zen, E. (1986). Aluminium in hornblende: An empirical igneous geobarometer. *American Mineralogist* **71**, 1297-1313.

Hart, S. R. (1984). A large-scale isotope anomaly in the Southern Hemisphere mantle. *Nature* **309**, 753-757.

Healy, J. (1962). *Structure and volcanism in the Taupo Volcanic Zone, New Zealand*. In: MacDonald, G. A. & Kuno, H. (eds) *The crust of the Pacific Basin. American Geophysical Union, Geophysical Monograph* **6**, 151-157.

Heiken, G. & Eichelberger, J. C. (1980). Eruptions at Chaos Crags, Lassen Volcano National Park, California. *Journal of Volcanology and Geothermal Research* **7**, 443-481.

Hirose, K. & Kushiro, I. (1993). Partial melting of a dry peridotite at high pressures: Determination of compositions of melts segregated from peridotite using aggregates of diamond. *Earth and Planetary Science Letters* **114**, 477-489.

Hollister, L. S., Grissom, G. C., Peters, E. K., Stowell, H. H. & Sisson, V. B. (1987). Confirmation of the empirical correlation of Al in hornblende with pressure of solidification of calc-alkaline plutons. *American Mineralogist* **72***,* 231-239.

Ingamells, C. O. (1980). Microprobe column. *Geostandards Newsletter* **4***,* 139.

Jackson, T. A., Lewis, J. F., Scott, P. W. & Manning, P. A. S. (1998). The Petrology of lamprophyre dikes in the Above Rocks Granitoid, Jamaica: evidence of rifting above a subduction zone during the early Tertiary. *Caribbean Journal of Science* **34**, 1-11.

Jaques, A. L. & Green, D. H. (1980). Anhydrous melting of peridotite at 0-15 kb pressure and the genesis of tholeiitic basalts. *Contributions to Mineralogy and Petrology* **73***,* 287-310.

Jarosewich, J. A., Nelen, J. A. & Norberg, J. A. (1980). Reference samples for electron microprobe analysis. *Geostandards Newsletter* **4***,* 43-47.

Johnson, M. C. & Rutherford, M. J. (1989). Experimentally determined conditions in the Fish Canyon Tuff, Colorado, magma chamber. *Journal of Petrology* **30**, 711-737.

Kay, R. W. (1978). Aleutian magnesian andesites: melts from subducted Pacific Ocean crust. *Journal of Volcanology and Geothermal Research* **4***,* 117-132.

Kay, R. W. & Kay, S. M. (1993). Delamination and delamination magmatism. *Tectonophysics* **219***,* 177-189.

Kelemen, P. B. (1995). Genesis of high Mg# andesites and the continental crust. *Contributions to Mineralogy and Petrology* **120***,* 1-19.

Klügel, A. Hansteen, T. H. & Galipp, K. (2005). Magma storage and underplating beneath Cumbre Vieja volcano, La Palma (Canary Islands). *Earth and Planetary Science Letters* **236***,* 211-226.

Le Bas, M. J., Le Maitre, R. W., Streckeisen, A. & Zanettin, B. (1986). A chemical classification of volcanic rocks based on the total alkali-silica diagram. *Journal of Petrology* **27***,* 745-750.

Lewis, J. F. (1960). *The Tauhara Volcano*. M.Sc. Thesis, Victoria University, Wellington, New Zealand.

Lewis, J. F. (1968a). Tauhara Volcano, Taupo Zone. Part 1 - geology and structure. *New Zealand Journal of Geology and Geophysics* **11***,* 212-224.

Lewis, J. F. (1968b). Tauhara Volcano, Taupo Zone. Part 2 - mineralogy and petrology. *New Zealand Journal of Geology and Geophysics* **11***,* 651-684.

Lindsley, D. H. (1983). Pyroxene thermometry. *American Mineralogist* **68***,* 477-493.

Liu, J., Bohlen, S. R. & Ernst, W. G. (1996). Stability of hydrous phases in subducting oceanic crust. *Earth and Planetary Science Letters* **143**, 161-171.

MacDonald, G. A. & Katsura, T. (1965). Eruption of Lassen Peak, Cascade Range, California, in 1915: example of mixed magmas. *Geological Society of America Bulletin* **76**, 475-482.

Marshall, P. (1907). Geology of centre and north of North Island. *Transactions and Proceedings of the New Zealand Institute* **40***,* 79-98.

Martin, H. & Moyen, J. –F. (2003). Secular changes in TTG composition: comparison with modern adakites. *Abstracts, EGS-AGU-EUG meeting*, Nice, France, abstract VGP7-1FR2O-001.

Martin, H., Smithies, R. H., Rapp, R., Moyen, J. –F. & Champion, D. (2005). An overview of adakite, tonalite-trondhjemite-granodiorite (TTG), and sanukitoid: relationships and some implications for crustal evolution. *Lithos* **79***,* 1-24.

Martin, V. M., Morgan, D. J., Jerram, D. A., Caddick, M. J., Prior, D. J. & Davidson. J. P. (2008). Bang! Month-scale eruption triggering at Santorini volcano. *Science* **321**, 1178.

McCulloch, M. T., Kyser, T. K., Woodhead, J. D. & Kinsley, L. (1994). Pb-Sr-Nd-O isotopic constraints on the origin of rhyolites from the Taupo Volcanic Zone of New Zealand: evidence for assimilation followed by fractionation from basalt. *Contributions to Mineralogy and Petrology* **115***,* 303-312.

Miyashiro, A. (1974). Volcanic rock series in island arcs and active continental margins. *American Journal of Science* **274***,* 321-355.

Morgan, D. J., Blake, S., Rogers, N. W., DeVivo, B., Rolandi, G., MacDonald, R. & Hawkesworth, C. J. (2004). Time scales of crystal residence and magma chamber volume from modelling of diffusion profiles in phenocrysts: Vesuvius 1944. *Earth and Planetary Science Letters* **222***,* 933-946.

Morris, P. A. (1995). Slab melting as an explanation of Quaternary volcanism and aseismicity in southwestern Japan. *Geology* **23***,* 395-398.

Moyen. J.-F., Martin, H. & Jayananda, M. (2003). Late Archaean granites; a typology based on the Dharwar Craton, India. *Precambrian Research* **127***,* 103-123.

Nicholls, I. A. & Ringwood, A. E. (1973). Effect of water on olivine stability in tholeiites and the production of silica-saturated magmas in the island-arc environment. *Journal of Geology* **81***,* 285-300.

Nockolds, S. R. & Allen, R. (1953). The geochemistry of some igneous rock series [part 1]. *Geochimica et Cosmochimica Acta* **4**, 105-142.

O'Neill, H. St. C. & Pownceby, M. L. (1993). Thermodynamic data from redox reactions at high temperatures. I. An experimental and theoretical assessment of the electrochemical method using stabilized zirconia electrolytes, with revised values for the Fe-"FeO", Co-CoO, Ni-NiO, and Cu-Cu_2O oxygen buffers, and new data for the W-WO_2 buffer. *Contributions to Mineralogy and Petrology* **114***,* 296-314.

Parson, L. M. & Wright, I. C. (1996). The Lau-Havre-Taupo back-arc basin: A southward-propagating, multi-stage evolution from rifting to spreading. *Tectonophysics* **263***,* 1-22.

Pertermann, M. & Hirschmann, M. M. (1999). Partial melting experiments on a MORB-like pyroxenite at 3.0 GPa and 1300-1500 °C. *EOS Transactions, American Geophysical Union* **80***,* 1112.

Price, R. C., McCulloch, M. T., Smith, I. E. & Stewart, R. B. (1992). Pb-Nd-Sr isotopic compositions and trace element characteristics of young volcanic rocks from Egmont Volcano and comparisons with basalts and andesites from the Taupo Volcanic Zone, New Zealand. *Geochimica et Cosmochimica Acta* **56***,* 941-953.

Putirka, K. D. (2008). *Thermometers and barometers for volcanic systems.* In: Putirka, K. D. & Tepley, F. J. III (eds) *Minerals, Inclusions and Volcanic Processes. Reviews in Mineralogy and Geochemistry* **69***,* 61-120.

Rapp, R. P., Watson, E. B. & Miller, C. F. (1991). Partial melting of amphibolite/eclogite and the origin of Archaean trondhjemites and tonalites. *Precambrian Research* **51***,* 1-25.

Rapp, R. P., Shimizu, N., Norman, M. D. & Applegate, G. S. (1999). Reaction between slab-derived melts and peridotite in the mantle wedge: experimental constraints at 3.8 GPa. *Chemical Geology* **160***,* 335-356.

Reid, F. W. & Cole, J. W. (1983). Origin of dacites of Taupo Volcanic Zone, New Zealand. *Journal of Volcanology and Geothermal Research* **18***,* 191-214.

Ridolfi, F., Renzulli, A. & Puerini, M. (2010). Stability and chemical equilibrium of amphibole in calc-alkaline magmas: an overview, new thermobarometric formulations and application to subduction-related volcanoes. *Contributions to Mineralogy and Petrology* **160***,* 45-66.

Rollison, H. (1993). *Using geochemical data: evaluation, presentation, interpretation.* Harlow, England: Pearson Prentice Hall.

Rosenberg, M. D. & Kilgour, G. N. (1993). Explosive volcanism at Tauhara Volcanic Complex: implications for the emplacement of Hipaua Dome. *Programme and Abstracts, Geological Society of New Zealand 2003 Annual Conference*, University of Otago, Dunedin, New Zealand, 1-4 December. *pp.* 125.

Rudnick, R. L. & Fountain, D. M. (1995). Nature and composition of the continental crust: a lower crustal perspective. *Reviews of Geophysics* **33**, 267-309.

Rutherford, M. J. & Hill, P. M. (1993). Magma ascent rates from amphibole breakdown: an experimental study applied to the 1980-1986 Mount St. Helens eruptions. *Journal of Geophysical Research* **93**, 11949-11959.

Rutherford, M. J. & Devine, J. D. (2002). Magmatic conditions and magma ascent as indicated by hornblende phase equilibria and reactions in the 1995-2002 Soufrière Hills magma. *Journal of Petrology* **44***,* 1433-1454.

Samsonov, A. V., Bogina, M. M., Bibikova, E. V., Petrova, A. Y. & Shchipansky, A. A. (2005). The relationship between adakitic, calc-alkaline volcanic rocks and TTGs: Implications for the tectonic setting of the Karelian greenstone belts, Baltic Shield. *Lithos* **79***,* 83-106.

Sanjona, F. G., Maury, R., Bellon, H., Cotten, J. & Defant, M. J. (1996). High field strength element enrichment of Pliocene-Pleistocene island arc basalts, Zamboanga Peninsula, western Mindanao (Philippines). *Journal of Petrology* **37**, 693-726.

Sauerzapf, U., Lattard, D., Burchard, M. & Engelmann, R. (2008). The titanomagnetite-ilmenite equilibrium: new experimental data and thermo-oxybarometric application to the crystallisation of basic to intermediate rocks. *Journal of Petrology* **49***,* 1161-1185.

Saunders, K. E., Baker, J. A. & Wysoczanski, R. J. (2010). Microanalysis of large volume silicic magma in continental and oceanic arcs: melt inclusions in Taupo Volcanic Zone and Kermadec Arc rocks, south west Pacific. *Journal of Volcanology and Geothermal Research* **190**, 203-218.

Schmidt, M. W. (1992). Amphibole composition in tonalite as a function of pressure; an experimental calibration of the Al-in-hornblende barometer*. Contributions to Mineralogy and Petrology* **110***,* 304-310.

Schmidt, M. W. & Poli, S. (1998). Experimentally based water budgets for dehydrating slabs and consequences for arc magma generation. E*arth and Planetary Science Letters* **163**, 361-379.

Schmitz, M. D. & Smith, I. E. M. (2004). The petrology of the Rotoiti eruption sequence, Taupo Volcanic Zone: an example of fractionation and mixing in a rhyolitic system*. Journal of Petrology* **45***,* 2045-2066.

Sekine, T. & Wyllie, P. J. (1982). Phase relationships in the system $KAlSiO_4$-Mg_2SiO_4-SiO_2-H_2O as a model for hybridization between hydrous siliceous melts and peridotite. *Contributions to Mineralogy and Petrology* **79***,* 368-374.

Sen, C. & Dunn, T. (1994). Dehydration melting of a basaltic composition amphibolite at 1.5 and 2.0 GPa: implications for the origin of adakites. *Contributions to Mineralogy and Petrology* **117***,* 394-409.

Severs, M. J., Beard, J. S., Fedele, L., Hanchar, J. M., Mutchler, S. R. & Bodnar, R. J. (2009). Partitioning behaviour of trace elements between dacitic melt and plagioclase, orthopyroxene, and clinopyroxene based on laser ablation ICPMS analysis of silicate melt inclusions. *Geochimica et Cosmochimica Acta* **73**, 2123-2141.

Shane, P., Nairn, I. A., Smith, V. C., Darragh, M., Beggs, K. & Cole, J. W. (2008). Silicic recharge of multiple rhyolite magmas by basaltic intrusion during the 22.6 ka Okareka Eruption Episode, New Zealand. *Lithos* **103***,* 527-549.

Shimoda, G., Tatsumi, Y., Nohda, S., Ishizaka, K. & Jahn, B. M. (1998). Setouchi high-Mg andesites revisited: geochemical evidence for melting of subducting sediments. *Earth and Planetary Science Letters* **160***,* 479-492.

Shirley, S. B. & Hanson, G. N. (1984). Mantle derived Archaean monzodiorites and trachyandesites. *Nature* **310***,* 222-224.

Sisson, T. W. (1994). Hornblende-melt trace element partitioning measured by ion microprobe. *Chemical Geology* **117***,* 331-344.

Smith, D. R. & Leeman, W. P. (1987). Petrogenesis of the Mount. St. Helens dacitic magmas. *Journal of Geophysical Research* **92***,* 10313-10334.

Smithies, R. H. & Champion, D. C. (1999). Late Archaean felsic alkaline igneous rocks in the Eastern Goldfields, Yilgarn Craton, Western Australia: A result of lower crustal delamination? *Journal of the Geological Society* **156***,* 561-576.

Sobolev, A. V., Migidosov, A. A. & Portnyagin, M. V. (1995). Incompatible element partitioning between clinopyroxene and basalt liquid revealed by the study of melt inclusions in minerals from Troodos Lavas, Cyprus. *Petrologiya* **4**, 307-317.

Sparks, R. S. J. & Marshall, L. A. (1986). Thermal and mechanical constraints on mixing between mafic and silicic magmas. *Journal of Volcanology and Geothermal Research* **29***,* 99-124.

Stern, C. R. & Kilian, R. (1996). Role of the subducted slab, mantle wedge and continental crust in the generation of adakites from the Austral Volcanic Zone. *Contributions to Mineralogy and Petrology* **123***,* 263-281.

Stern, T. A. (1985). A back-arc basin formed within continental lithosphere: the Central Volcanic Region of New Zealand. *Tectonophysics* **112***,* 385-409.

Stern, T. A. (1987). Asymmetric backarc spreading, heat flux and structure associated with the Central Volcanic Region of New Zealand. *Earth and Planetary Science Letters* **85**, 265-276.

Stipp, J. J. (1968). *The geochronology and petrogenesis of the Cenozoic volcanics of the North Island, New Zealand.* Ph.D. thesis, Australian National University, Canberra, Australia.

Stratford, W. R. & Stern, T. A. (2006). Crust and upper mantle structure of a continental backarc: central North Island, New Zealand. *Geophysical Journal International* **166,** 469-484.

Sun, S. -S. & McDonough, W. F. (1989). *Chemical and isotopic systematics of oceanic basalts; implications for mantle composition and processes*. In: Saunders, A. D. & Norry, M. J. (eds), *Magmatism in the ocean basins, Geological Society of London Special Publication* **42**, 313-345.

Sutton, A. N., Blake, S. & Wilson, C. J. N. (1995). An outline geochemistry of rhyolite eruptives from Taupo volcanic centre, New Zealand. *Journal of Volcanology and Geothermal Research* **68***,* 153-175.

Takahashi, E., Shimazaki, T., Tsuzaki, Y. & Yoshidam H. (1993). Melting study of a peridotite KLB-1 to 6.5 Gpa, and the origin of basaltic magmas. *Philosophical Transactions of the Royal Society of London, Series A* **342**, 105-120.

Tatsumi, Y. (2008). Making continental crust: the sanukitoid connection. *Chinese Science Bulletin* **53***,* 1620-1633

Tatsumi, Y. & Eggins, S. (1995). *Subduction zone magmatism*. Blackwell, Cambridge, MA.

Tatsumi, Y. & Kogiso, T. (2003). *The subduction factory: its role in the evolution of the Earth's crust and mantle*. In: Larter, R. D. & Leat, P. T. (eds) *Intra-oceanic subduction systems: tectonics and magmatic processes. Geological Society of London Special Publication* **219**, 55-80.

Tatsumi, Y. & Stern, R. J. (2006). Manufacturing continental crust in the subduction factory. *Oceanography* **19***,* 104-112.

Tatsumi, Y., Shukuno, H., Sato, K. Shibata, T. & Yoshika, M. (2003). The petrology and geochemistry of high-magnesium andesites at the western tip of the Setouchi Volcanic Belt, SW Japan. *Journal of Petrology* **44***,* 1561-1578.

Taylor, S. R. & McLennan, S. M. (1995). The geochemical evolution of the continental crust. *Reviews of Geophysics* **33***,* 241-265.

Thomas, W. & Ernst, W. G. (1990). *The aluminium content of hornblende in calc-alkaline granitic rocks; a mineralogic barometer calibrated experimentally to 12 kbars*. In: Spencer, R. J. & Chou, I. -M. (eds) *Fluid-mineral interactions: a tribute to H.P. Eugster. Geochemical Society Special Publications* **2**, 59-63.

Thomas, J. B., Watson, E. B., Spear F. S., Shemella, P. T., Nayak, S. K. & Lanzirotti, A. (2010). TitaniQ under pressure: the effect of pressure and temperature in the solubility of Ti in quartz. *Contributions to Mineralogy and Petrology* **160**, 743-759.

Turcotte, D. L. (1989). *Geophysical processes influencing the lower continental crust*. In: Mereu, R. F., Mueller, S. & Fountain, D. M. (eds) *Properties and processes of Earth's lower crust. American Geophysical Union Monographs* **51**, 321-329.

Ulmer, P. (2001). Partial melting in the mantle wedge - the role of H_2O in the genesis of mantle-derived 'arc-related' magmas. *Physics of the Earth and Planetary Interiors* **127**, 215-232.

Venezky, D. Y. & Rutherford, M. J. (1999). Petrology and Fe-Ti oxide re-equilibration of the 1991 Mount Unzen mixed magma. *Journal of Volcanology and Geothermal Research* **89**, 213-230.

Vucetich, C. G. & Howarth, R. (1976). Late Pleistocene tephrostratigraphy in the Taupo district, New Zealand. *New Zealand Journal of Geology and Geophysics* **19***,* 51-69.

Wark, D. A. & Spear, F. S. (2005). Ti in quartz: cathodoluminescence and thermometry. *Geochimica et Cosmochimica Acta* **69**, A592.

Wark, D. & Watson, E. B. (2006). TitaniQ: a titanium-in-quartz geothermometer. *Contributions to Mineralogy and Petrology* **152***,* 743-754.

Weaver, B. L. & Tarney, J. (1984). Empirical approach to estimating the composition of the continental crust. *Nature* **319**, 575-577.

Wells, P. R. A. (1997). Pyroxene thermometry in simple and complex systems. *Contributions to Mineralogy and Petrology* **62***,* 129-139.

Wilson, C. J. N. (1993). Stratigraphy, chronology, styles and dynamics of late Quaternary eruptions from Taupo volcano, New Zealand. *Philosophical Transactions of the Royal Society of London, Series A* **343**, 205-306.

Wilson, C. J. N., Houghton, B. F., McWilliams, M. O., Lanphere, M. A., Weaver, S. D. & Briggs, R. M. (1995). Volcanic and structural evolution of Taupo Volcanic Zone, New Zealand: a review. *Journal of Volcanology and Geothermal Research* **68***,* 1-28.

Wolf, M. B. & Wyllie, P. J. (1994). Dehydration melting of amphibolite at 10 kbar - the effects of temperature and time. *Contributions to Mineralogy and Petrology* **11**, 369-383.

Worthington, T. J. (1985). *Geology and petrology of the Tauhara Volcanic Complex, Taupo, New Zealand.* M.Sc. thesis, Victoria University, Wellington, New Zealand.

Wysoczanski, R. J., Wright, I. C., Gamble, J. A., Hauri, E. H., Luhr, J. F., Eggins, S. M. & Handler, M. R. (2006). Volatile contents of Kermadec Arc-Havre Trough pillow glasses: fingerprinting slab derived aqueous fluids in the mantle sources of arc and back-arc lavas. *Journal of Volcanology and Geothermal Research* **152**, 51-73.

Yasuda, A. Fujii, T. & Kurita, K. (1994). Melting phase relations of an anhydrous mid-ocean ridge basalt from 3 to 20 GPa; implications for the behaviour of subducted oceanic crust in the mantle. *Journal of Geophysical Research* **99***,* 9401-9414.

Yogodzinski, G. M., Kay, R. W., Volynets, O. N., Koloskov, A. V. & Kay, S. M. (1995). Magnesian andesite in the western Aleutian Komandorsky region: implications for slab melting and processes in the mantle wedge. *Geological Society of America Bulletin* **107***,* 505-519.

Zhang, Y. (2010). *Diffusion in minerals and melts: theoretical background*. In: Zhang, Y. & Cherniak, D. J. (eds) *Diffusion in Minerals and Melts. Reviews in Mineralogy and Geochemistry* **72**, 5-59.

Assembling dacite in a continental subduction zone:

a case study of Tauhara volcano

Chelsea May Tutt

APPENDICES

APPENDIX 1

SAMPLE INFORMATION

Plate 2: Mount Tauhara looking east from across Lake Taupo (photograph courtesy of Michael Gazley).

Table A1.1: Samples from the Tauhara volcano.

Table A1.2: Modal analyses – Worthington (1985).

Table A1.1: Sample information.

Sample #	VUW sample#	Dome	Easting*	Northing*	Rock name	Analyses	Notes
421	19421	Western	2784882	6275287	Dacite	WR-sol, gmass-iso	
425	19425	Western	2784070	6275776	Rhyolite	WR-sol, WR-iso, gmass-iso, min-maj, min-te, min-iso	
427	19427	Western	2784151	6275408	Dacite	WR-sol, gmass-iso	
428	19428	Western	2784524	6275672	Dacite	WR-sol	pink and grey intermixed groundmass
433	19433	Western	2783029	6274525	Dacite	WR-sol	pink and grey intermixed groundmass
436	19436	Western	2783392	6274423	Dacite	WR-sol	
437	19437	Western	2783668	6274507	Rhyolite	WR-sol, gmass-iso	
439	19439	Central	2783744	6273956	Dacite	WR-sol, gmass-iso	
440	19440	Central	2783744	6273956	Dacite	WR-sol, WR-iso, gmass-iso, min-maj, min-te, min-iso	
442	19442	Hipaua	2786631	6275795	Dacite	WR-sol	
443	19443	Hipaua	2786537	6275706	Dacite	WR-sol, gmass-iso	
444	19444	Hipaua	2786631	6275795	Dacite	WR-sol	
452	19452	Hipaua	2786535	6275615	Dacite	WR-sol	
455	19455	Hipaua	2786624	6275521	Dacite	WR-sol, gmass-iso	
456	19456	Hipaua	2786626	6275612	Dacite	WR-sol, WR-iso, gmass-iso, min-maj, min-te, min-iso	
473	19473	Trig M	2784536	6272836	Dacite	WR-sol, gmass-iso	
477	19477	Trig M	2784353	6272842	Dacite	WR-sol, WR-iso, gmass-iso, min-maj, min-te, min-iso	
478	19478	Trig M	2784353	6272842	Dacite	WR-sol, gmass-iso	
483	19483	Breached	2784193	6273669	Dacite	WR-sol, WR-iso, gmass-iso, min-maj, min-te, min-iso	
486	19486	Breached	2784468	6273661	Dacite	WR-sol, gmass-iso	
488	19488	Breached	2784661	6274022	Dacite	WR-sol	pink and grey intermixed groundmass
489	19489	Breached	2784102	6273672	Dacite	WR-sol	
495	19495	Breached	2783099	6273792	Dacite	WR-sol	pyroclastic flow
497	19497	Breached	2783462	6273690	Dacite	WR-sol, gmass-iso	pyroclastic flow
498	19498	Breached	2783739	6273773	Dacite	WR-sol	pyroclastic flow
506	19506	Main	2784882	6275387	Dacite	WR-sol	pumice
511	19511	Main	2784882	6275387	Dacite	WR-sol, gmass-iso	dark grey glassy groundmass
521	19521	Main	2785653	6273536	Dacite	WR-sol, gmass-iso	
522	19522	Main	2785948	6274260	Dacite	WR-sol, gmass-iso	
525	19525	Main	2786316	6274341	Dacite	WR-sol	pink rimmed plagioclase
527	19527	Main	2785240	6275103	Rhyolite	WR-sol, WR-iso, gmass-iso, min-maj, min-te, min-iso	
528	19528	Main	2785237	6275011	Dacite	WR-sol, gmass-iso	pink and grey intermixed groundmass
529	19529	Main	2785143	6274923	Dacite	WR-sol	

Abbreviations: gmass-iso: groundmass Sr-Pb isotopes; min-iso: Sr-Pb mineral isotopes; min-maj: EPMA mineral major elements; min-te: LA-ICP-MS mineral trace elements; WR-iso: whole rock Sr-Pb isotopes; WR-sol: solution ICP-MS whole rock trace elements. *Eastings and northings refer to the New Zealand Map Grid.

Table A1.2: Modal analyses – Worthington (1985).

Sample	**421**	**425**	**427**	**428**	**433**	**436**	**437**	**439**	**440**	**442**	**443**	**444**	**452**	**455**	**456**	**473**	**477**
Total phenocryst %	*13.1*	*23.4*	*9.6*	*14.8*	*22.2*	*22.5*	*15.4*	*14.0*	*22.8*	*15.9*	*14.2*	*23.0*	*20.0*	*12.0*	*16.6*	*12.9*	*12.4*
% of total phenocrysts																	
Plagioclase	32.8	52.8	40.0	25.8	54.4	48.5	46.1	42.7	48.2	53.1	26.1	54.4	49.0	50.0	60.6	45.6	54.1
PxT	27.7	2.9	11.7	43.5	3.9	6.2	15.5	18.0	15.2	12.6	43.1	18.9	230	18	14.9	24.9	6.5
OpxT	5.6	0.6	1.4	10.9	0.6	1.8	2.6	2.4	4.1	6.3	7.1	5.8	6.9	7.6	7.2	16.6	4.3
Opx A		0.3		0.5		0.6		1.4	2.9		1.9	1.5	2.9	0.5	2.4	3.1	2.2
Opx B	5.6	0.3	1.4	10.4	0.6	1.2	2.6	1.0	1.2	6.3	5.2	4.3	4.0	7.1	4.8	13.5	2.1
CpxT	22.1	2.3	10.3	32.6	3.3	4.4	12.9	15.6	11.1	6.3	36	13.1	16.0	11	7.6	8.3	2.2
Cpx A	7.2	1.7	1.4	19.9	1.5	0.6	9.5	4.3	2.9	1.3	24.6	11.3	11.0	0.5	3.2	4.1	1.6
Cpx B	14.9	0.6	8.9	12.7	1.8	3.8	3.4	11.3	8.2	5.0	11.4	1.8	4.9	10	4.4	4.2	0.6
Amph	23.6	28.1	40.7	24.4	31.5	24.9	17.2	28.0	19.0	29.7	24.2	7.3	16	20	8.0	16.6	24.9
Qtz	9.7	14.8	4.1	3.2	5.1	15.4	12.5	7.6	14.3	0.8	1.9	13.4	6.5	5.9	12.0	6.7	10.3
Opq	6.2	1.4	3.4	2.3	5.1	5.0	8.6	2.8	3.2	3.8	4.3	4.7	4.6	6.5	4.4	6.2	4.3
Bio				0.5				0.9			0.5	1.5	0.3				
Ol				0.5													

Sample	**477**	**478**	**483**	**486**	**488**	**489**	**495**	**497**	**498**	**506**	**511**	**521**	**522**	**525**	**527**	**528**	**529**
Total phenocryst %	*12.4*	*13.9*	*21.2*	*18.8*	*20.7*	*21.0*	*17.2*	*14.0*	*15.6*	*5.6*	*13.5*	*16.0*	*16.2*	*14.4*	*18.8*	*18.6*	*21.1*
% of total phenocrysts																	
Plag	54.1	55.3	51.4	60.3	53.4	51.0	42.5	27.0	45.1	67.9	58.3	44.0	51.9	47.2	62.5	65.8	69.6
PxT	6.5	23.6	20.8	19.1	12.0	10.0	40.2	49.0	30.2	21.4	20.1	40.0	24.3	37.5	8.6	23.4	20.6
OpxT	4.3	8.7	10.4	6.7	5.2	1.9	15.1	18.0	15.3	7.1	5.4	22.0	9.1	8.8	5.4	10.1	4.7
Opx A	2.2	1.4	4.1	2.8			3.5	3.0	2.6		1.5	2.4	2.1	4.2	1.8	5.0	3.2
Opx B	2.1	7.3	6.3	3.9	5.2	1.9	11.6	15.0	12.7	7.1	3.9	20.0	7.0	4.6	3.6	5.1	1.5
CpxT	2.2	14.9	10.4	12.4	6.8	8.4	25.1	31.0	14.9	14.3	14.7	18.0	15.2	28.7	3.2	13.3	15.8
Cpx A	1.6	5.3	8.8	10.6	2.6	7.4	18.9	21.0	9.8	2.4		2.0	2.5	10.6		0.4	0.6
Cpx B	0.6	9.6	1.6	1.8	4.2	1.0	6.2	10.0	5.1	11.9	14.7	16.0	12.7	18.1	3.2	12.9	15.2
Amph	24.9	11.1	7.3	9.2	10.0	21.0	6.2	12.0	20	6.0	7.4	6.9	15.2	7.9	3.6	2.5	3.2
Qtz	10.3	2.9	16.4	7.8	16.8	10.0	6.9	7.0	0.9		10.3	6.9	5.8	3.2	21.8	5.8	4.4
Opq	4.3	7.2	4.1	3.5	7.8	8.4	4.2	6.0	3.8	3.6	3.9	2.4	2.9	4.2	3.6	2.5	2.2
Bio										1.2							
Ol																	

Abbreviations: Amph: amphibole; Bio: biotite; CpxT: total clinopyroxene; CpxA: acicular clinopyroxene phenocrysts forming monomineralic clusters; CpxB: euhedral clinopyroxene phenocrysts; Ol: olivine; Opq: opaques = ilmenite and magnetite; OpxT: total orthopyroxene; OpxA: orthopyroxene = En_{44-51}; OpxB: orthopyroxene = En_{66-83}; Plag: plagioclase; PxT: Total clinopyroxene and orthopyroxene; Qtz: quartz

APPENDIX 2
MINERAL MAJOR ELEMENT DATA

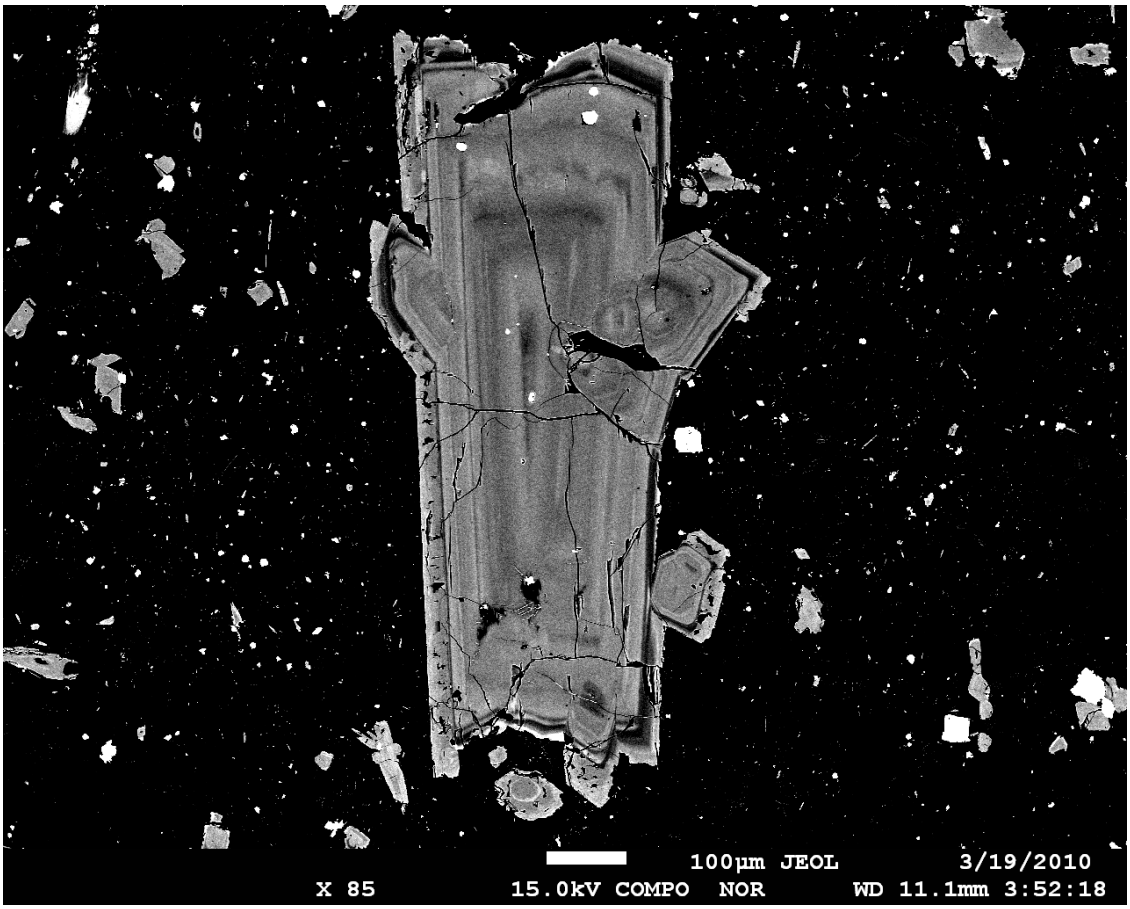

Plate 3. BSE image of an orthopyroxene phenocryst from sample 483

Table A2.1: Clinopyroxene data (6 samples; 149 analyses).

Table A2.2: Orthopyroxene data (4 samples; 104 analyses).

Table A2.3: Amphibole data (6 samples; 149 analyses).

Table A2.4: Plagioclase data (6 samples; 402 analyses).

Table A2.5: Ilmenite data (6 samples; 50 analyses).

Table A2.6: Magnetite data (6 samples, 124 analyses).

Table A2.7: Melt inclusion data (6 samples; 49 analyses).

Table A2.1: EPMA data for clinopyroxene phenocrysts from Tauhara volcano.

Sample #	425	425	425	425	425	425	425	425	425	425	425	425	425	425	425	425	425
Crystal	A	A	A	A	B	B	B	C	C	D	D	D	E	E	E	F	F
Zone	core	mid 1	mid 2	rim	core	mid	rim	core	rim	core	mid	rim	core	mid	rim	mid 1	mid 2
SiO_2	51.46	52.76	52.02	52.00	52.84	53.33	51.31	51.73	52.88	50.58	52.63	52.40	50.35	51.94	51.76	52.68	51.67
TiO_2	0.24	0.16	0.23	0.25	0.18	0.12	0.43	0.27	0.13	0.47	0.23	0.25	0.52	0.25	0.22	0.22	0.25
Cr_2O_3	0.04	0.23	0.18	0.05	0.21	0.29	0.04	0.32	0.00	0.00	0.23	0.10	0.04	0.11	0.06	0.28	0.02
Al_2O_3	3.36	2.13	2.06	2.61	1.91	1.72	3.45	3.46	1.76	4.12	2.62	2.43	4.09	3.67	2.56	2.40	2.88
FeO	7.30	4.41	7.56	7.12	3.96	3.49	6.29	5.05	7.25	9.40	4.87	8.01	9.91	4.67	8.26	4.97	8.80
MnO	0.19	0.11	0.25	0.13	0.11	0.08	0.13	0.09	0.19	0.20	0.10	0.23	0.23	0.09	0.26	0.07	0.24
MgO	15.35	17.05	14.75	15.87	16.66	17.52	16.86	16.50	15.60	14.08	16.98	14.58	13.87	16.74	15.16	17.03	14.42
CaO	21.76	22.97	22.63	21.70	23.92	23.25	21.24	22.35	21.95	20.76	22.12	21.67	20.53	22.34	21.40	22.17	21.32
Na_2O	0.31	0.19	0.31	0.27	0.21	0.19	0.27	0.22	0.25	0.41	0.24	0.33	0.46	0.19	0.32	0.18	0.40
Total	100.43	99.83	99.90	100.29	99.82	99.94	99.52	100.27	100.11	99.84	100.01	98.51	99.77	99.84	100.03	101.12	100.63
En	43.76	47.32	41.84	44.77	46.18	48.42	47.29	46.62	44.02	41.08	47.69	42.08	40.58	47.27	43.10	47.64	41.59
Fe	11.67	6.86	12.03	11.26	6.15	5.41	9.90	8.01	11.47	15.38	7.67	12.96	16.27	7.40	13.17	7.79	14.24
Wo	44.57	45.82	46.13	43.97	47.67	46.17	42.82	45.37	44.51	43.54	44.64	44.95	43.16	45.33	43.72	44.56	44.17
Mg#	78.95	87.33	77.67	79.90	88.24	89.95	82.69	85.34	79.33	72.75	86.15	76.45	71.38	86.46	76.60	85.94	74.50

Sample #	425	425	440	440	440	440	440	440	440	440	440	440	440	440	440	440	440
Crystal	F	F	A	A	B	B	B	B	C	C	C	D	D	E	F	F	F
Zone	mid 3	rim	mid	rim	core	mid	rim	v-rim	core	mid	rim	core	rim	mid	core	mid	rim
SiO_2	53.43	52.76	52.86	51.92	53.13	52.82	51.04	52.34	51.22	52.33	51.47	53.10	51.85	53.22	51.03	51.88	51.69
TiO_2	0.11	0.20	0.16	0.28	0.16	0.15	0.36	0.19	0.45	0.24	0.37	0.16	0.30	0.10	0.50	0.31	0.32
Cr_2O_3	0.11	0.05	0.49	0.05	0.23	0.35	0.01	0.05	0.12	0.50	0.07	0.12	0.02	0.00	0.01	0.34	0.02
Al_2O_3	1.54	1.89	1.92	2.39	1.98	2.02	3.61	1.91	3.73	2.71	2.86	1.88	2.68	0.81	2.98	2.98	2.91
FeO	5.93	6.81	3.76	7.43	4.09	4.71	8.56	7.91	7.09	4.60	8.07	4.75	7.77	8.22	9.16	4.95	7.76
MnO	0.18	0.19	0.10	0.15	0.08	0.11	0.20	0.23	0.13	0.09	0.18	0.07	0.18	0.28	0.21	0.07	0.17
MgO	17.90	16.92	16.72	14.94	16.86	17.05	14.29	15.10	15.19	16.05	14.72	16.76	14.56	15.50	14.74	15.67	14.40
CaO	20.64	20.92	23.77	22.55	23.29	22.56	21.56	21.95	21.75	23.28	21.91	22.97	22.34	21.65	21.10	23.52	22.36
Na_2O	0.17	0.24	0.23	0.29	0.18	0.22	0.36	0.32	0.31	0.21	0.35	0.19	0.30	0.22	0.27	0.29	0.37
Total	100.41	100.08	100.69	100.31	100.32	100.57	100.63	100.04	99.22	99.82	99.88	99.89	99.39	100.11	99.89	99.60	99.51
En	49.65	47.30	46.57	42.31	46.97	47.49	41.32	42.76	43.65	45.38	42.06	46.65	41.63	43.47	42.07	44.33	41.36
Fe	9.22	10.68	5.87	11.80	6.39	7.36	13.88	12.57	11.43	7.29	12.93	7.42	12.46	12.92	14.66	7.86	12.50
Wo	41.13	42.02	47.56	45.89	46.64	45.15	44.80	44.67	44.91	47.32	45.01	45.93	45.91	43.61	43.27	47.81	46.14
Mg#	84.34	81.58	88.81	78.19	88.02	86.58	74.86	77.28	79.24	86.16	76.49	86.28	76.97	77.09	74.16	84.94	76.80

Note: Oxides are normalised to 100%. Total refers to original analytical total. En=enstatite content: En=Mg/(Ca+Fe+Mg), Fe= ferrosilite: Fe/(Ca+Fe+Mg), Wo= wollastonite: Ca/(Ca+Fe+Mg), Mg#= Mg/(Mg+Fe). All cation normalised.

Table A2.1 *(continued)*: EPMA data for clinopyroxene phenocrysts from Tauhara volcano.

Sample #	440	440	440	440	440	440	440	440	440	440	440	440	440	440	440	440	440
Crystal	G	G	G	G	G	H	H	H	I	J	J	J	K	K	L	L	L
Zone	core	mid 1	mid 2	mid 3	rim	core	mid	rim	mid	core	mid	rim	core	rim	core	mid	rim
SiO_2	52.69	51.26	51.53	50.77	51.84	51.47	50.15	53.19	52.66	52.99	51.97	49.86	52.86	49.39	50.57	51.54	51.77
TiO_2	0.17	0.46	0.42	0.50	0.31	0.20	0.57	0.31	0.15	0.19	0.27	0.54	0.10	0.62	0.81	0.30	0.30
Cr_2O_3	0.00	0.04	0.04	0.06	0.04	0.06	0.00	0.00	0.00	0.07	0.04	0.00	0.01	0.00	0.12	0.02	0.09
Al_2O_3	1.29	3.85	3.72	3.99	2.91	3.77	3.93	1.29	1.12	1.51	2.58	4.26	0.90	5.00	4.43	3.01	2.90
FeO	9.28	6.52	5.93	7.00	8.06	6.01	10.92	7.43	9.42	6.27	7.97	10.77	9.83	10.92	6.91	7.56	7.76
MnO	0.28	0.13	0.10	0.16	0.20	0.15	0.43	0.51	0.24	0.13	0.19	0.30	0.34	0.33	0.12	0.14	0.16
MgO	15.32	15.34	15.47	15.26	14.63	15.72	12.83	15.46	15.02	16.67	14.75	12.50	15.54	11.77	15.04	14.52	14.34
CaO	20.69	22.10	22.51	21.95	21.67	22.43	20.82	21.45	21.09	21.96	21.89	21.40	20.17	21.53	21.68	22.54	22.39
Na_2O	0.30	0.31	0.28	0.31	0.33	0.20	0.35	0.36	0.29	0.21	0.35	0.37	0.26	0.44	0.32	0.36	0.29
Total	100.24	100.81	100.29	100.87	100.37	99.83	99.36	99.12	100.10	100.91	100.43	99.86	99.81	99.08	100.09	99.85	99.89
En	43.28	43.97	44.24	43.65	42.12	44.66	37.83	44.12	42.35	46.35	42.20	36.86	43.72	35.27	43.59	41.54	41.23
Fe	14.71	10.48	9.52	11.24	13.02	9.57	18.07	11.89	14.91	9.78	12.79	17.80	15.52	18.36	11.24	12.13	12.51
Wo	42.01	45.55	46.24	45.11	44.86	45.77	44.11	43.99	42.75	43.87	45.00	45.34	40.77	46.36	45.17	46.33	46.26
Mg#	74.64	80.75	82.30	79.53	76.39	82.36	67.68	78.77	73.97	82.58	76.74	67.43	73.81	65.76	79.51	77.40	76.73

Sample #	440	440	456	456	456	456	456	456	456	456	456	456	456	456	456	456	456
Crystal	M	M	A	B	C	C	C	D	D	D	E	F	G	G	H	H	H
Zone	core	rim	mid	core	core	mid	rim	core	mid	rim	mid	mid	core	rim	core	mid	rim
SiO_2	52.60	49.97	53.30	52.24	51.66	51.53	49.92	50.29	52.05	50.91	53.11	52.82	53.19	50.34	50.77	52.54	52.15
TiO_2	0.27	0.53	0.08	0.22	0.25	0.29	0.43	0.45	0.23	0.38	0.12	0.12	0.14	0.40	0.33	0.19	0.19
Cr_2O_3	0.04	0.00	0.03	0.01	0.01	0.42	0.02	0.01	0.40	0.05	0.00	0.00	0.33	0.02	0.34	0.61	0.03
Al_2O_3	2.08	5.21	0.61	2.15	2.69	3.20	4.61	4.25	2.78	3.68	1.03	0.81	1.80	3.78	4.21	2.38	2.16
FeO	6.73	10.80	8.32	8.64	8.24	6.28	9.35	9.44	6.59	8.40	9.01	9.31	5.43	9.59	7.26	5.25	8.56
MnO	0.15	0.27	0.21	0.24	0.22	0.17	0.19	0.26	0.16	0.20	0.21	0.25	0.15	0.23	0.16	0.14	0.23
MgO	16.06	12.08	15.99	15.40	15.47	16.40	13.87	14.36	16.93	14.38	15.23	15.33	17.25	14.47	15.15	17.29	15.78
CaO	21.91	20.32	21.13	20.84	21.23	21.47	21.32	20.63	20.62	21.72	21.06	21.14	21.53	20.85	21.47	21.38	20.64
Na_2O	0.17	0.82	0.32	0.25	0.24	0.25	0.28	0.30	0.24	0.28	0.23	0.21	0.19	0.31	0.30	0.22	0.25
Total	99.94	98.98	100.16	100.37	99.81	100.35	100.25	99.83	100.22	100.01	99.50	100.56	99.42	99.16	98.83	98.53	98.75
En	45.14	36.89	44.61	43.72	43.77	46.39	40.27	41.64	47.76	41.44	43.00	42.89	48.23	41.53	43.73	48.57	44.55
Fe	10.61	18.50	13.02	13.76	13.07	9.96	15.23	15.36	10.42	13.58	14.27	14.61	8.52	15.45	11.76	8.27	13.56
Wo	44.25	44.61	42.36	42.52	43.16	43.65	44.50	43.00	41.82	44.98	42.73	42.50	43.25	43.02	44.52	43.16	41.89
Mg#	80.97	66.60	77.40	76.07	77.01	82.32	72.56	73.05	82.09	75.32	75.09	74.59	84.99	72.89	78.81	85.45	76.67

Table A2.1 *(continued)*: EPMA data for clinopyroxene phenocrysts from Tauhara volcano.

Sample #	456	456	456	456	456	456	456	456	456	456	477	477	477	477	477	477	477
Crystal	I	I	I	I	J	K	L	L	L	M	A	A	A	B	C	C	D
Zone	core 1	core 2	mid	rim	mid	mid	core	mid	rim	mid	core	mid	rim	mid	core	rim	core
SiO_2	50.33	50.08	52.88	51.75	53.19	52.27	49.94	52.60	50.79	53.12	50.71	52.14	50.50	51.76	50.88	49.08	50.56
TiO_2	0.40	0.45	0.19	0.29	0.15	0.22	0.63	0.19	0.35	0.08	0.33	0.24	0.42	0.28	0.43	0.69	0.40
Cr_2O_3	0.02	0.01	0.64	0.02	0.00	0.05	0.00	0.61	0.04	0.01	0.20	0.58	0.12	0.11	0.02	0.02	0.15
Al_2O_3	5.00	3.52	2.24	2.97	0.91	2.31	5.12	2.30	3.91	0.67	3.83	2.56	4.33	2.97	3.35	5.53	4.42
FeO	7.53	14.00	4.76	8.94	9.33	8.17	8.95	4.88	8.63	8.34	6.81	5.53	7.06	6.64	9.52	9.16	6.92
MnO	0.13	0.28	0.15	0.21	0.25	0.20	0.24	0.12	0.20	0.20	0.14	0.14	0.15	0.12	0.23	0.20	0.13
MgO	15.17	12.42	17.32	14.87	15.69	15.22	13.90	17.05	14.30	15.43	15.53	16.67	15.56	16.44	14.31	13.97	15.58
CaO	21.23	18.88	21.63	20.67	20.26	21.29	20.80	22.06	21.52	21.87	22.21	21.90	21.61	21.46	20.87	21.07	21.60
Na_2O	0.20	0.36	0.19	0.29	0.22	0.27	0.42	0.18	0.27	0.26	0.24	0.25	0.25	0.22	0.40	0.27	0.26
Total	99.41	99.24	99.43	99.65	99.85	100.10	99.29	100.47	100.08	100.01	99.97	100.76	100.31	100.03	100.10	100.58	99.71
En	43.78	36.70	48.75	42.82	44.21	43.35	41.04	47.84	41.32	43.07	43.99	46.94	44.40	46.21	41.30	40.79	44.53
Fe	12.18	23.20	7.51	14.43	14.76	13.06	14.82	7.68	13.99	13.06	10.81	8.73	11.30	10.46	15.41	15.00	11.09
Wo	44.04	40.10	43.75	42.75	41.03	43.59	44.14	44.48	44.69	43.87	45.20	44.33	44.30	43.33	43.29	44.21	44.38
Mg#	78.23	61.27	86.66	74.80	74.98	76.85	73.46	86.17	74.71	76.73	80.27	84.32	79.71	81.54	72.82	73.11	80.06

Sample #	477	477	477	477	477	477	477	477	477	477	477	477	483	483	483	483	483
Crystal	D	D	D	E	E	F	F	F	G	H	H	H	A	A	A	B	C
Zone	mid 1	mid 2	rim	core	rim	core	mid	rim	mid	core	mid	rim	core	mid	rim	mid	core
SiO_2	52.22	50.73	49.56	50.93	49.94	53.30	53.42	51.68	53.47	50.64	50.38	49.64	51.86	51.32	52.81	53.27	51.46
TiO_2	0.22	0.38	0.58	0.34	0.50	0.08	0.07	0.30	0.07	0.43	0.45	0.52	0.32	0.32	0.26	0.08	0.32
Cr_2O_3	0.53	0.11	0.00	0.37	0.03	0.00	0.03	0.00	0.00	0.21	0.12	0.00	0.04	0.11	0.02	0.00	0.00
Al_2O_3	2.53	4.17	5.01	3.95	4.25	0.44	0.54	2.56	0.33	4.52	4.71	4.80	2.38	3.17	0.84	0.32	2.51
FeO	5.29	6.95	9.04	6.38	9.16	9.10	7.52	10.27	7.67	6.87	7.31	9.04	8.27	7.75	9.99	8.93	9.60
MnO	0.12	0.16	0.23	0.15	0.25	0.28	0.18	0.45	0.19	0.16	0.17	0.25	0.24	0.18	0.63	0.27	0.29
MgO	16.77	15.42	14.06	15.96	14.10	16.07	16.21	13.20	15.70	15.38	15.21	14.34	14.89	15.11	14.49	15.53	14.89
CaO	22.11	21.83	21.26	21.62	21.48	20.45	21.83	21.15	22.35	21.53	21.36	21.18	21.73	21.78	20.53	21.43	20.63
Na_2O	0.21	0.24	0.25	0.30	0.29	0.27	0.22	0.38	0.23	0.25	0.28	0.23	0.27	0.27	0.43	0.18	0.28
Total	99.86	100.37	99.98	99.19	99.71	99.42	99.37	100.14	99.50	99.38	99.47	99.16	99.44	99.63	99.19	99.68	100.19
En	47.07	44.04	40.86	45.50	40.67	44.80	44.88	38.64	43.53	44.31	43.89	41.41	42.37	43.04	41.59	43.20	42.42
Fe	8.33	11.14	14.74	10.20	14.82	14.24	11.68	16.87	11.93	11.11	11.82	14.64	13.20	12.37	16.08	13.94	15.34
Wo	44.60	44.82	44.40	44.29	44.51	40.96	43.44	44.49	44.54	44.58	44.29	43.95	44.43	44.58	42.33	42.86	42.24
Mg#	84.96	79.82	73.49	81.68	73.29	75.88	79.35	69.61	78.49	79.96	78.78	73.89	76.24	77.67	72.11	75.61	73.44

Table A2.1 *(continued)*: EPMA data for clinopyroxene phenocrysts from Tauhara volcano.

Sample #	483	483	483	483	483	483	483	483	483	483	527	527	527	527	527	527	527
Crystal	C	C	E	E	F	G	H	H	I	I	A	B	B	B	B	B	C
Zone	mid	rim	core	rim	core	mid	core	rim	mid	rim	rim	core	mid 1	mid 2	mid 3	rim	core
SiO_2	52.28	51.94	52.59	53.42	52.40	52.72	50.45	51.76	50.32	50.60	50.55	51.97	50.66	51.32	50.53	49.83	50.72
TiO_2	0.22	0.19	0.12	0.11	0.10	0.15	0.42	0.21	0.41	0.46	0.41	0.24	0.49	0.41	0.55	0.76	0.42
Cr_2O_3	0.05	0.00	0.00	0.01	0.01	0.00	0.07	0.00	0.08	0.02	0.17	0.09	0.15	0.01	0.14	0.00	0.17
Al_2O_3	2.34	2.25	0.66	0.60	0.66	0.97	3.74	1.68	4.14	3.47	4.20	2.45	4.30	2.37	4.13	4.23	4.22
FeO	8.10	9.70	9.00	6.91	10.96	10.25	8.58	9.34	8.13	9.99	7.67	7.66	7.80	9.22	7.55	9.77	7.26
MnO	0.21	0.27	0.28	0.17	0.60	0.33	0.19	0.33	0.18	0.30	0.13	0.17	0.18	0.42	0.16	0.27	0.20
MgO	15.74	15.06	14.83	16.39	13.24	16.21	14.93	15.10	14.71	13.78	15.25	16.75	15.30	14.97	15.27	14.33	15.52
CaO	20.83	20.30	22.25	22.16	21.75	19.13	21.35	21.30	21.73	21.01	21.29	20.42	20.78	20.98	21.41	20.49	21.19
Na_2O	0.22	0.29	0.27	0.22	0.28	0.23	0.27	0.27	0.30	0.36	0.31	0.25	0.33	0.30	0.27	0.33	0.30
Total	100.12	100.17	98.81	98.63	99.61	100.04	98.36	98.97	99.84	98.86	100.94	100.39	100.46	101.01	100.36	99.99	100.14
En	44.65	42.92	41.35	45.29	37.81	45.40	42.54	42.36	42.16	39.97	43.76	46.88	44.20	42.51	43.76	41.49	44.57
Fe	12.88	15.50	14.07	10.71	17.56	16.10	13.71	14.70	13.08	16.25	12.34	12.02	12.65	14.69	12.14	15.87	11.69
Wo	42.46	41.57	44.58	44.00	44.63	38.50	43.74	42.94	44.76	43.78	43.90	41.09	43.15	42.80	44.10	42.64	43.74
Mg#	77.61	73.46	74.61	80.88	68.29	73.83	75.62	74.24	76.33	71.09	78.00	79.59	77.75	74.32	78.29	72.33	79.22

Sample #	527	527	527	527	527	527	527	527	527	527	527	527	527	527	527	527	527
Crystal	C	C	C	D	D	E	F	F	G	G	H	I	I	J	J	J	K
Zone	mid 1	mid 2	rim	mid	rim	mid	core	mid	mid	rim	mid	core	mid	mid 1	mid 2	rim	mid
SiO_2	49.60	51.34	49.36	50.07	50.51	52.66	52.59	52.39	50.96	48.67	53.45	51.08	52.00	51.78	50.86	51.17	50.59
TiO_2	0.57	0.36	0.60	0.54	0.50	0.17	0.25	0.24	0.40	0.98	0.14	0.40	0.33	0.28	0.56	0.40	0.45
Cr_2O_3	0.00	0.12	0.00	0.03	0.20	0.01	0.00	0.14	0.17	0.01	0.01	0.26	0.13	0.09	0.04	0.26	0.20
Al_2O_3	4.80	3.46	5.01	4.16	4.51	0.87	1.64	2.46	3.69	5.70	0.58	3.42	2.77	2.66	3.36	3.74	3.74
FeO	9.23	7.00	9.51	9.62	7.22	9.76	8.34	6.93	7.07	10.15	7.98	7.56	7.02	7.29	8.81	6.51	7.74
MnO	0.23	0.15	0.23	0.20	0.18	0.23	0.25	0.21	0.14	0.29	0.21	0.18	0.21	0.21	0.25	0.18	0.16
MgO	14.31	15.71	14.07	14.28	15.18	15.83	16.13	16.50	15.67	14.36	16.56	15.26	16.23	15.47	14.70	15.83	15.62
CaO	20.96	21.59	20.90	20.74	21.37	20.21	20.59	20.86	21.61	19.55	20.86	21.56	21.12	21.90	21.13	21.67	21.28
Na_2O	0.30	0.28	0.31	0.37	0.32	0.26	0.22	0.27	0.28	0.29	0.21	0.28	0.20	0.31	0.29	0.24	0.22
Total	100.61	99.54	100.12	99.78	99.31	99.78	100.11	100.38	100.36	99.36	99.09	99.10	99.04	99.96	100.48	100.08	99.49
En	41.41	44.70	40.87	41.29	43.89	44.18	45.30	46.64	44.56	42.11	45.96	43.61	45.92	43.83	42.21	45.15	44.30
Fe	14.98	11.17	15.50	15.61	11.71	15.27	13.14	10.99	11.27	16.70	12.43	12.11	11.14	11.59	14.18	10.41	12.32
Wo	43.61	44.13	43.63	43.10	44.40	40.54	41.56	42.38	44.17	41.19	41.61	44.27	42.94	44.58	43.61	44.43	43.39
Mg#	73.43	80.00	72.50	72.57	78.94	74.31	77.52	80.93	79.81	71.60	78.71	78.26	80.48	79.09	74.85	81.26	78.24

Table A2.1 *(continued)*: EPMA data for clinopyroxene phenocrysts from Tauhara volcano.

Sample #	527	527	527	527	527	527	527	527	527	527	527	527	527
Crystal	K	L	M	M	M	N	N	N	O	O	O	O	O
Zone	rim	mid	core	mid	rim	mid 1	mid 2	rim	core	mid 1	mid 2	mid 3	mid 4
SiO_2	49.65	51.93	52.15	50.80	51.08	52.04	50.80	51.01	50.36	50.90	49.01	50.40	49.68
TiO_2	0.64	0.35	0.25	0.47	0.51	0.26	0.41	0.43	0.44	0.35	0.61	0.41	0.56
Cr_2O_3	0.06	0.04	0.07	0.17	0.00	0.03	0.21	0.17	0.09	0.20	0.00	0.18	0.03
Al_2O_3	4.18	2.45	2.47	4.15	2.80	1.92	3.91	3.65	3.49	3.41	4.72	3.98	4.70
FeO	10.17	7.52	6.88	7.53	9.12	8.68	7.30	7.47	9.07	7.42	10.35	7.66	9.31
MnO	0.22	0.19	0.16	0.19	0.41	0.25	0.16	0.23	0.18	0.14	0.19	0.15	0.21
MgO	14.93	16.14	16.49	15.25	14.66	15.48	15.88	15.72	14.46	15.57	14.10	15.25	14.60
CaO	19.85	21.13	21.28	21.12	21.08	21.06	21.01	21.01	21.56	21.72	20.70	21.63	20.64
Na_2O	0.30	0.26	0.24	0.33	0.33	0.27	0.31	0.30	0.35	0.29	0.32	0.33	0.27
Total	100.13	99.01	99.63	99.19	99.29	99.44	99.61	99.71	99.65	99.62	99.44	99.72	99.59
En	42.78	45.41	46.27	44.01	41.98	43.63	45.27	44.90	41.27	44.05	40.54	43.47	42.13
Fe	16.34	11.87	10.83	12.19	14.65	13.72	11.68	11.97	14.52	11.78	16.69	12.25	15.07
Wo	40.88	42.72	42.91	43.80	43.37	42.66	43.05	43.13	44.21	44.17	42.77	44.28	42.80
Mg#	72.36	79.28	81.04	78.31	74.13	76.08	79.49	78.95	73.97	78.90	70.84	78.02	73.65

Table A2.2: EPMA data for orthopyroxene phenocrysts from Tauhara volcano.

Sample #	456	456	456	456	456	456	456	456	456	456	456	456	456	456	477	477	477
Crystal	A	B	B	C	C	D	E	E	E	F	F	F	G	G	A	A	A
Zone	mid	core	rim	core	rim	rim	core	mid	rim	core	mid	rim	core	rim	core	mid 1	mid 2
SiO_2	53.35	50.89	50.77	50.66	54.40	50.84	53.97	53.62	54.06	52.65	55.54	54.24	53.43	53.62	54.16	52.78	53.02
TiO_2	0.15	0.13	0.09	0.12	0.12	0.10	0.12	0.18	0.11	0.18	0.08	0.11	0.15	0.14	0.20	0.26	0.19
Cr_2O_3	0.68	1.52	1.51	1.55	0.63	1.60	0.42	0.28	0.54	0.38	0.25	0.50	0.39	0.39	0.22	0.33	0.30
Al_2O_3	0.80	0.41	0.33	0.27	0.72	0.35	1.38	2.44	0.68	2.77	0.96	0.74	2.03	1.64	2.31	3.59	3.08
FeO	19.31	29.37	30.26	30.30	17.28	30.99	16.46	14.21	17.30	16.36	11.91	16.56	16.13	16.99	13.44	14.68	14.72
MnO	0.05	0.01	0.02	0.02	0.05	0.03	0.05	0.21	0.00	0.12	0.11	0.03	0.03	0.05	0.09	0.00	0.07
MgO	24.30	16.58	16.07	16.00	25.37	15.29	26.44	27.49	25.83	25.94	29.82	26.34	26.64	25.80	28.29	26.86	27.36
CaO	1.34	1.09	0.93	1.07	1.37	0.77	1.14	1.55	1.47	1.58	1.33	1.46	1.18	1.35	1.26	1.49	1.26
Na_2O	0.01	0.01	0.02	0.03	0.06	0.03	0.02	0.03	0.01	0.03	0.01	0.03	0.03	0.01	0.03	0.02	0.01
Total	100.61	101.74	101.94	101.91	100.41	101.31	100.55	100.67	100.17	100.88	100.37	100.32	100.65	100.50	100.78	101.64	101.85
En	67.32	48.99	47.67	47.38	70.38	46.03	72.46	75.16	70.59	71.56	79.61	71.82	72.91	71.07	77.01	74.27	74.91
Fe	30.01	48.69	50.36	50.34	26.89	52.31	25.30	21.80	26.52	25.31	17.83	25.33	24.76	26.25	20.52	22.77	22.61
Wo	2.67	2.31	1.98	2.28	2.73	1.66	2.24	3.05	2.89	3.13	2.55	2.86	2.32	2.68	2.47	2.96	2.48
Mg#	69.17	50.15	48.63	48.49	72.35	46.80	74.12	77.52	72.69	73.87	81.70	73.93	74.65	73.03	78.96	76.54	76.81

Sample #	477	477	477	477	477	477	477	477	477	477	477	477	477	477	477	477	477
Crystal	A	B	B	C	C	C	D	E	E	E	F	F	F	F	F	G	G
Zone	rim	mid 1	mid 2	mid 1	mid 2	mid 3	mid	mid 1	mid 2	mid 3	core	mid 1	mid 2	mid 3	rim	mid	rim
SiO_2	53.18	52.73	53.66	53.44	53.17	52.77	53.55	54.83	54.93	53.48	53.96	53.04	54.84	54.75	54.42	54.75	54.50
TiO_2	0.22	0.25	0.17	0.18	0.20	0.25	0.17	0.12	0.10	0.15	0.13	0.21	0.13	0.09	0.10	0.10	0.14
Cr_2O_3	0.41	0.35	0.26	0.30	0.51	0.41	0.32	0.29	0.38	0.51	0.27	0.23	0.24	0.26	0.36	0.27	0.35
Al_2O_3	2.52	3.63	3.56	3.16	1.96	3.02	2.85	1.61	0.94	1.60	2.36	3.97	1.64	1.74	1.41	1.66	1.28
FeO	16.26	14.40	12.38	14.04	17.45	16.05	13.74	12.23	13.50	17.10	14.16	12.93	11.79	12.39	14.20	12.44	14.57
MnO	0.01	0.00	0.21	0.00	0.00	0.00	0.00	0.05	0.01	0.01	0.12	0.09	0.16	0.04	0.00	0.05	0.00
MgO	25.89	27.13	28.65	27.74	25.46	25.78	28.06	29.50	28.57	26.02	28.00	28.29	29.79	29.39	28.13	29.29	27.67
CaO	1.50	1.48	1.10	1.13	1.22	1.69	1.28	1.37	1.56	1.15	0.98	1.22	1.41	1.32	1.36	1.43	1.47
Na_2O	0.00	0.02	0.02	0.00	0.04	0.02	0.04	0.00	0.03	0.00	0.00	0.02	0.00	0.02	0.02	0.00	0.02
Total	101.75	101.14	100.91	100.92	101.09	101.20	101.15	100.08	100.48	101.13	100.22	100.70	99.84	99.38	98.99	101.32	101.14
En	71.74	74.80	78.74	76.15	70.47	71.62	76.48	78.99	76.67	71.41	76.40	77.68	79.62	78.81	75.88	78.54	74.99
Fe	25.28	22.26	19.08	21.62	27.10	25.01	21.00	18.37	20.32	26.33	21.67	19.92	17.67	18.64	21.48	18.71	22.15
Wo	2.98	2.94	2.18	2.23	2.43	3.37	2.51	2.64	3.01	2.26	1.93	2.40	2.72	2.55	2.65	2.75	2.86
Mg#	73.95	77.07	80.50	77.89	72.22	74.12	78.45	81.14	79.05	73.06	77.90	79.59	81.84	80.88	77.94	80.76	77.20

Note: Oxides are normalised to 100%. Total refers to original analytical total. En=enstatite content: En=Mg/(Ca+Fe+Mg), Fe= ferrosilite: Fe/(Ca+Fe+Mg), Wo= wollastonite: Ca/(Ca+Fe+Mg), Mg#= Mg/(Mg+Fe). All cation normalised.

Table A2.2 *(continued)*: EPMA data for orthopyroxene phenocrysts from Tauhara volcano.

Sample #	483	483	483	483	483	483	483	483	483	483	483	483	483	483	483	483	483
Crystal	A	A	A	A	B	B	B	B	C	C	C	C	D	D	D	D	D
Zone	core	mid 1	mid 2	rim	core	mid 1	mid 2	rim	core	mid 1	mid 2	rim	core	mid 1	mid 2	mid 3	mid 4
SiO_2	51.85	53.61	53.02	52.62	53.84	54.00	53.99	53.14	52.89	52.98	53.07	53.02	52.82	53.30	53.38	53.02	53.10
TiO_2	0.16	0.13	0.20	0.25	0.11	0.12	0.13	0.13	0.14	0.20	0.17	0.17	0.19	0.16	0.17	0.17	0.19
Cr_2O_3	0.41	0.31	0.30	0.42	0.41	0.23	0.26	0.35	0.40	0.28	0.30	0.39	0.40	0.25	0.25	0.19	0.28
Al_2O_3	2.37	1.72	2.07	2.27	0.83	1.35	1.05	1.47	1.25	2.26	1.85	1.33	1.33	2.10	2.14	3.23	2.06
FeO	21.33	17.19	18.44	20.04	18.69	16.60	17.42	19.64	19.52	16.79	17.42	19.02	19.90	16.58	16.63	14.46	17.71
MnO	0.01	0.07	0.00	0.01	0.00	0.01	0.07	0.02	0.04	0.01	0.10	0.06	0.00	0.07	0.05	0.15	0.10
MgO	22.80	25.91	24.74	23.00	24.94	26.45	25.95	24.17	24.56	25.68	26.05	24.89	24.03	26.39	26.18	27.30	25.39
CaO	1.07	1.07	1.22	1.38	1.18	1.22	1.13	1.06	1.17	1.80	1.05	1.09	1.32	1.15	1.17	1.46	1.14
Na_2O	0.01	0.00	0.01	0.02	0.00	0.00	0.01	0.02	0.03	0.02	0.00	0.02	0.01	0.00	0.02	0.02	0.03
Total	101.73	101.39	101.01	103.61	101.03	101.56	101.10	101.52	101.19	100.76	100.16	100.43	101.48	101.47	101.19	101.71	101.24
En	64.16	71.33	68.79	65.29	68.77	72.20	71.03	67.23	67.57	70.57	71.23	68.48	66.49	72.28	72.01	74.87	70.24
Fe	33.68	26.55	28.77	31.90	28.90	25.41	26.75	30.64	30.12	25.88	26.71	29.36	30.88	25.47	25.67	22.24	27.49
Wo	2.16	2.12	2.44	2.81	2.33	2.39	2.22	2.13	2.31	3.55	2.05	2.16	2.63	2.26	2.32	2.88	2.27
Mg#	65.58	72.88	70.51	67.18	70.41	73.97	72.65	68.69	69.17	73.17	72.73	69.99	68.28	73.94	73.72	77.10	71.87

Sample #	483	483	483	483	483	483	483	483	483	483	483	483	483	483	483	483	483
Crystal	D	D	F	F	G	G	G	G	G	J	J	J	K	L	L	L	L
Zone	mid 5	rim	mid	rim	core	mid 1	mid 2	mid 3	rim	mid 1	mid 2	rim	mid	core	mid 1	mid 2	rim
SiO_2	52.89	52.99	53.29	53.32	53.37	52.10	51.85	52.45	53.34	51.51	52.93	52.51	50.43	52.15	53.78	53.55	53.57
TiO_2	0.20	0.25	0.18	0.20	0.19	0.20	0.23	0.20	0.23	0.21	0.17	0.20	0.12	0.21	0.11	0.11	0.08
Cr_2O_3	0.35	0.37	0.28	0.28	0.26	0.32	0.27	0.33	0.53	0.35	0.34	0.34	0.88	0.22	0.33	0.35	0.38
Al_2O_3	1.76	1.61	1.66	1.81	1.99	2.74	2.70	2.24	2.38	1.99	1.49	1.75	0.34	3.93	0.89	0.87	0.82
FeO	19.39	19.24	17.75	17.44	16.88	19.21	19.42	19.47	19.44	21.20	18.96	19.02	30.39	14.48	17.66	18.78	18.43
MnO	0.04	0.01	0.01	0.02	0.12	0.01	0.00	0.00	0.00	0.00	0.01	0.02	0.00	0.11	0.02	0.00	0.02
MgO	24.20	24.21	25.70	25.73	26.09	24.11	24.25	24.12	22.48	23.57	24.93	24.89	17.03	26.69	26.05	25.07	25.50
CaO	1.15	1.29	1.12	1.18	1.10	1.29	1.27	1.17	1.51	1.17	1.15	1.27	0.78	2.17	1.15	1.23	1.17
Na_2O	0.03	0.04	0.00	0.01	0.01	0.03	0.00	0.02	0.09	0.00	0.01	0.01	0.03	0.04	0.00	0.03	0.02
Total	101.60	100.97	101.77	101.53	101.04	101.49	101.79	101.10	101.69	101.35	100.75	100.88	102.19	100.42	101.16	101.13	100.96
En	67.39	67.39	70.48	70.77	71.78	67.33	67.26	67.23	65.21	64.93	68.50	68.24	49.17	73.38	70.83	68.71	69.53
Fe	30.30	30.03	27.31	26.90	26.05	30.09	30.21	30.43	31.64	32.75	29.22	29.25	49.21	22.32	26.93	28.86	28.18
Wo	2.31	2.58	2.21	2.33	2.18	2.58	2.54	2.33	3.16	2.31	2.28	2.50	1.62	4.29	2.25	2.43	2.30
Mg#	68.99	69.17	72.08	72.46	73.37	69.11	69.01	68.84	67.33	66.47	70.10	69.99	49.98	76.68	72.45	70.42	71.16

Table A2.2 *(continued)*: EPMA data for orthopyroxene phenocrysts from Tauhara volcano.

Sample #	483	483	483	483	483	483	483	527	527	527	527	527	527	527	527	527	527	527
Crystal	N	N	N	Q	Q	Q	Q	A	A	A	A	B	B	B	B	B	C	C
Zone	mid 1	mid 2	mid 3	core	mid 1	mid 2	rim	core	mid 1	mid 2	mid 3	core	mid 2	mid 3	mid 4	rim	mid 1	mid 2
SiO_2	51.60	53.11	53.06	45.24	44.76	44.98	45.02	53.29	53.38	53.37	52.02	53.34	52.50	53.63	52.86	53.16	54.57	54.29
TiO_2	0.19	0.19	0.20	2.28	2.32	2.39	2.31	0.18	0.18	0.18	0.30	0.13	0.22	0.20	0.21	0.19	0.13	0.14
Cr_2O_3	0.47	0.36	0.35	0.09	0.08	0.11	0.09	0.27	0.63	0.30	0.39	0.37	0.45	0.28	0.40	0.30	0.31	0.26
Al_2O_3	1.76	1.27	1.57	11.18	11.42	11.21	11.58	3.42	1.53	3.08	4.00	1.85	2.65	2.84	2.73	3.20	1.18	1.62
FeO	22.00	18.86	18.87	11.99	12.65	13.18	12.72	13.55	17.87	13.74	15.77	15.27	17.36	12.67	16.15	14.03	13.99	14.49
MnO	0.02	0.00	0.00	0.13	0.08	0.05	0.08	0.06	0.03	0.14	0.02	0.08	0.01	0.17	0.08	0.11	0.06	0.07
MgO	22.48	24.81	24.86	15.16	14.79	14.44	14.53	27.86	25.13	27.78	26.02	27.25	25.53	28.37	26.35	27.71	28.10	27.15
CaO	1.47	1.39	1.09	12.25	12.14	11.92	11.96	1.33	1.24	1.37	1.43	1.68	1.24	1.82	1.21	1.29	1.66	1.95
Na_2O	0.02	0.02	0.01	1.68	1.77	1.72	1.72	0.04	0.01	0.03	0.04	0.03	0.03	0.03	0.01	0.02	0.02	0.03
Total	101.60	101.33	100.99	98.75	98.64	98.84	98.87	100.68	101.50	101.41	101.41	100.36	100.51	100.67	100.36	101.11	101.49	100.51
En	62.67	68.18	68.63	49.40	48.32	47.51	48.03	76.51	69.73	76.17	72.49	73.60	70.61	77.13	72.63	75.90	75.67	74.03
Fe	34.39	29.08	29.21	21.91	23.18	24.31	23.57	20.87	27.81	21.13	24.64	23.14	26.93	19.32	24.98	21.56	21.12	22.16
Wo	2.94	2.75	2.15	28.69	28.50	28.18	28.40	2.62	2.46	2.70	2.87	3.26	2.46	3.55	2.39	2.54	3.21	3.81
Mg#	64.57	70.10	70.14	69.27	67.58	66.15	67.08	78.57	71.49	78.28	74.63	76.08	72.39	79.97	74.41	77.88	78.18	76.96

Sample #	527	527	527	527	527	527	527	527	527	527	527	527	527	527	527	527	527	527
Crystal	C	C	D	D	D	D	E	E	E	F	F	F	G	G	G	G	G	G
Zone	mid 3	mid 4	mid 1	mid 2	mid 3	rim	core	mid 1	mid 2	core	mid	rim	core	mid 1	mid 2	mid 3	mid 4	rim
SiO_2	53.49	53.93	53.65	54.58	54.02	54.25	53.68	53.24	53.46	53.39	53.18	53.33	53.13	53.15	53.41	52.03	53.43	53.40
TiO_2	0.23	0.19	0.21	0.16	0.17	0.17	0.20	0.15	0.22	0.20	0.21	0.24	0.17	0.22	0.20	0.22	0.17	0.18
Cr_2O_3	0.29	0.30	0.31	0.37	0.38	0.45	0.32	0.29	0.25	0.38	0.28	0.30	0.28	0.35	0.31	0.35	0.28	0.28
Al_2O_3	3.26	2.57	2.78	1.12	1.20	1.18	2.51	2.72	2.92	2.43	3.25	3.36	3.65	2.48	3.09	4.12	2.93	3.24
FeO	12.83	13.10	13.89	14.63	15.94	15.39	13.57	15.63	13.19	15.11	14.05	13.46	12.53	16.62	13.50	15.99	13.89	13.69
MnO	0.14	0.13	0.07	0.01	0.02	0.01	0.12	0.05	0.15	0.01	0.10	0.13	0.48	0.04	0.11	0.08	0.18	0.13
MgO	27.91	28.49	27.75	27.57	26.55	26.81	28.39	26.67	28.57	26.63	27.59	27.84	27.74	25.84	27.99	25.62	27.89	27.78
CaO	1.81	1.28	1.32	1.54	1.70	1.75	1.19	1.23	1.24	1.81	1.34	1.33	2.01	1.30	1.40	1.59	1.21	1.27
Na_2O	0.03	0.02	0.02	0.01	0.01	0.01	0.02	0.01	0.01	0.03	0.02	0.01	0.03	0.00	0.01	0.00	0.01	0.03
Total	101.47	100.90	100.70	100.59	100.78	101.12	100.56	100.02	99.94	100.66	100.46	100.49	100.54	100.86	100.66	100.65	101.02	100.97
En	76.66	77.51	76.04	74.75	72.32	73.05	77.02	73.42	77.51	73.14	75.73	76.60	76.61	71.58	76.55	71.69	76.31	76.37
Fe	19.76	19.99	21.35	22.25	24.34	23.53	20.65	24.14	20.07	23.28	21.63	20.77	19.41	25.82	20.70	25.10	21.31	21.11
Wo	3.58	2.50	2.60	3.00	3.34	3.42	2.33	2.44	2.42	3.58	2.64	2.62	3.98	2.60	2.75	3.21	2.38	2.52
Mg#	79.51	79.49	78.07	77.06	74.82	75.64	78.85	75.26	79.43	75.86	77.78	78.67	79.79	73.49	78.71	74.07	78.17	78.34

Table A2.3: EPMA data for amphibole phenocrysts from Tauhara volcano.

Sample #	425	425	425	425	425	425	425	425	425	425	425	425	425	425	425	425	425
Crystal	A	A	A	C	C	G	G	G	G	G	G	G	H	H	H	H	H
Zone	core	mid	rim	mid	rim	core	mid 1	mid 2	mid 3	mid 4	mid 5	rim	core	mid	rim	core	mid
SiO_2	45.48	45.93	47.32	45.71	45.43	46.28	46.16	45.66	46.69	46.37	47.28	45.41	45.28	45.79	45.33	45.54	45.43
TiO_2	1.63	1.46	1.38	1.50	1.47	1.34	1.43	1.58	1.22	1.42	0.98	1.46	1.64	1.44	1.53	1.58	1.42
Al_2O_3	10.45	10.21	9.77	10.34	9.46	9.54	10.05	9.87	10.49	9.97	9.46	9.92	10.44	10.13	10.13	10.26	10.19
Fe_2O_3	4.78	5.36	0.23	7.16	5.94	4.59	5.11	4.36	5.47	5.43	4.29	4.16	6.32	6.18	6.98	5.14	5.85
FeO	5.61	5.16	10.53	4.37	6.30	6.78	5.16	7.81	3.89	6.27	3.38	7.99	5.26	4.52	6.48	5.33	4.72
MnO	0.08	0.09	0.15	0.10	0.14	0.16	0.12	0.18	0.09	0.14	0.09	0.15	0.12	0.12	0.18	0.12	0.12
MgO	15.49	15.63	14.51	15.57	14.91	14.98	15.72	14.22	16.08	14.80	17.15	14.43	15.16	15.64	14.28	15.43	15.71
CaO	11.93	11.93	11.68	11.84	11.81	11.83	12.00	11.82	11.53	11.66	11.78	11.66	11.78	11.70	11.59	11.85	11.97
Na_2O	1.93	1.78	2.70	1.75	1.86	1.81	1.68	1.75	1.87	1.70	1.82	2.34	1.86	1.82	1.93	1.82	1.78
K_2O	0.44	0.41	0.58	0.43	0.41	0.40	0.43	0.43	0.46	0.41	0.47	0.45	0.44	0.43	0.42	0.40	0.42
H_2O	1.86	1.82	1.87	1.88	1.84	1.85	1.71	1.70	1.96	1.95	1.96	1.93	1.94	1.94	1.94	1.94	1.94
Total	99.84	99.99	100.87	100.76	99.71	99.69	99.94	99.71	99.77	100.13	98.67	99.91	100.25	99.72	100.79	99.41	99.55
Al#	0.17	0.17	0.27	0.14	0.12	0.18	0.18	0.18	0.23	0.20	0.23	0.16	0.15	0.16	0.13	0.17	0.15
Species	Mg-Hbl	Mg-Hbl	Xeno	Mg-Hbl	Mg-Hbl	Mg-Hbl	Mg-Hbl	Mg-Hbl	Xeno	Mg-Hbl	Xeno	Mg-Hbl	T-Prg	Mg-Hbl	Mg-Hbl	Mg-Hbl	Mg-Hbl

Sample #	425	425	425	425	425	425	425	425	425	425	425	425	425	425	425	425	425
Crystal	H	L	L	L	M	M	M	N	N	O	O	P	P	P	P	R	R
Zone	rim	mid 1	mid 2	rim	core	mid	rim	core	rim	core	rim	core	mid 1	mid 2	rim	core	rim
SiO_2	44.93	44.94	45.69	45.42	46.35	47.21	45.95	45.27	45.78	46.54	45.44	45.75	45.52	45.54	45.62	46.64	45.22
TiO_2	1.59	1.70	1.47	1.48	1.52	0.81	1.39	1.71	1.45	1.40	1.44	1.51	1.66	1.06	1.46	1.34	1.52
Al_2O_3	10.09	10.52	10.49	9.46	9.50	9.95	9.53	10.38	9.86	9.52	9.79	9.95	10.55	11.24	9.87	9.08	10.27
Fe_2O_3	5.34	6.15	6.15	6.06	5.58	7.63	4.13	4.75	5.77	4.75	4.46	5.49	5.18	6.55	6.61	5.78	6.30
FeO	7.75	5.84	4.80	6.84	5.51	0.62	7.66	5.72	6.25	5.27	7.15	5.89	5.40	3.26	5.67	6.86	6.21
MnO	0.13	0.13	0.12	0.17	0.12	0.06	0.17	0.12	0.10	0.13	0.15	0.14	0.10	0.10	0.15	0.15	0.16
MgO	14.02	14.78	15.51	14.69	15.55	17.77	14.86	15.53	14.90	16.08	14.74	15.23	15.50	15.96	15.05	14.79	14.56
CaO	11.57	11.78	11.87	11.42	11.84	11.60	11.64	12.01	11.76	12.05	11.72	12.03	11.98	11.74	11.82	11.42	11.77
Na_2O	2.19	1.87	1.80	2.45	1.74	1.84	2.45	2.01	1.84	1.82	2.10	1.71	1.86	1.82	1.81	2.14	1.78
K_2O	0.43	0.45	0.41	0.38	0.41	0.45	0.39	0.42	0.42	0.37	0.42	0.38	0.43	0.50	0.43	0.36	0.47
H_2O	1.92	1.94	1.95	1.93	1.95	1.97	1.94	1.95	1.94	1.96	1.93	1.94	1.95	1.95	1.94	1.95	1.93
Total	99.96	100.11	100.26	100.28	100.08	99.92	100.10	99.86	100.06	99.88	99.34	100.04	100.15	99.73	100.43	100.51	100.20
Al#	0.15	0.14	0.16	0.11	0.15	0.18	0.16	0.15	0.15	0.16	0.17	0.15	0.17	0.21	0.13	0.15	0.15
Species	Mg-Hbl	T-Prg	Mg-Hbl	Mg-Hbl	Mg-Hbl	Mg-Hbl	Mg-Hbl	Mg-Hbl	Mg-Hbl	Mg-Hbl	Mg-Hbl	Mg-Hbl	Mg-Hbl	T-Prg	Mg-Hbl	Mg-Hbl	Mg-Hbl

Note: Total refers to original analytical total. Al# = $Al_{VI}/(Al_{VI}+Al_{IV})$ on the basis of 13 cations. Abbreviated amphibole names: Mg-Hbl: magnesiohornblende; Mg-Hst: magnesiohastingsite; T-prg: tschermakitic pagasite; Xeno: Xenocryst.

Table A2.3 *(continued)*: EPMA data for amphibole phenocrysts from Tauhara volcano.

Sample #	425	440	440	440	440	440	440	440	440	440	440	440	440	440	440	440	440
Crystal	U	A	A	B	C	C	C	D	D	E	F	F	G	G	G	H	H
Zone	mid	core	rim	mid	core	mid	rim	core	rim	mid	core	rim	core	mid	rim	core	mid
SiO_2	44.72	46.17	45.35	43.05	45.12	47.56	45.25	46.25	45.40	45.94	47.05	45.51	45.25	45.90	45.11	45.71	45.59
TiO_2	1.69	1.23	1.73	1.87	1.51	1.06	1.70	1.64	1.59	1.39	0.97	1.62	1.66	1.23	1.57	1.27	1.38
Al_2O_3	10.85	10.58	9.86	12.66	10.62	9.65	10.31	9.22	10.14	9.14	9.38	9.35	9.72	9.94	9.51	8.91	9.41
Fe_2O_3	5.43	7.86	7.51	6.29	8.06	4.88	5.57	6.56	6.81	6.40	9.81	4.72	7.52	6.94	6.86	8.24	6.43
FeO	4.87	3.09	5.92	6.84	5.86	4.88	6.69	5.42	4.89	5.25	0.04	7.35	5.34	3.71	6.52	4.62	5.30
MnO	0.12	0.10	0.13	0.12	0.18	0.10	0.13	0.17	0.15	0.12	0.09	0.13	0.16	0.08	0.15	0.17	0.13
MgO	15.59	15.85	14.43	13.23	14.03	16.05	14.45	15.12	15.10	15.22	17.25	14.59	14.69	15.84	14.30	15.04	15.18
CaO	12.09	11.37	11.33	11.52	11.30	11.66	11.53	11.49	11.50	11.59	11.23	11.74	11.42	11.67	11.48	11.26	11.54
Na_2O	1.85	1.93	2.01	2.11	1.98	1.85	2.08	1.77	1.90	1.68	1.61	1.95	1.88	1.68	1.95	1.83	1.92
K_2O	0.43	0.40	0.37	0.46	0.43	0.34	0.40	0.32	0.38	0.33	0.34	0.34	0.31	0.37	0.35	0.35	0.33
H_2O	1.94	1.96	1.93	1.92	1.94	1.97	1.94	1.94	1.94	1.92	1.96	1.92	1.93	1.94	1.92	1.92	1.92
Total	99.59	100.53	100.57	100.08	101.04	99.98	100.05	99.90	99.80	98.99	99.72	99.21	99.87	99.29	99.73	99.31	99.12
Al#	0.15	0.17	0.11	0.19	0.14	0.23	0.16	0.13	0.14	0.14	0.13	0.14	0.11	0.16	0.11	0.09	0.13
Species	T-Prg	Mg-Hbl	Mg-Hbl	Tsch-Prg	T-Prg	Xeno	Mg-Hbl	Mg-Hbl	Mg-Hbl	Mg-Hbl	Mg-Hbl	Mg-Hbl	Mg-Hbl	Mg-Hbl	Mg-Hbl	Mg-Hbl	Mg-Hbl

Sample #	440	440	440	440	440	440	440	440	440	440	440	456	456	456	456	456	456
Crystal	I	J	K	K	L	M	M	N	Q	R	S	A	A	B1	B1	B2	B2
Zone	mid	mid	core	rim	rim	core	rim	core	mid	mid	mid	core	rim	core	rim	core	rim
SiO_2	45.23	44.86	44.95	45.07	45.04	44.97	45.25	45.10	45.71	45.38	45.95	44.94	43.67	44.07	43.98	44.06	43.84
TiO_2	1.61	1.43	1.43	1.74	1.55	1.47	1.67	1.62	1.67	1.70	1.44	1.31	1.79	1.48	1.70	1.41	1.77
Al_2O_3	10.15	10.00	10.30	9.93	9.59	10.13	9.82	10.22	9.60	9.66	9.48	11.12	11.17	11.20	11.38	11.44	11.25
Fe_2O_3	4.99	8.74	8.49	5.30	7.27	6.65	6.02	5.65	6.33	6.89	5.86	6.99	1.12	7.93	7.22	7.03	6.39
FeO	6.95	4.76	5.21	8.26	6.21	6.80	6.26	5.60	5.91	6.50	5.49	4.24	10.63	4.16	5.51	3.86	6.40
MnO	0.14	0.15	0.18	0.17	0.17	0.20	0.13	0.10	0.16	0.18	0.15	0.13	0.12	0.10	0.13	0.11	0.13
MgO	14.47	14.58	14.08	13.88	14.17	14.25	14.70	15.12	14.66	14.22	15.09	14.96	13.23	14.62	13.87	15.20	13.81
CaO	11.45	11.25	11.12	11.43	11.38	11.38	11.72	11.71	11.39	11.51	11.56	11.46	11.37	11.33	11.17	11.68	11.48
Na_2O	2.26	1.99	1.87	2.45	1.85	2.39	1.83	1.96	1.86	1.81	1.74	1.85	3.09	1.91	1.96	1.94	1.97
K_2O	0.34	0.38	0.40	0.39	0.33	0.40	0.38	0.41	0.31	0.34	0.33	0.39	0.47	0.39	0.45	0.38	0.42
H_2O	1.93	1.92	1.92	1.93	1.91	1.93	1.93	1.93	1.93	1.93	1.93	1.93	1.90	1.92	1.91	1.92	1.91
Total	99.50	100.06	99.93	100.55	99.48	100.56	99.68	99.43	99.54	100.12	99.02	99.32	98.57	99.11	99.29	99.04	99.37
Al#	0.17	0.10	0.14	0.13	0.12	0.12	0.13	0.15	0.15	0.12	0.16	0.19	0.22	0.16	0.17	0.17	0.16
Species	Mg-Hbl	T-Prg	T-Prg	Mg-Hbl	Mg-Hbl	Mg-Hst	Mg-Hbl	Mg-Hbl	Mg-Hbl	Mg-Hbl	Mg-Hbl	T-Prg	Xeno	T-Prg	T-Prg	T-Prg	T-Prg

Table A2.3 *(continued)*: EPMA data for amphibole phenocrysts from Tauhara volcano.

Sample #	456	456	456	456	456	456	456	456	456	456	456	456	456	456	456	456	456
Crystal	C1	C2	C2	C2	D	D	E	E	F	G	G	H	I	I	I	J	J
Zone	core	rim	core	rim	core	rim	core	rim	rim	core	rim	rim	core	mid	rim	core	rim
SiO_2	44.30	43.97	43.60	44.16	44.35	44.13	44.36	44.67	43.92	44.16	44.02	44.50	46.44	45.52	43.70	44.88	44.53
TiO_2	1.62	1.63	1.60	1.61	1.66	1.78	1.48	1.62	1.81	1.65	1.76	1.75	1.28	1.38	1.82	1.46	1.64
Al_2O_3	10.99	11.09	11.95	11.33	11.10	11.00	11.45	10.59	11.24	10.96	10.52	10.50	9.70	10.47	11.16	10.69	10.15
Fe_2O_3	7.90	8.11	5.94	7.32	6.81	6.69	6.55	5.58	6.37	7.28	6.46	5.91	7.42	6.59	8.14	7.41	6.91
FeO	3.67	4.26	5.10	5.15	4.78	5.97	4.90	6.22	6.06	4.62	6.07	6.06	2.82	4.43	5.22	4.07	5.58
MnO	0.11	0.13	0.09	0.13	0.11	0.12	0.12	0.12	0.14	0.12	0.14	0.13	0.09	0.11	0.14	0.14	0.16
MgO	15.14	14.52	14.59	14.26	14.88	13.90	14.80	14.55	13.84	14.61	14.27	14.44	16.49	15.38	14.15	15.35	14.71
CaO	11.48	11.27	11.68	11.34	11.55	11.24	11.65	11.64	11.30	11.32	11.57	11.59	11.70	11.69	11.40	11.67	11.47
Na_2O	1.91	1.93	2.03	1.99	2.05	1.96	1.99	2.00	1.97	1.96	1.94	1.89	1.72	1.77	2.04	1.90	2.16
K_2O	0.35	0.40	0.39	0.44	0.36	0.42	0.42	0.40	0.41	0.40	0.39	0.39	0.35	0.36	0.43	0.38	0.38
H_2O	1.93	1.91	1.92	1.92	1.93	1.91	1.93	1.92	1.91	1.92	1.91	1.92	1.96	1.94	1.92	1.94	1.92
Total	99.40	99.22	98.90	99.66	99.57	99.13	99.66	99.32	98.97	99.00	99.06	99.08	99.95	99.64	100.11	99.88	99.61
Al#	0.14	0.14	0.19	0.16	0.15	0.17	0.18	0.16	0.17	0.15	0.13	0.15	0.14	0.17	0.11	0.14	0.11
Species	T-Prg	T-Prg	T-Prg	T-Prg	T-Prg	T-Prg	T-Prg	T-Prg	T-Prg	T-Prg	T-Prg	T-Prg	Mg-Hbl	Mg-Hbl	T-Prg	T-Prg	T-Prg

Sample #	456	456	456	477	477	477	477	477	477	477	477	477	477	477	477	477	477
Crystal	K	L	L	A	B	C	D	E	F	F	G	H	I	I	I	J	J
Zone	rim	core	rim	mid	rim	mid	mid	mid	core	rim	mid	core	core	mid	rim	mid	rim
SiO_2	43.73	44.57	43.93	43.68	43.87	42.22	43.67	43.55	43.43	43.35	44.03	43.67	43.60	42.72	43.38	45.94	43.60
TiO_2	1.80	1.45	1.70	1.59	1.66	1.59	1.61	1.66	1.73	1.65	1.58	1.46	1.62	1.44	1.62	1.15	1.59
Al_2O_3	11.20	10.62	11.33	12.26	11.88	12.02	11.83	11.98	11.61	11.89	10.83	12.08	11.95	13.02	12.06	10.07	11.92
Fe_2O_3	8.46	8.63	7.01	7.40	7.35	8.24	7.47	8.05	9.03	9.01	8.58	9.12	8.49	9.59	8.73	6.13	8.28
FeO	5.54	3.08	5.67	2.89	3.88	2.40	3.11	2.76	3.66	3.56	2.32	3.20	2.43	2.99	3.22	3.46	3.34
MnO	0.15	0.12	0.12	0.07	0.12	0.12	0.12	0.12	0.16	0.10	0.09	0.13	0.10	0.13	0.09	0.11	0.11
MgO	13.93	15.61	14.25	15.56	15.37	15.49	15.66	15.64	14.58	14.84	15.93	14.82	15.48	14.24	14.94	16.15	15.04
CaO	11.47	11.63	11.57	11.63	11.77	11.76	11.89	11.81	11.33	11.56	11.55	11.36	11.46	11.22	11.45	11.66	11.49
Na_2O	2.00	1.92	2.03	2.14	2.26	2.05	2.05	2.05	2.09	2.10	2.02	2.12	2.09	2.08	2.10	1.80	2.09
K_2O	0.43	0.36	0.44	0.38	0.39	0.39	0.36	0.37	0.34	0.42	0.34	0.41	0.40	0.42	0.41	0.34	0.39
H_2O	1.92	1.93	1.92	1.94	1.94	1.90	1.94	1.94	1.92	1.93	1.92	1.93	1.93	1.92	1.93	1.94	1.93
Total	100.63	99.92	99.98	99.54	100.48	98.18	99.71	99.93	99.87	100.41	99.19	100.30	99.54	99.76	99.92	98.75	99.77
Al#	0.11	0.11	0.15	0.17	0.14	0.12	0.14	0.13	0.12	0.12	0.10	0.14	0.14	0.17	0.14	0.19	0.14
Species	T-Prg	T-Prg	T-Prg	T-Prg	Mg-Hst	T-Prg	T-Prg	T-Prg	T-Prg	T-Prg	T-Prg	T-Prg	T-Prg	T-Prg	T-Prg	Mg-Hbl	T-Prg

Table A2.3 *(continued)*: EPMA data for amphibole phenocrysts from Tauhara volcano.

Sample #	477	477	477	477	477	477	483	483	483	483	483	483	483	483	483	483	483
Crystal	K	M	N	O	P	P	A	A	A	C	C	D	D	D	D	F	F
Zone	core	core	mid	mid	core	mid	core	mid	rim	core	rim	core	mid 1	mid 3	rim	core	mid 1
SiO_2	44.08	44.43	43.85	43.06	44.35	43.77	44.46	44.90	44.47	44.84	45.46	46.34	45.66	44.70	46.37	44.87	46.31
TiO_2	1.60	1.52	1.54	1.56	1.58	1.65	1.70	1.26	1.66	1.33	1.42	1.23	1.74	1.69	1.15	1.70	1.19
Al_2O_3	11.33	11.36	12.04	11.93	11.17	11.68	10.73	11.10	10.90	11.19	10.22	10.03	10.06	10.89	10.30	10.95	10.30
Fe_2O_3	7.35	7.59	7.84	8.16	7.31	7.59	7.01	8.71	8.57	7.47	7.93	10.21	8.35	8.51	8.87	7.59	8.76
FeO	3.75	2.76	2.82	2.33	3.04	3.65	5.00	1.74	4.22	2.96	4.43	1.15	4.51	4.47	1.18	4.45	1.49
MnO	0.09	0.09	0.13	0.12	0.10	0.13	0.14	0.11	0.12	0.09	0.15	0.15	0.14	0.16	0.16	0.17	0.14
MgO	15.32	15.82	15.49	15.65	15.57	14.98	14.84	15.95	14.76	15.93	15.16	16.24	14.94	14.64	16.73	14.94	16.65
CaO	11.63	11.55	11.52	11.67	11.40	11.46	11.65	11.25	11.33	11.80	11.29	10.98	11.34	11.45	11.32	11.47	11.41
Na_2O	2.06	2.05	2.18	2.06	2.02	2.01	1.92	1.91	2.02	1.91	2.21	1.87	1.83	1.85	1.91	1.98	1.89
K_2O	0.35	0.37	0.37	0.39	0.36	0.37	0.39	0.42	0.41	0.35	0.31	0.36	0.37	0.41	0.35	0.40	0.37
H_2O	1.93	1.94	1.94	1.92	1.93	1.92	1.93	1.94	1.93	1.94	1.94	1.96	1.95	1.94	1.96	1.94	1.96
Total	99.49	99.47	99.70	98.86	98.83	99.21	99.76	99.28	100.39	99.81	100.52	100.52	100.89	100.71	100.29	100.48	100.50
Al#	0.14	0.15	0.16	0.13	0.16	0.16	0.13	0.16	0.12	0.16	0.13	0.13	0.11	0.12	0.15	0.14	0.14
Species	T-Prg	T-Prg	T-Prg	T-Prg	T-Prg	T-Prg	T-Prg	T-Prg	T-Prg	T-Prg	T-Prg	Mg-Hbl	Mg-Hbl	T-Prg	Mg-Hbl	Tsch-Prg	Mg-Hbl

Sample #	483	483	483	483	483	483	483	483	483	527	527	527	527	527	527	527	527
Crystal	F	F	F	F	H	H	I	M	M	A	B	B	C	C	C	C	D
Zone	mid 2	mid 3	mid 4	rim	core	rim	core	core	rim	mid	core	rim	core	mid 1	mid2	rim	core
SiO_2	45.39	46.35	45.24	44.88	44.76	44.62	46.02	45.36	44.78	46.73	45.58	45.10	46.13	45.54	44.75	47.51	44.53
TiO_2	1.62	1.22	1.69	1.67	1.68	1.84	1.46	1.58	1.66	1.50	1.47	1.84	1.22	1.20	1.50	1.44	1.77
Al_2O_3	10.56	10.29	10.25	10.77	11.11	10.73	10.04	10.46	10.66	6.51	9.98	10.43	9.95	10.86	11.16	7.62	10.58
Fe_2O_3	8.40	9.28	8.68	7.58	7.42	7.29	8.87	7.32	7.19	8.14	8.06	7.15	7.43	8.26	7.90	7.17	7.78
FeO	4.48	1.05	4.37	4.75	4.90	5.69	3.29	4.64	4.97	10.31	2.95	5.73	4.09	3.02	3.56	5.93	5.17
MnO	0.14	0.12	0.14	0.13	0.13	0.15	0.16	0.12	0.12	0.46	0.13	0.16	0.17	0.12	0.16	0.33	0.17
MgO	14.92	16.73	14.94	14.94	14.69	14.25	15.65	15.17	14.89	11.87	15.96	14.47	15.66	15.63	15.45	14.99	14.30
CaO	11.43	11.30	11.38	11.58	11.52	11.37	11.28	11.58	11.62	10.73	11.55	11.52	11.69	11.57	11.73	11.39	11.25
Na_2O	1.94	1.88	1.94	1.98	1.94	1.99	2.02	1.93	1.93	1.53	1.76	1.85	1.80	1.74	1.88	1.47	1.93
K_2O	0.39	0.39	0.38	0.40	0.41	0.41	0.37	0.37	0.39	0.35	0.37	0.42	0.38	0.43	0.42	0.39	0.40
H_2O	1.95	1.97	1.94	1.94	1.94	1.93	1.96	1.95	1.94	1.89	1.94	1.94	1.95	1.95	1.95	1.94	1.92
Total	101.21	100.57	100.96	100.63	100.50	100.26	101.12	100.48	100.14	100.03	99.75	100.63	100.48	100.33	100.45	100.18	99.80
Al#	0.12	0.14	0.10	0.13	0.15	0.14	0.11	0.14	0.13	0.00	0.12	0.13	0.14	0.16	0.14	0.09	0.13
Species	T-Prg	Mg-Hbl	T-Prg	T-Prg	T-Prg	T-Prg	Mg-Hbl	T-Prg	T-Prg	Mg-Hbl	Mg-Hbl	T-Prg	Mg-Hbl	T-Prg	T-Prg	Mg-Hbl	T-Prg

Table A2.3 *(continued)*: EPMA data for amphibole phenocrysts from Tauhara volcano.

Sample #	527	527	527	527	527	527	527	527	527	527	527	527	527
Crystal	D	E	E	F	F	F	G	G	H	I	I	J	K
Zone	rim	core	rim	core	mid	rim	core	rim	mid	core	rim	mid	mid
SiO_2	46.40	45.45	48.48	43.49	44.82	48.06	44.36	48.50	47.57	45.30	47.22	46.90	46.27
TiO_2	1.38	1.33	1.29	2.36	1.99	1.20	1.95	1.05	1.50	1.35	1.32	1.56	1.54
Al_2O_3	7.25	9.89	6.62	10.84	10.31	6.12	10.77	6.30	6.51	9.56	6.58	6.72	6.84
Fe_2O_3	8.02	7.53	7.21	7.58	5.75	9.02	7.10	7.91	8.45	7.91	7.85	7.67	9.45
FeO	9.53	4.21	5.73	6.56	6.03	6.28	7.00	5.80	9.86	4.37	7.77	10.44	10.71
MnO	0.42	0.15	0.40	0.16	0.13	0.48	0.15	0.41	0.45	0.15	0.46	0.38	0.49
MgO	12.40	15.31	15.37	13.65	14.85	14.31	13.46	15.29	12.39	15.04	13.67	12.21	11.15
CaO	10.90	11.44	11.24	11.43	11.68	10.78	11.33	11.29	10.82	11.40	10.95	10.94	10.51
Na_2O	1.71	1.87	1.51	2.03	2.01	1.51	1.93	1.47	1.64	1.72	1.57	1.67	1.64
K_2O	0.42	0.37	0.34	0.48	0.42	0.35	0.48	0.38	0.33	0.35	0.43	0.33	0.45
H_2O	1.90	1.93	1.94	1.92	1.93	1.92	1.92	1.94	1.92	1.92	1.90	1.90	1.88
Total	100.33	99.49	100.12	100.50	99.92	100.03	100.47	100.33	101.44	99.08	99.74	100.71	100.95
Al#	0.03	0.13	0.06	0.08	0.13	0.00	0.14	0.02	0.00	0.12	0.02	0.01	0.00
Species	Mg-Hbl	Mg-Hbl	Mg-Hbl	T-Prg	T-Prg	Mg-Hbl	T-Prg	Mg-Hbl	Mg-Hbl	Mg-Hbl	Mg-Hbl	Mg-Hbl	Mg-Hbl

Table A2.4: EPMA data for plagioclase phenocrysts from Tauhara volcano.

Sample #	425	425	425	425	425	425	425	425	425	425	425	425	425	425	425	425	425
Crystal	A	A	A	A	A	A	B	B	B	B	C	C	C	C	E	F	F
Zone	core	mid 1	mid 2	mid 3	mid 4	rim	core	mid 1	mid 2	rim	core	mid 1	mid 2	rim	mid	core	mid
SiO_2	57.54	58.81	60.64	60.74	60.97	60.96	61.38	60.69	60.72	55.52	59.65	56.79	63.09	55.41	61.52	57.55	61.00
TiO_2	0.06	0.00	0.01	0.00	0.00	0.03	0.00	0.00	0.00	0.00	0.03	0.01	0.00	0.01	0.00	0.00	0.00
Al_2O_3	27.14	26.40	25.07	25.07	24.64	20.96	24.65	25.10	24.75	28.48	25.76	27.70	23.60	28.29	24.67	26.99	24.67
FeO	0.30	0.22	0.19	0.16	0.21	0.40	0.18	0.25	0.26	0.37	0.28	0.17	0.23	0.65	0.18	0.32	0.23
MgO	0.02	0.01	0.00	0.01	0.00	0.00	0.00	0.01	0.02	0.01	0.01	0.00	0.01	0.02	0.00	0.03	0.01
CaO	8.57	7.71	6.19	6.20	5.81	1.99	5.73	6.31	6.18	10.06	7.10	9.30	4.32	10.05	5.36	8.74	6.10
Na_2O	5.81	6.19	6.93	6.82	6.96	3.66	7.11	6.80	6.58	4.91	6.44	5.58	7.56	5.00	7.33	5.84	6.68
K_2O	0.57	0.67	0.96	1.01	1.41	12.00	0.93	0.85	1.49	0.65	0.74	0.46	1.19	0.58	0.94	0.54	1.31
Total	100.14	100.34	100.28	100.30	100.27	100.71	100.16	99.86	99.94	100.50	99.81	100.36	100.33	101.14	100.09	100.31	99.68
An	43.35	39.14	31.17	31.40	28.94	8.68	29.07	32.14	31.10	51.03	36.14	46.60	22.24	50.81	27.13	43.83	30.87
Ab	53.23	56.83	63.08	62.49	62.67	28.90	65.29	62.70	59.97	45.05	59.37	50.67	70.48	45.73	67.18	52.97	61.24
Or	3.42	4.02	5.75	6.11	8.39	62.42	5.64	5.15	8.93	3.92	4.49	2.73	7.28	3.47	5.70	3.20	7.89

Sample #	425	425	425	425	425	425	425	425	425	425	425	425	425	425	425	425	425
Crystal	F	G	G	G	G	H	H	H	I	I	I	I	I	I	I	I	J
Zone	rim	core	mid 1	mid 2	rim	core	mid 1	mid 2	mid 3	mid 4	mid 5	mid 6	mid 7	mid 8	mid 9	rim	core
SiO_2	54.55	57.78	61.56	60.70	61.54	61.01	59.99	61.94	60.82	59.52	59.72	59.83	60.22	61.28	59.26	61.82	54.78
TiO_2	0.00	0.00	0.01	0.00	0.02	0.05	0.00	0.00	0.00	0.00	0.02	0.02	0.00	0.01	0.00	0.00	0.00
Al_2O_3	28.83	26.94	24.58	25.01	24.35	24.70	25.55	24.17	25.10	25.89	26.32	25.62	25.26	24.58	26.00	24.39	29.21
FeO	0.69	0.27	0.17	0.24	0.20	0.23	0.23	0.23	0.21	0.27	0.25	0.28	0.24	0.26	0.21	0.16	0.21
MgO	0.03	0.01	0.01	0.01	0.00	0.01	0.00	0.00	0.02	0.03	0.00	0.01	0.01	0.00	0.01	0.00	0.01
CaO	10.91	8.62	5.77	6.30	5.61	5.96	6.76	5.25	6.07	7.20	7.21	6.94	6.77	5.79	7.55	5.34	10.78
Na_2O	4.51	5.85	7.02	6.84	6.92	6.95	6.61	7.11	7.00	6.49	5.85	6.61	6.79	7.12	6.31	7.10	4.65
K_2O	0.49	0.54	0.89	0.90	1.37	1.09	0.85	1.30	0.79	0.62	0.63	0.69	0.71	0.96	0.66	1.19	0.36
Total	100.77	99.82	99.92	99.36	99.79	99.47	99.82	100.03	100.38	100.11	99.47	99.73	99.83	99.76	99.64	99.91	100.28
An	55.51	43.44	29.52	31.89	28.36	30.05	34.24	26.69	30.87	36.59	38.88	35.20	34.01	29.21	38.22	27.23	54.95
Ab	41.50	53.34	65.04	62.66	63.37	63.42	60.62	65.44	64.36	59.68	57.09	60.61	61.72	65.03	57.79	65.54	42.86
Or	2.99	3.22	5.44	5.45	8.28	6.53	5.15	7.87	4.77	3.73	4.03	4.18	4.26	5.75	3.99	7.24	2.19

Note: Oxides are normalised to 100%. Total refers to original analytical total. An= anorthite content: Ca/(Ca+Na+K), Ab= albite: Na/(Ca+Na+K), Or = orthoclase: K/(Ca+Na+K). All cation normalised.

Table A2.4 *(continued)*: EPMA data for plagioclase phenocrysts from Tauhara volcano.

Sample #	425	425	425	425	425	425	425	425	425	425	425	425	425	425	425	425	425
Crystal	J	J	K	K	K	K	L	M	M	M	M	N	N	N	O	P	Q
Zone	mid	rim	core	mid 1	mid 2	rim	mid	core	mid 1	mid 2	rim	c-dark	c-light	rim	mid	mid	core
SiO_2	58.30	61.91	57.68	62.24	62.08	62.69	60.86	58.27	60.68	60.50	61.96	61.19	57.95	60.26	61.04	62.77	60.61
TiO_2	0.00	0.03	0.03	0.00	0.01	0.00	0.00	0.02	0.00	0.01	0.00	0.00	0.00	0.00	0.01	0.00	0.00
Al_2O_3	26.60	24.10	27.08	24.00	24.07	23.35	24.99	26.57	25.00	25.49	23.82	24.68	26.74	25.01	24.74	23.33	25.03
FeO	0.21	0.19	0.30	0.19	0.14	0.17	0.23	0.26	0.26	0.24	0.22	0.33	0.33	0.42	0.16	0.19	0.28
MgO	0.00	0.00	0.00	0.01	0.00	0.00	0.01	0.00	0.01	0.01	0.00	0.00	0.00	0.00	0.00	0.01	0.01
CaO	8.24	5.40	8.66	4.89	5.21	4.60	6.32	8.27	6.39	6.40	5.27	5.92	8.31	6.34	5.92	4.28	6.29
Na_2O	5.96	7.06	5.71	7.52	7.34	7.30	6.80	6.01	6.75	6.48	6.97	6.94	5.83	6.56	6.93	7.18	6.83
K_2O	0.70	1.31	0.54	1.16	1.13	1.89	0.79	0.60	0.91	0.87	1.75	0.93	0.83	1.40	1.21	2.24	0.95
Total	99.58	99.84	99.89	99.63	99.65	99.30	99.69	99.78	100.00	99.56	99.85	100.23	100.15	100.53	100.21	100.20	100.17
An	41.50	27.38	44.12	24.60	26.26	22.91	32.28	41.63	32.45	33.42	26.36	30.22	41.84	31.89	29.74	21.45	31.79
Ab	54.33	64.74	52.63	68.47	66.94	65.85	62.89	54.78	62.06	61.17	63.19	64.10	53.16	59.73	63.02	65.16	62.51
Or	4.17	7.88	3.25	6.93	6.80	11.23	4.83	3.59	5.49	5.40	10.45	5.68	5.00	8.38	7.24	13.39	5.70

Sample #	425	425	425	425	425	425	425	425	425	425	425	425	425	425	425	425	425
Crystal	Q	Q	Q	R	S	S	S	S	T	U	V	V	X	X	ZB	ZB	ZE
Zone	mid 1	mid 2	rim	mid	core	mid 1	mid 2	mid 3	mid	mid	mid	rim	mid	rim	mid	rim	core
SiO_2	60.61	61.56	61.95	61.25	58.52	53.82	60.94	60.84	59.57	60.70	61.12	58.06	60.09	56.44	61.01	56.22	60.22
TiO_2	0.01	0.00	0.00	0.01	0.01	0.02	0.01	0.00	0.01	0.00	0.01	0.02	0.00	0.00	0.00	0.00	0.00
Al_2O_3	25.35	24.43	23.96	24.78	26.50	29.78	24.90	25.01	25.90	25.03	24.58	26.50	25.21	27.56	24.46	27.97	25.45
FeO	0.25	0.22	0.26	0.18	0.25	0.22	0.26	0.25	0.22	0.22	0.27	0.38	0.32	0.66	0.28	0.58	0.22
MgO	0.01	0.00	0.01	0.00	0.00	0.01	0.02	0.01	0.02	0.01	0.00	0.02	0.01	0.02	0.00	0.01	0.02
CaO	6.27	5.51	5.07	5.85	7.95	11.48	6.03	6.17	6.97	6.13	5.86	8.10	6.58	9.58	5.51	9.18	6.67
Na_2O	6.57	7.14	6.99	6.96	6.16	4.36	6.99	6.88	6.54	6.95	6.86	5.93	6.44	5.17	6.83	5.37	6.69
K_2O	0.92	1.13	1.76	0.96	0.61	0.31	0.85	0.84	0.77	0.97	1.30	0.98	1.36	0.56	1.91	0.67	0.73
Total	100.25	99.78	100.17	99.63	99.80	100.62	99.71	100.02	98.29	99.51	100.08	100.15	100.30	100.71	98.78	99.43	99.88
An	32.55	27.85	25.58	29.87	40.10	58.20	30.63	31.47	35.33	30.88	29.56	40.50	33.13	48.89	27.36	46.62	33.96
Ab	61.76	65.32	63.83	64.30	56.24	39.96	64.24	63.42	60.02	63.31	62.65	53.66	58.69	47.71	61.36	49.34	61.60
Or	5.69	6.83	10.59	5.82	3.65	1.84	5.12	5.11	4.65	5.81	7.79	5.84	8.18	3.40	11.28	4.05	4.44

Table A2.4 *(continued)*: EPMA data for plagioclase phenocrysts from Tauhara volcano.

Sample #	425	425	425	425	425	425	425	425	425	425	425	425	425	440	440	440	440
Crystal	ZE	ZE	ZE	ZF	ZF	ZF	ZF	ZG	ZG	ZL	ZL	ZL	ZQ	A	A	A	A
Zone	mid 1	mid 2	rim	core	mid 1	mid 2	rim	core	mid	core	mid	rim	mid	core	mid 1	mid 2	mid 3
SiO_2	56.71	62.49	57.69	59.45	58.98	60.52	60.74	57.75	60.71	57.52	62.94	58.91	60.87	59.97	56.69	61.22	59.75
TiO_2	0.02	0.00	0.00	0.00	0.00	0.01	0.01	0.03	0.00	0.00	0.01	0.02	0.01	0.00	0.00	0.00	0.00
Al_2O_3	27.68	23.75	26.83	26.11	26.24	25.20	25.05	26.99	25.05	27.26	23.48	25.66	24.66	25.25	27.48	24.34	25.36
FeO	0.29	0.19	0.44	0.23	0.22	0.25	0.21	0.27	0.24	0.23	0.18	0.47	0.24	0.27	0.24	0.22	0.22
MgO	0.01	0.00	0.02	0.01	0.01	0.01	0.01	0.00	0.00	0.00	0.00	0.01	0.00	0.02	0.00	0.02	0.01
CaO	9.32	4.90	8.53	7.01	7.41	6.12	6.06	8.41	5.84	8.80	4.60	7.45	6.20	6.74	9.33	5.75	6.86
Na_2O	5.47	7.12	5.73	6.49	6.44	6.96	6.93	6.01	7.22	5.78	7.62	5.55	6.76	6.98	5.80	7.55	7.07
K_2O	0.49	1.55	0.77	0.69	0.69	0.94	1.00	0.53	0.95	0.42	1.18	1.94	1.27	0.76	0.46	0.90	0.75
Total	100.01	99.96	99.89	98.94	99.31	99.64	99.67	99.24	99.32	99.37	99.63	98.90	99.24	98.53	98.93	98.45	98.24
An	47.06	24.96	43.06	35.80	37.25	30.87	30.60	42.23	29.13	44.54	23.22	37.61	31.09	33.25	45.81	28.08	33.42
Ab	49.97	65.61	52.30	59.99	58.64	63.51	63.37	54.58	65.20	52.91	69.68	50.75	61.31	62.28	51.53	66.72	62.26
Or	2.97	9.43	4.64	4.21	4.12	5.62	6.03	3.19	5.67	2.55	7.10	11.64	7.60	4.47	2.66	5.20	4.32

Sample #	440	440	440	440	440	440	440	440	440	440	440	440	440	440	440	440	440
Crystal	A	B	B	C	C	C	D	D	D	E	F	F	F	F	F	G	G
Zone	rim	core	rim	core	mid	rim	core	mid	rim	mid	core	mid 1	mid 2	mid 3	rim	core	mid
SiO_2	60.60	56.77	60.25	58.79	62.63	62.05	62.92	60.90	56.31	60.85	60.80	59.21	61.67	59.00	61.14	58.41	61.76
TiO_2	0.00	0.00	0.00	0.04	0.02	0.00	0.02	0.03	0.07	0.03	0.00	0.03	0.00	0.02	0.00	0.01	0.00
Al_2O_3	24.81	27.44	24.98	26.15	23.58	24.04	23.30	24.71	27.49	24.66	24.75	25.93	24.18	25.98	24.38	26.34	23.93
FeO	0.22	0.33	0.23	0.17	0.22	0.18	0.22	0.17	0.40	0.17	0.21	0.25	0.23	0.23	0.19	0.33	0.22
MgO	0.01	0.03	0.01	0.02	0.00	0.00	0.01	0.00	0.02	0.01	0.02	0.01	0.00	0.00	0.01	0.02	0.01
CaO	6.24	9.37	6.54	7.82	4.83	5.32	4.60	6.12	9.58	6.23	6.35	7.49	5.71	7.59	5.94	8.11	5.47
Na_2O	7.09	5.59	6.71	6.31	7.55	7.27	7.62	7.17	5.35	6.89	7.04	6.45	7.16	6.25	6.93	5.97	7.08
K_2O	1.02	0.48	1.28	0.70	1.17	1.14	1.32	0.88	0.77	1.16	0.83	0.64	1.04	0.94	1.40	0.80	1.52
Total	98.24	99.54	99.31	100.09	99.72	99.61	99.55	99.52	99.88	99.82	99.64	99.98	99.32	99.88	99.92	99.98	99.66
An	30.75	46.69	32.37	38.95	24.32	26.83	23.05	30.38	47.48	31.03	31.64	37.59	28.69	37.92	29.50	40.83	27.23
Ab	63.24	50.45	60.09	56.88	68.70	66.34	69.10	64.40	47.98	62.11	63.43	58.61	65.10	56.50	62.22	54.35	63.76
Or	6.02	2.85	7.53	4.17	6.98	6.83	7.85	5.21	4.54	6.86	4.93	3.80	6.21	5.58	8.28	4.82	9.01

Table A2.4 *(continued)*: EPMA data for plagioclase phenocrysts from Tauhara volcano.

Sample #	440	440	440	440	440	440	440	440	440	440	440	440	440	440	440	440	440
Crystal	G	H	H	H	I	I	I	I	J	J	J	J	K	K	L	L	L
Zone	rim	mid 1	mid 2	rim	core	mid 1	mid 2	rim	mid 1	mid 2	mid 3	rim	core	mid	core	mid	rim
SiO_2	58.22	59.98	59.90	61.99	58.27	60.82	58.58	60.07	61.29	61.36	58.78	60.33	52.58	61.42	57.43	61.27	62.14
TiO_2	0.00	0.00	0.01	0.00	0.01	0.00	0.06	0.03	0.00	0.00	0.00	0.02	0.00	0.00	0.00	0.01	0.00
Al_2O_3	26.34	25.45	25.36	23.98	26.56	24.92	26.42	25.24	24.50	24.45	26.21	25.01	30.21	24.30	27.14	24.57	23.83
FeO	0.45	0.21	0.28	0.22	0.19	0.16	0.32	0.22	0.24	0.22	0.20	0.23	0.30	0.18	0.23	0.19	0.24
MgO	0.01	0.01	0.01	0.00	0.00	0.00	0.01	0.01	0.01	0.00	0.02	0.00	0.00	0.01	0.01	0.00	0.00
CaO	8.20	6.92	6.95	5.30	8.39	6.34	8.00	6.72	5.78	5.84	7.76	6.45	12.63	5.74	8.96	5.88	5.12
Na_2O	5.96	6.73	6.79	7.31	5.87	7.03	6.04	6.65	7.21	7.18	6.12	6.74	3.86	6.85	5.76	7.20	7.27
K_2O	0.83	0.71	0.71	1.20	0.72	0.73	0.58	1.07	0.97	0.95	0.91	1.21	0.43	1.51	0.46	0.88	1.40
Total	99.61	99.52	100.22	99.93	99.77	99.83	99.84	100.11	100.10	99.52	99.73	100.29	100.25	99.59	99.90	99.87	100.10
An	41.06	34.73	34.59	26.53	42.25	31.80	40.77	33.56	28.96	29.24	38.95	32.10	62.77	28.80	44.94	29.43	25.68
Ab	53.97	61.06	61.20	66.28	53.47	63.85	55.73	60.08	65.27	65.11	55.62	60.73	34.72	62.20	52.29	65.31	65.95
Or	4.97	4.22	4.20	7.18	4.29	4.35	3.50	6.35	5.77	5.65	5.43	7.17	2.52	8.99	2.78	5.26	8.37

Sample #	440	440	440	440	440	440	440	440	440	440	440	440	440	440	440	440	440
Crystal	N	N	N	N	O	O	O	O	P	P	Q	Q	Q	Q	R	R	S
Zone	core	mid 1	mid 2	rim	mid 1	mid 2	mid 3	rim	core	rim	core	mid 1	mid 2	rim	mid	rim	core
SiO_2	59.81	59.75	55.88	61.19	58.98	60.93	61.07	62.26	55.86	62.05	62.18	61.80	61.87	60.70	61.42	61.16	60.29
TiO_2	0.00	0.02	0.02	0.03	0.03	0.01	0.00	0.00	0.02	0.00	0.02	0.00	0.00	0.01	0.03	0.00	0.01
Al_2O_3	25.64	25.55	28.19	24.32	26.12	24.69	24.77	23.60	28.00	24.03	24.11	24.29	24.13	25.14	24.53	24.68	25.28
FeO	0.26	0.24	0.21	0.26	0.32	0.22	0.19	0.20	0.46	0.10	0.19	0.14	0.19	0.14	0.19	0.18	0.20
MgO	0.01	0.00	0.00	0.00	0.01	0.01	0.01	0.01	0.02	0.01	0.00	0.01	0.01	0.00	0.00	0.00	0.01
CaO	7.07	7.24	9.97	5.74	7.72	6.20	6.09	5.23	9.98	5.40	5.28	5.57	5.30	6.41	5.86	5.96	6.77
Na_2O	6.55	6.53	5.09	6.60	6.08	6.96	6.89	7.14	5.28	7.02	7.29	7.30	7.45	6.83	7.13	7.12	6.79
K_2O	0.66	0.67	0.65	1.86	0.75	0.98	0.99	1.55	0.38	1.40	0.93	0.89	1.04	0.79	0.84	0.90	0.65
Total	99.85	99.70	100.05	99.88	99.87	100.05	99.96	99.64	100.72	99.89	99.66	100.30	100.38	100.30	99.94	100.19	100.39
An	35.87	36.49	49.97	28.86	39.34	31.09	30.85	26.16	49.94	27.33	26.97	28.08	26.48	32.52	29.67	29.94	34.16
Ab	60.13	59.49	46.18	59.99	56.12	63.09	63.20	64.59	47.79	64.27	67.39	66.59	67.36	62.72	65.30	64.70	61.97
Or	3.99	4.02	3.86	11.16	4.54	5.83	5.96	9.25	2.27	8.41	5.63	5.33	6.17	4.76	5.03	5.37	3.87

Table A2.4 *(continued)*: EPMA data for plagioclase phenocrysts from Tauhara volcano.

Sample #	440	440	440	440	440	440	440	440	440	440	440	440	440	440	440	440	440
Crystal	S	S	T	U	U	V	V	V	Y	Y	Z	Z	ZA	ZA	ZB	ZC	ZC
Zone	mid	rim	rim	mid	rim	core	mid	rim	core	rim	core	rim	core	rim	mid	mid 1	mid 2
SiO_2	61.26	60.41	58.40	62.57	57.19	60.42	62.12	61.40	55.93	59.12	62.12	60.34	56.12	60.75	60.42	61.05	58.39
TiO_2	0.04	0.00	0.10	0.00	0.03	0.02	0.00	0.00	0.00	0.00	0.00	0.00	0.03	0.00	0.00	0.00	0.01
Al_2O_3	24.57	25.02	26.17	23.86	27.00	25.22	23.80	24.33	28.17	25.94	24.06	25.18	27.88	24.70	25.00	24.72	26.49
FeO	0.23	0.27	0.40	0.14	0.46	0.25	0.22	0.13	0.34	0.24	0.22	0.23	0.29	0.24	0.26	0.19	0.32
MgO	0.01	0.00	0.01	0.01	0.02	0.00	0.00	0.01	0.03	0.00	0.00	0.00	0.02	0.00	0.00	0.01	0.02
CaO	5.90	6.46	8.01	5.10	9.00	6.57	5.24	5.66	10.10	7.48	5.26	6.58	10.00	6.25	6.36	6.18	8.14
Na_2O	7.09	6.61	5.90	7.27	5.67	6.67	7.19	6.92	5.10	6.27	7.37	6.62	5.18	6.69	6.92	7.11	6.07
K_2O	0.91	1.23	1.00	1.05	0.63	0.85	1.42	1.56	0.32	0.96	0.98	1.05	0.49	1.37	1.04	0.74	0.56
Total	100.14	100.52	100.71	99.84	100.33	100.33	100.33	100.02	100.35	100.15	100.41	100.26	100.31	99.75	100.96	100.77	100.71
An	29.78	32.45	40.28	26.15	44.96	33.43	26.28	28.25	51.27	37.49	26.62	33.23	50.11	31.26	31.63	31.03	41.12
Ab	64.78	60.17	53.72	67.45	51.28	61.42	65.24	62.50	46.78	56.80	67.49	60.48	46.96	60.60	62.20	64.55	55.50
Or	5.44	7.38	6.00	6.41	3.76	5.15	8.49	9.26	1.95	5.70	5.89	6.28	2.93	8.14	6.17	4.42	3.38

Sample #	440	456	456	456	456	456	456	456	456	456	456	456	456	456	456	456	456
Crystal	ZC	A	B	B	C	C	D	D	D	E	E	E	F	F	F	F	G
Zone	rim	mid	core	rim	core	rim	core	mid	rim	core	mid	rim	core	mid 1	mid 2	rim	core
SiO_2	61.15	61.61	52.78	62.09	60.72	62.31	61.21	59.26	61.97	60.16	59.10	59.20	60.05	57.16	58.72	61.38	59.21
TiO_2	0.00	0.00	0.09	0.03	0.00	0.03	0.00	0.03	0.00	0.00	0.02	0.00	0.04	0.00	0.00	0.00	0.00
Al_2O_3	24.47	24.22	29.90	23.84	24.91	23.72	24.63	25.88	24.03	25.28	25.86	25.97	25.54	27.38	26.35	24.51	26.06
FeO	0.26	0.20	0.57	0.14	0.29	0.08	0.24	0.19	0.08	0.18	0.21	0.15	0.19	0.24	0.26	0.14	0.21
MgO	0.01	0.00	0.04	0.01	0.01	0.01	0.01	0.01	0.02	0.01	0.00	0.00	0.00	0.01	0.01	0.01	0.02
CaO	5.79	5.57	12.27	5.32	6.20	5.04	6.04	7.39	5.36	6.71	7.47	7.42	6.96	9.25	8.00	5.83	7.53
Na_2O	6.99	6.98	4.07	6.92	6.93	7.21	6.93	6.36	7.06	6.77	6.39	6.30	6.66	5.60	6.09	6.87	6.22
K_2O	1.33	1.41	0.27	1.66	0.94	1.60	0.94	0.89	1.48	0.88	0.96	0.97	0.56	0.36	0.56	1.27	0.76
Total	100.87	99.98	100.89	99.52	100.03	99.77	100.10	99.75	99.56	99.86	99.99	100.03	99.75	100.10	99.97	99.58	100.15
An	28.94	28.03	61.48	26.85	31.22	25.20	30.63	37.03	26.91	33.53	37.03	37.13	35.36	46.69	40.62	29.48	38.26
Ab	63.15	63.52	36.89	63.19	63.13	65.30	63.67	57.67	64.23	61.23	57.32	57.09	61.24	51.15	55.98	62.87	57.17
Or	7.91	8.45	1.63	9.96	5.65	9.51	5.70	5.30	8.86	5.25	5.65	5.78	3.40	2.16	3.40	7.65	4.57

Table A2.4 *(continued)*: EPMA data for plagioclase phenocrysts from Tauhara volcano.

Sample #	456	456	456	456	456	456	456	456	456	456	456	456	456	456	456	456	456
Crystal	G	G	G	H	I	J	J	J	L	L	M	N	N	O	O	O	O
Zone	mid 1	mid 2	rim	rim	mid	core	mid	rim	core	rim	rim	mid	rim	core	mid 1	mid 2	rim
SiO_2	61.41	60.84	62.31	50.37	62.87	60.15	61.47	60.91	58.40	60.34	47.33	55.79	60.14	61.33	59.99	62.08	59.93
TiO_2	0.03	0.00	0.04	0.00	0.00	0.00	0.04	0.00	0.00	0.01	0.05	0.06	0.02	0.01	0.00	0.03	0.00
Al_2O_3	24.53	24.87	23.72	30.91	23.36	25.33	24.37	24.81	26.21	25.06	33.58	28.22	25.10	24.55	25.37	23.92	25.31
FeO	0.19	0.16	0.21	0.85	0.21	0.28	0.22	0.21	0.30	0.26	0.57	0.33	0.25	0.22	0.22	0.19	0.26
MgO	0.01	0.01	0.02	0.03	0.00	0.02	0.01	0.00	0.02	0.00	0.03	0.02	0.01	0.01	0.00	0.00	0.00
CaO	5.79	6.22	5.14	13.94	4.60	6.84	5.62	6.16	8.59	6.53	16.49	9.96	6.59	5.93	6.95	5.28	6.92
Na_2O	7.11	6.71	7.14	3.58	7.45	6.68	7.37	6.95	5.98	6.65	1.83	5.17	6.60	7.03	6.71	7.10	6.48
K_2O	0.94	1.20	1.42	0.32	1.51	0.71	0.90	0.96	0.51	1.15	0.13	0.45	1.28	0.92	0.75	1.40	1.10
Total	99.48	99.63	99.34	98.47	99.57	99.69	99.85	99.56	98.82	100.14	100.79	100.02	99.73	98.67	99.10	98.72	99.28
An	29.27	31.43	26.01	67.00	23.14	34.59	28.07	31.00	42.91	32.75	82.67	50.19	32.85	30.03	34.78	26.65	34.67
Ab	65.10	61.38	65.40	31.16	67.81	61.15	66.59	63.25	54.06	60.36	16.57	47.14	59.53	64.44	60.76	64.94	58.78
Or	5.63	7.19	8.58	1.83	9.05	4.25	5.34	5.75	3.03	6.89	0.76	2.68	7.62	5.53	4.46	8.41	6.55

Sample #	456	456	456	456	456	456	456	456	456	456	456	456	456	456	456	456	456
Crystal	P	P	P	Q	R	R	S	S	S	S	S	T	T	V	V	W	W
Zone	core	mid	rim	rim	mid	rim	core	mid 1	mid 2	mid 3	rim	core	mid	core	rim	core	mid 1
SiO_2	54.37	63.68	63.08	47.92	63.43	62.25	55.97	60.59	60.00	62.08	60.12	61.98	60.11	63.00	59.20	58.38	55.21
TiO_2	0.00	0.00	0.00	0.00	0.00	0.00	0.04	0.00	0.00	0.00	0.00	0.00	0.00	0.00	0.21	0.00	0.01
Al_2O_3	29.13	22.89	23.06	33.06	23.00	23.71	28.22	25.03	25.20	24.01	25.21	24.15	25.31	23.33	24.95	26.44	28.57
FeO	0.28	0.16	0.21	0.68	0.18	0.18	0.13	0.22	0.26	0.13	0.22	0.20	0.21	0.14	0.56	0.33	0.40
MgO	0.02	0.01	0.00	0.04	0.00	0.00	0.01	0.00	0.02	0.00	0.01	0.01	0.01	0.01	0.03	0.01	0.00
CaO	11.19	4.07	4.54	16.10	4.26	5.14	9.96	6.55	6.82	5.38	6.70	5.35	6.74	4.54	8.52	8.20	10.48
Na_2O	4.67	7.78	7.17	2.07	7.52	7.02	5.25	6.78	6.42	7.34	6.53	7.35	6.64	7.40	4.70	6.08	4.83
K_2O	0.34	1.41	1.94	0.13	1.62	1.71	0.42	0.83	1.27	1.06	1.20	0.96	0.97	1.59	1.82	0.56	0.50
Total	100.45	99.48	99.57	100.98	99.79	99.79	99.95	99.89	99.78	99.71	100.01	99.89	99.80	99.52	99.20	99.04	99.60
An	55.84	20.53	22.89	80.48	21.51	25.86	49.89	33.07	34.19	26.98	33.61	27.05	33.85	22.89	44.40	41.27	52.89
Ab	42.13	71.02	65.46	18.75	68.78	63.92	47.60	61.96	58.22	66.66	59.22	67.17	60.34	67.58	44.31	55.36	44.09
Or	2.03	8.45	11.65	0.78	9.71	10.22	2.51	4.97	7.59	6.36	7.17	5.79	5.82	9.54	11.29	3.37	3.02

Table A2.4 *(continued)*: EPMA data for plagioclase phenocrysts from Tauhara volcano.

Sample #	456	456	456	456	456	456	456	456	456	456	456	477	477	477	477	477	477
Crystal	W	W	X	X	ZI	ZJ	ZJ	ZJ	ZK	ZK	ZK	A	A	A	B	B	C
Zone	mid 2	rim	core	rim	mid	core	mid	rim	core	mid	rim	core	mid	rim	core	rim	mid
SiO_2	55.25	61.83	62.59	61.37	63.33	62.25	60.78	53.80	56.37	62.50	62.10	53.08	62.45	60.42	58.03	62.68	62.57
TiO_2	0.01	0.03	0.03	0.00	0.00	0.00	0.00	0.10	0.09	0.00	0.01	0.00	0.00	0.02	0.00	0.00	0.00
Al_2O_3	28.64	23.99	23.71	24.33	23.07	23.91	24.95	29.03	27.99	23.74	23.89	30.27	23.84	24.98	26.82	23.27	23.48
FeO	0.33	0.18	0.19	0.20	0.18	0.17	0.18	0.72	0.15	0.12	0.19	0.20	0.20	0.21	0.23	0.23	0.12
MgO	0.01	0.00	0.00	0.01	0.00	0.00	0.00	0.04	0.01	0.01	0.01	0.02	0.00	0.01	0.01	0.00	0.00
CaO	10.50	5.40	4.81	5.58	4.12	5.28	6.43	11.49	9.61	4.94	5.24	12.26	4.92	6.55	8.42	4.49	4.79
Na_2O	4.77	7.02	7.49	6.87	7.94	7.36	6.69	4.18	5.36	7.52	6.96	3.88	7.24	6.39	6.04	7.47	7.17
K_2O	0.48	1.55	1.17	1.65	1.36	1.04	0.97	0.65	0.43	1.17	1.60	0.29	1.35	1.42	0.45	1.87	1.87
Total	99.49	98.73	98.99	99.24	100.21	99.78	99.83	100.52	100.15	99.72	99.99	99.50	98.84	99.15	98.81	99.12	99.34
An	53.28	27.07	24.32	27.91	20.48	26.62	32.67	57.93	48.49	24.78	26.56	62.43	25.05	33.08	42.35	22.20	23.95
Ab	43.82	63.69	68.62	62.26	71.48	67.16	61.47	38.14	48.94	68.26	63.79	35.81	66.79	58.37	54.95	66.83	64.90
Or	2.90	9.24	7.06	9.83	8.04	6.22	5.86	3.93	2.57	6.96	9.64	1.76	8.16	8.56	2.70	10.98	11.15

Sample #	477	477	477	477	477	477	477	477	477	477	477	477	477	477	477	477	477
Crystal	D	D	D	E	E	E	F	F	F	G	G	G	H	H	H	J	K
Zone	core	mid	rim	core	mid	rim	core	mid	rim	core	mid	rim	core	mid	rim	mid	core
SiO_2	56.21	62.56	61.56	61.95	60.50	52.40	60.60	56.17	53.32	56.03	61.86	60.98	55.52	58.39	61.75	61.14	56.01
TiO_2	0.00	0.00	0.00	0.05	0.13	0.04	0.00	0.02	0.04	0.04	0.00	0.00	0.01	0.01	0.00	0.00	0.01
Al_2O_3	27.84	23.50	23.85	23.87	24.06	29.84	24.61	27.52	29.32	28.14	24.25	24.34	28.40	26.51	24.11	24.74	28.19
FeO	0.29	0.18	0.33	0.15	0.62	0.71	0.14	0.63	0.71	0.26	0.21	0.21	0.28	0.28	0.19	0.12	0.19
MgO	0.01	0.00	0.00	0.00	0.05	0.03	0.00	0.03	0.03	0.01	0.00	0.01	0.03	0.00	0.00	0.01	0.00
CaO	9.90	4.62	5.30	5.22	6.07	12.71	6.05	9.76	11.93	9.81	5.44	6.06	10.37	8.33	5.39	6.11	9.91
Na_2O	5.23	7.21	6.84	7.08	6.71	3.81	6.32	5.04	4.07	5.11	7.16	6.47	5.04	6.05	7.10	6.82	5.18
K_2O	0.51	1.93	2.13	1.68	1.87	0.47	2.28	0.85	0.59	0.60	1.08	1.92	0.35	0.43	1.45	1.08	0.50
Total	99.75	99.40	99.53	98.66	97.78	99.41	99.47	99.64	99.61	99.90	99.73	99.26	99.78	99.35	99.06	99.33	99.56
An	49.58	23.11	26.21	26.05	29.70	63.04	29.96	49.07	59.68	49.61	27.64	30.20	98.58	42.08	27.00	30.98	49.83
Ab	47.38	65.36	61.23	63.95	59.42	34.20	56.61	45.85	36.82	46.78	65.80	58.39	1.35	55.31	64.34	62.53	47.15
Or	3.04	11.53	12.56	9.99	10.88	2.75	13.43	5.08	3.50	3.61	6.56	11.41	0.06	2.61	8.66	6.49	3.02

Table A2.4 *(continued)*: EPMA data for plagioclase phenocrysts from Tauhara volcano.

Sample #	477	477	477	477	477	477	477	477	477	477	477	477	477	477	477	477	477
Crystal	K	K	L	L	M	M	M	N	O	O	P	Q	R	S	T	T	V
Zone	mid	rim	core	rim	core	mid	rim	core	mid	rim	mid	mid	mid	mid	mid	rim	core
SiO_2	60.82	60.20	62.65	52.47	59.46	57.27	60.94	60.90	49.34	49.57	63.03	61.18	60.63	61.41	57.70	61.89	60.16
TiO_2	0.04	0.21	0.00	0.05	0.02	0.04	0.00	0.00	0.01	0.10	0.00	0.02	0.04	0.11	0.00	0.16	0.00
Al_2O_3	24.57	20.24	23.41	29.88	25.84	27.37	24.42	24.81	25.65	25.61	23.40	24.55	25.07	18.41	26.80	18.80	24.99
FeO	0.27	0.68	0.19	0.82	0.25	0.20	0.26	0.20	0.27	0.28	0.13	0.12	0.19	0.30	0.30	0.47	0.29
MgO	0.01	0.00	0.00	0.03	0.00	0.01	0.01	0.01	0.04	0.00	0.00	0.00	0.01	0.00	0.03	0.00	0.01
CaO	6.06	3.64	4.62	12.43	7.32	8.85	5.92	6.20	10.08	9.53	4.55	5.91	6.29	0.83	8.51	0.93	6.37
Na_2O	6.85	4.35	7.11	3.80	6.43	5.72	6.66	6.92	13.21	12.93	7.38	7.08	6.84	4.09	5.94	4.43	6.73
K_2O	1.39	10.68	2.02	0.51	0.69	0.54	1.78	0.96	1.40	2.00	1.51	1.13	0.92	14.84	0.73	13.31	1.45
Total	99.50	98.58	99.92	100.86	99.60	100.12	99.42	99.48	49.06	48.73	99.20	98.90	99.84	99.53	99.60	100.15	99.88
An	30.15	15.02	23.23	62.38	37.02	44.62	29.44	31.19	28.27	27.00	23.12	29.45	31.85	3.20	42.28	3.74	31.41
Ab	61.61	32.51	64.71	34.54	58.82	52.15	59.99	63.06	67.07	66.27	67.77	63.83	62.62	28.56	53.40	32.36	60.05
Or	8.23	52.47	12.06	3.08	4.16	3.23	10.57	5.75	4.66	6.73	9.10	6.73	5.53	68.23	4.32	63.89	8.53

Sample #	477	477	477	477	477	477	477	483	483	483	483	483	483	483	483	483	483
Crystal	V	ZE	ZE	ZE	ZE	ZM	ZM	A	A	A	B	B	B	C	C	C	D
Zone	rim	core	mid 1	mid 2	rim	core	rim	core	mid	rim	core	mid	rim	core	mid	rim	core
SiO_2	60.48	60.51	56.64	57.70	60.82	60.21	57.58	61.79	60.22	60.12	59.76	57.08	51.87	58.44	56.51	52.49	60.18
TiO_2	0.00	0.00	0.03	0.00	0.00	0.01	0.03	0.00	0.00	0.00	0.00	0.00	0.01	0.00	0.01	0.03	0.00
Al_2O_3	25.04	24.80	27.71	27.09	24.46	25.29	26.72	24.55	25.35	25.53	25.63	27.46	30.35	26.67	27.81	29.79	25.34
FeO	0.21	0.19	0.34	0.23	0.21	0.17	0.36	0.20	0.27	0.25	0.26	0.25	0.75	0.25	0.23	0.75	0.20
MgO	0.01	0.01	0.00	0.01	0.01	0.00	0.02	0.00	0.01	0.00	0.00	0.00	0.06	0.02	0.02	0.07	0.01
CaO	6.52	6.31	9.40	8.61	5.96	6.69	8.45	5.27	6.47	6.69	6.92	9.05	12.79	7.90	9.59	12.52	7.02
Na_2O	6.84	6.77	5.39	5.80	6.40	6.45	5.71	7.22	6.86	6.64	6.75	5.73	3.92	6.13	5.44	4.04	6.56
K_2O	0.89	1.41	0.49	0.57	2.14	1.17	1.13	0.96	0.82	0.77	0.68	0.43	0.24	0.59	0.40	0.32	0.69
Total	99.51	100.13	100.58	100.52	100.37	100.45	100.93	99.00	99.08	99.05	98.37	98.64	98.71	98.40	98.59	98.11	99.30
An	32.67	31.15	47.62	43.52	29.69	33.84	41.98	27.06	32.58	34.11	34.69	45.39	63.40	40.08	48.15	61.96	35.61
Ab	62.02	60.54	49.40	53.06	57.65	59.10	51.32	67.04	62.50	61.21	61.26	52.02	35.17	56.34	49.46	36.17	60.20
Or	5.30	8.31	2.98	3.42	12.66	7.06	6.70	5.89	4.91	4.67	4.05	2.60	1.44	3.58	2.38	1.87	4.18

Table A2.4 *(continued)*: EPMA data for plagioclase phenocrysts from Tauhara volcano.

Sample #	483	483	483	483	483	483	483	483	483	483	483	483	483	483	483	483	483
Crystal	D	D	D	E	F	F	G	H	H	I	I	I	I	I	I	J	J
Zone	mid	rim	v-rim	mid	mid 1	mid 2	rim	core	rim	core	mid 1	mid 2	mid 3	mid 4	rim	mid	rim
SiO_2	63.26	62.23	56.06	63.40	57.73	59.95	52.39	55.86	61.49	61.77	60.74	59.46	62.70	60.66	55.55	60.29	60.55
TiO_2	0.00	0.00	0.02	0.00	0.00	0.00	0.01	0.02	0.01	0.00	0.00	0.00	0.01	0.00	0.02	0.00	0.01
Al_2O_3	23.43	24.05	27.73	23.21	27.11	25.60	30.07	27.99	24.51	24.38	25.07	25.90	23.56	25.04	28.13	25.28	24.99
FeO	0.14	0.29	0.62	0.21	0.22	0.26	0.80	0.42	0.21	0.23	0.22	0.27	0.25	0.25	0.66	0.22	0.36
MgO	0.00	0.02	0.03	0.00	0.00	0.01	0.07	0.03	0.02	0.01	0.01	0.01	0.00	0.00	0.06	0.01	0.02
CaO	4.69	5.24	10.16	4.42	8.43	6.73	12.31	10.13	5.84	5.67	6.56	7.40	4.88	6.65	9.90	6.40	6.68
Na_2O	7.40	7.13	4.90	7.57	5.95	6.70	3.99	5.17	7.06	7.08	6.68	6.32	7.54	6.66	5.14	6.95	6.64
K_2O	1.08	1.05	0.47	1.18	0.56	0.75	0.36	0.38	0.86	0.86	0.73	0.64	1.06	0.73	0.55	0.85	0.76
Total	99.07	99.84	99.65	99.50	98.66	98.14	98.96	100.09	99.16	99.71	99.28	99.65	99.84	99.09	98.01	98.07	99.72
An	24.22	27.90	51.84	22.65	42.45	34.07	61.68	50.83	29.76	29.06	33.60	37.76	24.64	33.96	49.88	32.01	32.07
Ab	69.13	65.71	45.28	70.17	54.20	61.41	36.19	46.91	65.02	65.71	61.94	58.36	68.97	61.59	46.85	62.90	62.56
Or	6.65	6.39	2.87	7.18	3.36	4.52	2.13	2.26	5.22	5.23	4.46	3.88	6.39	4.44	3.28	5.09	5.37

Sample #	483	483	483	483	483	483	483	483	483	483	483	483	483	483	483	483	483
Crystal	K	K	K	L	L	L	L	M	M	M	M	N	N	N	O	O	Q
Zone	core	mid	rim	core	mid 1	mid 2	rim	core	mid 1	mid 2	rim	core	mid	rim	core	rim	core
SiO_2	52.90	61.58	61.08	47.09	56.55	62.14	61.82	55.56	58.32	61.68	62.12	46.35	49.51	52.03	62.53	62.31	59.03
TiO_2	0.00	0.01	0.00	0.00	0.00	0.00	0.01	0.01	0.00	0.00	0.00	0.00	0.00	0.02	0.00	0.00	0.00
Al_2O_3	29.86	24.41	24.72	33.92	27.86	24.17	24.30	28.57	26.73	24.40	24.07	34.05	31.95	30.36	23.91	24.08	26.19
FeO	0.48	0.26	0.26	0.26	0.19	0.20	0.31	0.22	0.18	0.16	0.17	0.70	0.60	0.61	0.23	0.19	0.26
MgO	0.01	0.01	0.02	0.01	0.02	0.01	0.00	0.01	0.01	0.00	0.02	0.04	0.05	0.07	0.00	0.00	0.01
CaO	12.62	5.83	6.23	17.06	9.81	5.32	5.71	10.47	8.29	5.74	5.37	17.36	15.27	13.19	4.98	5.20	7.76
Na_2O	3.87	7.06	6.90	1.61	5.16	7.19	6.79	4.82	5.95	7.11	7.23	1.45	2.48	3.52	7.34	7.23	6.20
K_2O	0.26	0.84	0.79	0.06	0.40	0.96	1.06	0.34	0.52	0.91	1.02	0.06	0.13	0.21	1.01	0.99	0.55
Total	99.80	99.50	99.69	100.94	99.82	99.78	99.58	99.85	99.69	100.04	99.80	101.12	100.60	100.80	99.38	99.59	99.26
An	63.31	29.76	31.69	85.13	49.97	27.34	29.67	53.39	42.13	29.15	27.29	86.61	76.68	66.60	25.58	26.73	39.53
Ab	35.12	65.12	63.51	14.54	47.60	66.77	63.78	44.52	54.74	65.34	66.51	13.06	22.53	32.13	68.24	67.20	57.11
Or	1.57	5.12	4.80	0.33	2.44	5.90	6.55	2.09	3.13	5.51	6.20	0.33	0.79	1.27	6.18	6.08	3.36

Table A2.4 *(continued)*: EPMA data for plagioclase phenocrysts from Tauhara volcano.

Sample #	483	483	483	483	483	483	483	483	483	483	483	483	483	483	483	483	483
Crystal	Q	Q	S	T	T	T	U	U	V	V	W	X	Z	Z	ZA	ZC	ZC
Zone	mid	rim	rim	core	mid	rim	core	rim	mid	rim	mid	mid	mid	rim	rim	mid	rim
SiO_2	57.66	61.97	49.16	61.75	61.42	54.55	56.19	60.64	46.76	52.53	61.20	61.37	46.39	50.25	54.86	46.19	49.55
TiO_2	0.00	0.00	0.01	0.00	0.00	0.01	0.05	0.00	0.02	0.00	0.00	0.00	0.00	0.00	0.04	0.00	0.03
Al_2O_3	26.89	24.20	32.14	24.42	24.42	28.62	27.79	24.79	33.71	29.97	24.69	24.53	34.04	31.56	28.63	34.23	32.09
FeO	0.34	0.26	0.65	0.18	0.22	0.76	0.41	0.33	0.56	0.57	0.20	0.27	0.62	0.62	0.61	0.48	0.53
MgO	0.01	0.00	0.06	0.02	0.02	0.07	0.01	0.02	0.05	0.05	0.00	0.01	0.05	0.06	0.06	0.03	0.05
CaO	8.88	5.60	15.33	5.75	6.03	11.03	9.74	6.50	17.18	12.85	6.18	5.89	17.28	14.46	11.95	17.65	15.04
Na_2O	5.76	7.07	2.53	7.01	6.60	4.49	5.41	6.81	1.66	3.80	6.93	7.05	1.54	2.88	3.09	1.37	2.59
K_2O	0.47	0.91	0.11	0.87	1.29	0.46	0.39	0.91	0.05	0.22	0.81	0.89	0.08	0.17	0.78	0.04	0.12
Total	99.71	99.62	100.90	99.69	99.77	99.90	100.12	99.82	100.53	100.49	99.77	100.13	101.00	100.53	101.67	101.07	100.95
An	44.70	28.75	76.47	29.53	30.90	55.96	48.68	32.67	84.88	64.27	31.41	29.92	85.69	72.74	64.73	87.48	75.67
Ab	52.46	65.69	22.86	65.12	61.24	41.26	48.98	61.90	14.80	34.43	63.71	64.73	13.83	26.24	30.26	12.26	23.59
Or	2.84	5.55	0.68	5.34	7.86	2.78	2.33	5.43	0.32	1.31	4.89	5.35	0.48	1.02	5.01	0.26	0.73

Sample #	483	483	527	527	527	527	527	527	527	527	527	527	527	527	527	527	527
Crystal	ZD	ZD	A	A	A	A	A	B	B	B	C	C	D	D	E	E	E
Zone	mid	rim	c-dark	c-light	mid 1	mid 2	rim	mid 1	mid 2	rim	core	rim	core	rim	core	mid 1	mid 2
SiO_2	63.12	51.27	59.69	57.08	59.95	62.05	61.51	61.50	59.82	62.68	62.18	62.10	60.27	51.67	56.55	61.35	60.04
TiO_2	0.00	0.09	0.01	0.00	0.02	0.00	0.00	0.00	0.00	0.01	0.01	0.00	0.00	0.03	0.00	0.00	0.00
Al_2O_3	23.45	30.92	26.64	27.94	25.77	24.16	24.60	24.44	25.68	23.72	24.26	24.23	25.39	30.05	27.79	24.63	25.61
FeO	0.14	0.36	0.27	0.18	0.22	0.21	0.23	0.26	0.20	0.21	0.20	0.19	0.21	0.99	0.27	0.21	0.17
MgO	0.00	0.15	0.01	0.00	0.00	0.01	0.01	0.00	0.01	0.01	0.00	0.01	0.00	0.10	0.00	0.00	0.01
CaO	4.63	13.60	7.41	9.12	6.94	5.32	5.69	5.61	6.83	4.79	5.28	5.37	6.85	13.17	9.35	5.87	6.66
Na_2O	7.48	3.42	5.38	5.23	6.44	7.32	7.04	7.24	6.72	7.49	7.15	7.17	6.61	3.71	5.57	7.07	6.76
K_2O	1.17	0.18	0.59	0.45	0.66	0.93	0.91	0.95	0.74	1.09	0.92	0.93	0.65	0.27	0.47	0.87	0.75
Total	99.97	100.41	98.82	99.12	99.15	99.34	99.72	98.81	98.83	98.76	99.39	99.37	99.35	98.11	98.68	98.09	98.10
An	23.68	67.98	41.53	47.71	35.83	27.05	29.17	28.27	34.35	24.38	27.33	27.59	34.96	65.18	46.77	29.80	33.62
Ab	69.21	30.94	54.54	49.49	60.14	67.32	65.28	66.02	61.22	69.03	66.97	66.69	61.07	33.22	50.43	64.94	61.85
Or	7.12	1.08	3.93	2.80	4.03	5.64	5.55	5.71	4.44	6.60	5.70	5.72	3.98	1.60	2.80	5.27	4.53

Table A2.4 *(continued)*: EPMA data for plagioclase phenocrysts from Tauhara volcano.

Sample #	527	527	527	527	527	527	527	527	527	527	527	527	527	527	527	527	527
Crystal	E	E	F	F	F	F	G	G	G	G	G	G	H	H	H	H	I
Zone	mid 3	rim	core	mid 1	mid 2	rim	core	mid 1	mid 2	mid 3	mid 4	rim	core	mid 1	mid 2	rim	core
SiO_2	61.15	61.32	61.94	61.22	60.81	61.87	57.34	60.29	61.63	59.59	61.74	61.54	62.52	62.35	61.19	62.62	61.98
TiO_2	0.02	0.00	0.00	0.02	0.00	0.00	0.02	0.00	0.02	0.00	0.00	0.02	0.00	0.00	0.00	0.00	0.00
Al_2O_3	24.83	24.57	24.27	24.74	25.17	24.46	27.24	25.34	24.39	25.70	24.31	24.87	23.93	24.04	24.63	23.77	24.25
FeO	0.19	0.30	0.23	0.21	0.22	0.28	0.30	0.24	0.24	0.34	0.22	0.28	0.16	0.15	0.24	0.23	0.26
MgO	0.00	0.00	0.00	0.00	0.00	0.00	0.00	0.01	0.00	0.01	0.00	0.00	0.00	0.02	0.01	0.01	0.00
CaO	5.73	5.63	5.12	6.02	6.25	5.50	9.17	6.88	5.85	7.27	5.68	5.57	5.22	5.26	6.21	5.29	5.37
Na_2O	7.16	7.26	7.44	6.94	6.75	6.97	5.51	6.61	7.02	6.44	7.17	6.80	7.19	7.22	6.93	7.16	7.25
K_2O	0.91	0.93	1.01	0.85	0.81	0.92	0.43	0.65	0.84	0.65	0.88	0.93	0.99	0.97	0.79	0.93	0.90
Total	98.15	98.29	98.13	99.03	99.30	99.96	99.30	99.60	99.48	99.33	99.46	99.74	99.43	99.02	99.86	99.44	99.57
An	28.98	28.33	25.88	30.73	32.19	28.62	46.70	35.09	29.92	36.91	28.83	29.33	26.90	27.03	31.51	27.31	27.47
Ab	65.53	66.10	68.06	64.12	62.88	65.69	50.72	60.99	64.95	59.18	65.84	64.86	67.05	67.06	63.71	66.95	67.07
Or	5.49	5.58	6.06	5.14	4.94	5.69	2.58	3.92	5.13	3.91	5.32	5.81	6.06	5.91	4.79	5.74	5.46

Sample #	527	527	527	527	527	527	527	527	527	527	527	527	527	527	527	527	527
Crystal	I	I	I	J	J	J	J	K	K	K	L	L	L	M	M	M	N
Zone	mid 1	mid 2	rim	core	mid 1	mid 2	rim	core	mid	rim	core	mid	rim	core	mid	rim	core
SiO_2	61.00	61.93	61.72	59.53	61.17	60.75	62.16	58.67	61.56	62.30	57.23	60.06	62.54	58.48	58.46	62.01	52.96
TiO_2	0.01	0.00	0.01	0.00	0.00	0.00	0.00	0.00	0.00	0.02	0.00	0.00	0.01	0.00	0.00	0.00	0.00
Al_2O_3	24.73	25.40	24.41	25.84	24.71	25.06	24.09	26.48	24.64	23.95	27.36	25.47	23.84	26.48	26.53	24.13	30.11
FeO	0.23	0.28	0.18	0.27	0.27	0.20	0.26	0.24	0.20	0.19	0.27	0.24	0.20	0.27	0.24	0.26	0.30
MgO	0.03	0.01	0.00	0.03	0.01	0.00	0.01	0.01	0.01	0.02	0.01	0.00	0.00	0.01	0.02	0.00	0.00
CaO	6.14	6.19	5.70	7.41	6.07	6.44	5.32	7.73	5.75	5.21	8.70	6.59	4.93	8.21	8.26	5.46	12.03
Na_2O	7.05	5.36	7.09	6.29	6.97	6.81	7.23	6.28	7.04	7.34	5.92	6.87	7.42	6.00	5.96	7.18	4.29
K_2O	0.80	0.82	0.89	0.61	0.79	0.75	0.93	0.60	0.80	0.98	0.51	0.77	1.06	0.55	0.54	0.96	0.30
Total	99.25	98.57	99.39	99.50	99.18	99.24	99.41	98.21	99.19	99.57	98.28	98.18	98.57	99.31	99.55	99.16	98.50
An	30.95	36.68	29.09	37.95	30.93	32.76	27.27	39.00	29.59	26.51	43.46	33.03	25.11	41.61	41.94	27.87	59.68
Ab	64.23	57.52	65.50	58.30	64.27	62.67	67.08	57.42	65.52	67.58	53.53	62.36	68.47	55.09	54.77	66.27	38.54
Or	4.82	5.80	5.42	3.75	4.80	4.57	5.65	3.58	4.90	5.91	3.01	4.61	6.42	3.30	3.29	5.86	1.78

Table A2.4 *(continued)*: EPMA data for plagioclase phenocrysts from Tauhara volcano.

Sample #	527	527	527	527	527	527	527	527	527	527	527	527	527	527	527	527	527
Crystal	N	N	O	O	O	P	P	P	Q	Q	Q	Q	Q	R	R	R	R
Zone	mid	rim	core	mid	rim	core	mid	rim	core	mid 1	mid 2	mid 3	rim	core	mid 1	mid 2	rim
SiO_2	61.93	61.43	61.70	61.05	63.33	60.52	59.90	61.69	60.58	59.37	59.95	61.28	61.30	62.09	60.79	60.30	61.20
TiO_2	0.00	0.00	0.02	0.02	0.00	0.00	0.00	0.00	0.01	0.00	0.01	0.00	0.00	0.04	0.03	0.00	0.03
Al_2O_3	24.20	24.44	24.29	24.74	23.12	25.20	25.61	24.43	25.17	25.92	25.59	24.75	24.65	24.03	24.99	25.26	24.61
FeO	0.24	0.35	0.25	0.19	0.18	0.22	0.27	0.18	0.23	0.30	0.20	0.17	0.16	0.23	0.24	0.26	0.33
MgO	0.01	0.01	0.00	0.00	0.01	0.02	0.00	0.01	0.00	0.01	0.00	0.01	0.00	0.00	0.01	0.00	0.00
CaO	5.61	5.86	5.82	6.30	4.55	6.18	6.77	5.38	6.38	7.56	6.73	5.82	5.77	4.78	5.88	6.29	5.54
Na_2O	7.11	7.09	7.06	6.90	7.69	7.04	6.71	7.36	6.88	6.29	6.80	7.09	7.17	7.68	7.14	7.02	7.28
K_2O	0.90	0.81	0.87	0.81	1.13	0.82	0.74	0.95	0.74	0.56	0.72	0.89	0.95	1.14	0.92	0.87	1.01
Total	99.69	99.87	99.29	99.55	99.63	98.46	98.74	99.02	98.55	99.93	99.25	99.56	99.35	97.56	97.78	97.57	97.57
An	28.73	29.83	29.64	31.89	22.98	31.08	34.20	27.14	32.37	38.57	33.85	29.53	29.05	23.86	29.55	31.41	27.82
Ab	65.81	65.23	65.11	63.23	70.25	63.99	61.36	67.16	63.19	58.01	61.82	65.11	65.27	69.36	64.94	63.42	66.16
Or	5.46	4.93	5.25	4.87	6.77	4.93	4.44	5.70	4.44	3.43	4.34	5.36	5.68	6.79	5.51	5.17	6.02

Sample #	527	527	527	527	527	527	527	527	527	527	527
Crystal	S	S	S	S	S	T	T	T	T	U	U
Zone	core	mid 1	mid 2	mid 3	rim	core	mid 1	mid 2	rim	core	mid
SiO_2	60.29	56.42	61.14	61.88	61.82	59.57	54.64	59.56	61.72	59.35	60.52
TiO_2	0.00	0.03	0.00	0.00	0.00	0.00	0.000	0.000	0.000	0.02	0.00
Al_2O_3	25.37	27.89	24.81	24.27	24.33	25.88	29.18	25.78	24.40	25.71	25.06
FeO	0.25	0.32	0.22	0.29	0.20	0.24	0.169	0.235	0.228	0.44	0.30
MgO	0.00	0.00	0.01	0.00	0.00	0.00	0.000	0.013	0.002	0.03	0.01
CaO	6.50	9.44	6.16	5.34	5.63	7.29	10.74	7.04	5.28	7.57	6.67
Na_2O	6.86	5.50	6.90	7.28	7.12	6.41	4.94	6.67	7.38	6.26	6.73
K_2O	0.73	0.40	0.76	0.93	0.89	0.60	0.327	0.705	0.991	0.62	0.72
Total	98.56	98.97	99.64	99.87	99.91	100.30	98.86	98.71	98.27	99.79	100.19
An	32.87	47.52	31.52	38.55	27.21	28.75	53.53	35.28	26.64	37.21	53.53
Ab	62.75	50.10	63.87	57.79	67.12	65.84	44.53	60.51	67.40	59.14	44.53
Or	4.38	2.38	4.62	3.66	5.67	5.41	1.94	4.21	5.96	3.65	1.94

Table A2.5: EPMA data for ilmenite phenocrysts from Tauhara volcano.

Sample #	425	425	425	425	425	425	425	425	425	440	440	440	440	440	440	440	440
Crystal*	1	3	5	8	19	21	22	s5	s7	4	5	8	11	14	16	18	23
Zone	core	core	core	core	core	core	core	core	core	core	core	core	core	core	core	core	core
Host	plag	amph	plag	gmass	gmass	gmass	gmass	gmass	gmass	amph	amph	amph	plag	cpx	gmass	amph	cpx
SiO_2	0.11	0.04	0.01	0.03	0.28	0.00	0.01	0.01	0.03	0.00	0.00	0.03	0.35	0.00	0.01	0.00	0.00
TiO_2	40.28	41.81	45.78	42.61	42.93	29.72	39.02	31.13	34.25	40.91	41.11	44.02	41.55	41.41	38.14	41.88	42.25
Al_2O_3	0.21	0.77	0.12	0.49	0.30	0.26	0.20	0.24	0.23	0.16	0.19	0.13	0.36	0.08	0.08	0.11	0.15
Cr_2O_3	0.00	0.06	0.03	0.00	0.02	0.01	0.00	0.00	0.02	0.00	0.03	0.00	0.00	0.00	0.00	0.00	0.00
Fe_2O_3	7.15	6.09	4.29	5.38	5.34	11.59	11.17	12.98	10.35	8.33	7.83	6.52	7.13	7.70	9.67	7.27	7.10
FeO	45.17	42.90	45.68	39.99	41.23	43.42	51.01	47.72	44.74	45.18	44.16	44.71	44.93	45.36	46.64	45.09	44.52
MnO	1.41	0.27	1.31	0.93	0.72	0.47	0.56	0.64	0.50	0.74	0.64	1.06	1.18	1.01	0.91	0.89	1.26
MgO	1.53	3.96	1.23	4.57	4.06	2.39	2.27	1.99	2.66	3.48	3.76	3.28	2.95	2.74	2.43	2.80	2.98
CaO	0.26	0.08	0.00	0.00	0.02	0.00	0.00	0.00	0.01	0.00	0.00	0.00	0.00	0.00	0.00	0.00	0.00
Total	96.12	95.97	98.45	94.00	94.90	87.85	104.24	94.71	92.79	98.78	97.71	99.74	98.46	98.30	97.87	98.05	98.26
Ti#	41.26	43.74	45.39	46.09	45.62	33.17	36.50	32.04	36.30	41.13	41.94	43.91	42.13	41.61	38.27	42.19	42.74
$Fe^{3+}/\Sigma Fe$	0.12	0.11	0.08	0.11	0.10	0.19	0.16	0.20	0.17	0.14	0.14	0.12	0.12	0.13	0.16	0.13	0.13

Sample #	440	440	456	456	456	456	456	456	456	456	456	456	477	477	477	477	477
Crystal*	24	26	2	4	7	8	9	16	18	20	s2	s5	4	6	8	11	12
Zone	core	core	core	core	core	core	core	core	core	core	core	core	core	core	core	core	core
Host	gmass	plag	cpx	gmass	gmass	plag	plag	gmass	gmass	cpx	gmass	gmass	gmass	cpx	amph	gmass	plag
SiO_2	0.01	0.01	0.05	0.00	0.02	0.00	0.01	0.02	0.06	0.01	0.08	0.05	0.27	0.01	0.00	0.04	0.38
TiO_2	39.97	41.14	44.46	43.10	43.81	43.99	43.89	43.75	31.82	43.65	37.90	31.83	42.06	38.40	41.66	36.66	47.99
Al_2O_3	0.10	0.14	0.08	0.05	0.06	0.07	0.05	0.04	0.53	0.06	0.24	0.41	0.21	0.14	0.24	0.17	0.26
Cr_2O_3	0.01	0.00	0.02	0.03	0.04	0.00	0.01	0.03	0.02	0.01	0.07	0.00	0.00	0.01	0.00	0.00	0.00
Fe_2O_3	8.38	7.70	5.02	6.12	5.64	5.62	5.73	5.65	13.12	6.00	8.06	13.97	5.32	8.58	7.74	9.94	0.47
FeO	45.87	44.62	44.69	45.16	45.16	44.99	45.19	44.93	47.73	45.56	42.70	49.20	42.91	45.66	42.31	46.44	42.16
MnO	0.83	0.81	1.10	0.92	0.86	0.92	1.01	0.75	1.15	0.99	1.55	1.12	0.55	0.69	0.89	0.69	0.76
MgO	2.54	3.21	1.95	2.16	2.09	2.20	2.09	2.24	2.56	2.06	2.81	2.45	2.64	2.21	4.89	2.32	1.10
CaO	0.00	0.02	0.00	0.00	0.00	0.00	0.00	0.00	0.00	0.00	0.01	0.00	0.00	0.00	0.00	0.00	0.09
Total	97.71	97.65	97.36	97.55	97.67	97.79	98.00	97.42	96.99	98.35	93.41	99.03	93.95	95.71	97.73	96.25	93.19
Ti#	40.23	41.79	44.84	43.35	43.96	44.16	43.95	44.04	32.47	43.52	40.56	31.67	44.24	39.29	43.20	37.32	50.34
$Fe^{3+}/\Sigma Fe$	0.14	0.13	0.09	0.11	0.10	0.10	0.10	0.10	0.20	0.11	0.15	0.20	0.10	0.14	0.14	0.16	0.01

Note: Total refers to original analytical total. Ti#= cation normalised $Ti/(Ti+Fe^{2+}+Fe^{3+})$. Abbreviated host names: amph: amphibole; cpx: clinopyroxene; gmass: groundmass; plag: plagioclase. Crystal*: Ilmenite labelled with s# are <10 µm in diameter and are considered to have originated in the groundmass. Ilmenite crystals without s as a prefix have diameters > 50 µm and are phenocrysts or hosted by other phenocrysts such as clinopyroxene.

Table A2.5 *(continued)*: EPMA data for ilmenite phenocrysts from Tauhara volcano.

Sample #	477	477	477	477	483	483	483	527	527	527	527	527	527	527	527	527
Crystal*	15	17	19	21	3	8	9	11	13	15	18	21	23	s1	s9	s10
Zone	core	core	core	core	core	core	core	core	core	core	core	core	core	core	core	core
Host	cpx	amph	cpx	gmass	gmass	plag	plag	gmass	cpx	gmass	gmass	gmass	gmass	gmass	gmass	gmass
SiO_2	0.02	0.01	0.02	0.01	0.01	0.02	0.00	0.02	0.02	0.00	0.10	0.00	0.00	1.23	0.02	0.00
TiO_2	40.72	40.89	43.27	40.14	45.36	37.60	39.52	47.03	46.78	46.86	46.45	46.94	45.94	45.30	48.38	45.28
Al_2O_3	0.15	0.29	0.18	0.16	0.09	0.26	0.84	0.06	0.08	0.09	0.09	0.08	0.09	0.41	0.06	0.08
Cr_2O_3	0.00	0.01	0.00	0.00	0.00	0.02	0.03	0.00	0.03	0.00	0.00	0.00	0.00	0.00	0.00	0.00
Fe_2O_3	6.38	7.65	5.56	7.93	1.33	9.52	4.95	4.02	4.00	3.96	4.01	3.69	4.54	3.14	2.97	4.98
FeO	42.47	44.84	44.18	45.60	38.00	44.40	40.48	45.36	45.08	45.04	44.85	44.60	45.46	44.32	44.50	45.17
MnO	1.02	0.54	0.67	0.71	1.09	1.32	0.93	1.12	1.18	1.19	1.18	1.22	1.16	1.11	1.47	1.14
MgO	2.74	3.25	2.52	2.47	2.42	3.24	2.71	1.76	1.81	1.80	1.83	1.79	1.71	1.79	1.69	1.98
CaO	0.03	0.00	0.00	0.00	0.00	0.03	0.02	0.05	0.00	0.00	0.01	0.00	0.00	0.07	0.01	0.00
Total	93.52	97.48	96.40	97.01	88.31	96.41	89.49	99.42	98.97	98.94	98.51	98.32	98.90	97.36	99.12	98.62
Ti#	43.17	41.56	44.18	40.64	51.00	38.97	44.17	46.34	46.36	46.45	46.30	46.84	45.47	46.36	47.99	45.06
$Fe^{3+}/\Sigma Fe$	0.12	0.13	0.10	0.14	0.03	0.16	0.10	0.07	0.07	0.07	0.07	0.07	0.08	0.06	0.06	0.09

Table A2.6: EPMA data for magnetite phenocrysts from Tauhara volcano.

Sample #	425	425	425	425	425	425	425	425	425	425	425	425	425	425	425	425	425
Crystal*	2	6	7	9	10	12	13	14	15	16	17	18	20	s1	s10	s2	s3
Zone	core	core	core	core	core	core	core	core	core	core	core	core	core	core	core	core	core
Host	plag	plag	gmass	amph	amph	amph	amph	amph	gmass	gmass	gmass	gmass	gmass	gmass	gmass	gmass	gmass
SiO_2	1.07	0.07	0.07	0.01	0.07	0.06	0.03	0.02	0.06	0.04	0.06	0.02	0.02	0.03	0.05	0.01	0.04
TiO_2	1.19	6.81	4.41	18.51	5.19	5.79	31.21	6.42	4.88	4.83	3.96	2.62	20.12	3.83	5.93	4.29	5.83
Al_2O_3	2.10	1.76	1.19	0.21	1.27	1.42	0.11	1.41	1.28	1.23	1.27	1.44	0.21	0.97	0.95	0.94	0.91
Cr_2O_3	0.00	0.03	0.03	0.00	0.03	0.03	0.02	0.02	0.03	0.02	0.05	0.04	0.00	0.02	0.02	0.07	0.00
Fe_2O_3	46.16	47.28	47.62	39.77	47.19	47.23	38.56	45.29	47.10	46.99	47.64	47.83	32.36	47.11	47.17	47.38	47.30
FeO	42.52	40.16	38.66	32.88	37.83	40.60	32.23	40.18	38.13	37.81	39.46	41.47	24.11	38.42	37.15	38.27	36.83
MnO	0.18	0.62	0.83	0.62	0.87	0.66	0.29	0.23	0.85	0.99	0.76	0.59	0.56	0.90	0.91	0.86	1.01
MgO	0.13	1.65	2.36	1.33	2.62	1.26	1.26	0.68	2.42	2.43	1.99	1.13	2.57	2.10	2.84	2.34	3.00
CaO	0.06	0.06	0.00	0.04	0.00	0.00	0.00	0.11	0.00	0.00	0.00	0.00	0.00	0.00	0.00	0.00	0.00
Total	93.40	98.44	95.16	93.37	95.06	97.04	103.71	94.35	94.76	94.35	95.19	95.12	79.95	93.37	95.01	94.17	94.92
Ti#	1.25	6.89	4.64	19.52	5.50	5.90	29.56	6.66	5.17	5.14	4.15	2.71	25.37	4.09	6.28	4.55	6.20
$Fe^{3+}/\Sigma Fe$	0.49	0.51	0.53	0.52	0.53	0.51	0.52	0.50	0.53	0.53	0.52	0.51	0.55	0.52	0.53	0.53	0.54

Sample #	425	425	425	425	440	440	440	440	440	440	440	440	440	440	440	440	440
Crystal*	s4	s6	s8	s9	1	2	3	6	7	9	10	12	13	15	17	19	20
Zone	core	core	core	core	core	core	core	core	core	core	core	core	core	core	core	core	core
Host	gmass	gmass	gmass	gmass	cpx	gmass	amph	amph	amph	amph	gmass	plag	gmass	cpx	amph	plag	plag
SiO_2	0.02	1.13	0.05	0.04	0.30	0.04	0.01	0.05	0.05	0.03	0.03	0.06	0.02	1.25	0.06	0.03	0.04
TiO_2	6.18	7.19	6.45	6.34	4.80	3.11	4.53	6.59	4.56	20.74	6.62	4.36	6.16	5.15	6.09	6.70	6.49
Al_2O_3	0.81	0.95	1.03	0.96	1.31	0.75	1.86	1.67	1.41	0.85	1.18	1.56	1.24	1.85	1.34	1.19	1.21
Cr_2O_3	0.06	0.03	0.04	0.05	0.02	0.01	0.05	0.02	0.06	0.02	0.01	0.02	0.03	0.00	0.02	0.02	0.02
Fe_2O_3	47.38	45.17	46.58	47.02	49.36	32.22	49.88	48.79	49.55	43.43	48.46	48.43	49.09	46.73	48.43	48.67	48.65
FeO	36.53	35.44	36.00	36.10	42.36	27.83	42.65	41.39	42.81	34.11	41.03	43.00	41.85	40.39	41.07	41.33	41.25
MnO	0.96	0.97	0.97	0.94	0.57	0.28	0.50	0.52	0.57	0.86	0.65	0.58	0.67	0.62	0.69	0.82	0.89
MgO	3.21	2.75	3.19	3.34	1.33	0.80	1.71	1.77	1.25	2.64	1.54	0.61	1.42	1.29	1.53	1.39	1.40
CaO	0.00	0.00	0.00	0.00	0.03	0.00	0.00	0.00	0.00	0.00	0.00	0.00	0.00	0.03	0.03	0.00	0.00
Total	95.13	93.63	94.30	94.78	100.08	65.02	101.20	100.79	100.26	102.69	99.53	98.63	100.48	97.29	99.24	100.14	99.94
Ti#	6.56	7.84	6.93	6.78	4.74	4.69	4.45	6.50	4.49	20.31	6.58	4.33	6.05	5.32	6.08	6.61	6.42
$Fe^{3+}/\Sigma Fe$	0.54	0.53	0.54	0.54	0.51	0.51	0.51	0.51	0.51	0.53	0.52	0.50	0.51	0.51	0.51	0.51	0.51

Note: Total refers to original analytical total. Ti#= cation normalised $Ti/(Ti+Fe^{2+}+Fe^{3+})$. Abbreviated host names: amph: amphibole; cpx: clinopyroxene; gmass: groundmass; plag: plagioclase. Crystal*: Magnetite labelled with s# are <10 μm in diameter and are considered to have originated in the groundmass. Magnetite crystals without s as a prefix have diameters > 50 μm and are phenocrysts or hosted by other phenocrysts such as clinopyroxene.

Table A2.6 *(continued)*: EPMA data for magnetite phenocrysts from Tauhara volcano.

Sample #	440	440	440	440	440	440	440	440	440	440	440	440	456	456	456	456	456
Crystal*	22	27	s1	s10	s2	s3	s4	s5	s6	s7	s8	s9	1	3	6	10	11
Zone	core	core	core	core	core	core	core	core	core	core	core	core	core	core	core	core	core
Host	cpx	gmass	gmass	gmass	gmass	gmass	gmass	gmass	gmass	gmass	gmass	gmass	cpx	cpx	gmass	gmass	gmass
SiO_2	0.04	0.04	0.06	0.10	0.08	0.06	0.05	0.05	0.76	0.09	0.10	0.02	3.59	0.08	0.07	0.04	0.06
TiO_2	5.38	7.05	4.37	4.24	7.36	8.04	7.90	5.28	7.61	4.66	6.80	8.53	4.70	4.85	4.27	5.39	6.39
Al_2O_3	1.33	1.34	1.26	1.44	1.08	1.01	1.02	1.16	1.07	1.10	1.05	1.06	1.88	1.40	1.26	1.40	0.99
Cr_2O_3	0.02	0.03	0.02	0.07	0.00	0.03	0.01	0.03	0.00	0.03	0.04	0.03	0.04	0.02	0.09	0.03	0.06
Fe_2O_3	48.92	48.12	49.41	49.74	47.66	47.43	47.01	48.84	48.10	49.20	48.14	47.93	44.98	48.62	49.02	48.31	49.07
FeO	41.80	40.82	42.40	42.91	39.61	38.98	39.73	41.66	39.62	42.07	40.56	39.90	33.79	42.70	42.94	42.17	42.52
MnO	0.77	0.65	0.58	0.54	0.70	0.72	0.77	0.59	0.73	0.53	0.65	0.77	0.45	0.60	0.56	0.59	0.68
MgO	1.34	1.56	1.33	1.32	1.63	1.64	1.41	1.41	2.04	1.38	1.58	1.80	0.77	0.81	0.86	0.95	0.94
CaO	0.00	0.00	0.00	0.00	0.33	0.61	0.00	0.00	0.03	0.00	0.03	0.00	4.84	0.00	0.00	0.00	0.00
Total	99.59	99.60	99.44	100.35	98.45	98.52	97.90	99.01	99.95	99.05	98.96	100.04	95.03	99.06	99.08	98.89	100.71
Ti#	5.34	7.01	4.33	4.17	7.43	8.14	7.98	5.25	7.63	4.63	6.79	8.46	5.38	4.80	4.23	5.36	6.22
$Fe^{3+}/\Sigma Fe$	0.51	0.51	0.51	0.51	0.52	0.52	0.52	0.52	0.52	0.51	0.52	0.52	0.54	0.51	0.51	0.51	0.51

Sample #	456	456	456	456	456	456	456	456	456	456	456	456	456	456	477	477	477
Crystal*	12	13	14	15	17	19	s1	s10	s3	s4	s6	s7	s8	s9	1	2	3
Zone	core	core	core	core	core	core	core	core	core	core	core	core	core	core	core	core	core
Host	gmass	plag	gmass	gmass	plag	gmass	gmass	gmass	gmass	gmass	gmass	gmass	gmass	gmass	gmass	cpx	amph
SiO_2	0.06	0.04	0.29	0.05	0.07	0.05	0.03	0.08	0.07	0.06	0.05	0.05	1.19	0.08	0.06	0.04	0.05
TiO_2	19.52	5.04	5.66	4.78	5.39	6.53	5.94	5.91	5.39	5.98	4.89	4.25	5.07	8.49	9.90	9.91	7.57
Al_2O_3	0.72	1.49	0.93	0.91	1.45	0.96	1.03	1.00	0.99	0.89	1.08	1.06	1.23	0.87	1.29	1.37	1.62
Cr_2O_3	0.06	0.03	0.05	0.02	0.03	0.04	0.09	0.25	0.07	0.00	0.18	0.01	0.03	0.00	0.04	0.06	0.03
Fe_2O_3	39.68	48.75	48.69	49.23	49.46	48.50	48.01	48.40	48.62	48.98	48.73	49.12	48.05	47.06	45.80	45.45	43.47
FeO	31.78	42.77	42.27	42.93	42.87	41.98	41.76	42.26	42.43	42.72	42.83	43.15	42.03	40.33	38.49	38.28	33.22
MnO	1.06	0.59	0.70	0.60	0.63	0.66	0.58	0.59	0.56	0.52	0.60	0.53	0.56	0.84	0.66	0.71	0.50
MgO	1.90	0.88	0.85	0.79	1.14	0.95	0.92	0.85	0.84	0.82	0.71	0.71	0.81	1.00	1.67	1.62	3.67
CaO	0.00	0.00	0.00	0.00	0.00	0.00	0.00	0.01	0.00	0.00	0.00	0.00	0.06	0.00	0.01	0.00	0.00
Total	94.79	99.58	99.45	99.31	101.03	99.66	98.36	99.35	98.97	99.97	99.05	98.88	99.04	98.65	97.91	97.45	90.14
Ti#	20.65	4.97	5.58	4.69	5.26	6.42	5.92	5.83	5.33	5.83	4.83	4.19	5.08	8.46	10.05	10.12	8.61
$Fe^{3+}/\Sigma Fe$	0.47	0.51	0.51	0.51	0.51	0.51	0.51	0.51	0.51	0.51	0.51	0.51	0.51	0.51	0.52	0.52	0.54

Table A2.6 *(continued)*: EPMA data for magnetite phenocrysts from Tauhara volcano.

Sample #	477	477	477	477	477	477	477	477	477	477	477	477	477	477	477	477	477
Crystal*	5	7	9	10	13	14	16	18	20	22	s1	s10	s2	s3	s4	s5	s6
Zone	core	core	core	core	core	core	core	core	core	core	core	core	core	core	core	core	core
Host	gmass	cpx	amph	gmass	plag	gmass	cpx	amph	cpx	gmass	gmass	gmass	gmass	gmass	gmass	gmass	gmass
SiO_2	0.06	0.07	0.03	1.54	0.08	0.13	0.07	0.05	0.06	0.04	0.09	0.06	0.09	0.07	0.08	0.11	0.11
TiO_2	10.31	8.90	8.37	10.49	12.01	10.64	9.64	9.56	10.52	7.86	10.57	9.49	10.20	9.85	9.04	8.15	9.78
Al_2O_3	1.52	0.85	1.72	1.36	1.27	1.63	1.57	2.54	0.92	1.44	0.84	0.94	0.94	1.01	0.72	0.78	1.25
Cr_2O_3	0.06	0.04	0.05	0.03	0.02	0.07	0.05	0.06	0.02	0.00	0.00	0.04	0.03	0.02	0.02	0.00	0.05
Fe_2O_3	44.50	44.68	46.77	43.27	45.99	43.67	46.05	46.01	44.95	47.13	44.33	45.79	44.27	44.93	45.34	44.35	45.00
FeO	36.44	37.80	37.88	38.06	38.52	34.31	39.44	38.63	37.50	41.19	37.65	38.81	37.27	37.79	38.16	36.68	38.49
MnO	0.81	0.59	0.91	0.54	0.57	0.19	0.66	0.52	0.76	0.14	0.50	0.61	0.72	0.66	0.72	0.66	0.56
MgO	2.18	1.36	2.53	0.73	1.79	3.35	1.38	2.28	1.59	1.18	1.30	1.37	1.41	1.50	1.36	1.71	1.30
CaO	0.00	0.00	0.00	0.00	0.00	0.00	0.00	0.00	0.00	0.00	0.00	0.00	0.00	0.01	0.00	0.05	0.02
Total	95.87	94.29	98.26	96.01	100.25	94.00	98.86	99.66	96.32	98.98	95.28	97.10	94.92	95.83	95.43	92.49	96.56
Ti#	10.81	9.31	8.60	10.92	11.91	11.51	9.69	9.71	10.82	7.80	10.93	9.64	10.63	10.18	9.34	8.74	10.02
$Fe^{3+}/\Sigma Fe$	0.52	0.52	0.53	0.51	0.52	0.53	0.51	0.52	0.52	0.51	0.51	0.51	0.52	0.52	0.52	0.52	0.51

Sample #	477	477	477	483	483	483	483	483	483	483	483	483	483	483	483	483	483
Crystal*	s7	s8	s9	1	4	7	10	11	12	13	15	16	s1	s10	s2	s4	s5
Zone	core	core	core	core	core	core	core	core	core	core	core	core	core	core	core	core	core
Host	gmass	gmass	gmass	gmass	gmass	plag	gmass	gmass	amph	cpx	gmass	gmass	gmass	gmass	gmass	gmass	gmass
SiO_2	0.07	0.07	0.06	0.10	0.08	0.04	0.14	0.07	0.06	0.07	0.10	0.08	0.10	0.08	0.07	0.12	0.05
TiO_2	6.59	8.65	8.90	10.84	8.05	4.94	21.69	12.10	9.36	24.27	7.86	10.79	8.36	12.19	7.44	6.52	8.78
Al_2O_3	0.70	0.65	1.04	1.66	1.26	1.37	0.88	1.22	1.87	0.81	1.40	2.00	1.18	1.26	1.51	1.12	1.25
Cr_2O_3	0.04	0.01	0.01	0.03	0.04	0.00	0.01	0.04	0.04	0.00	0.03	0.05	0.17	0.25	0.04	0.01	0.17
Fe_2O_3	45.84	45.52	45.49	40.61	43.54	41.64	41.40	41.03	43.60	39.93	45.86	42.49	43.21	43.37	43.33	44.81	45.31
FeO	39.38	38.50	38.86	34.04	38.23	35.88	35.33	34.76	38.04	32.26	39.30	37.02	35.58	36.01	37.63	37.17	37.56
MnO	0.52	0.61	0.57	0.58	0.38	0.46	0.57	0.64	0.46	0.68	0.59	0.22	0.80	0.58	0.38	0.45	0.73
MgO	1.00	1.30	1.26	1.72	0.82	1.14	1.11	1.34	1.16	1.96	1.33	1.36	1.90	1.92	1.15	1.92	1.93
CaO	0.05	0.00	0.00	0.04	0.00	0.04	0.00	0.00	0.00	0.05	0.00	0.00	0.02	0.01	0.00	0.05	0.00
Total	94.18	95.30	96.18	89.61	92.40	85.52	101.12	91.19	94.60	100.02	96.47	94.00	91.33	95.67	91.55	92.16	95.78
Ti#	6.85	8.92	9.12	12.14	8.56	5.71	21.19	13.18	9.83	24.25	8.07	11.42	9.18	12.75	8.03	7.03	9.16
$Fe^{3+}/\Sigma Fe$	0.51	0.52	0.51	0.52	0.51	0.51	0.51	0.52	0.51	0.53	0.51	0.51	0.52	0.52	0.51	0.52	0.52

Table A2.6 *(continued)*: EPMA data for magnetite phenocrysts from Tauhara volcano.

Sample #	483	483	483	483	527	527	527	527	527	527	527	527	527	527	527	527	527
Crystal*	s6	s7	s8	s9	12	14	16	17	19	20	22	24	25	26	27	s2	s3
Zone	core	core	core	core	core	core	core	core	core	core	core	core	core	core	core	core	core
Host	gmass	gmass	gmass	gmass	cpx	cpx	gmass	gmass	plag	plag	gmass	gmass	cpx	gmass	gmass	gmass	gmass
SiO_2	0.08	0.06	0.10	0.12	0.29	0.06	0.06	0.27	0.05	0.07	0.06	0.07	0.07	0.04	0.08	0.10	1.03
TiO_2	6.09	7.52	12.45	10.52	8.81	9.15	8.54	8.33	8.99	9.55	9.13	8.41	8.32	8.53	8.00	5.65	5.73
Al_2O_3	1.34	1.53	0.96	1.12	1.42	1.34	1.47	1.39	1.40	1.69	1.37	1.47	1.48	1.45	1.40	4.39	4.03
Cr_2O_3	0.02	0.02	0.26	0.02	0.01	0.03	0.03	0.02	0.04	0.02	0.01	0.03	0.00	0.02	0.00	0.06	0.02
Fe_2O_3	44.13	47.57	44.35	44.59	45.91	47.33	47.08	45.71	47.06	44.84	46.81	46.26	46.83	47.27	46.90	45.84	46.04
FeO	37.22	40.64	37.19	37.77	40.45	41.19	41.52	39.90	41.29	39.77	40.78	41.06	41.19	41.55	41.24	39.39	39.14
MnO	0.68	0.73	0.70	0.65	0.68	0.68	0.66	0.71	0.67	0.48	0.68	0.54	0.65	0.65	0.61	0.31	0.37
MgO	1.55	1.42	1.57	1.39	0.66	0.94	0.69	0.81	0.78	0.73	0.91	0.60	0.75	0.77	0.74	2.62	2.64
CaO	0.00	0.00	0.00	0.00	0.00	0.00	0.00	0.06	0.00	0.00	0.00	0.00	0.00	0.00	0.00	0.00	0.05
Total	91.12	99.49	97.58	96.19	98.24	100.72	100.05	97.20	100.28	97.15	99.74	98.44	99.30	100.26	98.97	98.35	99.04
Ti#	6.65	7.50	12.69	10.84	8.84	8.95	8.39	8.47	8.81	9.69	9.01	8.39	8.24	8.36	7.94	5.93	6.02
$Fe^{3+}/\Sigma Fe$	0.52	0.51	0.52	0.52	0.51	0.51	0.51	0.51	0.51	0.50	0.51	0.50	0.51	0.51	0.51	0.51	0.51

Sample #	527	527	527	527	527
Crystal*	s4	s5	s6	s7	s8
Zone	core	core	core	core	core
Host	gmass	gmass	gmass	gmass	gmass
SiO_2	0.80	0.29	0.04	0.38	0.06
TiO_2	5.72	5.61	8.24	6.36	6.86
Al_2O_3	3.67	4.43	1.41	2.90	1.48
Cr_2O_3	0.05	0.03	0.03	0.00	0.04
Fe_2O_3	46.28	45.71	47.99	45.97	47.94
FeO	39.10	39.81	42.18	38.65	42.19
MnO	0.36	0.32	0.66	0.44	0.63
MgO	2.68	2.32	0.75	2.42	0.77
CaO	0.00	0.00	0.00	0.00	0.00
Total	98.67	98.52	101.30	97.12	99.98
Ti#	5.99	5.87	7.99	6.67	6.75
$Fe^{3+}/\Sigma Fe$	0.52	0.51	0.51	0.52	0.51

Table A2.7: EPMA data for melt inclusions from Tauhara volcano.

Sample #	425	425	425	425	425	425	425	425	425	425	425	440	440	440	440	440	440
Crystal	B	C	C	E	E	G	G	G	H	H	H	A	B	C	E	E	E
XL type	qtz	qtz	qtz	qtz	qtz	qtz	qtz	qtz	qtz	qtz	qtz	qtz	qtz	qtz	qtz	qtz	qtz
MI	1	1	2	1	2	1	2	3	1	2	3	1	1	1	1	2	3
SiO_2	76.97	77.59	76.04	77.77	78.53	77.63	75.95	77.64	76.66	78.22	77.32	76.70	77.57	79.11	76.66	76.40	76.84
TiO_2	0.08	0.10	0.13	0.10	0.09	0.10	0.11	0.07	0.10	0.08	0.10	0.08	0.07	0.22	0.09	0.10	0.09
Al_2O_3	12.48	11.82	12.76	12.12	11.88	12.12	13.17	12.09	12.63	11.68	12.22	12.63	11.96	11.39	12.71	12.96	12.75
FeO	1.09	1.42	1.31	1.07	0.69	1.12	1.17	0.97	1.14	1.12	1.14	1.03	0.61	0.43	1.09	0.83	0.92
MnO	0.03	0.00	0.04	0.02	0.00	0.05	0.06	0.01	0.00	0.00	0.01	0.02	0.00	0.04	0.03	0.01	0.06
MgO	0.05	0.05	0.06	0.10	0.07	0.11	0.02	0.10	0.08	0.09	0.07	0.07	0.00	0.01	0.08	0.07	0.05
CaO	0.71	0.69	0.69	0.54	0.23	0.58	0.62	0.78	0.61	0.63	0.63	0.61	0.25	0.38	0.55	0.59	0.52
Na_2O	2.80	3.32	3.57	3.43	2.60	3.25	3.59	2.61	3.63	2.79	2.89	3.05	2.43	2.36	3.45	3.02	3.48
K_2O	5.79	5.01	5.40	4.84	5.91	5.05	5.31	5.73	5.15	5.39	5.63	5.83	7.11	6.07	5.33	6.02	5.30
Total	99.62	100.29	99.56	99.50	99.90	99.90	99.39	99.43	98.50	98.74	97.04	98.12	99.74	100.53	100.20	99.40	100.20
Tot. alk.	8.59	8.33	8.96	8.28	8.51	8.30	8.90	8.35	8.78	8.18	8.51	8.87	9.54	8.44	8.79	9.04	8.78
Class	Rhy	Rhy	Rhy	Rhy	Rhy	Rhy	Rhy	Rhy	Rhy	Rhy	Rhy	Rhy	Rhy	Rhy	Rhy	Rhy	Rhy

Sample #	456	477	477	477	477	483	527	527	527	527	527	527	527	527	527	527	527
Crystal	B	A	A	A	C	D	A	B	C	C	D	E	F	G	G	H	H
XL type	qtz	qtz	qtz	qtz	qtz	opx	qtz	cpx	qtz	qtz	cpx	cpx	qtz	qtz	qtz	qtz	qtz
MI	1	1	2	3	1	1	1	1	1	2	1	1	1	1	2	1	2
SiO2	79.48	79.25	78.85	78.01	77.29	79.19	78.84	78.38	79.05	78.79	76.83	77.92	78.74	78.11	78.25	77.91	78.16
TiO2	0.06	0.02	0.05	0.09	0.07	0.06	0.11	0.10	0.09	0.09	0.10	0.13	0.10	0.09	0.10	0.09	0.09
Al2O3	12.11	11.18	11.18	11.53	11.91	11.80	11.98	12.10	11.99	11.66	12.60	12.13	11.99	12.27	12.22	12.38	12.15
FeO	0.35	0.76	0.87	0.99	0.98	1.27	0.92	0.93	0.86	1.11	1.57	1.77	0.78	1.12	0.92	0.96	0.95
MnO	0.00	0.04	0.01	0.00	0.06	0.03	0.04	0.05	0.02	0.03	0.02	0.05	0.07	0.01	0.02	0.03	0.04
MgO	0.00	0.03	0.06	0.07	0.08	0.06	0.11	0.09	0.12	0.07	0.10	0.12	0.08	0.10	0.11	0.12	0.06
CaO	1.35	0.36	0.45	0.49	0.70	0.82	0.66	0.75	0.76	0.66	1.02	0.87	0.67	0.74	0.76	0.94	0.72
Na_2O	3.88	2.92	2.87	2.98	4.16	2.88	3.37	3.43	3.19	3.60	3.55	3.29	3.13	3.50	3.60	3.57	3.17
K_2O	2.77	5.44	5.65	5.83	4.75	3.88	3.97	4.16	3.92	3.99	4.21	3.72	4.45	4.04	4.02	4.00	4.67
Total	100.30	98.94	97.88	98.58	98.33	100.29	95.52	95.87	95.42	93.75	96.76	97.47	94.71	96.27	96.22	96.88	93.04
Tot. alk.	6.65	8.36	8.52	8.82	8.91	6.76	7.34	7.60	7.11	7.59	7.75	7.00	7.58	7.54	7.61	7.57	7.84
Class	Rhy	Rhy	Rhy	Rhy	Rhy	Rhy	Rhy	Rhy	Rhy	Rhy	Rhy	Rhy	Rhy	Rhy	Rhy	Rhy	Rhy

Note: Oxides are normalised to 100%. Total refers to original analytical total Abbreviated terms: class: melt classification; cpx: clinopyroxene; opx: orthopyroxene; plag: plagioclase; qtz: quartz; rhy: rhyolite; Tot. Alk.: total alkali = $Na_2O + K_2O$ wt%; XL: crystal

Table A2.7 *(continued)*: EPMA data for melt inclusions from Tauhara volcano.

Sample #	527	527	527	527	527	527	527	527	527
Crystal	I	J	J	K	L	L	M	M	M
XL type	qtz	qtz	qtz	qtz	qtz	qtz	qtz	qtz	qtz
MI	1	1	2	1	1	2	1	2	3
SiO_2	79.17	80.31	80.64	79.29	78.07	77.92	80.10	78.35	78.53
TiO_2	0.08	0.14	0.06	0.06	0.10	0.09	0.09	0.09	0.11
Al_2O_3	11.42	10.49	10.69	11.36	12.02	12.33	11.06	11.95	11.81
FeO	0.87	1.41	0.93	1.06	0.96	0.99	0.83	0.80	1.06
MnO	0.04	0.04	0.01	0.08	0.05	0.04	0.05	0.05	0.06
MgO	0.08	0.26	0.08	0.07	0.09	0.09	0.09	0.08	0.06
CaO	0.65	1.07	0.67	0.65	0.75	0.81	0.71	0.76	0.61
Na_2O	3.67	2.79	2.93	3.37	3.77	3.62	3.60	4.12	3.74
K_2O	4.02	3.49	4.00	4.06	4.19	4.13	3.46	3.82	4.02
Total	95.33	96.10	95.39	96.27	96.60	97.10	99.16	93.57	96.30
Tot. alk.	7.69	6.28	6.93	7.43	7.96	7.74	7.06	7.93	7.76
Class	Rhy	Rhy	Rhy	Rhy	Rhy	Rhy	Rhy	Rhy	Rhy

APPENDIX 3

MINERAL TRACE ELEMENT DATA

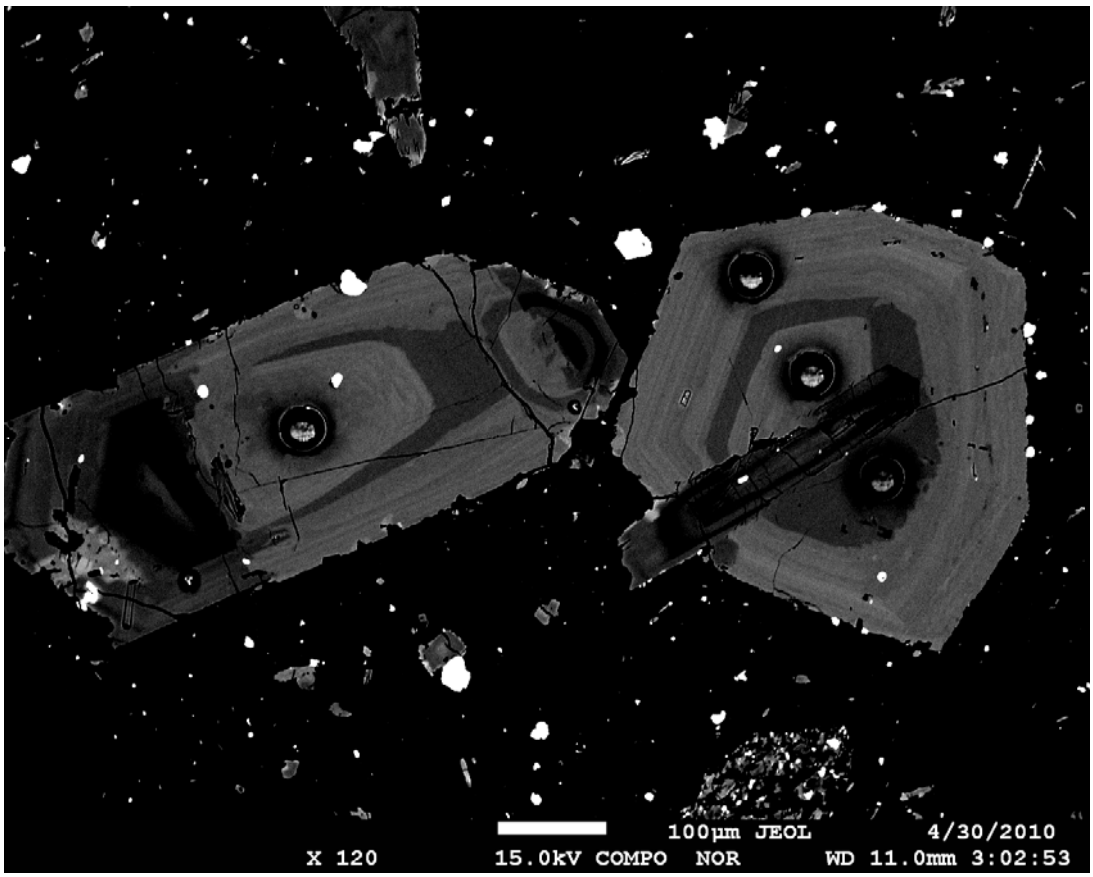

Plate 4: BSE image of clinopyroxene phenocrysts from sample 456 with 35 µm laser pits

Table A3.1: Clinopyroxene LA-ICP-MS data (6 samples, 53 analyses).

Table A3.2: Amphibole LA-ICP-MS data (6 samples, 66 analyses).

Table A3.3: Plagioclase LA-ICP-MS data (6 samples, 126 analyses).

Table A3.4: Melt inclusion LA-ICP-MS data (3 samples, 19 analyses).

Table A3.1: Clinopyroxene LA-ICP-MS data.

Sample	425	425	425	425	425	425	425	440	440	440	440	440	440	440	440	440	440
Crystal	A	A	B	C	C	D	D	C	D	D	E	F	F	F	I	K	L
Zone	core	mid 1	core	core	rim	core	mid	core	core	rim	mid	core	mid	rim	mid	core	core
CaO (wt. %)*	21.76	22.97	23.92	22.35	21.95	20.76	22.12	21.75	22.97	22.34	21.65	21.10	23.52	22.36	21.09	20.17	21.68
Li (ppm)	2.38	37.9	43.4	30.1	64.1	7.40	52.8	115	65.9	105	72.0	61.8	61.4	107	67.6	128	170
B	b.d.l.	b.d.l.	b.d.l.	0.920	b.d.l.	b.d.l.	b.d.l.	b.d.l.	0.792	0.084	b.d.l.	0.515	2.43	1.81	b.d.l.	b.d.l.	1.12
Sc	99.6	57.6	44.6	63.2	70.8	104	62.9	61.9	54.4	65.1	23.7	106	65.9	69.3	30.3	61.5	67.0
Ti (wt. %)	0.287	0.222	0.152	0.256	0.345	0.447	0.204	0.251	0.190	0.409	0.113	0.403	0.197	0.363	0.167	0.355	0.433
V (ppm)	258	128	79.5	147	213	287	147	234	190	291	108	428	143	294	151	300	281
Cr	542	5985	2490	4086	1599	18.0	1411	717	1354	290	6.43	81.2	1408	789	1.86	497	460
Mn (wt. %)	0.190	0.092	0.092	0.110	0.162	0.211	0.114	0.201	0.102	0.227	0.285	0.235	0.121	0.175	0.259	0.277	0.203
Ni (ppm)	44.4	536	623	635	494	8.07	426	367	71.6	180	128	34.1	352	195	109	194	347
Cu	1.37	3.23	2.73	2.32	8.54	1.88	6.59	6.06	2.79	4.21	2.35	2.77	3.74	9.39	17.2	4.48	30.8
Zn	32.6	19.4	17.5	20.1	34.0	39.7	21.4	51.5	24.7	54.2	70.3	60.7	31.6	50.0	71.5	56.0	79.2
Rb	b.d.l.	0.047	b.d.l.	0.026	0.026	b.d.l.	b.d.l.	0.049	0.018	0.008	b.d.l.	0.041	b.d.l.	0.642	0.909	0.429	3.18
Sr	17.3	97.0	95.0	68.6	63.0	21.8	65.2	73.0	106	73.0	37.8	20.1	88.8	79.0	60.3	47.1	116
Y	9.44	3.9	2.74	5.10	12.5	9.89	5.29	10.2	2.31	15.7	12.9	27.4	5.32	20.4	17.8	22.1	27.1
Zr	13.7	7.41	3.16	6.62	18.4	9.40	7.38	13.2	3.81	29.8	6.75	26.8	9.50	27.3	10.4	32.1	41.6
Nb	b.d.l.	b.d.l.	0.045	0.032	0.040	b.d.l.	b.d.l.	0.003	0.015	0.037	0.021	0.024	0.004	0.028	b.d.l.	0.011	0.318
Cs	b.d.l.	b.d.l.	0.004	b.d.l.	b.d.l.	b.d.l.	b.d.l.	b.d.l.	b.d.l.	b.d.l.	b.d.l.	b.d.l.	b.d.l.	b.d.l.	0.103	0.024	0.231
Ba	b.d.l.	0.318	0.035	0.118	b.d.l.	0.107	0.231	0.408	b.d.l.	0.140	0.077	0.144	0.419	2.18	2.86	1.84	27.0
La	0.826	1.62	0.971	1.08	1.93	0.524	0.923	1.46	0.827	2.93	1.39	2.15	1.58	4.16	2.44	2.01	7.65
Ce	3.73	6.14	3.90	4.24	7.83	2.68	4.01	8.37	3.57	13.3	6.30	10.5	5.08	16.1	10.1	10.9	26.6
Pr	0.636	1.16	0.712	0.932	1.52	0.549	0.843	1.49	0.742	2.51	1.25	2.01	1.24	3.40	2.04	1.92	4.62
Nd	3.83	6.61	3.97	5.20	9.37	2.77	5.39	8.62	3.50	15.14	6.90	11.4	6.09	15.1	11.9	10.6	23.4
Sm	1.24	1.98	0.697	1.35	2.83	1.42	1.52	2.90	1.18	4.29	2.73	4.28	1.27	5.00	3.06	3.66	5.58
Eu	0.508	0.500	0.263	0.541	0.779	0.427	0.472	0.807	0.330	1.06	0.518	0.585	0.366	1.24	0.698	0.779	1.30
Gd	1.74	1.27	0.991	1.67	2.79	1.66	1.56	3.04	0.769	3.76	2.40	4.93	2.27	4.94	3.19	3.56	6.08
Tb	0.349	0.233	0.079	0.142	0.454	0.204	0.177	0.390	0.118	0.630	0.361	0.763	0.204	0.751	0.458	0.609	0.764
Dy	1.80	0.841	0.876	1.45	2.57	1.73	1.34	2.12	0.709	3.32	2.06	4.82	1.11	4.22	3.47	3.47	4.84
Ho	0.377	0.165	0.103	0.240	0.451	0.469	0.166	0.459	0.113	0.638	0.506	1.06	0.211	1.11	0.669	0.798	0.815
Er	0.829	0.538	0.313	0.515	1.53	1.16	0.630	1.38	0.220	1.58	1.45	2.95	0.521	2.53	2.04	2.24	2.48
Tm	0.133	0.021	0.043	0.076	0.203	0.115	0.059	0.150	0.046	0.294	0.180	0.391	0.077	0.341	0.278	0.305	0.362
Yb	0.854	0.392	0.093	0.288	1.14	0.952	0.374	0.946	0.205	1.90	0.941	2.73	0.640	2.34	1.79	2.36	2.37
Lu	0.081	0.050	0.037	0.053	0.135	0.110	0.037	0.144	0.016	0.212	0.226	0.463	0.082	0.259	0.258	0.361	0.424
Hf	0.562	0.324	0.168	0.359	0.815	0.271	0.496	0.668	0.210	1.63	0.362	1.21	0.276	1.46	0.567	1.52	2.26
Ta	b.d.l.	b.d.l.	b.d.l.	0.001	b.d.l.	b.d.l.	0.030	b.d.l.	b.d.l.	b.d.l.	b.d.l.	b.d.l.	b.d.l.	0.009	b.d.l.	0.011	0.040
W	b.d.l.	0.005	0.010	b.d.l.	b.d.l.	0.032	0.016	b.d.l.	b.d.l.	0.036	0.000	b.d.l.	0.026	0.061	0.054	0.074	0.134
Pb	0.041	0.070	0.069	0.043	0.036	0.103	0.013	0.190	0.055	b.d.l.	0.197	0.130	0.115	0.112	0.216	0.142	2.41
Th	0.328	0.007	b.d.l.	0.014	0.018	0.026	b.d.l.	0.039	b.d.l.	0.076	0.015	0.016	0.041	0.116	0.056	0.067	0.536
U	0.010	b.d.l.	b.d.l.	b.d.l.	b.d.l.	b.d.l.	0.007	0.020	0.010	0.023	b.d.l.	b.d.l.	0.008	b.d.l.	b.d.l.	0.006	0.043

Note: b.d.l.= below detection limits. *CaO (wt. %) from EPMA data, used as an internal standard.

Table A3.1 *(continued)*: Clinopyroxene LA-ICP-MS data.

Sample	440	456	456	456	456	456	456	456	456	456	456	456	456	477	477	477	477	477
Crystal	M	A	B	C	C	C	D	F	I	I	I	J	K	A	A	B	C	D
Zone	core	mid	core	core	mid	rim	core	mid	core	mid	rim	mid	mid	core	rim	mid	core	mid 2
CaO (wt. %)	21.91	21.13	20.84	21.23	21.47	21.32	20.63	21.14	21.23	21.63	20.67	20.26	21.29	22.21	21.61	21.46	20.87	21.83
Li (ppm)	370	91.6	150	47.4	57.8	134	96.6	102	12.7	89.6	158	106	118	2.95	8.09	42.2	3.58	1.70
B	2.14	b.d.l.	0.522	b.d.l.	0.267	0.120	0.006	b.d.l.	0.114	b.d.l.	1.58	b.d.l.	0.175	0.436	1.37	2.79	0.268	b.d.l.
Sc	65.3	18.4	83.6	86.6	67.1	88.7	92.8	27.7	90.6	60.9	82.1	30.4	70.7	88.1	88.0	64.6	134	68.3
Ti (wt. %)	0.598	0.094	0.278	0.364	0.183	0.439	0.487	0.151	0.387	0.200	0.385	0.157	0.224	0.398	0.389	0.225	0.453	0.366
V (ppm)	457	87.1	211	267	136	290	264	151	357	149	250	149	214	239	246	158	439	187
Cr	595	1.26	194	92.7	1810	474	140	b.d.l.	74.9	4368	145	0.091	270	903	973	1062	60.3	749
Mn (wt. %)	0.235	0.253	0.274	0.272	0.202	0.298	0.249	0.269	0.182	0.155	0.258	0.293	0.279	0.160	0.155	0.182	0.257	0.170
Ni (ppm)	311	167	196	190	583	184	197	159	129	421	160	160	199	261	310	385	6.00	256
Cu	10.2	2.35	4.38	3.21	2.53	22.8	1.74	4.76	1.13	3.71	5.37	2.95	4.31	1.96	2.78	2.96	1.27	1.47
Zn	58.8	56.2	55.3	58.8	34.8	82.2	48.5	68.2	36.7	27.2	59.8	67.9	62.0	34.1	31.6	33.2	54.0	34.9
Rb	8.07	b.d.l.	0.074	0.000	0.052	0.267	b.d.l.	b.d.l.	b.d.l.	b.d.l.	0.017	0.023	b.d.l.	0.016	0.007	b.d.l.	0.007	b.d.l.
Sr	126	32.3	22.8	26.7	27.1	25.4	26.5	29.6	28.3	34.3	30.1	31.0	23.4	35.5	35.3	29.0	21.3	34.7
Y	17.1	5.69	19.5	22.3	7.22	30.6	21.1	12.1	11.7	5.24	25.1	15.6	14.0	9.91	9.38	6.16	17.2	7.68
Zr	49.1	2.68	18.7	26.3	4.51	68.6	28.4	8.01	10.2	3.66	28.1	9.78	13.1	15.1	11.6	5.70	11.5	11.3
Nb	0.974	0.000	0.003	0.029	b.d.l.	0.230	0.052	0.040	b.d.l.	0.018	0.116	0.054	b.d.l.	0.016	b.d.l.	b.d.l.	0.014	0.029
Cs	0.408	b.d.l.	0.028	b.d.l.	b.d.l.	0.020	0.009	0.021	b.d.l.	b.d.l.	b.d.l.	b.d.l.	b.d.l.	b.d.l.	b.d.l.	b.d.l.	b.d.l.	0.007
Ba	68.7	0.059	0.071	b.d.l.	0.336	0.650	0.060	b.d.l.	0.065	b.d.l.	0.518	0.048	0.168	b.d.l.	b.d.l.	b.d.l.	b.d.l.	b.d.l.
La	3.33	0.501	1.32	1.49	0.429	5.36	1.81	1.40	0.650	0.462	2.61	1.78	1.05	0.864	0.704	0.369	0.880	0.846
Ce	16.1	2.50	5.57	7.37	2.05	20.8	7.07	5.48	3.29	2.07	10.5	7.39	4.91	3.78	3.61	2.05	4.41	3.54
Pr	3.09	0.487	1.12	1.44	0.387	3.39	1.40	1.09	0.680	0.332	2.11	1.40	0.870	0.703	0.728	0.421	0.864	0.699
Nd	16.2	2.76	8.08	9.11	2.47	18.9	9.04	6.77	3.86	2.29	12.3	9.04	5.97	4.64	4.29	2.91	5.47	4.20
Sm	4.22	0.901	2.31	3.39	0.876	4.85	3.37	2.00	1.74	0.826	4.33	2.26	2.20	1.31	1.82	0.978	2.00	1.49
Eu	1.15	0.277	0.687	0.853	0.351	0.951	0.906	0.529	0.449	0.321	1.08	0.812	0.511	0.704	0.631	0.449	0.802	0.527
Gd	4.74	1.03	3.89	4.18	1.45	6.05	4.51	2.92	1.47	1.09	4.03	3.32	2.95	2.80	2.41	1.27	3.16	1.78
Tb	0.682	0.151	0.519	0.717	0.169	0.859	0.625	0.272	0.416	0.125	0.646	0.523	0.369	0.311	0.280	0.251	0.476	0.267
Dy	3.68	0.694	3.90	4.62	1.19	6.21	4.37	1.90	2.25	0.864	4.91	3.09	2.57	1.67	1.87	1.34	3.31	1.51
Ho	0.613	0.185	0.879	1.06	0.319	1.18	0.962	0.394	0.480	0.195	0.923	0.738	0.551	0.320	0.340	0.186	0.610	0.378
Er	1.76	0.667	2.32	2.90	0.768	3.43	2.14	1.58	1.39	0.595	3.17	1.72	1.61	0.974	1.06	0.744	2.09	0.898
Tm	0.235	0.024	0.315	0.272	0.182	0.485	0.324	0.114	0.131	0.084	0.416	0.247	0.298	0.107	0.122	0.076	0.215	0.092
Yb	1.77	0.439	2.06	2.28	0.628	3.53	2.21	0.945	1.20	0.340	2.24	1.41	1.29	0.743	0.910	0.259	1.39	0.777
Lu	0.227	0.060	0.298	0.348	0.113	0.515	0.289	0.216	0.111	0.056	0.353	0.233	0.241	0.089	0.091	0.027	0.208	0.074
Hf	2.04	0.150	0.984	1.15	0.110	3.30	1.60	0.398	0.488	0.309	1.44	0.487	0.869	0.663	0.469	0.290	0.436	0.506
Ta	0.113	b.d.l.	0.002	b.d.l.	b.d.l.	0.044	b.d.l.	0.033	b.d.l.	b.d.l.	0.003	b.d.l.	b.d.l.	0.005	b.d.l.	b.d.l.	b.d.l.	0.021
W	0.214	b.d.l.	b.d.l.	b.d.l.	b.d.l.	0.464	0.026	b.d.l.	b.d.l.	0.021	0.074	b.d.l.	b.d.l.	b.d.l.	b.d.l.	b.d.l.	b.d.l.	b.d.l.
Pb	1.50	0.095	0.101	0.109	b.d.l.	0.528	0.121	0.295	0.051	0.023	0.347	0.056	0.070	0.081	0.064	b.d.l.	0.027	0.010
Th	0.998	b.d.l.	0.003	0.039	0.007	0.740	0.055	0.022	0.032	b.d.l.	0.290	0.049	0.064	0.016	0.004	0.027	b.d.l.	b.d.l.
U	0.248	0.003	0.015	0.020	0.017	0.057	b.d.l.	0.004	b.d.l.	b.d.l.	0.006	b.d.l.	0.013	b.d.l.	b.d.l.	0.018	b.d.l.	b.d.l.

Table A3.1 *(continued)*: Clinopyroxene LA-ICP-MS data.

Sample	477	477	477	483	483	483	483	483	527	527	527	527	527	527	527	527	527
Crystal	E	F	H	A	B	C	E	G	B	E	F	I	J	K	M	N	O
Zone	core	mid	mid	core	mid	mid	core	mid	mid 1	mid	mid	mid	mid 1	mid	mid	mid 2	mid 1
CaO (wt. %)	21.62	21.83	21.36	21.78	21.43	20.83	22.16	19.13	20.78	20.21	20.86	21.12	21.90	21.28	21.12	21.01	21.72
Li (ppm)	1.95	38.1	1.91	4.72	5.12	5.83	13.9	28.6	2.35	7.58	2.32	2.85	2.97	2.31	3.57	2.66	2.64
B	1.51	b.d.l.	0.921	b.d.l.	b.d.l.	b.d.l.	b.d.l.	b.d.l.	1.41	b.d.l.	b.d.l.	b.d.l.	b.d.l.	b.d.l.	b.d.l.	1.29	2.07
Sc	86.4	33.6	82.6	109	18.7	89.8	27.6	36.5	77.8	25.8	89.5	80.0	91.2	91.7	93.8	90.2	101
Ti (wt. %)	0.345	0.099	0.394	0.364	0.080	0.313	0.134	0.175	0.316	0.128	0.372	0.330	0.395	0.374	0.477	0.435	0.432
V (ppm)	226	91.6	230	288	101	291	165	172	224	126	253	240	296	227	302	295	285
Cr	2389	2.82	1794	350	b.d.l.	400	12.4	0.448	888	b.d.l.	1027	990	851	1400	1061	1491	997
Mn (wt. %)	0.146	0.290	0.153	0.270	0.351	0.374	0.209	0.303	0.210	0.280	0.173	0.204	0.197	0.187	0.199	0.190	0.194
Ni (ppm)	383	130	391	101	70.8	165	157	78.6	228	112	235	210	264	247	227	256	229
Cu	1.14	2.69	1.66	0.920	1.74	2.48	1.26	3.07	1.50	1.30	1.61	1.54	1.73	0.415	1.46	1.61	1.28
Zn	31.2	69.2	30.3	56.7	69.3	78.0	43.8	63.5	39.1	79.8	38.6	38.9	44.9	33.6	35.0	36.7	34.1
Rb	b.d.l.	0.103	0.006	0.053	b.d.l.	0.051	0.017	0.076	0.027	b.d.l.	b.d.l.	b.d.l.	b.d.l.	b.d.l.	b.d.l.	0.036	b.d.l.
Sr	37.3	29.3	34.0	25.8	30.7	25.6	39.4	24.3	23.9	29.1	31.9	28.0	39.9	32.1	27.5	29.0	31.1
Y	7.48	17.3	8.43	24.1	9.51	21.4	5.02	16.2	10.9	14.2	14.4	12.0	19.6	15.2	13.2	14.3	20.2
Zr	9.64	6.29	10.0	23.2	2.48	21.9	4.26	12.8	11.3	6.03	15.2	12.1	23.6	17.0	17.8	18.7	20.8
Nb	b.d.l.	b.d.l.	b.d.l.	0.083	b.d.l.	b.d.l.	0.003	0.023	b.d.l.	b.d.l.	b.d.l.	0.026	b.d.l.	b.d.l.	b.d.l.	b.d.l.	b.d.l.
Cs	0.024	0.005	b.d.l.	b.d.l.	b.d.l.	0.005	0.013	b.d.l.	b.d.l.	b.d.l.	b.d.l.	b.d.l.	b.d.l.	b.d.l.	b.d.l.	b.d.l.	0.041
Ba	1.95	1.401	b.d.l.	0.338	b.d.l.	0.194	0.016	0.129	b.d.l.	b.d.l.	b.d.l.	0.070	b.d.l.	b.d.l.	b.d.l.	b.d.l.	b.d.l.
La	0.607	2.02	0.657	1.93	0.686	1.56	0.683	1.45	0.688	1.18	0.958	0.825	1.86	0.913	1.05	1.12	1.46
Ce	3.02	8.25	3.49	9.00	3.46	7.86	2.80	6.61	3.67	5.63	4.50	4.53	8.65	4.58	5.06	5.29	7.69
Pr	0.586	1.42	0.604	1.83	0.647	1.51	0.549	1.22	0.712	1.22	0.867	0.805	1.71	0.857	0.992	1.19	1.49
Nd	4.03	8.15	4.10	10.3	3.45	8.56	2.74	7.31	4.76	6.17	6.09	5.10	10.2	6.45	5.85	5.38	8.18
Sm	1.52	2.23	1.48	3.36	0.913	3.01	0.600	2.72	2.13	1.96	1.77	1.85	4.11	1.74	1.73	2.35	3.45
Eu	0.523	0.463	0.542	0.805	0.267	0.625	0.445	0.705	0.395	0.504	0.552	0.481	0.821	0.672	0.712	0.714	0.773
Gd	1.57	2.89	1.73	3.91	1.21	4.09	0.803	2.72	1.63	2.03	2.39	1.91	3.64	2.57	2.60	2.15	3.17
Tb	0.233	0.487	0.253	0.702	0.162	0.774	0.103	0.516	0.371	0.401	0.456	0.275	0.555	0.399	0.525	0.394	0.649
Dy	1.38	3.06	1.80	4.69	1.64	4.30	0.681	3.45	1.86	2.10	2.68	2.55	4.12	2.99	3.09	2.97	4.17
Ho	0.289	0.677	0.356	0.807	0.241	0.863	0.227	0.631	0.498	0.545	0.543	0.491	0.894	0.612	0.560	0.530	0.726
Er	0.631	1.62	0.776	3.14	0.527	1.78	0.667	1.73	0.990	1.09	1.46	1.23	1.81	1.33	1.69	1.35	2.10
Tm	0.063	0.300	0.104	0.336	0.135	0.466	0.026	0.269	0.093	0.216	0.218	0.155	0.294	0.162	0.253	0.208	0.316
Yb	0.649	1.74	0.462	2.35	0.735	2.68	0.436	1.41	0.507	1.58	1.53	1.40	2.08	1.07	1.33	1.23	1.96
Lu	0.064	0.224	0.104	0.288	0.087	0.263	0.096	0.201	0.157	0.173	0.256	0.158	0.178	0.191	0.258	0.159	0.306
Hf	0.615	0.120	0.806	1.14	0.039	1.09	0.140	0.444	0.511	0.243	0.580	0.504	0.884	0.712	0.947	0.965	1.12
Ta	b.d.l.	b.d.l.	b.d.l.	b.d.l.	b.d.l.	0.034	0.011	b.d.l.	b.d.l.	b.d.l.	0.007	0.005	b.d.l.	b.d.l.	b.d.l.	0.007	0.008
W	b.d.l.	b.d.l.	b.d.l.	b.d.l.	b.d.l.	b.d.l.	b.d.l.	b.d.l.	b.d.l.	b.d.l.	b.d.l.	b.d.l.	b.d.l.	b.d.l.	b.d.l.	b.d.l.	b.d.l.
Pb	b.d.l.	0.220	0.031	0.189	0.073	0.016	0.008	0.021	0.073	b.d.l.	b.d.l.	0.073	b.d.l.	0.092	0.005	0.028	0.035
Th	0.003	0.228	0.004	0.050	b.d.l.	0.023	0.002	0.015	b.d.l.	b.d.l.	0.022	0.018	b.d.l.	0.012	b.d.l.	0.020	0.019
U	0.010	0.010	b.d.l.	b.d.l.	b.d.l.	b.d.l.	0.012	0.000	b.d.l.	b.d.l.	b.d.l.	b.d.l.	0.010	b.d.l.	0.001	b.d.l.	b.d.l.

Table A3.2: Amphibole LA-ICP-MS data.

Sample	425	425	425	425	425	425	425	425	440	440	440	440	440	440	440	440	440
Crystal	A	A	C	M	M	N	R	U	F	F	G	H	H	I	J	K	K
Zone	core	rim	mid	core	mid	core	core	mid	core	rim	core	core	mid	mid	mid	core	rim
CaO (wt. %)	11.93	11.68	11.84	11.84	11.60	12.01	11.42	12.09	11.23	11.74	11.42	11.26	11.54	11.45	11.25	11.12	11.43
Li (ppm)	76.8	65.1	118	35.6	33.2	112	17.5	126	44.6	145	115	46.8	94.9	53.5	114	31.8	193
B	b.d.	0.898	1.24	b.d.l.	0.601	b.d.l.	b.d.l.	b.d.l.	0.281	1.37	b.d.l.	1.71	0.815	b.d.l.	2.14	0.819	b.d.l.
Sc	79.2	66.8	64.1	65.8	53.5	71.2	57.3	67.9	52.2	58.9	57.4	61.2	59.4	59.6	51.2	23.0	61.5
Ti (wt. %)	1.68	1.43	1.51	1.43	0.990	1.72	1.66	1.57	0.942	1.52	1.59	1.28	1.43	1.57	1.25	0.150	1.47
V (ppm)	462	367	467	487	342	571	555	496	336	529	541	417	475	563	445	130	471
Cr	331	331	168	504	729	658	200	629	739	606	436	214	626	604	410	73.1	215
Mn (wt. %)	0.124	0.223	0.134	0.130	0.107	0.132	0.168	0.132	0.113	0.154	0.156	0.148	0.149	0.158	0.154	0.329	0.192
Ni (ppm)	734	367	453	361	654	524	252	536	1009	462	402	269	450	435	367	97.1	274
Cu	163	233	129	137	117	120	102	107	1.37	6.48	6.83	4.39	8.04	7.94	5.39	1.85	18.1
Zn	69.7	136	73.8	104	60.4	78.9	103	71.8	50.4	97.4	103	81.2	85.3	90.8	90.4	77.8	102
Rb	1.66	3.62	1.18	2.42	1.29	1.57	1.08	1.36	0.635	1.00	1.03	0.881	1.07	1.02	1.07	0.027	0.863
Sr	307	273	266	242	196	306	260	271	136	201	217	140	187	206	175	5.26	150
Y	33.4	56.4	33.3	46.4	20.3	36.7	46.8	34.8	12.9	33.5	33.7	31.4	32.8	37.4	31.2	37.5	43.2
Zr	41.6	78.4	46.9	51.8	44.1	41.9	50.5	45.3	33.8	35.9	37.3	36.4	38.4	36.1	35.9	48.5	37.1
Nb	2.73	5.65	2.98	3.63	1.79	2.97	3.49	2.81	0.919	2.58	2.69	2.66	2.77	2.92	2.23	0.079	3.35
Cs	0.035	0.188	b.d.l.	0.083	b.d.l.	b.d.l.	b.d.l.	b.d.l.	0.013	b.d.l.	b.d.l.	0.007	b.d.l.	b.d.l.	b.d.l.	0.010	b.d.l.
Ba	68.1	133.7	61.2	66.1	47.7	77.5	61.2	69.0	24.9	39.5	43.6	46.0	44.3	38.3	40.5	0.235	44.7
La	5.00	14.7	5.67	7.37	4.08	6.09	6.79	5.55	1.66	3.78	7.86	3.64	3.71	3.96	3.77	18.7	4.13
Ce	21.6	44.5	24.3	32.8	18.7	25.7	32.1	23.0	7.33	17.3	26.0	16.9	17.8	17.6	16.5	86.0	18.0
Pr	3.77	7.17	4.45	5.66	2.99	4.88	5.65	4.15	1.57	3.56	4.73	3.09	3.42	3.22	3.08	14.4	3.42
Nd	22.4	32.6	24.5	34.1	18.3	26.4	32.6	24.8	7.45	20.0	24.4	16.7	19.1	18.5	16.6	61.5	18.5
Sm	7.42	10.2	7.25	9.65	5.26	7.79	8.52	7.44	2.40	7.16	6.98	6.11	6.68	6.86	5.21	12.3	6.73
Eu	1.84	2.18	2.08	2.38	1.27	2.04	2.12	1.77	1.00	1.89	1.77	1.70	1.43	1.71	1.18	1.25	1.57
Gd	7.41	11.6	7.31	7.68	3.72	8.38	8.63	7.62	2.52	7.54	6.53	6.91	5.81	7.09	5.92	9.91	7.42
Tb	1.29	1.64	1.10	1.56	0.775	1.35	1.61	1.22	0.407	1.05	1.09	0.913	1.05	1.10	1.01	1.22	1.23
Dy	6.09	9.89	6.66	10.1	4.35	7.96	9.58	7.15	2.69	6.80	6.05	6.09	6.42	6.54	5.96	7.51	7.98
Ho	1.21	1.75	1.22	1.97	0.783	1.48	1.72	1.43	0.533	1.47	1.25	1.30	1.39	1.52	1.13	1.55	1.84
Er	4.15	6.77	3.59	5.95	2.51	3.79	4.90	3.71	1.47	3.75	3.50	3.63	3.74	3.91	3.09	3.91	5.19
Tm	0.536	0.776	0.503	0.751	0.258	0.526	0.549	0.471	0.235	0.528	0.483	0.415	0.533	0.553	0.435	0.531	0.706
Yb	2.44	5.09	3.16	5.37	1.79	3.50	4.82	3.14	1.16	3.32	3.12	2.92	3.04	3.39	2.62	3.11	3.79
Lu	0.412	0.730	0.431	0.682	0.212	0.391	0.505	0.416	0.122	0.450	0.443	0.464	0.456	0.535	0.466	0.416	0.566
Hf	2.23	3.66	2.17	2.26	2.31	2.30	2.88	2.30	2.02	1.65	1.98	2.11	1.72	1.58	1.39	1.57	2.01
Ta	0.186	0.275	0.133	0.110	0.079	0.176	0.151	0.079	0.039	0.152	0.132	0.127	0.171	0.163	0.094	0.013	0.188
W	0.051	0.306	b.d.l.	0.077	b.d.l.	b.d.l.	b.d.l.	b.d.l.	b.d.l.	b.d.l.	0.111	0.139	b.d.l.	0.077	b.d.l.	0.019	b.d.l.
Pb	0.606	1.02	0.443	1.05	0.186	0.449	0.589	0.457	0.204	0.493	1.13	0.517	0.282	0.351	0.418	0.230	0.513
Th	0.247	1.442	0.139	0.373	0.125	0.138	0.133	0.110	0.086	0.124	0.365	0.077	0.110	0.067	0.105	1.15	0.016
U	0.032	0.239	b.d.l.	0.049	0.016	0.013	0.019	0.026	0.014	0.007	0.019	0.019	0.010	b.d.l.	0.010	0.043	0.011

Note: b.d.l.= below detection limits. *CaO (wt. %) from EPMA data, used as an internal standard.

Table A3.2 *(continued)*: Amphibole LA-ICP-MS data.

Sample	440	440	440	456	456	456	456	456	456	456	456	456	456	456	456	477	477
Crystal	Q	R	S	A	B1	B2	C2	D	I	I	J	J	K	L	L	A	B
Zone	mid	mid	mid	core	core	core	core	core	mid	rim	core	rim	rim	core	rim	mid	rim
CaO (wt. %)	11.39	11.51	11.56	11.46	11.33	11.68	11.68	11.55	11.69	11.40	11.67	11.47	11.47	11.63	11.57	11.63	11.77
Li (ppm)	35.6	38.3	31.5	98.5	101	70.7	100	97.0	86.7	129	91.0	122	119	52.6	107	260	184
B	0.201	0.401	1.32	0.788	2.13	0.978	0.449	b.d.l.	3.39	0.872	b.d.l.	3.29	0.540	b.d.l.	0.133	b.d.l.	0.509
Sc	49.9	64.4	57.2	64.3	56.6	67.7	75.0	80.7	69.7	74.8	74.3	79.6	69.3	72.2	80.8	86.7	89.7
Ti (wt. %)	1.34	1.67	1.39	1.38	1.46	1.50	1.57	1.53	1.36	1.59	1.39	1.70	1.58	1.47	1.69	1.57	1.72
V (ppm)	430	569	494	420	461	430	449	455	478	547	371	559	487	412	566	469	489
Cr	685	240	633	738	180	483	589	824	570	640	255	511	407	151	1098	1294	857
Mn (wt. %)	0.130	0.188	0.163	0.127	0.143	0.131	0.133	0.129	0.123	0.136	0.127	0.148	0.140	0.135	0.140	0.110	0.118
Ni (ppm)	632	224	386	520	335	511	489	663	379	485	551	473	426	506	513	725	709
Cu	3.56	1.92	1.32	9.76	4.79	18.8	5.64	5.50	3.02	7.34	4.56	8.07	10.8	1.38	7.14	71.5	29.1
Zn	77.2	118	96.5	60.1	72.8	71.3	67.3	62.1	63.7	77.5	60.7	88.1	68.6	71.2	74.9	51.1	56.6
Rb	0.842	1.14	1.68	1.01	1.01	1.26	0.951	1.08	0.800	1.18	0.679	1.41	0.936	0.867	1.23	0.699	0.966
Sr	226	271	157	167	168	187	182	180	172	145	170	153	182	179	168	216	245
Y	24.2	52.9	32.0	17.6	19.6	20.0	21.5	23.2	19.9	27.6	19.8	31.9	24.6	21.1	33.5	15.2	17.1
Zr	29.3	51.2	34.3	20.1	21.5	23.5	25.1	24.3	26.7	29.9	21.5	27.3	25.4	22.7	30.1	17.7	25.0
Nb	2.12	4.38	2.71	1.52	1.45	1.34	1.52	1.36	1.81	1.91	1.68	2.66	1.77	1.56	2.37	0.728	1.20
Cs	b.d.	0.009	0.030	0.011	b.d.l.	b.d.l.	b.d.l.	b.d.l.	0.010	b.d.l.	0.017	0.003	b.d.l.	0.000	0.013	0.006	b.d.l.
Ba	35.3	59.5	44.1	43.0	43.3	48.7	46.5	45.1	34.3	42.9	40.4	54.1	57.5	44.1	58.8	42.3	54.9
La	3.21	7.02	3.38	1.45	1.67	2.06	1.94	2.15	2.10	2.55	2.00	2.70	2.46	1.95	2.88	1.33	1.89
Ce	14.7	31.5	16.0	7.68	8.09	8.96	9.45	8.54	9.51	10.9	8.52	12.6	11.4	8.35	13.2	5.78	8.79
Pr	3.06	6.35	3.05	1.49	1.56	1.75	1.75	1.73	1.90	2.25	1.64	2.44	2.03	1.46	2.34	1.07	1.62
Nd	16.1	35.3	18.8	8.40	8.87	10.5	10.5	10.0	10.1	14.7	9.60	14.0	12.2	8.79	14.9	6.80	9.52
Sm	5.14	12.4	6.96	2.42	3.19	3.32	3.23	3.34	3.90	5.04	3.71	4.71	4.53	3.79	4.70	2.88	2.74
Eu	1.24	2.32	1.57	1.01	1.03	1.19	1.30	1.03	1.30	1.31	1.30	1.40	1.43	1.25	1.45	0.931	1.09
Gd	4.72	10.4	6.00	3.05	3.08	3.73	3.78	4.71	4.28	5.82	4.61	5.52	5.09	4.11	5.50	3.51	2.74
Tb	0.759	1.61	1.01	0.409	0.580	0.657	0.647	0.732	0.625	0.778	0.617	0.994	0.607	0.580	0.913	0.423	0.513
Dy	4.29	10.3	5.59	3.23	3.78	3.91	3.86	4.12	4.28	6.16	3.79	5.85	5.14	4.73	6.20	2.97	3.26
Ho	0.888	2.19	1.04	0.547	0.763	0.830	0.839	0.917	0.759	1.22	0.725	1.13	0.943	0.827	1.15	0.578	0.719
Er	2.53	6.13	3.34	2.14	2.12	2.25	2.49	2.32	2.31	3.34	2.96	3.30	2.84	2.22	3.27	1.59	1.88
Tm	0.296	0.787	0.443	0.226	0.243	0.287	0.227	0.298	0.334	0.449	0.357	0.545	0.293	0.264	0.560	0.167	0.209
Yb	2.14	5.23	3.15	1.59	1.82	1.85	2.06	2.16	2.17	2.94	2.25	3.29	2.66	2.16	3.67	1.24	1.59
Lu	0.265	0.741	0.440	0.205	0.215	0.241	0.253	0.253	0.265	0.411	0.291	0.384	0.337	0.237	0.447	0.086	0.180
Hf	1.41	2.47	1.56	0.890	1.05	1.13	1.17	1.28	1.30	1.44	1.39	1.48	1.06	1.05	1.35	0.793	1.41
Ta	0.085	0.141	0.139	0.049	0.050	0.083	0.102	0.073	0.139	0.022	0.119	0.106	0.103	0.086	0.134	0.018	0.006
W	0.069	0.009	b.d.	0.062	b.d.l.	b.d.l.	b.d.l.	0.058	b.d.l.	b.d.l.	b.d.l.	b.d.l.	b.d.l.	b.d.l.	b.d.l.	b.d.l.	b.d.l.
Pb	0.513	0.572	0.434	0.358	0.312	0.723	0.355	0.384	0.399	0.407	0.406	0.720	0.547	0.480	0.532	0.228	0.456
Th	0.042	0.100	0.048	0.051	0.023	0.056	0.040	b.d.l.	0.065	0.119	0.033	0.056	0.029	0.081	0.045	b.d.l.	0.025
U	b.d.l.	0.043	0.034	0.002	b.d.l.	0.024	0.010	0.005	0.041	0.000	0.011	b.d.l.	b.d.l.	b.d.l.	0.009	0.019	b.d.l.

Table A3.2 *(continued)*: Amphibole LA-ICP-MS data.

Sample	477	477	477	477	477	477	477	477	483	483	483	483	483	483	483	483	483
Crystal	C	D	G	H	I	K	O	P	C	C	D	D	F	F	H	H	I
Zone	mid	mid	mid	core	core	core	mid	core	core	rim	mid 1	rim	core	rim	core	rim	core
CaO (wt. %)	11.76	11.89	11.55	11.36	11.46	11.63	11.67	11.40	11.80	11.29	11.34	11.32	11.47	11.58	11.52	11.37	11.28
Li (ppm)	243	265	201	187	203	184	262	282	309	395	540	460	212	500	525	509	487
B	1.48	0.624	1.35	b.d.l.	0.918	b.d.l.	1.89	b.d.l.	b.d.l.	b.d.l.	0.591	b.d.l.	b.d.l.	b.d.l.	0.336	0.352	b.d.l.
Sc	87.2	87.0	94.7	77.2	85.5	89.9	86.7	90.0	65.8	63.5	72.8	81.0	83.8	74.7	84.9	74.4	61.1
Ti (wt. %)	1.61	1.65	1.56	1.52	1.57	1.68	1.51	1.44	1.22	1.27	1.38	1.16	1.42	1.26	1.63	1.39	1.41
V (ppm)	457	474	433	482	482	486	450	396	453	449	543	467	539	486	615	569	437
Cr	1821	1438	612	199	326	110	1044	397	1526	398	399	887	715	1018	282	632	294
Mn (wt. %)	0.105	0.111	0.110	0.122	0.115	0.117	0.093	0.103	0.108	0.117	0.148	0.134	0.136	0.121	0.151	0.147	0.157
Ni (ppm)	790	782	681	476	631	510	680	634	326	311	301	421	363	420	263	311	432
Cu	48.0	81.5	23.7	35.4	30.8	18.7	55.8	42.9	13.4	8.03	37.1	47.7	2.75	38.2	22.9	12.6	27.8
Zn	51.4	50.7	51.5	63.1	49.4	56.0	50.9	57.6	57.3	58.7	71.7	54.6	64.6	55.9	73.9	68.6	83.4
Rb	0.552	0.632	0.738	0.839	0.781	1.20	0.841	0.623	0.590	0.822	1.42	1.11	1.12	0.884	1.27	1.22	1.18
Sr	245	224	208	187	201	204	213	234	182	190	157	161	150	179	148	146	233
Y	14.0	14.1	15.2	16.2	16.0	18.5	13.3	16.6	13.9	15.8	22.7	14.6	20.0	16.7	28.6	23.6	33.3
Zr	16.6	16.1	21.5	23.9	16.7	22.2	16.0	20.4	19.9	24.8	35.1	30.0	24.3	26.7	28.4	30.4	61.2
Nb	0.910	0.738	1.13	1.16	1.04	1.23	0.832	1.27	0.966	1.19	1.48	1.43	1.43	0.885	2.13	1.38	3.77
Cs	b.d.l.	b.d.l.	b.d.l.	0.006	b.d.l.	0.019	0.001	b.d.l.	b.d.l.	b.d..	0.017	b.d.l.	b.d.l.	b.d.l.	b.d.l.	b.d.l.	b.d.l.
Ba	49.9	44.7	43.9	42.2	44.4	56.0	44.2	45.6	30.2	35.0	50.3	36.4	40.1	42.9	47.0	42.3	60.9
La	1.38	1.16	1.28	1.18	1.26	1.59	1.18	1.26	1.33	1.86	2.81	1.81	1.95	2.06	2.41	2.35	6.02
Ce	5.89	5.68	5.86	5.83	5.51	7.50	5.62	5.52	6.03	8.04	12.1	6.83	8.71	8.65	11.2	10.5	25.1
Pr	1.20	1.04	1.28	1.08	1.09	1.35	1.22	1.04	1.14	1.53	2.36	1.20	1.65	1.64	2.18	1.80	4.58
Nd	6.94	6.70	7.43	6.47	6.80	8.98	7.48	7.25	7.03	9.42	11.8	7.15	9.38	8.77	12.4	11.5	24.0
Sm	2.06	2.71	2.29	2.53	2.14	3.02	2.11	2.63	2.26	3.04	3.96	2.86	3.87	3.19	4.39	3.37	7.14
Eu	0.975	1.01	0.991	0.876	0.779	1.06	1.03	0.877	0.986	1.12	1.30	0.886	1.06	0.978	1.26	1.20	1.86
Gd	3.41	3.02	3.21	2.99	3.19	3.58	2.93	3.08	2.59	3.19	4.70	2.41	3.01	3.17	4.12	4.04	6.72
Tb	0.454	0.416	0.500	0.376	0.395	0.606	0.509	0.522	0.432	0.450	0.601	0.432	0.537	0.485	0.667	0.704	1.01
Dy	2.39	2.96	2.82	3.12	2.53	3.87	2.98	3.00	2.44	3.09	5.14	3.14	4.00	3.39	5.66	4.81	6.65
Ho	0.534	0.553	0.558	0.732	0.540	0.552	0.531	0.475	0.516	0.656	0.893	0.571	0.790	0.670	1.09	0.893	1.31
Er	1.38	1.72	1.60	1.72	1.39	2.09	1.33	1.46	1.35	1.85	2.26	1.41	2.48	1.75	2.74	2.69	3.97
Tm	0.238	0.203	0.250	0.262	0.122	0.263	0.218	0.306	0.105	0.130	0.270	0.134	0.250	0.208	0.302	0.362	0.381
Yb	1.12	0.95	1.31	1.64	0.897	1.94	1.32	1.52	1.23	1.30	2.10	0.848	2.03	1.73	2.28	2.28	2.79
Lu	0.135	0.158	0.122	0.165	0.130	0.212	0.140	0.168	0.185	0.185	0.350	0.132	0.280	0.149	0.367	0.284	0.383
Hf	0.748	0.578	0.811	1.06	0.523	1.12	0.754	1.18	0.853	1.23	1.40	1.85	1.20	1.22	1.02	1.60	3.48
Ta	0.027	0.028	0.095	0.093	0.016	0.046	0.031	0.046	0.057	0.093	0.103	0.103	0.050	0.018	0.089	0.082	0.094
W	0.001	b.d.l.	0.075	b.d.l.	b.d.l.	b.d..	b.d.l.	b.d.l.	b.d.l.	b.d.l.	b.d.l.	0.033	b.d.l.	b.d.l.	0.104	b.d.l.	0.076
Pb	0.284	0.272	0.486	0.097	0.199	0.375	0.399	0.464	0.295	0.391	0.193	0.509	0.428	0.197	0.225	0.420	0.373
Th	0.008	0.003	0.080	0.030	0.010	0.039	0.039	0.042	b.d.l.	0.051	0.087	0.130	0.025	0.131	0.069	0.081	0.038
U	0.010	b.d.l.	b.d.l.	0.007	0.009	b.d.l.	0.017	0.015	0.009	b.d.l.	0.039	0.038	b.d.l.	b.d.l.	b.d.l.	0.001	0.011

Table A3.2 *(continued)*: Amphibole LA-ICP-MS data.

Sample	483	483	527	527	527	527	527	527	527	527	527	527	527	527	527
Crystal	M	M	A	B	B	C	C	D	E	F	G	H	I	J	K
Zone	core	rim	mid	core	rim	core	rim	core	core	core	core	mid	core	mid	mid
CaO (wt. %)	11.58	11.62	10.73	11.55	11.52	11.69	11.39	11.25	11.44	11.43	11.33	10.82	11.40	10.94	10.51
Li (ppm)	319	469	7.45	5.04	16.5	5.35	8.20	14.1	15.8	8.35	38.9	7.78	10.5	17.8	7.15
B	b.d.l.	2.43	1.64	0.278	0.330	b.d.l.	b.d.l.	b.d.l.	2.82	b.d.l.	0.283	b.d.l.	1.02	b.d.l.	0.353
Sc	99.6	85.1	273	70.8	74.3	61.0	75.5	72.4	57.0	89.1	71.4	262.9	50.2	278	345
Ti (wt. %)	1.63	1.45	1.40	1.47	1.84	1.15	1.81	1.51	1.25	2.22	1.78	1.43	1.33	1.46	1.49
V (ppm)	573	569	164	509	645	376	580	479	446	694	623	211	483	185	147
Cr	437	650	2.05	481	283	226	252	791	145	193	569	1.25	252	9.11	3.65
Mn (wt. %)	0.153	0.147	0.440	0.137	0.207	0.160	0.187	0.171	0.170	0.157	0.190	0.449	0.169	0.499	0.480
Ni (ppm)	299	305	21.9	375	222	234	168	506	264	258	258	16.9	358	24.9	20.0
Cu	7.74	27.9	0.584	2.41	1.43	1.34	1.57	6.27	3.56	4.46	6.11	0.002	0.507	1.43	1.05
Zn	69.2	67.0	223	67.0	117	80.2	103	93.7	89.8	93.2	115	230	102	254	248
Rb	0.992	1.26	0.860	1.04	1.35	0.967	1.56	1.30	1.39	1.40	1.94	0.798	1.00	1.90	1.06
Sr	153	136	24.5	219	167	148	184	154	138	163	161	26.9	144	29.1	25.7
Y	29.8	25.4	260	23.5	44.1	34.1	52.9	36.0	29.1	50.5	43.1	203	29.7	284	335
Zr	35.1	30.5	72.1	29.5	35.9	40.9	46.7	50.2	35.5	40.7	32.6	61.8	28.3	63.0	60.3
Nb	2.29	1.40	17.4	2.22	3.99	3.06	4.66	3.12	2.77	4.79	3.77	16.2	2.83	20.4	26.3
Cs	b.d.	b.d.	0.004	0.027	b.d.l.	b.d.l.	b.d.l.	0.018	0.008	b.d.l.	b.d.l.	b.d.l.	b.d.l.	0.033	b.d.l.
Ba	46.6	43.8	54.5	53.3	68.5	40.3	78.9	59.4	49.9	82.9	65.4	45.7	42.0	65.8	83.6
La	2.46	2.35	24.3	2.70	4.46	4.37	6.83	4.76	3.22	4.72	4.71	17.7	3.02	24.7	33.7
Ce	11.7	11.2	114	13.0	22.4	20.3	30.2	20.6	13.9	21.9	20.5	86.2	13.1	113	157
Pr	2.28	2.24	21.8	2.54	4.31	4.16	5.47	3.61	2.58	4.40	3.61	15.9	2.55	21.2	29.7
Nd	12.5	11.4	122	12.9	22.9	20.6	31.8	19.5	14.5	22.7	20.1	89.2	14.4	132	170
Sm	4.26	4.23	45.9	4.44	6.63	6.75	9.03	6.79	4.87	8.04	7.36	28.7	5.52	47.2	56.9
Eu	1.45	1.40	3.38	1.30	1.66	1.60	2.29	1.60	1.35	1.86	1.60	3.46	1.31	3.58	4.22
Gd	5.49	5.44	52.9	4.95	7.60	6.02	9.43	6.59	6.00	8.41	8.06	39.1	5.59	51.6	70.4
Tb	0.957	0.887	8.38	0.742	1.25	1.11	1.56	1.23	0.852	1.47	1.39	6.73	0.837	7.88	11.4
Dy	6.11	5.41	56.0	4.87	8.50	7.25	11.5	8.11	5.84	9.54	8.48	42.0	5.63	51.0	71.1
Ho	1.20	1.16	10.2	0.881	1.55	1.21	2.18	1.40	1.18	2.13	1.83	8.01	1.05	9.71	12.8
Er	3.53	3.45	29.46	2.94	4.78	3.85	6.38	4.48	2.97	5.73	4.93	22.6	3.17	27.2	36.9
Tm	0.378	0.338	4.20	0.318	0.685	0.509	0.777	0.501	0.372	0.780	0.661	3.17	0.400	3.87	5.30
Yb	2.72	3.09	24.3	2.29	4.31	3.61	5.52	3.84	3.11	5.52	5.51	20.2	2.62	20.3	28.1
Lu	0.381	0.468	3.14	0.298	0.697	0.537	0.702	0.602	0.305	0.607	0.615	2.45	0.402	3.33	4.19
Hf	1.96	1.52	3.86	1.73	1.48	2.34	2.39	2.42	1.53	1.68	1.74	3.06	1.42	2.82	3.69
Ta	0.053	0.073	0.447	0.148	0.138	0.207	0.268	0.243	0.146	0.245	0.185	0.441	0.100	0.399	0.757
W	b.d.l.	b.d.l.	0.037	b.d.l.	0.089	0.099	0.036	0.052	b.d.l.	b.d.l.	b.d.l.	b.d.l.	b.d.l.	b.d.l.	b.d.l.
Pb	0.351	0.339	0.767	0.602	0.753	0.356	0.630	0.612	0.575	0.842	0.752	0.611	0.404	0.934	0.754
Th	0.006	0.055	0.065	0.037	0.077	0.068	0.165	0.153	0.062	0.051	0.060	0.127	b.d.l.	0.173	0.127
U	0.018	0.029	0.013	0.017	0.024	0.013	0.036	0.015	0.001	0.000	0.021	0.038	0.020	0.023	0.029

Table A3.3: Plagioclase LA-ICP-MS data.

Sample	425	425	425	425	425	425	425	425	425	425	425	425	425	425	425	425	425
Crystal	A	A	B	I	I	I	J	K	K	L	M	M	P	R	ZB	ZE	ZE
Zone	core	mid 3	mid 1	mid 3	mid 6	rim	mid	core	mid 2	mid	core	mid 2	mid	mid	mid	core	mid 1
CaO (wt. %)	8.57	6.20	6.31	6.07	6.94	5.34	8.24	8.66	5.21	6.32	8.27	6.40	4.28	5.85	5.51	6.67	9.32
Li (ppm)	34.8	48.4	48.0	47.2	43.8	43.1	60.5	58.1	45.8	49.8	38.6	56.7	39.4	42.9	35.0	40.1	28.0
Mg	142	58.9	67.4	84.3	93.7	53.9	90.3	68.4	39.2	66.3	69.7	68.0	54.2	55.1	58.4	94.5	87.2
Rb	0.515	1.15	0.668	0.637	0.480	1.66	0.975	0.762	1.15	0.713	0.383	1.48	6.86	0.945	1.03	0.701	0.310
Sr	254	242	230	183	217	180	283	310	168	216	266	237	147	200	177	163	199
Y	0.685	0.135	0.173	0.149	0.179	0.133	0.162	0.427	0.114	0.184	0.197	0.173	0.006	0.173	0.146	0.321	0.335
Cs	0.029	b.d.l.	b.d.l.	b.d.l.	0.003	b.d.l.	0.038	b.d.l.	b.d.l.	0.005	0.002	b.d.l.	0.048	b.d.l.	b.d.l.	0.106	0.112
Ba	154	914	491	449	287	597	740	504	636	507	198	908	1065	524	553	390	59
La	4.14	10.8	7.17	8.41	5.18	6.88	11.2	8.79	7.71	6.65	3.52	10.2	9.30	7.28	7.50	7.02	1.51
Ce	6.76	14.0	9.39	12.5	8.04	10.1	14.8	14.0	11.5	9.69	5.92	14.5	11.8	10.6	10.3	14.3	6.81
Pr	0.577	1.01	0.876	0.805	0.664	0.763	1.09	1.075	0.786	0.726	0.492	1.01	0.767	0.734	0.851	0.719	0.355
Nd	2.40	2.58	2.30	3.03	1.79	2.25	3.59	2.55	2.24	2.10	1.16	2.80	2.45	2.26	2.31	2.00	1.33
Sm	b.d.l.	0.263	0.207	0.432	0.196	0.283	0.083	0.263	0.114	0.015	0.188	0.252	0.098	0.067	0.179	0.847	0.908
Eu	1.04	2.71	2.11	1.44	1.60	1.86	2.66	2.60	2.06	2.10	1.37	2.82	2.07	1.80	1.84	0.89	0.711
Gd	b.d.l.	b.d.l.	b.d.l.	b.d.l.	b.d.l.	0.068	b.d.l.	0.187	0.070	0.132	0.006	b.d.l.	b.d.l.	0.086	0.010	0.609	0.663
Pb	4.07	8.33	5.93	6.24	4.51	7.75	9.06	9.23	8.29	6.39	3.39	10.3	10.4	6.64	6.87	6.24	5.44

Sample	425	425	425	425	425	440	440	440	440	440	440	440	440	440	440	440	440
Crystal	ZE	ZF	ZF	ZG	ZG	B	B	D	E	G	G	H	H	H	L	L	O
Zone	mid 2	core	rim	core	mid	core	rim	mid	mid	core	mid	core	mid 2	rim	core	rim	mid 2
CaO (wt. %)	4.90	7.01	6.06	8.41	5.84	9.37	6.54	6.12	6.23	8.11	5.47	6.92	6.95	5.30	8.96	5.12	6.20
Li (ppm)	31.2	49.0	38.5	47.2	34.4	35.7	46.5	53.2	41.9	41.9	34.4	43.1	37.8	36.6	44.3	41.3	48.2
Mg	37.9	75.8	58.9	108	57.9	158	65.6	59.3	68.2	164	675	88.4	85.9	54.5	84.1	49.6	64.7
Rb	1.21	0.678	1.07	0.468	0.778	0.266	1.23	1.05	0.872	0.535	9.08	0.468	0.409	0.834	0.405	1.03	0.789
Sr	130	268	195	247	186	285	243	221	217	266	293	210	224	196	288	163	208
Y	0.335	0.228	0.168	0.251	0.279	0.154	0.242	0.156	0.140	0.184	1.16	0.198	0.200	0.147	0.254	0.149	0.109
Cs	0.138	0.002	b.d.l.	0.008	0.125	b.d.l.	b.d.l.	0.032	b.d.l.	b.d.l.	0.310	b.d.l.	b.d.l.	0.018	0.023	b.d.l.	0.012
Ba	524	415	461	288	527	150	822	700	478	425	685	445	301	720	212	586	564
La	5.66	7.90	6.43	6.55	5.51	3.79	10.17	7.80	7.05	6.84	14.7	8.93	5.25	8.29	3.61	7.76	7.37
Ce	10.0	11.2	9.00	8.31	10.8	5.23	13.3	11.2	10.1	9.83	26.9	12.9	7.88	11.0	5.72	10.9	10.6
Pr	0.534	0.833	0.644	0.681	0.525	0.414	0.950	0.721	0.693	0.729	2.00	1.00	0.693	0.812	0.496	0.709	0.690
Nd	1.49	2.31	2.09	2.00	2.03	1.25	2.62	2.44	2.26	2.64	6.03	2.75	1.69	2.56	2.05	2.23	2.39
Sm	0.591	0.425	0.216	0.289	0.791	b.d.l.	b.d.l.	0.231	0.056	0.373	0.813	0.133	0.293	0.193	0.294	0.392	0.240
Eu	1.34	2.09	1.94	1.35	1.56	0.988	2.18	2.63	1.90	1.66	0.990	1.37	1.73	2.08	2.68	1.90	1.72
Gd	0.662	b.d.l.	0.149	0.124	0.592	0.057	0.041	0.113	0.048	0.096	0.481	b.d.l.	0.142	0.048	0.248	0.005	b.d.l.
Pb	6.52	5.32	6.37	4.72	6.70	2.73	8.13	7.36	6.62	5.38	9.44	6.90	4.61	6.47	5.19	8.26	6.97

Note: b.d.l.= below detection limits. *CaO (wt. %) from EPMA data, used as an internal standard.

Table A3.3 *(continued)*: Plagioclase LA-ICP-MS data.

Sample	440	440	440	440	440	440	440	440	440	440	440	440	456	456	456	456	456
Crystal	Q	Q	R	R	S	S	T	U	V	V	Z	Z	B	B	C	E	G
Zone	core	rim	mid	rim	core	rim	rim	mid	core	mid	core	rim	core	rim	rim	core	core
CaO (wt. %)	5.28	6.41	5.86	5.96	6.77	6.46	8.01	5.10	6.57	5.24	5.26	6.58	12.27	5.32	5.04	6.71	7.53
Li (ppm)	49.7	50.2	46.9	43.0	44.0	40.1	38.3	45.2	39.4	40.4	41.9	39.1	34.6	46.6	39.6	45.3	46.8
Mg	53.1	58.3	58.0	57.8	69.9	66.6	155	64.8	63.1	50.2	61.8	68.9	251	56.0	38.1	65.4	64.3
Rb	0.729	0.986	0.659	0.908	0.527	2.65	1.98	0.720	0.488	1.59	0.880	1.19	0.132	1.19	2.06	0.444	0.349
Sr	219	245	212	210	238	207	268	203	237	184	191	207	336	206	173	209	204
Y	0.132	0.206	0.133	0.143	0.193	0.132	0.264	0.112	0.120	0.190	0.111	0.210	0.258	0.134	0.083	0.218	0.152
Cs	b.d.l.	b.d.l.	b.d.l.	b.d.l.	0.001	b.d.l.	b.d.l.	b.d.l.	b.d.l.	b.d.l.	0.024	0.002	b.d.l.	b.d.l.	b.d.l.	b.d.l.	0.033
Ba	526	536	525	650	320	435	264	526	256	639	619	456	84	888	573	322	284
La	5.95	8.54	7.23	7.78	5.81	6.27	5.28	5.51	4.34	8.47	7.34	7.57	1.87	8.59	7.45	5.65	4.83
Ce	8.61	12.4	9.92	11.0	8.86	9.83	8.16	8.67	6.13	10.9	9.78	10.7	3.55	13.1	10.6	7.93	7.41
Pr	0.649	0.827	0.754	0.877	0.654	0.727	0.666	0.645	0.517	0.787	0.702	0.775	0.285	0.932	0.812	0.664	0.645
Nd	1.86	2.13	2.40	2.61	2.23	2.12	2.01	1.97	1.30	2.52	2.08	2.41	1.19	2.37	2.31	1.91	1.88
Sm	0.040	0.194	0.219	0.199	0.247	0.012	0.167	b.d.l.	0.099	0.361	0.214	0.197	0.295	0.328	0.141	0.069	0.141
Eu	2.42	2.09	2.31	2.24	1.99	1.90	1.52	2.57	1.91	1.94	1.92	1.97	0.926	1.97	2.05	1.50	1.68
Gd	0.143	0.164	0.181	b.d.l.	0.109	0.097	b.d.l.	0.111	0.007	0.126	0.251	b.d.l.	0.068	0.129	b.d.l.	0.060	b.d.l.
Pb	5.95	6.49	6.20	7.60	4.97	7.25	4.27	6.18	5.16	7.19	5.76	6.47	1.26	8.30	6.65	5.16	5.72

Sample	456	456	456	456	456	456	456	456	456	456	456	456	456	456	456	456	456
Crystal	G	G	I	J	J	L	L	O	P	P	T	T	W	X	X	ZI	ZJ
Zone	mid 1	rim	mid	core	rim	core	rim	core	core	mid	core	mid	mid 2	core	rim	mid	core
CaO (wt. %)	5.79	5.14	4.60	6.84	6.16	8.59	6.53	5.93	11.19	4.07	5.35	6.74	10.50	4.81	5.58	4.12	5.28
Li (ppm)	49.0	44.6	53.0	60.2	52.7	52.5	45.7	63.4	45.4	54.7	59.5	50.4	56.0	51.9	31.8	54.9	54.6
Mg	54.4	46.4	33.7	67.6	60.2	114	63.9	66.0	280	27.7	60.7	68.4	163	34.3	757	26.6	54.7
Rb	0.739	2.45	1.26	0.701	0.769	0.307	3.59	1.01	1.27	1.62	1.05	0.528	0.354	1.05	36.3	1.32	0.918
Sr	199	155	158	254	222	271	238	230	304	119	216	225	309	159	188	141	202
Y	0.156	0.150	0.121	0.118	0.154	0.161	0.170	0.148	0.166	0.107	0.199	0.165	0.234	0.115	6.77	0.079	0.121
Cs	0.032	b.d.l.	0.001	b.d.l.	0.011	b.d.l.	0.008	b.d.l.	0.004	b.d.l.	b.d.l.	0.019	b.d.l.	b.d.l.	0.960	b.d.l.	b.d.l.
Ba	539	639	754	432	507	209	460	690	177	929	636	412	230	694	797	917	623
La	8.01	7.53	8.25	6.95	7.77	4.66	6.93	9.17	4.86	7.93	7.40	6.42	6.04	7.90	17.7	8.56	6.57
Ce	11.4	9.97	10.5	9.85	10.5	7.50	10.7	12.9	7.71	11.1	9.97	9.79	8.60	10.6	31.8	10.7	9.53
Pr	0.862	0.751	0.788	0.680	0.786	0.665	0.841	0.965	0.622	0.757	0.720	0.713	0.653	0.770	2.61	0.766	0.696
Nd	2.21	2.18	1.70	2.06	2.05	1.66	2.40	2.27	1.91	1.58	2.19	2.03	2.43	2.03	8.44	2.33	1.86
Sm	0.026	0.079	0.184	0.235	0.156	0.219	0.270	0.395	0.175	0.118	0.365	0.271	0.071	0.152	1.11	0.155	0.155
Eu	1.84	1.93	1.98	2.61	1.76	1.86	2.12	2.37	0.991	1.71	2.34	1.88	1.93	1.84	1.90	2.13	2.36
Gd	0.183	0.077	b.d.l.	0.187	0.090	0.247	b.d.l.	0.016	0.050	b.d.l.	0.200	b.d.l.	0.229	0.058	1.02	0.049	0.160
Pb	5.86	7.22	8.83	6.07	7.27	3.83	6.71	7.51	4.08	9.47	6.00	6.33	4.00	7.91	11.6	9.20	6.65

Table A3.3 *(continued)*: Plagioclase LA-ICP-MS data.

Sample	456	456	456	477	477	477	477	477	477	477	477	477	477	477	477	477	477
Crystal	ZJ	ZK	ZK	A	A	B	B	C	D	D	E	H	H	H	J	M	M
Zone	mid	core	mid	core	mid	core	rim	mid	core	rim	core	core	mid	rim	mid	core	mid
CaO (wt. %)	6.43	9.61	4.94	12.26	4.92	8.42	4.49	4.79	9.90	5.30	5.22	10.37	8.33	5.39	6.11	7.32	8.85
Li (ppm)	52.4	51.8	57.5	24.8	33.6	38.2	26.6	26.0	24.0	24.1	30.7	35.4	40.2	34.3	39.4	46.6	33.8
Mg	66.8	49.5	33.9	94.3	57.5	144	43.1	32.3	144	55.4	57.1	133	149	52.3	57.8	107	78.3
Rb	0.686	0.270	1.21	0.170	0.556	0.370	2.26	0.553	0.348	0.988	0.673	0.226	0.361	0.760	0.980	0.655	0.343
Sr	214	311	164	163	163	272	160	159	195	170	169	231	260	210	209	247	259
Y	0.146	0.403	0.125	0.335	0.117	0.248	0.064	0.127	0.205	0.141	0.146	0.302	0.200	0.150	0.166	0.195	0.330
Cs	b.d.l.	b.d.l.	0.002	0.014	b.d.l.	b.d.l.	b.d.l.	0.014	b.d.l.	b.d.l.	b.d.l.	b.d.l.	b.d.l.	0.020	b.d.l.	b.d.l.	b.d.l.
Ba	468	347	665	107	396	213	666	434	71	665	407	206	174	584	598	386	271
La	7.21	7.99	7.09	3.00	5.52	4.83	7.14	5.63	2.10	7.88	6.32	5.96	4.23	7.58	8.62	6.82	4.85
Ce	10.2	13.9	10.5	4.78	7.66	6.99	10.1	8.24	3.26	11.3	8.65	8.19	6.26	10.5	11.8	10.8	7.88
Pr	0.784	1.16	0.796	0.424	0.646	0.652	0.678	0.583	0.309	0.774	0.720	0.666	0.551	0.735	0.810	0.763	0.694
Nd	2.27	3.68	1.99	1.27	1.71	1.86	1.87	1.79	1.06	2.30	2.20	1.76	1.85	2.31	2.29	2.52	2.08
Sm	0.119	0.539	0.276	0.298	0.122	0.224	b.d.l.	0.292	0.198	0.049	0.086	0.188	0.159	b.d.l.	0.394	0.238	0.272
Eu	1.93	2.40	2.05	0.816	1.64	1.80	2.05	1.57	0.769	1.90	1.74	1.55	1.60	2.33	2.07	1.95	1.78
Gd	b.d.l.	0.228	0.068	0.133	b.d.l.	0.192	0.074	b.d.l.	b.d.l.	b.d.l.	0.041	0.187	b.d.l.	0.093	b.d.l.	0.093	b.d.l.
Pb	6.64	7.42	8.12	4.81	5.37	3.64	7.73	6.04	2.15	7.49	5.66	6.16	3.24	6.89	6.94	4.96	6.32

Sample	477	477	477	477	477	477	483	483	483	483	483	483	483	483	483	483	483
Crystal	M	N	R	T	V	V	A	D	D	E	H	H	J	K	K	M	M
Zone	rim	core	mid	mid	core	rim	core	core	rim	mid	core	rim	mid	core	rim	core	rim
CaO (wt. %)	5.92	6.20	6.29	8.51	6.37	6.52	5.27	7.02	5.24	4.42	10.13	5.84	6.40	12.62	6.23	10.47	5.37
Li (ppm)	43.1	38.9	39.4	41.9	26.3	46.3	32.6	29.9	21.3	23.5	25.3	26.6	26.9	19.0	23.4	23.9	21.4
Mg	65.7	69.0	64.8	140	52.1	66.6	57.3	67.2	55.9	32.6	162.0	73.7	62.5	117	69.4	61.6	52.9
Rb	0.877	0.586	0.511	0.323	0.498	0.869	0.961	0.675	0.739	1.06	0.238	0.669	0.977	0.541	0.872	0.231	0.588
Sr	198	220	210	283	175	226	206	249	185	151	292	197	200	310	229	282	175
Y	0.156	0.085	0.201	0.223	0.398	0.167	0.125	0.125	0.160	0.126	0.182	0.182	0.208	0.159	0.171	0.472	0.132
Cs	b.d.l.	b.d.l.	0.020	0.021	0.004	b.d.l.	b.d.l.	b.d.l.	0.007	b.d.l.	b.d.l.	b.d.l.	b.d.l.	0.008	b.d.l.	0.023	b.d.l.
Ba	571	431	486	195	297	540	601	417	505	739	123	500	660	119	596	131	363
La	7.41	5.83	7.37	4.72	5.71	7.41	8.04	4.98	6.73	7.82	3.30	6.65	6.71	2.55	9.54	2.88	5.58
Ce	11.8	8.04	10.3	7.03	9.02	11.0	10.5	7.82	11.0	11.2	5.20	10.3	10.5	4.69	13.4	4.29	7.86
Pr	0.816	0.710	0.846	0.535	0.705	0.912	0.741	0.618	0.808	0.717	0.438	0.746	0.777	0.400	1.01	0.362	0.566
Nd	2.10	2.04	2.52	2.07	2.34	2.81	2.11	1.73	2.42	1.83	1.46	1.82	2.25	1.63	2.44	1.54	1.86
Sm	0.123	0.041	0.335	0.127	b.d.l.	0.021	0.114	0.170	0.085	0.140	b.d.l.	0.192	b.d.l.	0.043	0.218	0.032	0.072
Eu	1.99	2.59	1.95	2.11	1.15	2.22	2.32	2.80	1.67	1.85	1.17	1.63	1.81	1.26	1.44	1.66	1.56
Gd	b.d.l.	b.d.l.	b.d.l.	b.d.l.	0.092	0.273	0.029	0.178	b.d.l.	0.048	0.091	b.d.l.	b.d.l.	0.039	0.143	0.097	0.013
Pb	6.74	6.01	6.89	3.48	5.78	7.80	6.31	5.99	7.19	8.00	1.76	5.88	8.27	3.21	6.80	5.52	5.57

Table A3.3 *(continued)*: Plagioclase LA-ICP-MS data.

Sample	483	483	483	483	483	527	527	527	527	527	527	527	527	527	527	527	527
Crystal	N	O	V	W	Z	A	B	C	D	F	F	G	G	G	I	J	J
Zone	mid	core	mid	mid	mid	mid 2	mid 1	core	core	core	mid 2	core	mid 1	mid 4	core	core	mid 2
CaO (wt. %)	15.27	4.98	17.18	6.18	17.28	5.32	5.61	5.28	6.85	5.12	6.25	9.17	6.88	5.68	5.37	7.41	6.44
Li (ppm)	11.3	27.2	8.38	24.0	6.43	28.5	36.2	46.6	31.8	39.0	23.1	56.0	56.4	22.9	44.7	33.8	16.7
Mg	528.6	49.1	413	57.7	338	61.0	53.9	55.3	68.1	61.4	59.1	102	83.0	52.5	57.2	77.2	57.8
Rb	0.133	0.840	0.094	0.832	b.d.l.	0.940	0.927	0.591	0.453	0.852	1.28	0.357	0.807	0.733	0.711	0.945	1.44
Sr	367	177	354	202	339	207	194	177	202	204	210	284	226	187	197	190	190
Y	0.158	0.110	0.678	0.177	0.057	0.127	0.223	0.167	0.205	0.141	0.165	0.116	0.182	0.100	0.104	0.007	b.d.l.
Cs	b.d.l.	0.008	b.d.l.	0.019	0.024	0.001	0.028	b.d.l.	b.d.l.	0.008	0.007	0.008	0.002	b.d.l.	b.d.l.	b.d.l.	b.d.l.
Ba	50.7	534	32.7	519	27.4	464	645	407	386	505	734	213	479	382	526	336	616
La	1.62	6.27	1.75	7.46	0.948	6.30	8.39	7.00	8.45	7.19	8.92	4.18	8.06	6.21	6.85	3.81	6.77
Ce	2.96	8.98	3.80	10.8	2.02	9.02	11.3	9.42	12.2	10.1	13.1	5.51	10.9	9.41	9.49	6.68	11.7
Pr	0.258	0.641	0.432	0.753	0.195	0.679	0.712	0.684	0.970	0.674	0.922	0.355	0.890	0.608	0.723	0.493	0.766
Nd	0.738	1.79	1.31	2.34	0.386	1.94	2.63	1.95	2.76	1.71	2.47	1.12	2.12	1.69	2.25	2.08	2.72
Sm	0.009	0.069	0.361	0.156	0.004	0.010	0.228	0.177	0.159	0.263	0.322	0.205	0.111	0.023	0.138	b.d.l.	0.090
Eu	0.272	1.91	0.270	1.94	0.130	2.22	2.00	1.73	1.58	2.06	2.20	1.21	2.06	2.09	2.33	1.50	2.11
Gd	b.d.l.	0.006	0.390	0.234	b.d.l.	0.037	0.058	b.d.l.	0.150	0.056	b.d.l.	b.d.l.	0.133	0.020	0.001	b.d.l.	0.199
Pb	1.13	6.24	0.95	6.78	0.840	5.99	7.58	5.91	6.27	6.32	7.91	4.11	6.99	6.34	6.33	5.82	7.93

Sample	527	527	527	527	527	527	527
Crystal	P	Q	Q	S	S	T	T
Zone	mid	mid 1	mid 3	mid 1	mid 3	mid 1	mid 2
CaO (wt. %)	6.77	7.56	5.82	9.44	5.34	10.74	7.04
Li (ppm)	47.1	37.5	42.2	56.1	25.1	22.4	23.2
Mg	74.1	68.1	62.3	85.4	49.0	82.4	61.4
Rb	0.942	0.506	0.749	0.530	0.989	0.739	0.287
Sr	242	269	197	251	155	232	173
Y	0.200	0.157	0.183	b.d.l.	b.d.l.	0.422	0.412
Cs	0.029	b.d.l.	0.022	b.d.l.	b.d.l.	b.d.l.	b.d.l.
Ba	647	310	535	119	496	161	155
La	10.1	5.44	7.47	1.01	5.57	2.57	3.20
Ce	13.3	9.10	10.6	4.58	8.67	6.86	5.39
Pr	0.932	0.730	0.842	0.374	0.650	0.702	0.559
Nd	2.38	1.75	2.06	2.21	2.33	2.53	1.56
Sm	0.089	0.177	0.156	b.d.l.	b.d.l.	0.128	0.216
Eu	2.11	2.35	1.93	2.03	1.53	0.993	0.931
Gd	b.d.l.	0.108	0.179	b.d.l.	b.d.l.	0.047	0.153
Pb	7.58	5.96	6.73	2.92	6.52	5.51	3.96

Table A3.4: Melt inclusion LA-ICP-MS data.

Sample	425	425	425	425	425	440	527	527	527	527	527	527	527	527	527
Crystal	G	G	H	H	H	A	A	G	G	I	J	J	M	M	M
XL type	qtz	qtz	qtz	qtz	qtz	qtz	qtz	qtz	qtz	qtz	qtz	qtz	qtz	qtz	qtz
MI	1	3	1	2	3	1	1	1	2	1	1	2	1	2	3
SiO_2	77.6	77.6	76.7	78.2	77.3	76.7	78.8	78.1	78.3	79.2	80.3	80.6	80.1	78.4	78.5
Li (ppm)	465	350	436	354	382	418	32.8	55.5	49.9	46.6	33.3	35.7	27.9	90.0	43.9
B	22.9	44.0	33.3	51.9	b.d.l.	24.9	46.8	31.8	25.8	30.2	19.4	20.7	37.4	28.5	8.07
Mg	524	654	538	569	389	528	735	747	747	591	1727	565	658	620	606
Ca (wt. %)	0.543	0.617	0.461	0.416	0.660	0.520	0.475	0.660	0.587	0.568	0.876	0.576	0.564	0.617	0.355
Sc (ppm)	5.59	0.22	5.57	3.06	3.11	5.41	4.64	5.44	3.92	6.12	5.16	2.96	b.d.l.	5.06	4.66
Ti	740	450	599	558	575	655	985	787	694	662	924	534	774	680	817
V	0.285	b.d.l.	0.857	3.02	b.d.l.	0.573	b.d.l.	1.06	0.735	1.54	8.32	1.19	0.979	0.836	2.11
Cr	b.d.l.	b.d.l.	b.d.l.	10.2	b.d.l.	b.d.l.	b.d.l.	10.2	0.583	5.32	b.d.l.	b.d.l.	5.54	5.80	1.07
Mn	245	276	268	282	270	265	332	281	291	286	230	257	230	301	251
Ni	b.d.l.	5.14	12.1	2.40	b.d.l.	0.560	b.d.l.	b.d.l.	b.d.l.	b.d.l.	b.d.l.	b.d.l.	0.762	1.04	2.96
Cu	1.03	b.d.l.	1.77	7.93	b.d.l.	1.52	b.d.l.	8.69	12.2	53.6	2.98	10.9	10.9	9.08	19.7
Zn	24.9	27.4	36.3	80.8	47.7	40.2	37.0	61.4	31.2	39.0	32.1	32.0	53.5	41.9	1.62
Rb	157	144	176	419	170	161	166	141	136	158	124	115	137	148	166
Sr	31.4	104	30.7	37.2	35.7	29.2	46.7	43.2	38.1	35.1	79.2	34.8	49.2	36.6	36.5
Y	16.4	16.1	15.7	20.0	20.9	17.7	21.2	18.1	16.2	19.7	14.9	16.3	14.4	17.4	22.8
Zr	78.6	72.4	72.9	99.4	94.8	70.5	82.9	74.8	64.6	81.9	62.7	57.3	73.9	72.3	73.0
Nb	7.06	8.88	6.92	8.08	7.60	7.34	4.33	7.15	5.98	7.42	5.91	5.87	4.96	6.83	7.86
Cs	7.10	7.83	7.45	7.42	8.53	7.64	7.10	7.15	6.09	7.93	5.49	5.79	7.70	7.08	8.00
Ba	515	617	537	666	659	610	732	672	640	743	325	498	660	325	745
La	17.1	18.2	17.5	17.7	22.9	18.4	22.8	18.9	18.3	22.2	14.8	17.2	16.1	16.9	20.9
Ce	43.3	46.4	45.0	54.0	51.2	47.2	44.4	42.8	42.6	52.7	34.7	39.8	44.4	45.2	46.6
Pr	3.82	3.64	3.49	5.47	5.36	3.96	2.89	4.61	3.72	4.78	3.54	3.80	3.96	4.42	5.20
Nd	12.5	14.3	13.5	16.7	21.7	12.5	20.2	15.6	13.7	17.7	12.5	13.6	13.4	14.0	11.6
Sm	2.44	0.976	2.86	4.46	3.44	2.40	3.66	3.86	2.55	3.59	2.74	1.84	2.88	2.72	3.94
Eu	0.266	0.481	0.170	0.131	0.587	0.282	0.203	0.273	0.172	0.381	0.369	0.365	0.014	0.173	b.d.l.
Gd	2.52	6.55	1.86	1.05	2.75	1.96	1.60	1.94	1.69	2.76	1.93	1.99	b.d.l.	2.31	3.45
Tb	0.336	0.664	0.306	0.661	0.482	0.371	0.126	0.373	0.331	0.581	0.341	0.129	0.442	0.358	0.554
Dy	2.57	b.d.l.	2.65	5.08	4.20	2.27	1.61	3.17	2.66	3.47	2.21	2.86	0.625	2.92	2.87
Ho	0.574	1.42	0.623	0.497	0.780	0.464	0.395	0.567	0.618	0.698	0.495	0.422	0.180	0.500	0.760
Er	1.60	2.31	1.83	0.753	1.95	1.67	1.22	2.04	1.67	2.65	1.48	1.82	1.21	1.41	0.552
Tm	0.198	0.691	0.242	0.338	0.064	0.328	b.d.l.	0.343	0.302	0.334	0.202	0.081	b.d.l.	0.22	b.d.l.

Note: b.d.l.= below detection limits. *SiO_2 (wt. %) from EPMA data, used as an internal standard.

Table A3.4 *(continued)*: Melt inclusion LA-ICP-MS data.

Sample	425	425	425	425	425	440	527	527	527	527	527	527	527	527	527
Crystal	G	G	H	H	H	A	A	G	G	I	J	J	M	M	M
XL type	qtz	qtz	qtz	qtz	qtz	qtz	qtz	qtz	qtz	qtz	qtz	qtz	qtz	qtz	qtz
MI	1	3	1	2	3	1	1	1	2	1	1	2	1	2	3
Yb	2.12	0.649	1.98	4.35	2.41	1.94	1.98	2.48	2.30	2.84	1.14	2.21	b.d.l.	1.81	2.37
Lu	0.249	0.055	0.329	0.377	0.045	0.383	0.493	0.357	0.271	0.491	0.189	0.231	b.d.l.	0.163	b.d.l.
Hf	2.82	3.65	2.24	1.39	2.87	1.99	b.d.l.	2.57	1.61	2.68	2.18	1.60	2.72	1.96	2.43
Ta	0.622	1.27	0.737	0.342	0.761	0.644	1.27	0.662	0.763	0.753	0.598	0.433	0.465	0.494	0.680
W	1.93	1.08	1.78	1.51	4.01	1.61	1.10	1.92	1.60	1.84	0.952	0.911	1.87	1.15	b.d.l.
Pb	15.9	19.4	17.0	15.4	19.7	17.6	15.1	20.0	13.1	20.1	9.21	13.7	17.6	16.3	18.5
Th	11.0	12.5	11.7	11.7	13.9	11.0	16.9	12.6	10.1	12.2	8.98	9.70	12.2	10.6	11.6
U	3.18	3.37	3.46	4.04	3.42	3.82	3.32	3.69	3.76	3.82	2.51	2.84	3.23	3.17	3.44

APPENDIX 4

WHOLE ROCK MAJOR AND TRACE ELEMENT DATA

Table A4.1: XRF whole rock major element data (33 samples).

Table A4.2: Solution ICP-MS whole rock trace element data (33 samples).

Table A4.1: Whole rock XRF major element data (Worthington, 1985).

Sample	421	425	427	428	433	436	437	439	440	442	443	444	452	455	456	473	477
Dome	WD	WD	WD	WD	WD	WD	WD	CD	CD	HD	HD	HD	HD	HD	HD	TD	TD
SiO_2	65.01	70.26	67.23	66.16	69.93	69.18	71.36	68.48	71.05	66.75	66.74	68.46	67.20	67.65	69.42	64.61	65.56
TiO_2	0.43	0.31	0.39	0.41	0.32	0.35	0.33	0.37	0.33	0.39	0.39	0.36	0.38	0.37	0.34	0.45	0.44
Al_2O_3	16.09	14.52	14.84	15.05	14.70	14.76	14.61	14.94	14.38	14.91	14.92	14.51	14.83	14.83	14.53	15.72	15.82
Fe_2O_3	4.72	3.23	4.07	4.25	3.29	3.51	3.09	3.78	3.18	4.47	4.47	3.99	4.28	4.31	3.65	5.25	5.03
MnO	0.05	0.07	0.07	0.08	0.07	0.06	0.06	0.07	0.08	0.08	0.08	0.06	0.10	0.07	0.06	0.14	0.08
MgO	2.91	1.70	2.63	2.96	1.77	2.05	1.13	2.07	1.28	2.63	2.83	2.33	2.57	2.33	1.92	3.01	2.76
CaO	5.21	3.58	4.98	5.41	3.87	4.11	3.21	4.72	3.40	4.80	4.92	4.30	4.65	4.31	3.78	5.56	4.79
Na_2O	3.56	3.76	3.45	3.38	3.83	3.53	3.72	3.46	3.70	3.68	3.48	3.62	3.73	3.81	3.84	3.46	3.44
K_2O	1.94	2.51	2.23	2.19	2.45	2.37	2.47	2.03	2.53	2.20	2.09	2.30	2.18	2.24	2.39	1.70	2.00
P_2O_5	0.08	0.06	0.11	0.11	0.07	0.08	0.02	0.08	0.07	0.09	0.08	0.07	0.08	0.08	0.07	0.10	0.08
(LOI)	2.41	0.31	0.29	0.85	0.33	0.41	0.80	1.14	0.55	1.02	0.04	0.11	0.11	0.55	0.12	0.73	1.19
(Total)	100.03	99.70	99.74	99.83	99.81	99.63	99.80	99.62	100.17	99.61	99.49	99.75	100.26	99.79	100.45	99.77	100.14
Tot. alk.	5.50	6.27	5.68	5.57	6.28	5.90	6.19	5.49	6.23	5.88	5.57	5.92	5.91	6.05	6.23	5.16	5.44

Sample	478	483	486	488	489	495	497	498	506	511	521	522	525	527	528	529
Dome	TD	BD	BD	BD	BD	BD	BD	BD	MD	MD	MD	MD	MD	MD	MD	MD
SiO_2	66.22	68.19	68.37	68.55	68.07	67.01	64.74	65.83	67.25	69.28	64.62	65.55	68.30	71.54	67.50	68.81
TiO_2	0.44	0.33	0.34	0.41	0.34	0.42	0.49	0.46	0.41	0.37	0.50	0.46	0.40	0.32	0.41	0.38
Al_2O_3	15.65	15.08	14.99	14.33	15.30	14.90	15.44	15.31	14.82	14.36	15.26	15.21	14.34	14.09	14.81	14.58
Fe_2O_3	4.84	4.09	3.96	4.59	4.08	4.40	5.11	4.90	4.39	3.70	5.26	4.96	4.19	3.09	4.37	3.91
MnO	0.07	0.09	0.06	0.09	0.12	0.10	0.10	0.10	0.09	0.07	0.10	0.07	0.08	0.07	0.08	0.08
MgO	2.56	2.03	1.95	2.11	2.04	2.62	3.04	2.75	2.49	1.96	3.20	2.87	2.36	1.29	2.41	2.11
CaO	4.72	4.08	4.21	3.85	4.06	4.83	5.61	5.08	4.59	3.96	5.71	5.28	4.38	3.14	4.60	4.21
Na_2O	3.38	3.78	3.79	3.70	3.74	3.50	3.42	3.38	3.62	3.79	3.30	3.49	3.48	3.76	3.55	3.47
K_2O	2.05	2.26	2.27	2.29	2.20	2.13	1.94	2.08	2.25	2.42	1.93	2.00	2.40	2.66	2.18	2.38
P_2O_5	0.07	0.07	0.06	0.08	0.05	0.09	0.11	0.11	0.09	0.09	0.12	0.11	0.07	0.04	0.09	0.07
(LOI)	0.77	0.55	1.57	0.92	1.53	0.58	0.98	1.49	2.12	0.45	0.91	0.86	1.74	2.30	0.95	1.82
(Total)	99.60	99.77	99.29	99.50	99.85	100.13	100.16	99.66	99.33	100.05	99.93	100.03	99.98	99.74	99.91	100.22
Tot. alk.	5.43	6.04	6.06	5.99	5.94	5.63	5.36	5.46	5.87	6.21	5.23	5.49	5.88	6.42	5.73	5.85

Note: Oxides are normalised to 100%. Total refers to original analytical total. Abbreviations: BD: Breached Dome; CD: Central Dome; HD: Hipaua Dome; MD: Main Dome; TD: Trig M Dome; WD: Western Dome; Tot. alk.: Total alkali = $Na_2O + K_2O$ (wt. %).

Table A4.2: Whole rock solution ICP-MS trace element data.

Sample	421	425	427	428	433	436	437	439	440	442	443	444	452	455	456	473	477
Dome	WD	WD	WD	WD	WD	WD	WD	CD	CD	HD	HD	HD	HD	HD	HD	TD	TD
CaO (wt. %)	5.21	3.58	4.98	5.41	3.87	4.11	3.21	4.72	3.40	4.80	4.92	4.30	4.65	4.31	3.78	5.56	4.79
Sc (ppm)	13.3	8.28	11.2	11.6	8.48	9.60	8.46	8.96	7.34	11.4	11.6	10.3	11.3	10.8	9.24	12.9	12.3
V	97.8	37.7	54.8	76.4	45.3	56.2	43.9	65.4	46.0	84.7	85.1	67.7	82.0	78.5	61.7	108	100
Cr	72.0	25.9	57.5	61.1	25.6	39.8	18.3	35.5	21.4	45.7	52.2	41.4	44.9	41.9	31.3	36.0	32.5
Ni	50.5	18.6	42.3	47.0	18.0	28.0	14.4	22.8	12.7	33.3	37.4	29.4	34.2	30.5	24.5	30.8	29.0
Cu	56.8	27.5	47.6	42.9	30.4	31.5	26.9	26.9	34.3	18.9	20.7	13.1	20.6	13.4	16.6	19.1	17.7
Zn	46.2	41.2	49.6	48.1	37.7	47.1	40.9	45.5	48.6	52.8	50.8	45.7	51.4	49.1	44.5	62.1	54.5
Ga	17.3	n.d.	n.d.	16.1	n.d.	15.8	16.0	n.d.	n.d.	15.9	15.9	n.d.	16.2	15.8	15.2	16.9	16.8
Rb	52.2	74.1	57.0	58.9	66.9	69.4	74.3	58.9	71.6	65.7	61.2	59.7	63.8	66.9	73.4	43.1	53.6
Sr	658	394	549	610	383	459	461	538	406	330	336	246	331	297	267	389	346
Y	12.1	15.8	16.1	16.2	15.2	16.8	14.9	13.8	14.4	16.6	16.6	14.8	17.3	16.0	17.1	15.8	14.8
Zr	112	75.7	83.3	107	83.8	97.7	80.2	92.9	62.6	100.3	95.2	58.1	97.5	91.3	56.4	85.4	81.7
Nb	5.19	5.60	5.03	4.81	5.15	5.37	6.01	4.64	5.45	4.92	4.71	4.38	4.98	4.94	5.12	4.41	4.69
Mo	0.868	0.340	0.398	0.689	0.630	0.679	0.657	0.792	0.535	0.879	0.494	0.353	0.895	0.685	0.922	0.769	0.801
Cs	2.42	2.45	1.87	2.50	2.18	2.12	1.76	2.62	2.07	2.93	2.37	1.66	1.88	1.91	2.28	2.10	1.24
Ba	617	573	533	532	496	580	608	460	518	483	463	384	501	494	519	433	481
La	18.9	19.5	22.4	23.4	17.3	21.7	25.5	16.9	18.2	17.1	16.6	14.3	17.7	16.8	18.8	16.0	14.6
Ce	35.2	38.5	43.9	45.4	34.0	42.8	48.2	33.2	40.5	34.2	33.9	28.3	35.1	35.8	36.8	31.9	29.4
Pr	3.95	4.28	5.04	5.27	3.76	5.02	5.35	3.73	3.94	3.89	3.83	3.17	4.04	3.97	4.35	3.77	3.30
Nd	14.4	15.6	18.6	19.4	13.9	18.4	18.1	13.7	14.3	14.5	14.3	11.7	15.2	14.6	16.0	14.5	12.6
Sm	2.80	3.09	3.53	3.66	2.74	3.42	3.09	2.59	2.69	2.93	2.91	2.33	3.15	3.02	3.24	3.03	2.68
Eu	1.00	0.762	0.867	0.935	0.701	0.885	0.837	0.697	0.711	0.784	0.765	0.558	0.797	0.748	0.745	0.809	0.788
Gd	2.80	2.98	3.36	3.49	2.76	3.52	3.29	2.60	2.79	3.08	2.95	2.36	3.16	2.99	3.18	3.04	2.73
Tb	0.401	0.443	0.468	0.492	0.406	0.499	0.467	0.377	0.403	0.465	0.450	0.352	0.484	0.453	0.493	0.460	0.429
Dy	2.33	2.66	2.70	2.83	2.41	2.83	2.70	2.24	2.36	2.79	2.75	2.08	2.91	2.70	2.95	2.72	2.55
Ho	0.463	0.538	0.536	0.563	0.490	0.585	0.543	0.452	0.476	0.572	0.567	0.427	0.590	0.560	0.595	0.561	0.527
Er	1.38	1.63	1.62	1.69	1.47	1.78	1.61	1.38	1.43	1.75	1.72	1.27	1.80	1.68	1.76	1.66	1.60
Tm	0.207	0.247	0.240	0.248	0.220	0.263	0.233	0.209	0.208	0.261	0.257	0.191	0.272	0.251	0.259	0.246	0.235
Yb	1.43	1.66	1.58	1.64	1.50	1.77	1.60	1.40	1.41	1.77	1.75	1.26	1.86	1.72	1.72	1.67	1.61
Lu	0.216	0.252	0.242	0.253	0.230	0.277	0.240	0.221	0.210	0.271	0.270	0.193	0.290	0.269	0.256	0.256	0.253
Hf	3.42	2.44	2.61	3.08	2.32	2.94	2.57	2.67	1.92	2.81	2.79	1.58	2.93	2.67	1.91	2.57	2.50
Ta	0.701	0.595	0.483	0.489	0.473	0.604	0.626	0.468	0.499	0.466	0.429	0.356	0.486	0.461	0.508	0.561	0.469
Pb	11.3	10.2	8.53	8.58	9.85	13.4	11.8	11.1	11.4	11.6	10.2	7.6	11.2	6.85	10.5	9.76	9.09
Th	8.91	8.50	7.80	8.26	7.16	8.86	8.76	7.04	6.61	7.61	7.26	5.11	7.91	7.46	7.14	6.79	7.01
U	2.13	1.74	1.42	1.75	1.57	2.04	1.75	1.52	1.54	1.75	1.66	1.13	1.79	1.73	1.59	1.55	1.58

Note: CaO (wt. %) used as an internal standard. Values from XRF analyses (Worthington 1985). Abbreviations: n.d.: not determined; BD: Breached Dome; CD: Central Dome; HD: Hipaua Dome; MD: Main Dome; TD: Trig M Dome; WD: Western Dome.

Table A4.2 *(continued)*: Whole rock solution ICP-MS trace element data.

Sample	478	483	486	488	489	495	497	498	506	511	521	522	525	527	528	529
Dome	TD	BD	BD	BD	BD	BD	BD	BD	MD	MD	MD	MD	MD	MD	MD	MD
CaO (wt. %)	4.72	4.08	4.21	3.85	4.06	4.83	5.61	5.08	4.59	3.96	5.71	5.28	4.38	3.14	4.60	4.21
Sc (ppm)	11.8	9.88	9.50	13.0	10.0	13.2	15.0	13.9	12.9	10.6	15.8	14.7	11.8	8.08	12.8	12.2
V	96.7	56.8	62.0	80.8	55.0	86.1	113	94.3	74.3	63.6	115	100	74.1	44.3	85.0	75.7
Cr	29.1	21.2	19.6	36.4	20.9	40.5	45.5	38.0	44.1	34.9	48.4	41.6	40.6	17.4	38.6	35.4
Ni	33.7	12.6	11.3	18.1	12.3	19.1	22.6	19.1	23.3	17.4	23.6	20.7	20.5	8.42	17.6	16.5
Cu	24.3	13.4	12.4	12.5	16.0	15.8	22.7	21.8	24.9	18.4	14.2	16.8	16.8	12.1	15.2	13.4
Zn	56.2	46.3	49.3	57.3	49.5	50.6	57.8	57.6	55.9	48.5	60.2	58.8	47.6	39.6	53.6	52.2
Ga	16.3	15.7	n.d.	16.4	n.d.	14.8	16.4	27.8	14.8	15.5	15.5	n.d.	14.7	n.d.	15.6	15.5
Rb	56.0	71.6	67.6	69.2	62.6	61.6	55.7	60.1	62.1	75.5	53.1	58.5	67.2	70.7	68.6	76.7
Sr	345	286	277	311	273	282	361	321	292	270	342	333	282	185	292	268
Y	14.0	16.4	16.7	14.9	15.8	18.1	18.7	18.2	18.2	19.0	17.6	18.0	17.7	17.0	19.9	19.3
Zr	79.3	75.5	83.2	85.3	86.0	92.4	114	106	100	101	104	107	98.3	68.4	97.0	90.9
Nb	4.52	5.24	5.03	5.65	4.97	5.37	5.33	5.45	5.29	5.77	4.98	5.30	5.28	5.14	5.55	5.81
Mo	1.22	0.993	1.11	1.13	0.274	0.968	0.832	0.935	0.892	1.15	0.871	0.918	0.977	1.00	0.935	1.12
Cs	1.99	3.11	3.05	2.60	2.72	2.77	2.53	2.68	2.82	3.50	2.42	2.67	2.96	3.09	3.06	3.64
Ba	487	529	482	532	480	472	467	470	475	551	420	457	500	465	527	537
La	14.6	17.8	16.7	21.0	15.8	17.1	18.0	16.9	18.2	19.1	16.4	16.5	17.8	16.1	19.2	19.6
Ce	28.0	35.2	34.0	41.2	32.6	35.4	36.6	35.4	37.4	39.2	33.4	33.6	35.1	32.5	39.0	39.0
Pr	3.20	3.97	3.86	4.43	3.61	4.07	4.35	4.01	4.15	4.50	3.94	3.96	4.13	3.66	4.50	4.48
Nd	12.0	14.7	14.4	14.7	13.4	15.2	16.7	15.3	15.5	16.5	15.2	15.0	15.2	13.5	17.0	17.3
Sm	2.56	3.01	2.91	2.65	2.78	3.15	3.41	3.11	3.12	3.39	3.08	3.08	3.10	2.70	3.44	3.41
Eu	0.768	0.788	0.728	0.828	0.723	0.818	0.918	0.814	0.785	0.793	0.810	0.826	0.795	0.659	0.899	0.83
Gd	2.52	3.06	2.93	2.76	2.83	3.28	3.50	3.18	3.27	3.46	3.10	3.19	3.26	2.80	3.58	3.39
Tb	0.397	0.471	0.454	0.411	0.438	0.492	0.524	0.484	0.501	0.516	0.477	0.485	0.475	0.430	0.543	0.542
Dy	2.44	2.84	2.74	2.60	2.63	3.05	3.17	2.93	2.99	3.17	2.90	2.93	2.92	2.60	3.30	3.25
Ho	0.491	0.577	0.566	0.542	0.546	0.608	0.652	0.608	0.609	0.644	0.591	0.602	0.602	0.541	0.696	0.672
Er	1.49	1.71	1.74	1.68	1.67	1.84	1.96	1.83	1.81	1.99	1.74	1.82	1.81	1.64	2.10	2.05
Tm	0.221	0.256	0.262	0.258	0.255	0.275	0.287	0.275	0.271	0.295	0.255	0.269	0.273	0.248	0.318	0.312
Yb	1.54	1.75	1.78	1.76	1.73	1.89	1.92	1.83	1.78	1.97	1.76	1.83	1.82	1.68	2.13	2.06
Lu	0.237	0.268	0.274	0.274	0.271	0.291	0.309	0.288	0.275	0.320	0.274	0.283	0.291	0.261	0.336	0.317
Hf	2.44	2.50	2.53	2.61	2.65	2.73	3.14	2.84	2.78	2.91	2.71	2.79	2.80	2.04	2.89	2.74
Ta	0.488	0.902	0.827	0.867	0.759	0.565	0.504	0.505	0.473	0.683	0.477	0.489	0.546	0.530	0.599	0.626
Pb	12.4	10.7	11.6	18.1	10.1	11.7	11.6	10.2	11.3	10.1	7.6	10.9	11.6	10.8	14.3	9.8
Th	6.85	7.47	7.46	7.95	7.75	7.31	7.12	6.91	7.74	8.46	6.10	6.51	7.76	7.11	8.25	8.25
U	1.60	1.58	1.73	1.66	1.67	1.66	1.66	1.62	1.67	2.04	1.49	1.53	1.80	1.64	1.90	1.99

APPENDIX 5

ISOTOPIC DATA

Table A5.1: Groundmass Sr-Pb isotopic data (21 samples).

Table A5.2: Whole rock Sr-Pb isotopic data (6 samples)**.**

Table A5.3: Mineral Sr-Pb isotopic data (6 samples).

Table A5.4: Sr-Pb isotope data for whole rock standards.

Table A5.1: Groundmass Sr-Pb isotopic data.

Sample #	$^{87}Sr/^{86}Sr$	$^{206}Pb/^{204}Pb$	$^{207}Pb/^{204}Pb$	$^{208}Pb/^{204}Pb$
Western Dome				
421	0.704402 ± 12	18.801 ± 12	15.614 ± 11	38.676 ± 30
425	0.704558 ± 8	18.818 ± 13	15.622 ± 12	38.705 ± 35
427	0.704245 ± 6	18.811 ± 11	15.619 ± 10	38.695 ± 26
437	0.704322 ± 11	18.832 ± 12	15.627 ± 13	38.724 ± 35
Central Dome				
439	0.704513 ± 8	18.811 ± 9	15.621 ± 10	38.706 ± 25
440	0.704158 ± 9	18.835 ± 11	15.631 ± 9	38.737 ± 23
Hipaua Dome				
443	0.704696 ± 9	18.811 ± 11	15.621 ± 11	38.701 ± 28
455	0.704946 ± 11	18.813 ± 12	15.620 ± 12	38.699 ± 32
456	0.704764 ± 7	18.828 ± 9	15.630 ± 9	38.731 ± 23
Trig M Dome				
473	0.704758 ± 7	18.812 ± 11	15.624 ± 9	38.717 ± 25
477	0.705029 ± 13	18.804 ± 11	15.613 ± 11	38.680 ± 29
478	0.704802 ± 7	18.811 ± 11	15.617 ± 10	38.691 ± 26
Breached Dome				
483	0.705041 ± 9	18.815 ± 12	15.627 ± 11	38.719 ± 26
486	0.705037 ± 12	18.813 ± 10	15.624 ± 10	38.710 ± 25
497	0.704842 ± 13	18.797 ± 10	15.618 ± 10	38.688 ± 25
498	0.704853 ± 13	18.799 ± 13	15.613 ± 14	38.675 ± 39
Main Dome				
511	0.705205 ± 10	18.823 ± 12	15.627 ± 11	38.719 ± 30
521	0.704866 ± 9	18.797 ± 11	15.618 ± 9	38.691 ± 24
522	0.704825 ± 14	18.805 ± 12	15.621 ± 11	38.699 ± 28
527	0.705098 ± 11	18.829 ± 16	15.629 ± 17	38.725 ± 50
528	0.704677 ± 10	18.810 ± 13	15.617 ± 11	38.686 ± 28

Table A5.2: Whole rock Sr-Pb isotopic data

Dome	Sample #	$^{87}Sr/^{86}Sr$	$^{206}Pb/^{204}Pb$	$^{207}Pb/^{204}Pb$	$^{208}Pb/^{204}Pb$
Western	425	0.704561 ± 9	18.820 ± 17	15.623 ± 19	38.707 ± 50
Central	440	0.704420 ± 11	18.831 ± 19	15.625 ± 13	38.718 ± 35
Hipaua	456	0.704995 ± 11	18.823 ± 31	15.628 ± 14	38.723 ± 38
Trig M	477	0.705000 ± 9	18.811 ± 17	15.621 ± 18	38.705 ± 47
Breached	483	0.705082 ± 9	18.818 ± 17	15.629 ± 15	38.724 ± 30
Main	527	0.705098 ± 9	18.836 ± 9	15.632 ± 13	38.737 ± 30

Table A5.3 Mineral Sr-Pb isotopic data.

Dome	Sample #	Mineral	$^{87}Sr/^{86}Sr$	$^{206}Pb/^{204}Pb$	$^{207}Pb/^{204}Pb$	$^{208}Pb/^{204}Pb$
Western	425	big plag 1	0.705468 ± 35	18.849 ± 88	15.635 ± 76	38.750 ± 192
		big plag 2	0.705098 ± 41	18.849 ± 88	15.635 ± 79	38.744 ± 192
		small plag	0.705194 ± 24	18.849 ± 17	15.635 ± 15	38. 748 ± 37
		cpx	0.704643 ± 87			
		amph	0.704833 ± 22			
Central	440	big plag 1	0.705544 ± 22	18.851 ± 39	15.635 ± 33	38.742 ± 85
		big plag 2	0.705307 ± 37	18.852 ± 44	15.637 ± 40	38.749 ± 93
		small plag	0.705305 ± 10	18.843 ± 13	15.630 ± 12	38.732 ± 34
		cpx	0.704624 ± 34			
Hipaua	456	big plag 1	0.705858 ± 23	18.854 ± 51	15.644 ± 44	38.774 ± 108
		small plag	0.705338 ± 13	18.842 ± 25	15.632 ± 25	38.734 ± 58
		cpx	0.705035 ± 12			
		amph	0.705054 ± 24			
Trig M	477	big plag 1	0.706134 ± 87	18.833 ± 69	15.623 ± 60	38.704 ± 146
		big plag 2	0.705229 ± 83	18.844 ± 69	15.635 ± 408	38.743 ± 145
		small plag	0.705285 ± 15	18.829 ± 14	15.632 ± 14	38.723 ± 35
		cpx	0.705009 ± 9			
		amph	0.705115 ± 12			
Breached	483	big plag 1	0.705716 ± 47	18.840 ± 41	15.628 ± 37	38.728 ± 91
		big plag 2	0.705255 ± 17	18.849 ± 54	15.636 ± 42	38.745 ± 113
		small plag	0.705352 ± 10	18.847 ± 18	15.636 ± 18	38.748 ± 46
		cpx	0.705058 ± 9			
		amph	0.705125 ± 26			
Main	527	big plag 1	0.705302 ± 15	18.844 ± 46	15.638 ± 41	38.745 ± 103
		big plag 2	0.705212 ± 33	18.850 ± 45	15.637 ± 41	38.752 ± 103
		small plag	0.705395 ± 10	18.850 ± 39	15.635 ± 28	38.750 ± 67
		cpx	0.704907 ± 13			
		amph	0.704743 ± 68			

Note: Abbreviatons: amph: bulk amphibole phenocrysts; big plag: individual plagioclase phenocrysts >2 mm; cpx: bulk clinopyroxene phenocrysts; small plag: bulk whole plagioclase phenocrysts >2 mm.

Table A5.4: Sr-Pb isotope data for whole rock standards.

JB-2	$^{206}Pb/^{204}Pb$	$^{207}Pb/^{204}Pb$	$^{208}Pb/^{204}Pb$
Value	18.344	15.562	38.276
Blanks			< 14 pg

BHVO-2	$^{87}Sr/^{86}Sr$
Value	0.703469
Blanks	< 90 pg

APPENDIX 6

GEOTHERMOBAROMETRY, HYGROMETRY AND OXYBAROMETRY

A6.1: Introduction.

A6.2: Two-pyroxene thermometry (Brey and Köhler, 1990).

A6.3: Amphibole thermobarometry, hygrometry and oxybarometry (Ridolfi et al., 2010).

A6.4: Iron-titanium oxide thermometry (Ghiorso and Evans, 2008).

A6.1 INTRODUCTION

The study of eruption products provides a means to ascertain physical parameters such as temperature and pressure for sub-volcanic processes which cannot be directly measured. Thermometry, oxybarometry, barometry and hygrometry use *in situ* major and minor element chemistries of crystals and their host melt to determine the physical condition of the magma. These techniques have been developed and calibrated for a wide range of igneous and metamorphic rocks. To obtain meaningful results, the selection of techniques for samples suites is important (e.g. thermometers calibrated on silicic rocks should only be applied to silicic rocks over the compositional and temperature range they have been calibrated for).

The Tauhara dacite contains a wide range of phenocrysts from rare olivine through to quartz, however not all phenocrysts can be used to calculate magmatic conditions. With magma mixing as the primary process for genesis of the Tauhara dacite, most crystals are antecrysts and therefore equilibrium amongst phases and/or the melt required by many techniques is unlikely. This rules out phenocryst-melt techniques such as plagioclase-melt and clinopyroxene-melt thermometers (Putirka, 2008) and most techniques which require more than one crystal phase such as Al in hornblende barometers (e.g. Hammarstrom and Zen, 1986). The techniques used in this thesis are Fe-Ti oxide thermometry and oxybarometry (Ghiorso and Evans, 2008) and two-pyroxene thermometry (Brey and Köhler, 1990), which both require the co-existence of two phases in equilibrium (Fe-Ti: titano-magnetite and ilmentite; 2-px: clinopyroxene and orthopyroxene). An equilibrium test is therefore imperative for these thermometers and only pairs that fall within equilibrium envelopes are used. A new hornblende thermobarometer, oxybarometer and hygrometer developed by Ridolfi et al. (2010) is also used in this thesis. This technique is independent of other phases and based on major element chemistry of amphibole alone.

Ti in quartz thermometry (Wark and Watson, 2006) was not applied in this study, owing to potential complications introduced by a large pressure dependence (Thomas et al., 2010) that cannot be independently constrained for quartz in the mixed Tauhara dacites.

A6.2 TWO-PYROXENE THERMOMETRY

Two-pyroxene thermometry is based on the partitioning of Ca between co-existing orthopyroxene and clinopyroxene. With higher temperature, Ca content increases in orthopyroxene and decreases in clinopyroxene. This dependence is used to determine the temperature of pyroxene crystallisation in the magma (Lindsley, 1983).

As two-pyroxene thermometry is based on the co-existence of two pyroxene phases, an equilibrium text must be applied. The equilibrium test (equation A1) applied in this thesis uses Fe-Mg exchange from Putirka (2008) where all cation fractions are calculated on a 6 oxygen basis. Clinopyroxene-orthopyroxene pairs with K_D of 1.09 ± 0.14 (3 s.e.) are interpreted to be in equilibrium.

A1) $$K_D(Fe-Mg)^{cpx-opx} = \left(X_{Fe}^{cpx}/X_{Mg}^{cpx}\right)/\left(X_{Fe}^{opx}/X_{Mg}^{opx}\right) = 1.09 \pm 0.14$$

Clinopyroxene-orthopyroxene pairs in equilibrium were determined by cross correlating core, middle and rim zones between the phases. This resulted in multiple pairs for a single zone. To avoid bias, the clinopyroxene-orthopyroxene pair with K_D closest to the equilibrium middle value of 1.09 was chosen to represent each pyroxene zone.

There are three two-pyroxene thermometers commonly used in magmatic studies; Wells (1977), QUILF by Andersen *et al*. (1973) and T_{BKN} (Brey and Köhler, 1990). Recent experiments by Blundy and Cashman (2008) using large data sets have revealed that Wells (1977) and QUILF impose large uncertainties of ± 99 °C and ± 114 °C average absolute deviation (aad) respectively. The T_{BKN} thermometer is more precise with ± 66 °C aad which is significantly larger than the 30 °C (2 s.d.) error quoted in Brey and Köhler (1990). The T_{BKN} precision improves to ± 50 °C aad when only data from Mg-rich systems (Mg_{cpx} # >0.75) is considered (Putirka, 2008). Putirka (2008) also proposes two new thermometers with slightly lower uncertainties than that of T_{BKN}. However, since T_{BKN} has been used widely in the literature and has a reasonable uncertainty, it has been used in this study.

Two-pyroxene temperatures were therefore calculated based on the Brey and Köhler (1990) model T_{BKN} (equation A2) using a spreadsheet from Putirka (2008).

A2) $$T_{\mathrm{BKN}} = \frac{23664+\left(24.9+126.3\,X_{Fe}^{cpx}\right)P}{13.38+\left(\ln K_D^*\right)^2+11.59\,X_{Fe}^{opx}}$$

With T_{BKN} in degrees Kelvin, P in kilobars and:

$$X_{Fe}^{px} = Fe/(Fe + Mg)$$

$$K_D^* = \left[1 - \left(X_{Ca}^{cpx}/(1 - X_{Na}^{cpx})\right)\right] / \left[1 - \left(X_{Ca}^{opx}/(1 - X_{Na}^{opx})\right)\right]$$

This thermometer requires a pressure input. The pressure input was derived from Putirka (2008) equation 38 (equation A3) which is temperature independent, utilising the strategy of Mercier *et al*. (1984). Equation A3 has a resolution of ± 3.7 kbar and the calculated pressure has only been used to input into the T_{BKN} thermometer as the associated uncertainty is too large to be useful as a barometer in its own right.

A3)

$$P(kbar) = -279.8 + 293\left(X_{Al(VI)}^{opx}\right) + 455\left(X_{Na}^{opx}\right) + 229\left(X_{Cr}^{opx}\right) + 519\left(X_{Fm_2Si_2O_6}^{opx}\right) - 563\left(X_{En}^{opx}\right) + 371\left(X_{Di}^{opx}\right) + 327\left(a_{En}^{opx}\right) + \frac{1.19}{K_f}$$

Where:

$$X_{En}^{opx} = \left(X_{Fm_2Si_2O_6}^{opx}\right)\left(X_{Mg}^{opx}/\left(X_{Mg}^{opx} + X_{Mn}^{opx} + X_{Fe}^{opx}\right)\right)$$

$$X_{Di}^{opx} = \left(X_{CaFmSi_2O_6}^{opx}\right)\left(X_{Mg}^{opx}/\left(X_{Mg}^{opx} + X_{Mn}^{opx} + X_{Fe}^{opx}\right)\right)$$

$$a_{En}^{opx} = \left(\frac{0.5X_{Mg}^{opx}}{X_{Ca}^{opx} + 0.5X_{Mg}^{opx} + 0.5X_{Fe^{2+}}^{opx} + X_{Mn}^{opx} + X_{Na}^{opx}}\right)\left(\frac{0.5X_{Mg}^{opx}}{0.5X_{Fe^{2+}}^{opx} + X_{Fe^{3+}}^{opx} + X_{Al(VI)}^{opx} + X_{Ti}^{opx} + X_{Cr}^{opx} + 0.5X_{Mg}^{opx}}\right)$$

$$X_{Fe^{2+}}^{opx} = X_{Fe}^{opx} - X_{Fe^{3+}}^{opx}$$

$$Fe^{3+} = Al(IV) + Na - Al(VI) - Cr - 2Ti$$

$$K_f = X_{Ca}^{opx}/\left(1 - X_{Ca}^{cpx}\right)$$

All cation fractions were calculated on a six oxygen basis. Temperatures, pressures and equilibrium values are given in Table A6.1.

Table A6.1: Two-pyroxene temperatures (Brey and Köhler, 1990).

Sample# 456 Hipaua Dome

Clinopyroxene		Orthopyroxene		Eqn 38	T_{BKN}	K_D (Fe-Mg)$^{cpx\text{-}opx}$
Crystal	Zone	Crystal	Zone	P(kbar)	°C	1.09 ± 0.14
D	core	G	core	6.50	955	1.09
L	core	G	core	6.69	935	1.06
A	mid	E	mid	7.08	945	1.01
C	mid	F	mid	7.49	962	0.96
D	mid	F	mid	5.84	1021	0.97
E	mid	E	mid	6.23	957	1.14
F	mid	E	mid	5.42	949	1.17
J	mid	E	mid	5.82	1006	1.15
K	mid	E	mid	6.08	939	1.04
M	mid	E	mid	5.33	889	1.05
C	rim	F	rim	4.02	903	1.07
G	rim	F	rim	3.90	933	1.05
L	rim	F	rim	3.45	895	0.96

Sample# 477 Trig M Dome

Clinopyroxene		Orthopyroxene		Eqn 38	T_{BKN}	K_D (Fe-Mg)$^{cpx\text{-}opx}$
Crystal	Zone	Crystal	Zone	P(kbar)	°C	1.09 ± 0.14
F	core	F	core	5.88	993	1.12
B	mid	F	mid 2	2.44	967	1.02
F	mid	G	mid	2.42	926	1.09
G	mid	F	mid 1	3.32	864	1.07
H	mid	B	mid 2	4.42	953	1.11
C	rim	A	rim	4.74	921	1.04
D	rim	A	rim	4.59	910	1.02
E	rim	A	rim	4.67	887	1.03
H	rim	A	rim	3.24	918	1.00

Sample# 483 Breached Dome

Clinopyroxene		Orthopyroxene		Eqn 38	T_{BKN}	K_D (Fe-Mg)$^{cpx\text{-}opx}$
Crystal	Zone	Crystal	Zone	P(kbar)	°C	1.09 ± 0.14
A	core	L	core	4.68	904	1.02
C	core	G	core	7.09	948	1.00
E	core	L	core	4.33	844	1.12
F	core	B	core	7.31	836	1.11
H	core	L	core	4.87	930	1.06
A	mid	D	mid 3	4.19	897	0.97
B	mid	D	mid 3	4.24	931	1.09
C	mid	D	mid 3	5.03	975	0.97
G	mid	B	mid 1	7.57	1030	1.01
I	mid	D	mid 3	4.18	891	1.04
A	rim	F	rim	7.09	933	1.02
C	rim	F	rim	7.39	962	0.95
I	rim	F	rim	6.54	904	1.07

Table A6.1 *(continued)*: Two-pyroxene temperatures (Brey and Köhler, 1990).
Sample# 527 Main Dome

Clinopyroxene		Orthopyroxene		Eqn 38	T_{BKN}	K_D (Fe-Mg)$^{cpx\text{-}opx}$
Crystal	Zone	Crystal	Zone	P(kbar)	°C	1.09 ± 0.14
B	core	G	core	4.07	1021	1.01
C	core	G	core	3.76	966	1.04
F	core	E	core	3.97	998	1.08
I	core	G	core	5.37	937	1.10
O	core	F	core	4.44	886	1.11
A	mid 2	C	mid 4	6.06	806	1.11
B	mid 1	E	mid 2	4.25	979	1.10
B	mid 2	B	mid 1	3.07	942	1.10
B	mid 3	C	mid 3	3.05	946	1.08
C	mid 1	E	mid 1	3.87	934	1.10
C	mid 2	B	mid 3	3.11	939	1.00
D	mid	B	mid 4	4.36	937	1.10
D	mid 2	B	mid 3	2.84	921	1.01
E	mid	B	mid 1	4.10	994	1.10
F	mid 2	B	mid 1	3.40	910	1.09
G	mid	B	mid 3	3.41	934	1.01
G	mid 1	B	mid 3	3.53	892	0.95
G	mid 3	B	mid 3	5.44	900	1.03
H	mid	B	mid 3	3.08	997	1.08
I	mid	B	mid 3	3.72	984	0.97
J	mid 1	B	mid 3	3.24	903	1.06
J	mid 2	B	mid 1	4.04	935	1.07
K	mid	C	mid 3	3.78	959	1.08
L	mid	B	mid 3	5.71	973	1.04
M	mid	B	mid 3	5.48	966	1.11
N	mid 1	F	mid	3.17	952	1.10
N	mid 2	B	mid 3	6.85	977	1.03
O	mid 1	B	mid 3	3.90	920	1.07
O	mid 2	B	mid 2	6.18	929	1.08
O	mid 3	C	mid 4	2.94	912	1.09
O	mid 4	E	mid 1	5.01	959	1.09
A	rim	F	rim	3.95	939	1.04
B	rim	D	rim	4.61	963	1.19
B	rim	F	rim	4.93	880	1.08
C	rim	D	rim	4.40	937	1.18
D	rim	F	rim	3.57	935	0.98
G	rim	D	rim	3.55	1015	1.23
K	rim	D	rim	3.89	999	1.19
M	rim	D	rim	2.96	925	1.08
N	rim	F	rim	4.62	963	0.98

A6.3 AMPHIBOLE THERMOBAROMETRY, OXYBAROMETRY AND HYGROMETRY

Most thermobarometers require an equilibrium of two or more phases, which is a requirement not commonly met by many igneous rocks, especially those of hybrid or mixed origins. Although single phase barometers such as Al-in-hornblende have been calibrated for calc-alkaline granites and rhyolites (Hammarstrom and Zen, 1986; Hollister et al., 1987; Johnson and Rutherford, 1989; Thomas and Ernst, 1990; Schmidt, 1992) these barometers require buffering assemblages in equilibrium with the amphibole. The Hammarstrom and Zen (1986) barometer, for example, requires a buffering assemblage of plagioclase + K-feldspar + quartz + hornblende + biotite + sphene + magnetite (or Ilmenite). This assemblage is not applicable to the Tauhara dacite where K-feldspar and sphene are absent, and most mineral phases are not in equilibrium.

Ridolfi *et al.* (2010) provides a new single phase thermometer, oxybarometer and hygrometer that is independent of buffering assemblages and is based exclusively on the amphibole composition. Element indexes (Si*, Mg* and Al*) are calculated by adding fractions of the amphibole major cations to Si, Mg and Al respectively where Si* (equation A4) correlates with temperature with an uncertainty of ±22 °C, Mg* (equation A5) correlates to ΔNNO with ±0.22 log unit and Al* (equation A6) correlates with with H_2O_{melt} (wt %) ±0.41 wt%. Pressure correlates with Al_T (equation A7) with ±54 MPa.

A4) $$T = -151.487\, Si^{*} + 2041$$

Where $Si^{*} = Si + \frac{Al}{15} - 2Ti - \frac{Al}{2} - \frac{Ti}{1.8} + \frac{Fe^{3+}}{9} + \frac{Fe^{2+}}{3.3} + \frac{Mg}{26} + \frac{^{B}Ca}{5} + \frac{^{B}Na}{1.3} - \frac{^{A}Na}{15} + \frac{^{A}[\,]}{2.3}$

A5) $$\Delta NNO = 1.644\, Mg^{*} - 4.01$$

Where $Mg^{*} = Mg + \frac{Si}{47} - \frac{Al}{9} - 1.3\, Ti + \frac{Fe^{3+}}{3.7} + \frac{Fe^{2+}}{5.2} - \frac{^{B}Ca}{20} - \frac{^{A}Na}{2.8} + \frac{^{A}[\,]}{9.5}$

A6) $$H_2O_{melt} = 5.215\, Al^{*} + 12.28$$

Where $Al^{*} = Al + \frac{Al}{13.9} - \frac{Si+Ti}{5} - \frac{Fe^{2+}}{3} - \frac{Mg}{1.7} + \frac{^{B}Ca + ^{A}[\,]}{1.2} + \frac{^{A}Na}{2.7} - 1.56\, K - \frac{Fe\#}{1.6}$

A7) $$P = 19.209e^{(1.438 Al_T)}$$

Amphibole temperatures, pressures, logfO_2 and H_2O melt (wt %) are given in Table A6.2.

Table A6.2: Amphibole temperatures, pressures, oxygen fugacity and H_2O_{melt} calculated from Ridolfi *et al.* (2010).

Sample# 425 Western Dome

Crystal	Zone	T (°C)	P (MPa)	Depth* (km)	logfO_2	ΔNNO	H_2O_{melt} (wt.%)
A	core	908	244	9.2	-10.31	1.41	6.11
A	mid	897	229	8.6	-10.39	1.53	6.21
C	mid	900	232	8.8	-10.32	1.56	6.07
C	rim	884	196	7.4	-10.76	1.40	5.64
G	core	875	198	7.5	-10.94	1.39	6.13
G	mid 1	893	220	8.3	-10.43	1.57	6.21
G	mid 2	882	217	8.2	-11.08	1.12	6.44
G	mid 4	876	216	8.2	-10.96	1.34	6.53
G	rim	892	220	8.3	-10.90	1.12	5.70
H	core	905	243	9.2	-10.40	1.38	6.12
H	mid	895	225	8.5	-10.38	1.58	6.03
H	rim	889	226	8.5	-10.87	1.20	6.14
H	core	901	235	8.9	-10.40	1.45	6.26
H	mid	904	230	8.7	-10.21	1.59	6.03
H	rim	894	230	8.7	-10.94	1.04	5.96
L	mid 1	907	250	9.5	-10.48	1.26	6.20
L	mid 2	903	243	9.2	-10.32	1.50	6.32
L	rim	884	195	7.3	-10.90	1.27	5.16
M	core	880	193	7.3	-10.71	1.54	5.77
M	mid	888	206	7.8	-9.77	2.32	5.49
M	rim	884	198	7.5	-10.93	1.25	5.42
N	core	913	241	9.1	-10.25	1.39	5.92
N	rim	885	213	8.0	-10.77	1.37	6.05
O	core	885	193	7.3	-10.49	1.66	5.75
O	rim	890	214	8.1	-10.80	1.26	5.85
P	core	893	217	8.2	-10.57	1.43	6.20
P	mid 1	910	248	9.4	-10.28	1.41	6.21
P	mid 2	915	291	11.0	-9.87	1.70	6.65
P	rim	890	212	8.0	-10.63	1.43	5.88
R	core	860	175	6.6	-11.26	1.36	5.56
R	rim	896	236	8.9	-10.67	1.27	6.24
U	mid	926	272	10.3	-9.96	1.44	6.26

Sample# 440 Central Dome

Crystal	Zone	T (°C)	P (MPa)	Depth* (km)	logfO_2	ΔNNO	H_2O_{melt} (wt.%)
A	core	893	243	9.2	-10.29	1.70	6.28
A	rim	883	212	8.0	-10.94	1.24	5.87
B	mid	949	431	16.3	-10.27	0.69	7.75
C	core	893	253	9.6	-10.84	1.15	6.46
C	rim	896	239	9.0	-10.80	1.14	6.22
D	core	868	181	6.8	-11.00	1.47	5.83
D	rim	893	227	8.6	-10.56	1.43	6.10
E	mid	869	181	6.8	-10.87	1.58	5.88
F	core	868	181	6.8	-10.15	2.32	5.58
F	rim	880	193	7.3	-11.01	1.24	5.86
G	core	884	207	7.8	-10.82	1.36	6.00
G	mid	887	215	8.1	-10.35	1.75	6.18
G	rim	880	199	7.5	-10.99	1.25	5.82
H	core	863	171	6.5	-10.95	1.63	5.42
H	mid	879	194	7.3	-10.73	1.53	5.77
I	mid	894	233	8.8	-10.84	1.14	6.17
J	mid	889	221	8.4	-10.67	1.41	5.87
K	core	885	239	9.0	-10.88	1.27	6.44
K	rim	891	219	8.3	-11.10	0.94	5.68
L	rim	878	204	7.7	-11.03	1.25	6.08
M	core	895	229	8.6	-10.82	1.15	5.71
M	rim	890	213	8.1	-10.77	1.29	6.03
N	core	903	235	8.9	-10.45	1.37	6.00
Q	mid	876	202	7.6	-11.01	1.31	6.16
R	mid	878	205	7.7	-11.07	1.20	6.17
S	mid	874	197	7.4	-10.87	1.49	6.17

*Depth is based on average continental rock density of 2700 kg/m^3.

Table A6.2 *(continued)*: Amphibole temperatures, pressures, oxygen fugacity and H_2O_{melt} calculated from Ridolfi *et al.* (2010).

Sample# 456 Hipaua Dome

Crystal	Zone	T (°C)	P (MPa)	Depth* (km)	logfO_2	ΔNNO	H_2O_{melt} (wt.%)
A	core	909	290	10.9	-10.26	1.43	6.99
B1	core	917	301	11.4	-10.20	1.34	6.80
B1	rim	915	316	12.0	-10.52	1.05	6.99
B2	core	932	317	12.0	-9.85	1.45	6.83
B2	rim	920	308	11.6	-10.52	0.98	6.92
C1	core	919	282	10.6	-10.08	1.44	6.52
C2	rim	917	293	11.1	-10.27	1.29	6.63
C2	core	942	364	13.8	-9.93	1.17	7.25
C2	rim	918	309	11.7	-10.36	1.16	6.81
D	core	921	290	11.0	-10.18	1.29	6.58
D	rim	909	290	11.0	-10.64	1.04	6.80
E	core	926	315	11.9	-10.11	1.28	6.88
E	rim	908	260	9.8	-10.52	1.20	6.43
F	rim	916	309	11.7	-10.56	0.99	7.00
G	core	915	285	10.8	-10.31	1.29	6.56
G	rim	911	259	9.8	-10.52	1.15	6.31
H	rim	906	256	9.7	-10.57	1.18	6.45
I	core	885	199	7.5	-10.25	1.91	5.78
I	mid	899	245	9.3	-10.35	1.53	6.55
I	rim	923	295	11.2	-10.34	1.11	6.38
J	core	912	259	9.8	-10.15	1.51	6.31
J	rim	904	233	8.8	-10.51	1.29	5.76
K	rim	922	296	11.2	-10.41	1.06	6.47
L	core	916	254	9.6	-9.95	1.64	6.03
L	rim	925	309	11.7	-10.29	1.11	6.63

Sample# 477 Trig M Dome

Crystal	Zone	T (°C)	P (MPa)	Depth* (km)	logfO_2	ΔNNO	H_2O_{melt} (wt.%)
A	mid	955	379	14.3	-9.46	1.44	6.94
B	rim	949	342	12.9	-9.64	1.35	6.47
C	mid	969	377	14.2	-9.14	1.52	6.50
D	mid	952	342	12.9	-9.46	1.49	6.63
E	mid	955	353	13.3	-9.42	1.48	6.64
F	core	935	328	12.4	-9.98	1.26	6.72
F	rim	945	346	13.1	-9.74	1.31	6.54
G	mid	928	270	10.2	-9.67	1.69	5.91
H	core	940	360	13.6	-9.79	1.34	6.89
I	core	947	352	13.3	-9.54	1.49	6.64
I	mid	958	462	17.5	-9.62	1.19	7.70
I	rim	947	363	13.7	-9.69	1.34	6.78
J	mid	893	224	8.5	-10.20	1.80	6.28
J	rim	943	351	13.3	-9.73	1.36	6.79
K	core	932	305	11.5	-9.85	1.43	6.52
M	core	931	304	11.5	-9.71	1.59	6.45
N	mid	947	359	13.5	-9.57	1.45	6.81
O	mid	957	358	13.5	-9.31	1.55	6.55
P	core	925	295	11.2	-9.88	1.54	6.49
P	mid	936	335	12.7	-9.87	1.34	6.88

Table A6.2 *(continued)*: Amphibole temperatures, pressures, oxygen fugacity and H_2O_{melt} calculated from Ridolfi *et al.* (2010).

Sample# 483 Breached Dome

Crystal	Zone	T (°C)	P (MPa)	Depth* (km)	logfO_2	ΔNNO	H_2O_{melt} (wt.%)
A	core	915	265	10.0	-10.29	1.31	6.32
A	mid	915	284	10.7	-9.82	1.77	6.39
A	rim	912	272	10.3	-10.31	1.33	6.23
C	core	925	289	10.9	-9.75	1.66	6.56
C	rim	893	228	8.6	-10.52	1.47	5.95
D	core	879	212	8.0	-10.31	1.94	5.84
D	mid 1	885	218	8.2	-10.73	1.41	6.02
D	mid 3	908	269	10.2	-10.41	1.30	6.44
D	rim	893	226	8.5	-10.00	2.00	5.95
F	core	912	273	10.3	-10.31	1.32	6.41
F	mid 1	894	226	8.5	-10.01	1.97	5.88
F	mid 2	898	244	9.2	-10.52	1.38	6.19
F	mid 3	893	224	8.5	-10.00	2.00	5.80
F	mid 4	895	229	8.6	-10.56	1.41	5.92
F	rim	911	261	9.9	-10.34	1.34	6.23
H	core	914	285	10.8	-10.36	1.25	6.63
H	rim	905	264	10.0	-10.64	1.12	6.40
I	core	887	214	8.1	-10.47	1.64	5.71
M	core	901	242	9.1	-10.42	1.43	6.20
M	rim	909	258	9.7	-10.36	1.33	6.29

Sample# 527 Main Dome

Crystal	Zone	T (°C)	P (MPa)	Depth* (km)	logfO_2	ΔNNO	H_2O_{melt} (wt.%)
A	mid	775	97	3.7	-13.52	0.88	5.14
B	core	894	216	8.1	-10.22	1.76	5.83
B	rim	898	242	9.2	-10.71	1.19	6.25
C	core	886	212	8.0	-10.45	1.67	6.02
C	mid 1	904	263	9.9	-10.12	1.67	6.54
C	mid 2	922	285	10.8	-9.95	1.51	6.42
C	rim	822	123	4.6	-11.78	1.61	5.10
D	core	901	257	9.7	-10.64	1.20	6.37
D	rim	800	116	4.4	-12.88	0.97	5.10
E	core	887	215	8.1	-10.51	1.59	5.96
E	rim	796	96	3.6	-12.16	1.79	4.56
F	core	921	275	10.4	-10.64	0.85	5.99
F	mid	908	239	9.0	-10.52	1.20	5.86
F	rim	779	86	3.2	-12.64	1.68	4.43
G	core	902	269	10.2	-10.93	0.89	6.48
G	rim	789	89	3.4	-12.24	1.87	4.28
H	mid	776	95	3.6	-13.38	1.00	5.00
I	core	879	201	7.6	-10.68	1.58	5.97
I	rim	791	98	3.7	-12.68	1.39	4.51
J	mid	785	101	3.8	-13.29	0.89	5.06
K	mid	787	105	4.0	-13.39	0.75	5.20

A6.4 Fe-Ti OXIDE THERMOMETRY AND OXYBAROMETRY

Two discrete phases of Fe-Ti oxide; ilmenite and magnetite, are present in many volcanic rocks. Solid solution of cubic oxides (titanomagnetite) occurs close to the ulvöspinel–magnetite binary and solid solution of rhombic oxides (ilmenite) occurs close to the haematite-ilmenite binary (Blundy and Cashman, 2008). Fe-Ti thermometry is based on the temperature dependent exchange of Fe^{2+} + Ti^{4+} for 2 Fe^{3+} between ilmenite and magnetite phases along their binaries based on the reaction:

$$FeTiO_3 + Fe_3O_4 = Fe_2TiO_4 + Fe_2O_3$$
ulvöspinel + haematite = ilmenite + magnetite

The magnetite-haematite iron redox reaction can be used to determine oxygen fugacity where:

$$4Fe_3O_4 + O_2 = 6Fe_2O_3$$
haematite + oxygen = magnetite

Fe-Ti thermometry requires the two oxide phases of ilmenite and titanomagnetite to be in equilibrium. Oxide pairs in contact with each other and pairs hosted inside phenocrysts were targeted as likely to be in equilibrium. However, the oxides may have been inherited from different parental magmas or re-equilibration and/or exsolution may have occurred in one or both oxides phases so an equilibrium test was applied. The Mg-Mn equilibrium test from Bacon and Hirschmann (1988) (equation A8) was applied to all touching and phenocryst hosted pairs and pairs that fell inside the ±2σ error envelope were accepted.

A8) $$\log\left(\frac{X_{Mg}}{X_{Mn}}\right)_{mt} = 0.9317^{+0.0113}_{-0.0104} \times \log\left(\frac{X_{Mg}}{X_{Mn}}\right)_{ilm} - 0.0909^{+0.0785}_{-0.0787}$$

Where Mg and Mn are atomic fractions in titanomagnetite (mt) and ilmenite (ilm). Ilmenite and titanomagnetite crystals that were in the groundmass but not in contact were also considered. These were first categorised by size, where crystals with diameters >70 µm were interpreted to be phenocrysts/antecrysts and crystals with diameters <20 µm were interpreted to be microlites representing the final melt conditions. The equilibrium test was applied for phases from each category. In total, six groundmass oxide pairs and 10 phenocryst hosted pairs met the criteria set for equilibrium, as shown in Figure A6.1.

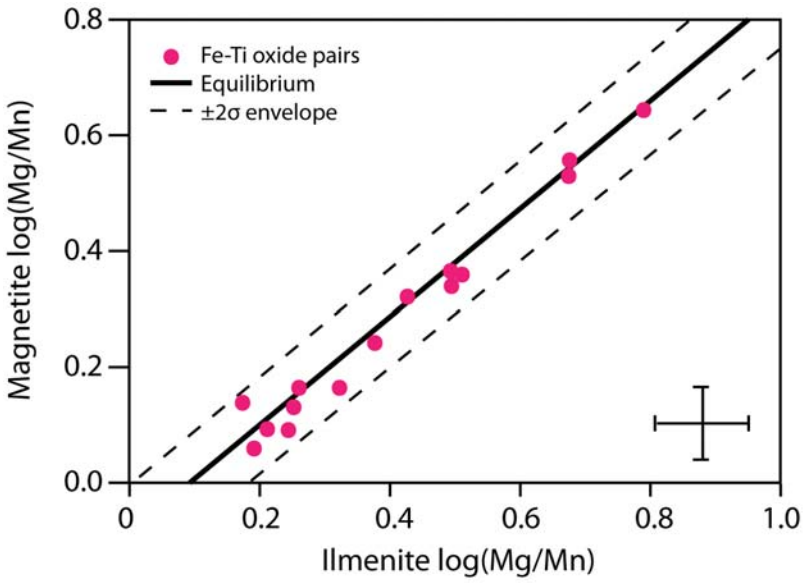

Figure A6.1: log Mg/Mn for 16 ilmenite-magnetite pairs. Middle solid line is the equilibrium equation (A8) and the ±2σ envelope is represented by dashed lines. Error bars show analytical uncertainty of 1 s.d.

Re-equilibration of oxides in response to changes in temperature and fO_2 can occur within a few days (Gardner et al., 1995) and therefore temperatures and oxygen fugacities calculated from Fe-Ti thermometry can represent eruption and cooling processes. Oxide cores were therefore targeted for EPMA analysis to minimise such effects.

Multiple Fe-Ti oxide thermometers have been calibrated under various temperature and fO_2 conditions resulting in a range of thermodynamic calculations. The two most widely used thermometers are those of QUILF (Andersen et al., 1993) and Ghiorso and Sack (1991). Ghiorso and Sack (1991) has been revised and corrected by Ghiorso and Evans (2008) to account for minor solid solution components including Mg, Mn and Al which can substitute for both Fe and Ti in the oxides and, as a result, influence the binary reactions and distort temperature calculations. Both QUILF and Ghiorso and Evans (2008) have been reviewed by Blundy and Cashman (2008) together with older thermometers by Andersen and Lindsley (1988). Of the revised thermometers, Andersen and Lindsley (1988) has the smallest error of ±33 °C (aad) but is valid over a small range of temperatures, and underestimates temperatures above 860 °C and overestimates temperatures below 860 °C. The QUILF thermometer encompasses a wider range of temperatures but systematically underestimates temperatures and has an uncertainty of ±60 °C (aad). A new thermo-oxybarometer by Sauerzapf et al. (2008) has also been calibrated and is only applicable for basic to intermediate rocks. Ghiorso and Evans (2008) has been used in this thesis as it provides the best thermometer that produces correct temperatures over the widest range,

with ±44 °C and is calibrated for silicic volcanic rocks. The Ghiorso and Evans (2008) thermometer is calibrated over 800-1300 °C and NNO-3 to NNO+3. An online thermometer has been set up by Ghiorso and Evans and is available at *http://ctserver.ofm-research.org/OxideGeotherm/OxideGeotherm.php* or can be downloaded as an excel spreadsheet. Fe-Ti oxide temperatures and oxygen fugacities are given in Table A6.3.

Table A6.3: Fe-Ti oxide temperatures and oxygen fugacities.

Pairs

Sample#	Ilmenite	Magnetite	T (°C)	ΔNNO	logfO_2
425	s5	s1	804	1.58	-12.24
425	s7	s9	812	1.55	-12.10
456	s2	s10	790	1.21	-12.91
527	s1	s8	860	0.03	-12.67
527	s10	s8	899	0.31	-11.67
527	18	17	767	0.26	-14.37

Crystal hosted pairs

Sample#	Host	Ilmenite	Magnetite	T (°C)	ΔNNO	logfO_2
440	amphibole	4	3	724	1.49	-14.15
440	amphibole	8	7	697	1.24	-15.09
440	amphibole	18	17	741	1.25	-13.98
440	clinopyroxene	23	22	741	1.22	-14.01
456	clinopyroxene	2	3	682	0.99	-15.73
456	clinopyroxene	20	19	755	0.94	-13.96
477	clinopyroxene	6	7	895	1.01	-11.04
477	clinopyroxene	15	16	884	0.77	-11.48
477	amphibole	17	18	911	1.02	-10.75
527	clinopyroxene	13	14	776	0.20	-14.22

Individual crystals in groundmass; s= <20 µm in groundmass; no s = >70 µm.

APPENDIX 7

DIFFUSION MODELLING

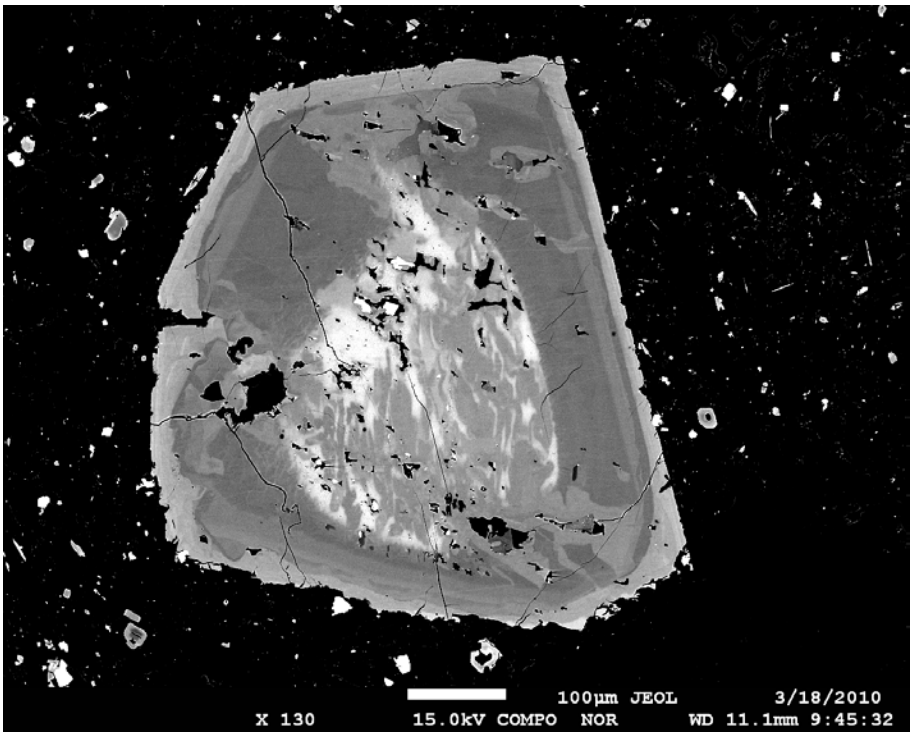

Plate 5: Back scattered electron image of a clinopyroxene phenocryst with a dissolution textured core and a normally zoned, Fe-rich rim.

A7.1: Introduction.

A7.2: Ti diffusion in quartz (Cherniak et al., 2007).

A7.3: Fe-Mg interdiffusion in clinopyroxene (Dimanov and Wiedenbeck, 2006).

A7.1 INTRODUCTION

Compositional zoning in minerals suggests disequilibrium in the system and records events where the physical and chemical conditions have changed, as observed in volcanic systems where there may be rapid crystallisation, short lived cooling and heating, magma mixing, magma recharge and fluctuations in oxygen fugacity caused by degassing. At magmatic temperatures these initially sharp boundaries will smooth out over time via the process of diffusion, forming increasingly broader chemical profiles, as illustrated in Figure A7.1. The rapid quenching that occurs on magma eruption preserves these compositional features. If the diffusion coefficient and physical conditions such as temperature and oxygen fugacity are known, the time elapsed between the disequilibrium event and magma eruption can be calculated (Costa and Chakraborty, 2004).

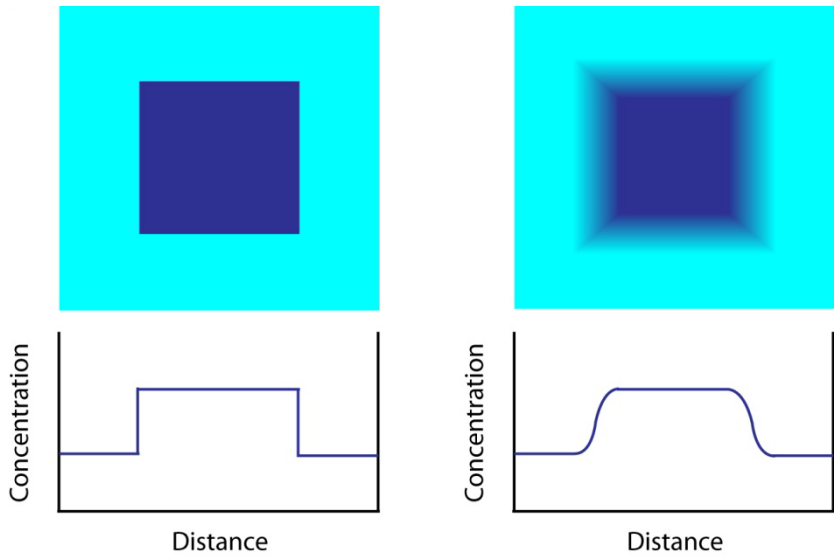

Figure A7.1: Schematic diagram of a zoned crystal before and after diffusion where the core is enriched in element X relative to the rim. The initial crystal shows a sharp boundary between the core and rim. After diffusion, this sharp boundary has been broadened by the exchange of X across the boundary, generating chemical profiles that resemble an error function curve.

Diffusion in minerals occurs due to the atomic-scale random motion of particles, which is thermally activated (Zhang, 2010). Different forms of diffusion are present in minerals: self diffusion (isotopic chemical potential), tracer diffusion (no chemical gradients) and chemical diffusion (chemical gradients), which can further be distinguished as trace element diffusion (one element, < 1 wt% concentration), interdiffusion (two component exchange), multispecies (when the diffusing component is present in two or more forms), mutlicomponent (interdiffusion of three or more components) and effective binary diffusion (when the diffusion of a component is treated simply by its own chemical gradient

in a multicomponent system) (Zhang, 2010). The chemical diffusion processes of interdiffusion (Fe-Mg in clinopyroxene) and trace element diffusion (Ti in quartz) are modelled in this study using the 1-D method of Morgan et al. (2004).

The relative diffusion modelling applied here is based on grey-scale compositional images of clinopyroxene and quartz images. These greyscale images are utilised for relative diffusion modelling where greyscale profiles across the selected boundaries are averaged and quantified using the software ImageJ (http://rsb.info.nih.gov/ij/). When selecting profiles, the modelled boundaries must be straight, and where multiple straight boundaries are present for the same crystal zone, the narrowest boundary zone was used as it will be the closest to perpendicular to the boundary.

Greyscale profiles share the same trend as an error function, and this relationship is used to calculate the timescales. Residence times are calculated using the grey scale contrast and the width of the boundary using the formulae:

$$C_{(x,t)} = \frac{n}{2(n+1)} = 1 - \left[0.5 erfc\left(\frac{x}{2\sqrt{Dt}}\right)\right]$$

where C represents the compositional contrast on a scale of 0 - 0.5 between the junction and the observed maximum extent of diffusion at the half-width x (see figure A7.2), t is the time since the formation of the rim boundary, n is the quantitative greyscale contrast (C_1-C_0) across the boundary, and D is the diffusion coefficient (for Ti in quartz and Fe-Mg interdiffusion in clinopyroxene).

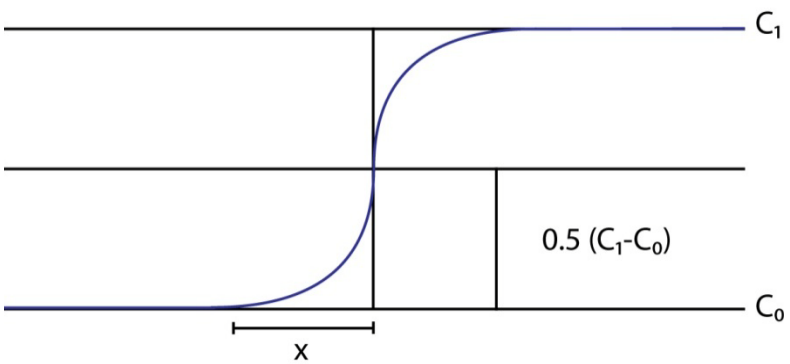

Figure A7.2: Diffused distribution of half-width x across the compositional range between C_0 and C_1. Figure taken from Morgan et al. (2004).

The diffusion coefficients describe the probability of ions moving in the crystal lattice, which is highly dependent on temperature. Increased thermal energy both facilitates the formation of more intrinsic lattice vacancies and increases the number of ions with sufficient energy to move around the crystal lattice (Costa and Morgan, 2010). The uncertainties in diffusion modelling are therefore greatly dependent on the reliability of the temperature constraints used to define the partition coefficients.

Variations in oxygen fugacity can also affect diffusion rates in two ways. The first effect is a direct effect where differently charged ions diffuse as different rates e.g. Fe (Fe^{2+} and Fe^{3+}), as the diffusivity of the lower valence species is higher than the high valence species due to weaker bonding with the crystal lattice. The second effect is indirect, and effects the numbers of vacancies through which the elements can diffuse. Vacancies in the crystal structure can be generated by balancing charges. For Fe, for example, three Fe^{2+} ions are equivalent to two Fe^{3+} ions and one vacancy (Zhang, 2010).

A7.2 Ti DIFFUSION IN QUARTZ

Titanium zoning in quartz can be revealed by cathodoluminesence (CL) imaging where luminescence intensity correlates with Ti concentration (Wark and Spear, 2005). The inclusion of Ti into the quartz crystal lattice is dependent on temperature and the Ti concentration in the melt (Wark and Watson, 2006), and new experiments by Thomas et al. (2010) indicate that there may also be large dependence on pressure.

The Ti diffusion rate in quartz has been determined experimentally by Cherniak et al. (2007) at dry 1-atm conditions where the rate of diffusion is dependent only on temperature. The experiments used both synthetic and natural quartz coupled with natural titanite powder and rutile, over a temperature range of 700-1150 °C. The resulting diffusion rate parallel to the crystal c-axis (0001) is defined by:

$$D_{Ti}(m^2/s) = 7\,x\,10^{-8}\exp\left(-\frac{273 \pm 12\ (kJ/mol)}{RT}\right)$$

where R = 8.314 J K^{-1} mol^{-1} (gas constant) and T = temperature in Kelvin.

Diffusivities normal to the c-axis do not differ significantly from those parallel to the c-axis (Cherniak, 2010).

For this study, diffusion modelling for quartz was conducted using the 1-D method of Morgan et al. (2004) with temperatures taken from amphibole thermometry (Ridolfi et al., 2010). As diffusion modelling is highly dependent on temperature, amphibole thermometry was used as it carries the smallest uncertainties of the thermometry methods applied here, and likely records the temperature in the mixed magma. Figure A7.3 shows the modelled quartz phenocrysts and the measured profiles. The modelling estimates the time lapsed between formation of the boundary and eruption. The rims of quartz are interpreted to have formed during the magma mixing event and therefore amphibole-derived temperatures are relevant as the amphibole crystallised during the mixing event. Table A7.1 presents the timescales calculated from the quartz rims. An indication of the uncertainties (1 s.e.) in the timescales is given by the Hot and Cold columns, which are based on the uncertainties on the temperatures determined by amphibole thermometry: ± 22 ^{o}C (1 s.e.). Higher temperatures (Hot) yield a lower timescale.

Table A7.1: Quartz rim diffusion ages for Tauhara volcano.

Sample	Dome	Crystal	T (°C)	D_{Ti}	**Age (years)**	Hot	Cold
425	Western	bH	889	3.76E-20	**0.30**	0.18	0.58
425	Western	bO	889	3.76E-20	**0.51**	0.30	0.93
425	Western	bW	889	3.76E-20	**0.33**	0.20	0.61
440	Central	bM	886	3.49E-20	**0.76**	0.44	1.41
440	Central	sT	886	3.49E-20	**0.74**	0.43	1.37
477	Trig M	bG	945	1.38E-19	**0.34**	0.22	0.56
477	Trig M	sH	945	1.38E-19	**0.24**	0.15	0.39
477	Trig M	sI	945	1.38E-19	**0.06**	0.04	0.10
477	Trig M	sL	945	1.38E-19	**0.08**	0.05	0.14
477	Trig M	sQ	945	1.38E-19	**0.07**	0.05	0.11
477	Trig M	sY	945	1.38E-19	**0.22**	0.14	0.36
483	Breached	bM	904	5.39E-20	**0.74**	0.45	1.32
483	Breached	sP	904	5.39E-20	**0.22**	0.15	0.39
483	Breached	bR	904	5.39E-20	**0.19**	0.11	0.34
527	Main	sY	894	4.24E-20	**0.25**	0.15	0.46

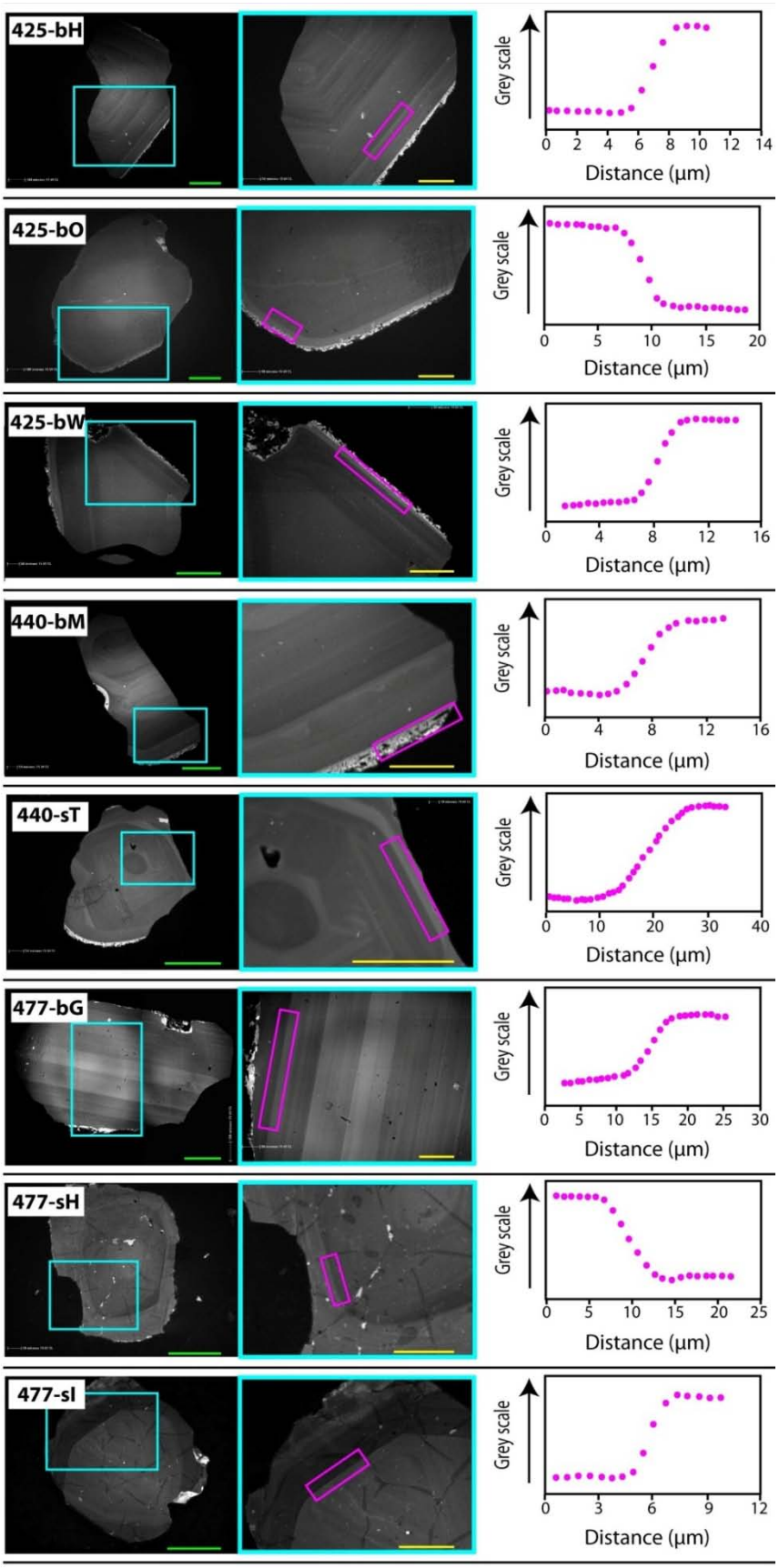

Figure A7.3: Images used in Ti in quartz diffusion modelling, showing the whole crystal, a close up of the modelled zone, and the measured grey scale intensity across the zone. Each pink dot represents the average grey scale at a specific distance across the profile. Green scale bars on the images are 200 µm and yellow scale bars are 100 µm.

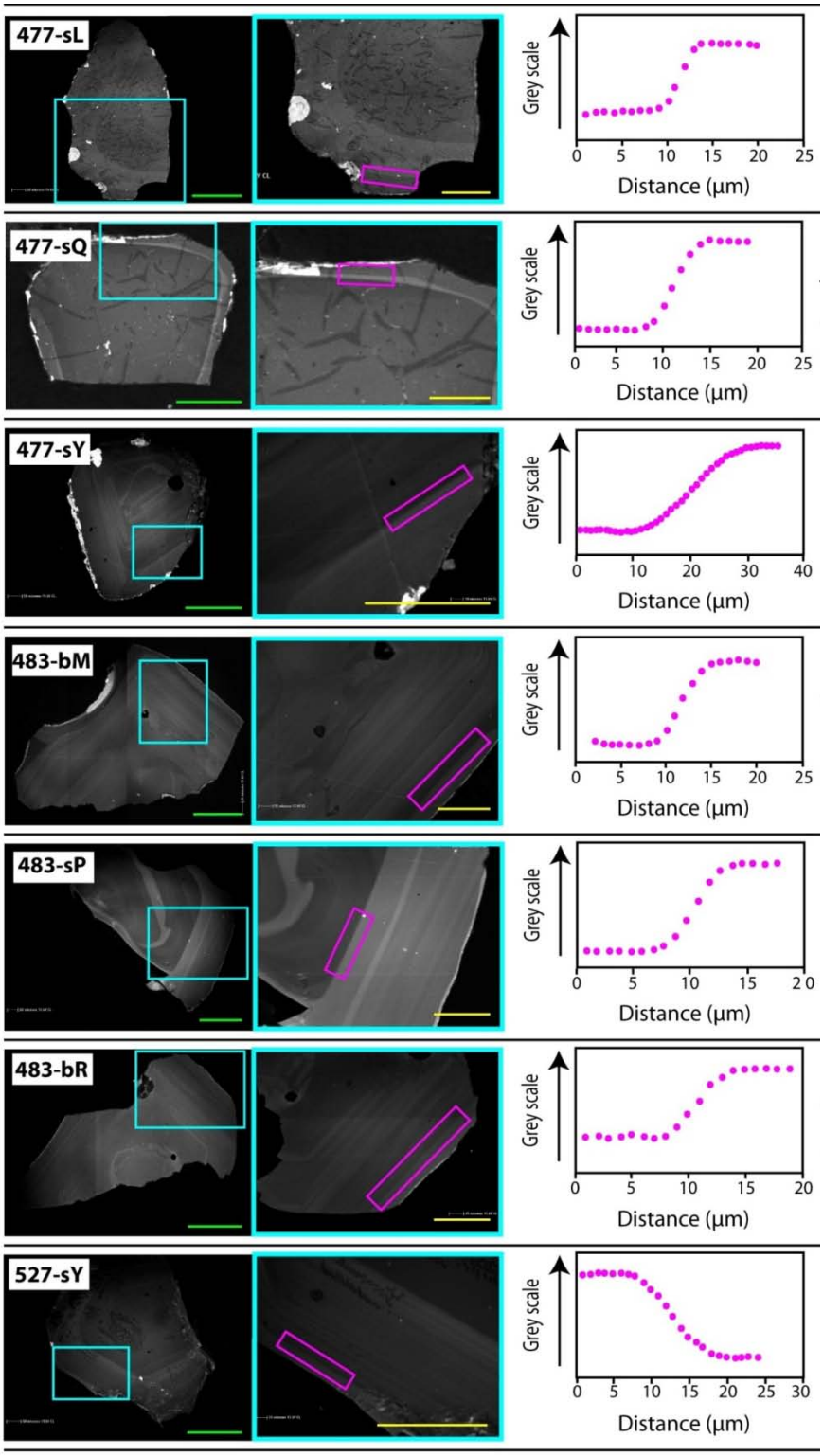

Figure A7.3 *(continued).*

A7.3: Fe-Mg INTERDIFFUSION IN CLINOPYROXENE

Fe-Mg interdiffusion experiments in clinopyroxene were first carried out by Dimanov and Sautter (2000) on natural diopside between 900-1240 °C. However, oxygen fugacity varied with temperature (10^{-18} to 10^{-13} atm) in these experiments, which may have led to an overestimation of the activation energy if the diffusion mechanism is vacancy-related. (Cherniak and Dimanov, 2010). This issue was resolved by the study of Dimanov and Wiedenbeck (2006), which focused on the effects of oxygen fugacity. Dimanov and Wiedenbeck investigated Fe-Mg interdiffusion in natural diopside along the (001) axis at temperatures between 1000 - 1200 °C and oxygen fugacities between $10^{-18.5}$ and 10^{-6} obtaining the following Arrhenius relation:

$$D\ (cm^2/s) = 7.68\ x\ 10^{-2}\left(\frac{pO_2}{pO_2^{ref}}\right)^{-0.22\pm0.02} \exp\left(-\frac{297 \pm 31\ (kJ/mol)}{RT}\right)$$

where R= 8.314 J K^{-1} mol^{-1} (gas constant), T= temperature in Kelvin, and pO_2^{ref} = 0.21 atm.

This relationship was used to calculate the diffusion rate used in diffusion modelling here. Two-pyroxene temperatures (Brey and Köhler, 1990) were used for the samples where orthopyroxene was present: Hipaua, Trig M, Breached and Main Domes. Where orthopyroxene was absent in the thin sections (Western and Central Domes), temperatures were taken from amphibole thermometry (Ridolfi et al., 2010). Oxygen fugacities determined from amphibole (Al# 0.10 – 0.24) were used for all samples (Ridolfi et al., 2010) as the amphibole, clinopyroxene and orthopyroxene crystallised during the magma mixing events.

Figure A7.4 shows the images used for modelling diffusion in clinopyroxene phenocrysts together with the measured profiles. For clinopyroxene, back scattered electron (BSE) imaging was used, where intensity reflects the average atomic number at the electron beam focus point. Brighter points on BSE images indicate higher average atomic mass, which for clinopyroxene corresponds to greater FeO concentration. Rim boundaries were targeted as these are interpreted to reflect pyroxene growth in the physical and chemical conditions of the dacitic melt prior to eruption.

Table A7.2 presents the timescales calculated from the clinopyroxene rims. Uncertainties (1 s.e.) in the timescale are indicated by the Hot and Cold columns, which are based on the 1

s.e. uncertainties in temperature (± 22 °C) and oxygen fugacity (± 0.4 log units). Hotter temperatures yield lower diffusion ages.

Table A7.2: Diffusion ages for clinopyroxene phenocryst rims from the Tauhara volcano.

Sample	Dome	Crystal	T °C	pO_2	D	**Age (years)**	Hot	Cold
425	Western	A	889	2.00E-05	2.00E-21	**1.72**	0.61	4.97
425	Western	D	889	2.00E-05	2.00E-21	**2.83**	1.00	8.16
440	Central	A	886	1.84E-05	1.80E-21	**2.28**	0.80	6.60
440	Central	F	886	1.84E-05	1.80E-21	**1.86**	0.65	5.37
440	Central	G	886	1.84E-05	1.80E-21	**1.06**	0.37	3.06
456	Hipaua	C	910	2.85E-05	4.16E-21	**1.13**	0.41	3.13
456	Hipaua	D	910	2.85E-05	4.16E-21	**1.03**	0.38	2.85
456	Hipaua	H	910	2.85E-05	4.16E-21	**1.90**	0.70	5.29
456	Hipaua	I	910	2.85E-05	4.16E-21	**0.23**	0.09	0.65
456	Hipaua	L	910	2.85E-05	4.16E-21	**1.47**	0.54	4.09
477	Trig M	A	909	6.00E-05	5.92E-21	**0.04**	0.01	0.10
527	Main	B	951	4.14E-06	4.30E-21	**0.45**	0.16	1.31
527	Main	M	951	4.14E-06	4.30E-21	**0.73**	0.26	2.16

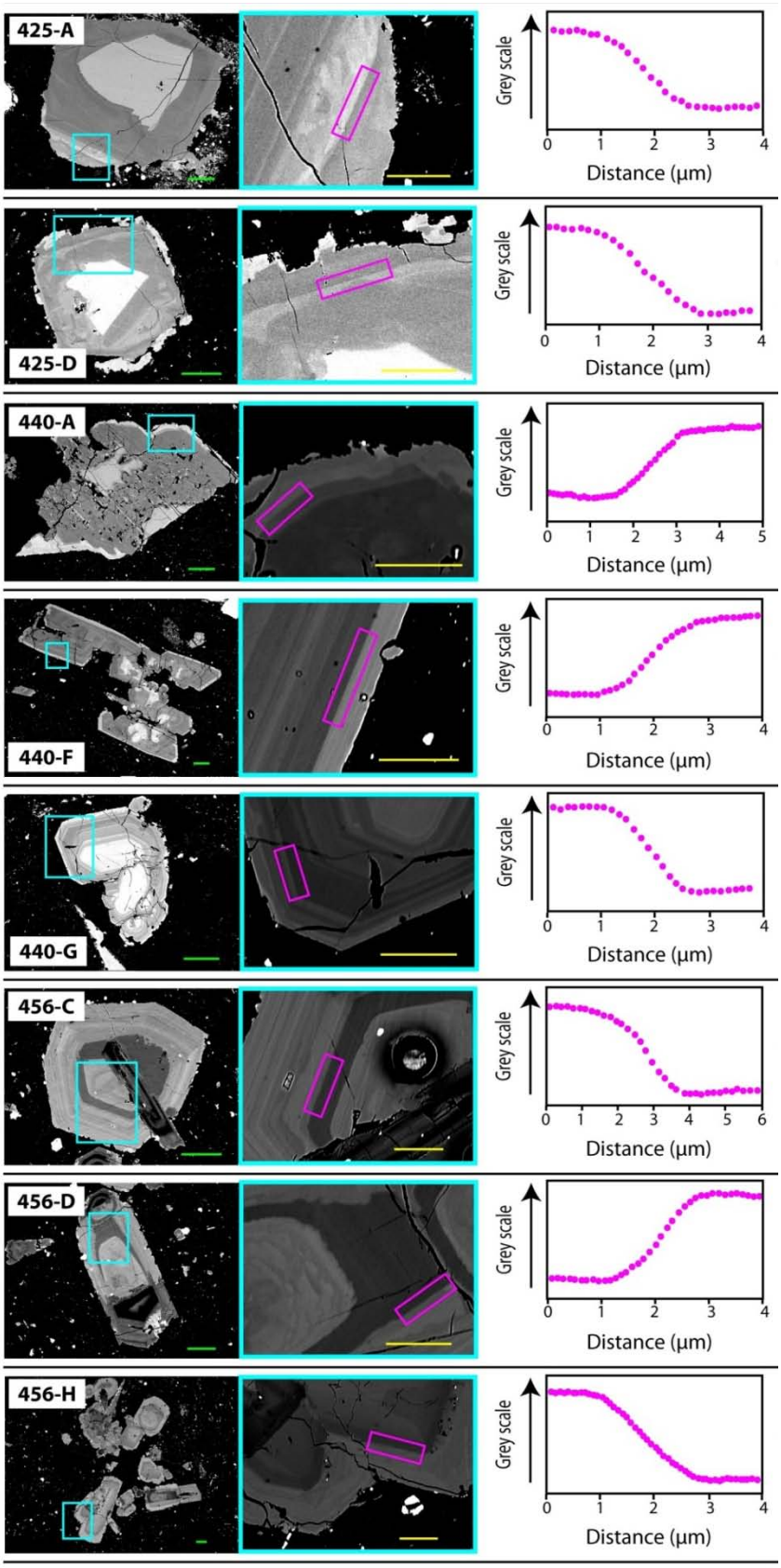

Figure A7.4: Back scattered electron images of clinopyroxene crystals used for Fe-Mg interdiffusion modelling, showing the whole crystal and a close up of the modelled boundary zone. Graphs show the measured grey scale intensity across the zone, where each pink dot represents the average grey scale at a specific distance across the profile. Green scale bars in the BSE images are 100 µm and yellow scale bars are 50 µm.

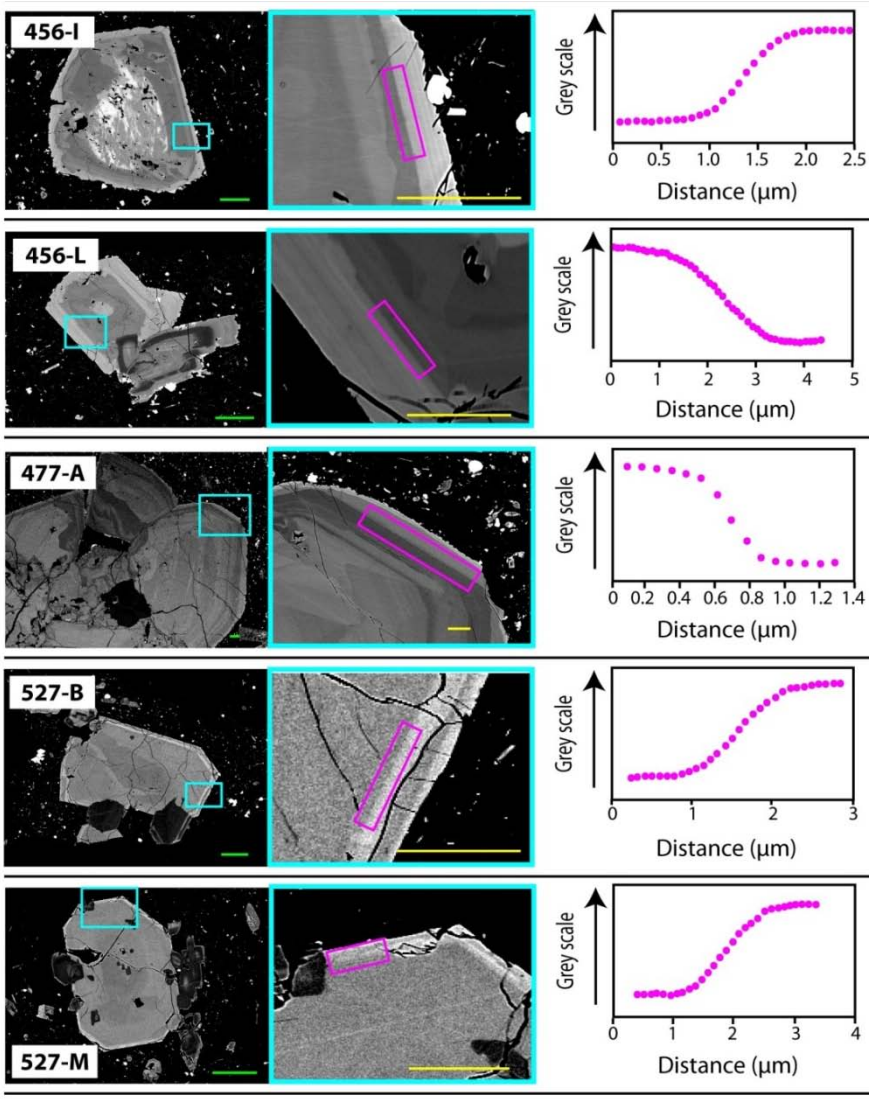

Figure A7.4 *(continued).*